STUDIES AND PREVENTION OF CARBON STEEL CORROSION AND SOLVENT DEGRADATION DURING AMINE-BASED CO_2 CAPTURE FROM INDUSTRIAL GAS STREAMS

A Thesis

Submitted to the Faculty of Graduate Studies and Research
In Partial Fulfillment of the Requirements
for the Degree of
Doctor of Philosophy
in Engineering
University of Regina

By

Pathamaporn Wattanaphan
Regina, Saskatchewan
January 2012

Copyright 2012: P. Wattanaphan

UNIVERSITY OF REGINA

FACULTY OF GRADUATE STUDIES AND RESEARCH

SUPERVISORY AND EXAMINING COMMITTEE

Pathamaporn Wattanaphan, candidate for the degree of Doctor of Philosophy in Engineering**,** has presented a thesis titled, ***Studies and Prevention of Carbon Steel Corrosion and Solvent Degradation during Amine-Based CO_2 Capture from Industrial Gas Streams,*** in an oral examination held on December 22, 2011. The following committee members have found the thesis acceptable in form and content, and that the candidate demonstrated satisfactory knowledge of the subject material.

External Examiner:	*Dr. Moetaz I. Attalla, CSIRO Energy Technology
Co-Supervisor:	Dr. Raphael Idem, Industrial Systems Engineering
Co-Supervisor:	Dr. Paitoon Tontiwachwuthikul, Industrial Systems Engineering
Committee Member:	Dr. Stephanie Young, Environmental Systems Engineering
Committee Member:	Dr. David deMontigny, Process Systems Engineering
Committee Member:	Dr. Renata Raina, Department of Chemistry & Biochemistry
Chair of Defense:	Dr. Dongyan Blachford, Faculty of Graduate Studies & Research

*Not present at defense

ABSTRACT

This research is focused on simultaneous inhibition of carbon steel (1020) corrosion and oxidative monoethanolamine (MEA) degradation in a carbon dioxide (CO_2) capture process from simulated post-combustion coal-fired flue gas, where components typically present in the flue gas partly contribute to such problems. Therefore, in this work, various additives were selected to study in the effects of flue gas composition on both carbon steel (1020) corrosion and oxidative MEA degradation. Sodium chloride (NaCl), ferrous chloride ($FeCl_2$), and hydrochloric acid (HCl) were selected to represent different sources of chlorides in the flue gas. Sulphurous acid (H_2SO_3), sulphuric acid (H_2SO_4), and nitric acid (HNO_3) were selected to represent the aqueous solutions of sulphur dioxide (SO_2), sulphur trioxide (SO_3), and nitrogen dioxide (NO_2), respectively. In addition, sodium bisulfite ($NaHSO_3$), sodium sulfite (Na_2SO_3), sodium sulphate (Na_2SO_4), and ferrous sulphate heptahydrate ($FeSO_4 \cdot 7H_2O$) were additionally selected in the study of corrosion. All the experiments were conducted under the base-case conditions containing MEA, CO_2, and O_2.

In the carbon steel (1020) corrosion study, the results illustrate that NaCl, HCl, Na_2SO_4, $FeSO_4 \cdot 7H_2O$, H_2SO_4, and HNO_3 all accelerated the corrosion process, while $FeCl_2$ slowed down metal corrosion. Surprisingly, H_2SO_3, $NaHSO_3$, and Na_2SO_3, either behaved as corrosion promoters or corrosion inhibitors depending strongly on their concentrations. Finally, the mixed additives were studied by mixing HCl, H_2SO_3, H_2SO_4, and HNO_3. The modified power law rate equation of the systems containing all four additives provided an acceptable percentage of average absolute deviations (%AAD) of 8.6%.

$$r_{corrosion} = (8.922E+09)\cdot e^{\frac{-6430}{T}} \cdot [H^+]^{0.118} \cdot ([Cl^-]^{0.106} + [HSO_3^-]^{0.007} + [SO_3^{2-}]^{0.006} + [SO_4^{2-}]^{0.006} + [NO_3^-]^{0.102})$$

In the oxidative MEA degradation study, $FeCl_2$, HCl, H_2SO_4, and HNO_3 essentially accelerated oxidative solvent degradation. On the other hand, NaCl and H_2SO_3 (below 250 ppm) appeared to prevent MEA degradation. Finally, the mixed additives study was performed by mixing HCl, H_2SO_3, H_2SO_4, and HNO_3 in the concentration ranges equivalent to the mixed additives in the corrosion study. The modified power law rate equation of the systems containing all four additives provided an acceptable %AAD of 9.4%.

$$r_{\deg radation} = (8.25E+05)\cdot e^{\frac{-8555}{T}} \cdot [H^+]^{0.37} \cdot ([Cl^-]^{0.24} + [HSO_3^-]^{-0.29} + [SO_3^{2-}]^{-0.02} + [SO_4^{2-}]^{0.05} + [NO_3^-]^{0.17})$$

In the inhibition study, both carbon steel corrosion and oxidative solvent degradation were inhibited simultaneously by introducing various inhibitors. Inhibitor A prevented carbon steel corrosion and oxidative MEA degradation by behaving as a hydrogen ion (H^+) scavenger. It provided the maximum efficiency of 88.9% inhibition on carbon steel corrosion and 97.3% inhibition on oxidative solvent degradation. Inhibitor B behaved primarily as an oxygen scavenger where it minimized carbon steel corrosion at the maximum of 92.4% inhibition and 59.9% inhibition on solvent degradation. Inhibitor C behaved as a free radical scavenger where it provided the maximum efficiency only at 42.7% inhibition on carbon steel corrosion but 92.6% inhibition on oxidative MEA degradation. Finally, the mixed inhibitors (A and C) were performed where the mixed inhibitors ratio III provided the best overall inhibitors' performance at 90.2% inhibition for carbon steel corrosion and 65.2% inhibition for oxidative MEA degradation. In conclusion, this work helped to establish "ultimate" inhibitors that were able to inhibit corrosion and solvent degradation simultaneously, which was essentially a successful achievement.

ACKNOWLEDGEMENTS

I would like to express my appreciation for the support I received during the course of my Ph.D. program from my mentors, colleagues, friends, and family. Without their support, I would never have fulfilled my goal.

I am greatly appreciative of my supervisors, Dr. Raphael Idem and Dr. Paitoon Tontiwachwuthikul, for giving me the incredible opportunity to pursue my Ph.D. Their technical suggestions and constructive advice were valuable guidance for keeping me on the right track. Most importantly, I cannot thank them enough for the belief they had in me that allowed me to independently develop my research ideas and skills.

I would like to thank my colleagues and friends at ITC, Ms. Robyn Fahlman, Ms. Lauren Bradshaw, Dr. Teeradet Supap for their technical support and friendship. Thanks are also given to the Engineering Workshop, Science Workshop, and Science Store, at the University of Regina, for their assistance whenever I had equipment difficulties or shortages of chemical supplies. Moreover, a special thank you goes to Dr. Renata Raina for not only kindly serving on my research committee but also for valuable technical support in using the analytical equipment.

Finally, financial support from The Natural Science and Engineering Research Council (NSERC) and the Faculty of Graduate Studies and Research, University of Regina, along with the International Test Centre for CO_2 capture (ITC), University of Regina, which provided me equipment and facilities for my research, are gratefully acknowledged.

DEDICATION

I would like to express my enormous appreciation to my parents, Mr. Phairat and Mrs. Prathoom Wattanaphan, for their endless love and support. There were times I secretly doubted myself and my ability, but the belief they have in me helped push me to move forward. My parents are my best inspiration; without them I have nothing. Their love and comfort have been constantly sent to me even when we are continents apart. Their words are inspiring and they always came in at all the right times. Lastly, my special appreciation goes to my boyfriend, Mr. Teerawat Sema, for his unbelievably understanding. Over the course of time, he has been not only my boyfriend but also my family, which he will always continue to be.

TABLE OF CONTENTS

ABSTRACT **i**

ACKNOWLEDGEMENTS **iii**

DEDICATION **iv**

TABLE OF CONTENTS **v**

LIST OF TABLES **xii**

LIST OF FIGURES **xv**

NOMENCLATURE AND ABBREVATIONS **xxi**

CHAPTER ONE: INTRODUCTION TO CARBON DIOXIDE (CO_2) CAPTURE PROCESS IN MONOETHANOLAMINE SOLUTION **1**

1.1 Background to carbon dioxide (CO_2) capture technology 1

1.2 Typical carbon dioxide (CO_2) capture process from post-combustion flue gas 8

1.3 Carbon dioxide (CO_2) absorption using monoethanolamine (MEA) solution 10

1.4 Absorption mechanisms in MEA-CO_2-H_2O system 15

1.5 Problem statement 16

1.6 Research objectives 18

CHAPTER TWO: CORROSION IN MEA-BASED CO_2 CAPTURE PROCESS **23**

2.1 Background to corrosion 23

2.2 Corrosion mechanism 25

2.3 Corrosion kinetics 31

2.3.1 Determination of the corrosion rate by using electrochemical technique 32

2.3.2 Corrosion kinetics in typical MEA-based CO_2 capture process 35

2.4 Corrosion prevention 38

2.4.1 Brief background of corrosion prevention 38

2.4.2 Corrosion inhibitors 39

CHAPTER THREE: SOLVENT DEGRADATION IN MEA-BASED CO_2 CAPTURE PROCESS 43

3.1 Background on MEA degradation 43

3.2 Oxidative MEA degradation mechanism 45

3.3 Kinetics of oxidative MEA degradation 55

3.4 Oxidative MEA degradation prevention 59

3.4.1 Oxygen scavengers and/or reaction inhibitors 60

3.4.2 Chelating agents 62

3.4.3 Stable salts 62

CHAPTER FOUR: EXPERIMENTAL APPARATUS AND PROCEDURES 64

4.1 List of chemicals and gases 64

4.2 Solvent preparation 68

4.3 Corrosion experiment 69

4.3.1 Specimen preparation 69

4.3.2 Experimental apparatus 71

4.3.3 Experimental procedures 75

4.3.4 Corrosion rate calculation 76

4.4 Oxidative MEA degradation experiment 79

4.5 Analytical techniques 84

4.5.1 Gas chromatography with mass spectrometry (GC-MS) 84

4.5.2 High performance liquid chromatography with refractive index detection (HPLC-RID) 85

4.5.3 Capillary electrophoresis with diode array detection (CE-DAD) 87

4.5.4 Inductively coupled plasma with mass spectrometry (ICP-MS) 88

4.5.5 Scanning electron microscopy with x-ray microanalysis (SEM-EDS) 89

CHAPTER FIVE: RESULTS AND DISCUSSION OF CARBON STEEL (1020) CORROSION 90

5.1 Experimental conditions 90

5.2 The effects of different types of chloride compounds on carbon steel (1020) corrosion 95

5.2.1 The effect of sodium chloride (NaCl) on the corrosion rate 97

5.2.2 The effect of hydrochloric acid (HCl) on the corrosion rate 102

5.2.3 The effect of ferrous chloride ($FeCl_2$) on the corrosion rate 103

5.2.4 Summary of the effects of cations (Na^+, H^+, and Fe^{2+}) and chloride ion (Cl^-) on the corrosion rates 107

5.3 The effects of different types of sulphate compounds on carbon steel (1020) corrosion 108

5.4 The effect of sulphurous acid (H_2SO_3) on carbon steel (1020) corrosion 111

5.4.1 The effect of sulphurous acid (H_2SO_3) on the corrosion rate 112

5.4.2 The influences of sulfite (SO_3^{2-}) and bisulfite (HSO_3^-) ions on the corrosion behaviour of sulphurous acid (H_2SO_3) 119

5.5 The effect of nitric acid (HNO_3) on carbon steel (1020) corrosion 122

5.6 The products of carbon steel (1020) corrosion in systems containing various additives (NaCl, HCl, $FeCl_2$, Na_2SO_4, H_2SO_4, $FeSO_4 \cdot 7H_2O$, Na_2SO_3, H_2SO_3, and HNO_3) under the base-case conditions 126

5.7 Kinetic study of mixed additives on carbon steel (1020) corrosion 135

CHAPTER SIX: RESULTS AND DISCUSSION OF OXIDATIVE MEA DEGRADATION 145

6.1 Experimental conditions 145

6.2 The effects of different types of chloride compounds on oxidative MEA degradation 148

6.2.1 The effect of sodium chloride (NaCl) on the degradation rate 148

6.2.2 The effect of hydrochloric acid (HCl) on the degradation rate 151

6.2.3 The effect of ferrous chloride ($FeCl_2$) on the degradation rate 153

6.2.4 The summary of the effects of cations (Na^+, H^+, and Fe^{2+}) and chloride ion (Cl^-) on the oxidative MEA degradation rates 159

6.3 The effect of sulphuric acid (H_2SO_4) on oxidative MEA degradation 162

6.4 The effect of sulphurous acid (H_2SO_3) on oxidative MEA degradation 165

6.5 The effect of nitric acid (HNO_3) on oxidative MEA degradation 170

6.6 The oxidative MEA degradation products in systems containing various additives (NaCl, HCl, $FeCl_2$, H_2SO_4, H_2SO_3, and HNO_3) under the base-case conditions 174

6.7 Kinetic study of mixed additives on oxidative MEA degradation 190

CHAPTER SEVEN: THE INHIBITION STUDIES OF CARBON STEEL CORROSION AND OXIDATIVE MEA DEGRADATION 197

7.1 Inhibitor screening 197

7.2 Experimental conditions 203

7.3 The calculation of inhibitor's efficiency (%) 205

7.4 The effects of various inhibitors in single inhibitor systems on carbon steel (1020) corrosion and oxidative MEA degradation 206

7.4.1 Inhibitor A 206

7.4.1.1 The inhibitor's efficiency of Inhibitor A on carbon steel (1020) corrosion 206

7.4.1.2 The inhibitor's efficiency of Inhibitor A on oxidative MEA degradation 212

7.4.2 Inhibitor B 216

7.4.2.1 The inhibitor's efficiency of Inhibitor B on carbon steel (1020) corrosion 216

7.4.2.2 The inhibitor's efficiency of Inhibitor B on oxidative MEA degradation 222

7.4.3 Inhibitor C 226

7.4.3.1 The inhibitor's efficiency of Inhibitor C on carbon steel (1020) corrosion 226

7.4.3.2 The inhibitor's efficiency of Inhibitor C on oxidative MEA degradation 231

7.4.4 The comparisons of inhibitors based on their maximum inhibiting performances 235

7.5 The effects of mixed inhibitors on carbon steel (1020) corrosion and oxidative MEA degradation 238

7.5.1 The selection of the mixed inhibitors 238

7.5.2 The inhibiting efficiency of the mixed inhibitors on carbon steel (C1020) corrosion and oxidative MEA degradation 242

CHAPTER EIGHT: CONCLUSIONS AND RECOMMENDATIONS 246

8.1 Summary of thesis study 246

8.2 Conclusions of thesis study 247

8.3 Recommendations for future work 252

REFERENCES 254

APPENDIX A: EXPERIMENTAL DATA OF THE CORROSION STUDY 263

APPENDIX B: EXPERIMENTAL DATA OF THE OXIDATIVE MEA DEGRADATION STUDY 267

APPENDIX C: EXPERIMENTAL DATA OF THE INHIBITION STUDY 278

APPENDIX D: DETERMINATION OF HYDROGEN (H^+), SULFITE (SO_3^{2-}), AND BISULFITE (HSO_3^-) IONS CONCENTRATIONS IN AQUEOUS SOLUTION OF SULPHUROUS ACID (H_2SO_3) 290

LIST OF TABLES

Table 1.1	The advantages and disadvantages of post-combustion capture, pre-combustion capture, and oxy-combustion.	3
Table 1.2	Average fuel carbon contents.	7
Table 1.3	The overall forward rate constant for CO_2-amine reactions.	12
Table 1.4	Heat of vapourization of various alkanolamines.	14
Table 1.5	Typical flue gas composition.	21
Table 1.6	Ion concentration (ppm) presented in IMC Chemicals Facility in Trona, CA, USA.	22
Table 4.1	A full list of chemicals and gases.	65
Table 4.2	The composition of carbon steel 1020.	70
Table 4.3	Parr reactor model 5523 specifications.	81
Table 5.1	The base-case conditions (no additive) of carbon steel (C1020) corrosion.	93
Table 5.2	The concentration ranges of additives in the carbon steel (C1020) corrosion study.	93
Table 5.3	The concentration ranges of the acid gas typically present in a flue gas, the calculated dissolved-gas concentration in aqueous solution, and the experimental concentration of the aqueous acid solution that were used in this work.	94
Table 5.4	Standard electrode potential (E_0^0) at 25°C.	101
Table 5.5	EDS elemental analysis for iron oxide (Fe-O) compound.	106

Table 5.6 The EDS scans of the corrosion products in the systems containing various additives under the base-case conditions and the standard iron compounds. 127

Table 5.7 Total iron ions (Fe^{2+} and Fe^{3+}) concentrations after performing the corrosion experiments in systems containing various additives under the base-case conditions. 130

Table 5.8 The experimental conditions of the kinetic study of the mixed additives on carbon steel (C1020) corrosion. 136

Table 5.9 The modified power law rate equations of single, binary, tertiary, and four additives systems. 141

Table 6.1 The base-case conditions (no additive) of oxidative MEA degradation. 146

Table 6.2 The concentration ranges of additives in oxidative MEA degradation study. 146

Table 6.3 The rate constants of the reactions of oxygen intermediates with amines at 25°C. 157

Table 6.4 The EDS scan for the precipitate particles found after performing an oxidative MEA degradation experiment. 157

Table 6.5 Initial MEA concentrations in different chlorides systems. 161

Table 6.6 Initial MEA concentrations in the systems containing various concentrations of H_2SO_3. 169

Table 6.7 Initial MEA concentrations in the systems containing various concentrations of HNO_3. 173

Table 6.8 Identification of the oxidative MEA degradation products. 176

Table 6.9 The experimental conditions in the kinetic study of the oxidative MEA degradation. 191

Table 6.10 The modified power law rate equation of single and four additives system. 196

Table 7.1 The effects of the MEA degradation products on carbon steel (1020) corrosion. 202

Table 7.2 The base-case conditions (no inhibitor) of the carbon steel (C1020) corrosion and oxidative MEA degradation experiments. 204

Table 7.3 pH of the solutions which containing different concentrations of Inhibitor A (%error: 0.17%). 211

Table 7.4 The concentrations of Inhibitor A before and after the corrosion experiments (%error: 2.8%). 211

Table 7.5 pH of the solutions which containing different concentrations of Inhibitor A (%error: 0.21%). 215

Table 7.6 The concentrations of Inhibitor C before and after the corrosion experiments (%error: 6.3%). 230

Table 7.7 The maximum efficiency of a single inhibitor on both carbon steel (C1020) corrosion and oxidative MEA degradation. 236

Table 7.8 HMIS (Hazardous Materials Identification System) of Inhibitor A, Inhibitor B, and Inhibitor C. 241

Table 7.9 The mixed inhibitors (Inhibitor A + Inhibitor C) performance with respected to single inhibitor systems (%error: 3.5%). 245

LIST OF FIGURES

Figure 1.1	Process diagrams of post-combustion capture, pre-combustion capture, and oxy-combustion.	5
Figure 1.2	Process diagram of typical carbon dioxide (CO_2) capture unit.	9
Figure 1.3	Commonly-used alkanolamines in the CO_2 capture process.	11
Figure 2.1	A simplified corrosion process involving iron and water.	26
Figure 2.2	Tafel plot.	34
Figure 3.1	Carbamate dimerization of MEA.	46
Figure 3.2	Oxidative MEA degradation mechanism.	48
Figure 3.3	Oxidative degradation mechanism through the reaction between MEA and acetic acid.	50
Figure 3.4	Oxidative degradation mechanism through electron abstraction.	52
Figure 3.5	Oxidative degradation mechanism through hydrogen abstraction.	54
Figure 4.1	Electrochemical apparatus for a corrosion experiment.	72
Figure 4.2	A corrosion cell.	73
Figure 4.3	A Tafel plot.	78
Figure 4.4	A fully equipped reactor.	82
Figure 4.5	Reactor's head.	83
Figure 5.1	The effects of different types of chloride compounds on the corrosion rates of carbon steel 1020 (%error: 5.8%, 4.5%, and 3.9% in NaCl, HCl, and $FeCl_2$ systems, respectively).	96
Figure 5.2	SEM-EDS scanning result for iron oxide (Fe-O) compound.	105

Figure 5.3 The effects of different types of sulphate compounds on the corrosion rates of carbon steel 1020 (%error: 5.9%, 5.0%, and 3.9% in Na_2SO_4, H_2SO_4, and $FeSO_4 \cdot 7H_2O$ systems, respectively). 110

Figure 5.4 The corrosion behaviour of H_2SO_3 on carbon steel 1020 (5.5 %error). 113

Figure 5.5 Tafel plots of 0 (no H_2SO_3), 24, 30, and 100 ppm H_2SO_3. 116

Figure 5.6 Tafel plots of 0 (no H_2SO_3), 100, 200, and 400 ppm H_2SO_3. 118

Figure 5.7 The corrosion behaviours of Na_2SO_3, $NaHSO_3$, and H_2SO_3 systems on carbon steel 1020 (%error: 6.3%, 3.2%, and 5.5% in Na_2SO_3, $NaHSO_3$, and H_2SO_3 systems, respectively). 120

Figure 5.8 The corrosion behaviour of HNO_3 system on carbon steel 1020 (1.6 %error). 124

Figure 5.9 SEM-EDS scan for the corrosion product in HNO_3 system. 125

Figure 5.10 SEM-EDS scan for a base-case system. 131

Figure 5.11 SEM-EDS scans for (a) NaCl system, (b) HCl system, and (c) $FeCl_2$ system. 132

Figure 5.12 SEM-EDS scans for (a) Na_2SO_4 system, (b) H_2SO_4 system, and (c) $FeSO_4 \cdot 7H_2O$ system. 133

Figure 5.13 SEM-EDS scans for (a) Na_2SO_3 system and (b) H_2SO_3 system. 134

Figure 6.1 The effect of sodium chloride (NaCl) on the oxidative MEA degradation rates (%error: 1.0%, 1.1%, 2.5% in 500, 1000, and 2000 ppm NaCl systems, respectively). 150

Figure 6.2 The effect of hydrochloric acid (HCl) on the oxidative MEA degradation rates (%error: 3.4%, 2.7%, 2.1% in 500, 1000, and 2000 ppm HCl systems, respectively). 152

Figure 6.3 SEM-EDS scan for particle generated when mixing $FeCl_2$ and 5M MEA. 154

Figure 6.4 The effect of ferrous chloride ($FeCl_2$) on the oxidative MEA degradation rates (%error: 2.94%, 2.85%, 2.44% in 500, 1000, and 2000 ppm $FeCl_2$ systems, respectively). 156

Figure 6.5 SEM-EDS scan for the precipitate particles found after performing an oxidative MEA degradation experiment. 158

Figure 6.6 The effect of sulphuric acid (H_2SO_4) on the oxidative MEA degradation rates (%error: 4.08%, 2.11%, and 2.76% in 4, 8, and 12 ppm H_2SO_4 systems, respectively). 164

Figure 6.7 The effect of sulphurous acid (H_2SO_3) on the oxidative MEA degradation rates (%error: 1.29%, 1.42%, 1.90%, 3.15%, 2.32% in 5, 15, 100, 250, and 400 ppm H_2SO_3 systems, respectively). 167

Figure 6.8 The effect of nitric acid (HNO_3) on the oxidative MEA degradation rates (%error: 1.91%, 1.40%, and 1.73% in 100, 250, and 400 ppm HNO_3 systems, respectively). 172

Figure 6.9 GC analysis of the oxidative MEA degradation products obtained from the base-case system. 177

Figure 6.10 Mass spectra of carbon dioxide (CO_2) obtained from (a) the sample solution and (b) MS-NIST98 database. 178

Figure 6.11 Mass spectra of water obtained from (a) the sample solution and (b) MS-NIST98 database. 179

Figure 6.12 Mass spectra of MEA obtained from (a) the sample solution and (b) MS-NIST98 database. 180

Figure 6.13 Mass spectra of 3-methylpyridine (A) obtained from (a) the sample solution, (b) MS-NIST98 database, and (c) the standard chemical. 181

Figure 6.14 Mass spectra of 1-methyl-azetidine (B) obtained from (a) the sample solution and (b) MS-NIST98 database. 182

Figure 6.15 Mass spectra of glycine anhydride (C) obtained from (a) the sample solution, (b) MS-NIST98 database, and (c) the standard chemical. 183

Figure 6.16 Mass spectra of n-acetylethanolamine (D) obtained from (a) the sample solution, (b) MS-NIST98 database, and (c) the standard chemical. 184

Figure 6.17 Mass spectra of 2-oxazolidone (E) obtained from (a) the sample solution and (b) the standard chemical. 185

Figure 6.18 Mass spectra of Compound A (G) obtained from (a) the sample solution, (b) MS-NIST98 database, and (c) the standard chemical. 186

Figure 6.19 Mass spectra of n-methyl caprolactam (H) obtained from (a) the sample solution, (b) MS-NIST98 database, and (c) the standard chemical. 187

Figure 6.20 Mass spectra of 1-2-hydroxyethyl-2-imidazolidinone (I) obtained from (a) the sample solution, (b) MS-NIST98 database, and (c) the standard chemical. 188

Figure 6.21 Mass spectra of diethyl fumarate (J) obtained from (a) the sample solution, (b) MS-NIST98 database, and (c) the standard chemical. 189

Figure 7.1 The corrosion rate and inhibitor's efficiency of Inhibitor A in the systems containing various concentrations of Inhibitor A (%error: 3.4%). 207

Figure 7.2 Tafel plots of the systems containing various concentrations of Inhibitor A. 208

Figure 7.3 The degradation rate and inhibitor's efficiency of Inhibitor A in the systems containing various concentrations of Inhibitor A (%error: 3.8%). 214

Figure 7.4 The corrosion rate and inhibitor's efficiency of Inhibitor B in the systems containing various concentrations of Inhibitor B (%error: 1.7%). 218

Figure 7.5 Tafel plots of the systems containing Inhibitor B in a concentration range between 0 to 100 ppm. 219

Figure 7.6 Tafel plots of the systems containing Inhibitor B in a concentration range between 100 to 10000 ppm. 221

Figure 7.7 The degradation rate and inhibitor's efficiency of Inhibitor B in the systems containing various concentrations of Inhibitor B (%error: 2.1%). 224

Figure 7.8 Inhibitor B's derivative in the system containing Inhibitor B concentration of 500 ppm (%error: 1.04%). 225

Figure 7.9 The corrosion rate and inhibitor's efficiency of Inhibitor C in the systems containing various concentrations of Inhibitor C (%error: 2.4%). 227

Figure 7.10 Tafel plots of the systems containing various concentrations of Inhibitor C. 228

Figure 7.11 The degradation rate and inhibitor's efficiency of Inhibitor C in the systems containing various concentrations of Inhibitor C (%error: 2.9%). 233

Figure 7.12 Inhibitor C concentration in the degradation system containing 80000 ppm of Inhibitor C (%error: 2.9%). 234

Figure 7.13 The comparison between the performances of Inhibitor A and Inhibitor B. 239

NOMENCLATURE AND ABBREVIATIONS

%AAD	Percentage of average absolute deviation
%wt	Percent weight
A	Surface area of a corrosion specimen (cm^2)
°C	Temperature in degree Celsius
d	Density of a corrosion specimen (g/cm^3)
Da	Dalton
E	Activation energy (J/mol)
E_0^0	Standard electrode potential for a half cell reduction reactions at 25°C (V)
E_{corr}	Corrosion potential (V)
EW	Equivalent weight of a corrosion specimen (g)
hp	Horse power
H_T	Temperature sensitivity constant in liquid phase (K)
i_{corr}	Corrosion current (μA)
I_{CORR}	Corrosion current density ($\mu A/cm^2$)
k	Rate constant
k_0	Pre-exponential factor or collision constant
K	Temperature in degree Kelvin
M	Molarity (mol/l)
MDL	Method detection limit
mpy	Milli-inches per year
Pa	Pascal

ppm	Parts per million
psi	Pound per square inch
r_{Exp}	Experimental rate
$r_{\mathrm{Pr}edicted}$	Predicted rate
R	Gas constant (8.314 J/(mol·K))
$R_{uninhibited}$	Rate of the uninhibited system (without inhibitor)
$R_{inhibited}$	Rate of the inhibit system (with inhibitor)
ROS	Reactive oxygen species
rpm	Round per minute
T	Temperature

Abbreviations

AOAC	Association of Official Analytical Chemists
ASU	Cryogenic air separation unit
CFCs	Chlorofluorocarbons
CH_3CN	Acetonitrile
CH_4	Methane
CO_2	Carbon dioxide
CRCLA	Compensation and Liability Act
DEA	Diethanolamine
DOE	U.S. Department of Energy
EIA	Energy Information Administration

$FeCl_2$	Ferrous chloride
FeO	Ferrous oxide
FeOOH	Goethite
Fe_2O_3	Ferric oxide
Fe_3O_4	Iron (II,III) oxide or Magnetite
$FeSO_4 \cdot 7H_2O$	Ferrous sulphate heptahydrate
GHG	Greenhouse gases
H_2	Hydrogen
He	Helium
HMIS	Hazardous Materials Identification System
HCl	Hydrochloric acid
H_2O	Water
HNO_3	Nitric acid
H_3PO_4	Phosphoric acid
H_2SO_3	Sulphurous acid
H_2SO_4	Sulphuric acid
ITC	International Test Center for CO_2 capture, University of Regina
KH_2PO_4	Potassium dihydrogen phosphate
MDEA	methyldiethanolamine
MEA	Monoethanolamine
N_2	Nitrogen
NaOH	Sodium hydroxide
NIST	National Institute of Standards and Technology

N_2O	Nitrous oxide
NaCl	Sodium chloride
$NaHSO_3$	Sodium bisulfite
Na_2SO_3	Sodium sulfite
Na_2SO_4	Sodium sulphate
NO_2	Nitrogen dioxide
NSERC	Natural Science and Engineering Research Council
O_2	Oxygen
O_3	Ozone
SO_2	Sulphur dioxide
SO_3	Sulphur trioxide
TEA	Triethylamine
TSCA	Toxic Substances Control Act
WGS	Water-gas-shift reaction

CHAPTER ONE

INTRODUCTION TO CARBON DIOXIDE (CO_2) CAPTURE PROCESS IN MONOETHANOLAMINE SOLUTION

1.1 Background to carbon dioxide (CO_2) capture technology

Carbon dioxide (CO_2) is known to be one of the major greenhouse gases (GHG) released to the atmosphere by an enormous number of industries and human activities. Greenhouse gases increasingly accumulate in the atmosphere, introducing problems such as climate change and global warming due to the fact that they behave as a heat barrier in the atmosphere that absorbs and reflects heat back to the earth surface, ultimately leading to rapid increase in global average temperature.

Due to their use in energy production, fossil fuels (coal, oil, and natural gas) are known to be one of the major sources of carbon dioxide emissions. Fossil fuels by themselves currently supply around 85% of the energy requirements in the United States and about the same percentage of energy used worldwide (Herzog, 1998). Fossil fuels are widely used due to their low cost, extensive availability, and the fact that existing fossil fuel-based technologies for energy production are highly reliable. The Energy Information Administration (EIA) at the U.S. Department of Energy (DOE) estimates the consumption of fossil fuels will increase by 27% over the next 20 years (Figueroa et al., 2008). Therefore, concerns over the amount of future carbon dioxide emissions have been raised, along with questions concerning the capability of industry to reduce them.

For years, numerous techniques have been applied in order to reduce the amount of carbon dioxide in gas emissions. The techniques are mainly divided into three categories: post-combustion capture, pre-combustion capture, and oxy-combustion (Figueroa et al., 2008). Post-combustion is primary applied to coal-fired power plants. Carbon dioxide is removed from flue gas after the air-driven combustion, so it contains a high percentage of nitrogen (N_2) and generates a flue gas that is released at atmospheric pressure and consists of less than 15% carbon dioxide. Pre-combustion is mostly applied in gasification processes. A primary fuel is chemically reacted with either steam or oxygen to generate a synthesis gas containing mainly hydrogen (H_2), carbon dioxide (CO_2), and trace gases. Then, the synthesis gas is processed through a water-gas-shift reaction (WGS) to produce a CO_2/H_2 (40%/55%) rich stream. Since carbon dioxide in the synthesis gas has high partial pressure, it is easy to remove, usually by physical or physical/chemical absorption (Blomen et al., 2009). In oxy-combustion, fuel is burnt in a highly-purified oxygen (O_2) stream, typically produced using cryogenic air separation units (ASU), which results in a very high carbon dioxide concentration flue gas. The advantages and disadvantages of each process are summarized in Table 1.1, and the process diagrams are presented in Figure 1.1.

Table 1.1: The advantages and disadvantages of post-combustion capture, pre-combustion capture, and oxy-combustion. (Figueroa et al., 2008 and Blomen et al., 2009).

Process	Advantage	Disadvantage
Post-combustion	▪ Mature technology ▪ Applications are already installed in many coal-fired power plants as solvent scrubbing facilities.	▪ Low carbon dioxide partial pressure (13 to 15%vol in coal-fired flue gas), which requires high performance chemical absorption in order to achieve a satisfactory removal efficiency. ▪ Traces of impurities in flue gas can possibly cause severe solvent degradation and material corrosion.
Pre-combustion	▪ High concentration and pressure of carbon dioxide in exhaust gas helps as a driving force in the separation process. ▪ Hydrogen-rich gas is produced and can be used in subsequent applications.	▪ Not suitable for fuel gas that has many impurities.

Oxy-combustion	▪ High carbon dioxide concentration in flue gas normally varies from 70 to 95% depending on fuel types ▪ 60 to 70% reduction of NO_x emissions compared to air-fired combustion	▪ The production of highly-purified oxygen might not be cost effective because the power consumption in cryogenic air separation units (ASU) is substantial.

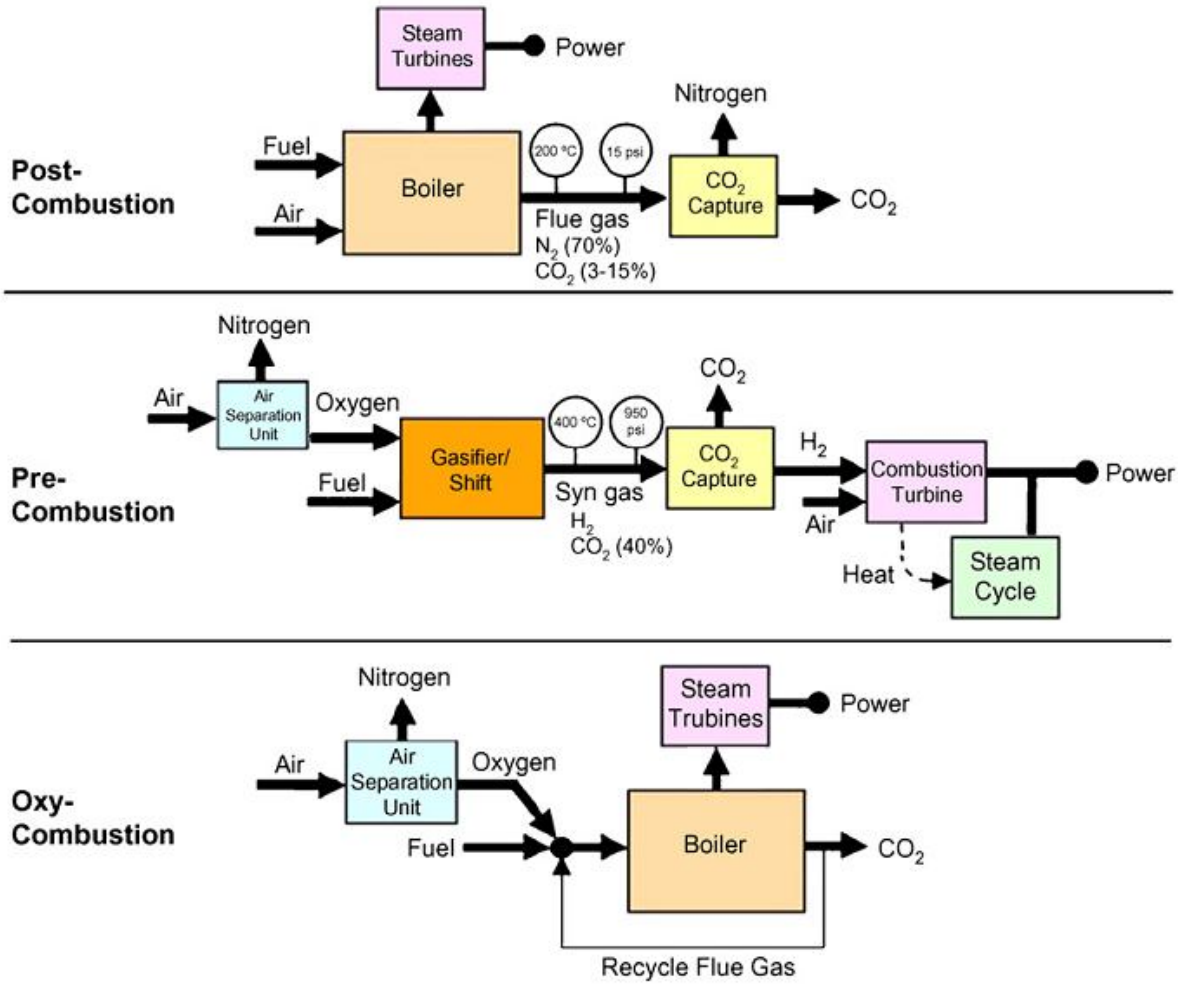

Figure 1.1: Process diagrams of post-combustion capture, pre-combustion capture, and oxy-combustion. (Figueroa et al., 2008) (Original in colour)

As mentioned earlier, fossil fuels (coal, oil, and natural gas) have played a major role in global energy production and their continued consumption is expected to remain high for at least a few decades (Figueroa et al., 2008). Among all the fossil fuels, coal is the most abundant and least expensive. Thus, coal is widely used as a source of energy supply. In fact, approximately 60% of worldwide electricity has been produced from coal (Krumbeck, 2007). Unfortunately, coal has the highest average carbon content, as illustrated in Table 1.2, which leads to greater carbon dioxide emissions when compared to oil and natural gas combustion processes (Wilson, 1990). As was also mentioned above, there are a several techniques that can be applied for carbon dioxide capture (post-combustion capture, pre-combustion capture, and oxy-combustion) (Figueroa et al., 2008). However, post-combustion is the most suitable for application of carbon dioxide capture from coal-fired power plants for several reasons (Herzog et al., 2009). First, it is compatible with existing coal-fired power plant facilities and can be used to retrofit conventional infrastructure for carbon dioxide capture without requiring substantial changes in the basic combustion technology. In addition, it offers flexibility; specifically, if the capture plant shuts down, the power plant can still operate. The other two capture options are highly integrated with the power plant, so if the capture element of the system fails, the entire plant must shut down. Lastly, pre-combustion and oxy-combustion technologies have not been yet commercialized, whereas post-combustion capture is ready for commercial deployment. Consequently, post-combustion capture is still the leading candidate for applications in coal-fired power plants. Therefore, based on all of the above reasons, this research will focus mainly on processes associated with carbon dioxide capture from simulated post-combustion coal-fired flue gas.

Table 1.2: Average fuel carbon contents. (Wilson, 1990)

Fuel	**gram carbon per MJ**	**gram carbon dioxide (CO_2) released per MJ**
Brown coal and lignite	25.2	92
Bituminous coal	23.7	87
Oil	19.9	73
Natural gas	13.5	49

1.2 Typical carbon dioxide (CO_2) capture process from post-combustion flue gas

A typical post-combustion gas treating facility mainly consists of two units, an absorber and a stripper. The process starts when a post-combustion flue gas enters the absorber through the bottom while a solvent, mostly amines, flows downward from the upper section and flows counter current with the flue gas. Carbon dioxide (CO_2) that is carried within the flue gas then has a chance to react with the amine to form a reversible compound such as carbamate (if it is a primary or secondary amine). In the absorber, carbon dioxide is removed from "sour gas or acid gas" by reacting with the amine, leaving an exhaust gas that carries mainly nitrogen (N_2) and oxygen (O_2) or so called "sweet gas". The carbon dioxide-rich solution leaves the bottom of the absorber and enters the stripper unit where heat is applied to the solution, usually from a steam reboiler, in order to reverse the chemical equilibrium and liberate the carbon dioxide. Then, the released carbon dioxide flows upward, passes through a condenser, and exits the process. The remaining amine solution is then fed through an exchanger in order to remove some of the heat before it re-enters the absorber as a recycled stream. The exchanger behaves as heat-integrated equipment by using the heat carried by the amine leaving the stripper as a heat source to pre-heat the rich amine solution. A process diagram of a typical carbon dioxide capture unit is presented in Figure 1.2 (Mofarahi et al., 2008).

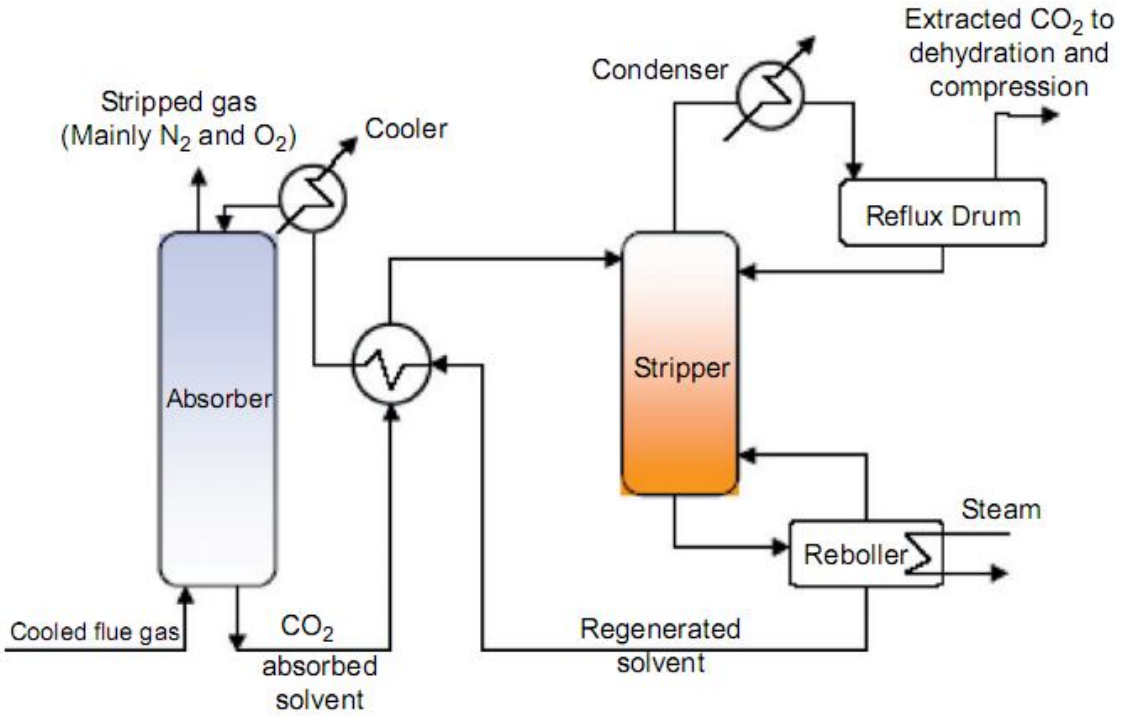

Figure 1.2: Process diagram of typical carbon dioxide (CO_2) capture unit. (Mofarahi et al., 2008) (Original in colour)

1.3 Carbon dioxide (CO_2) absorption using monoethanolamine (MEA) solution

Amines chemically react with carbon dioxide (CO_2) to form water soluble compounds, consequently they are able to capture CO_2 at a low partial pressure within a flue gas. However, capturing capacity is normally equilibrium limited (Mandal et al., 2001). Amines typically exist in three forms (primary, secondary, and tertiary amines). Alkanolamine solution is well known to be one of the most promising solvents for CO_2 absorption due to the fact that it either provides high reactivity with CO_2 or simply has satisfactory removal capacity (Chakma, 1997). A hydroxyl group in alkanolamine helps to reduce the vapour pressure and increase the water solubility, while an amino group provides the necessary alkalinity in aqueous solution for the CO_2 absorption (Kohl and Nielsen, 1997). Some commonly-used alkanolamines in the CO_2 capture process are monoethanolamine (MEA), diethanolamine (DEA), and methyldiethanolamine (MDEA), which are illustrated in Figure 1.3 (Astarita et al., 1983). Aqueous monoethanolamine (MEA), a primary amine, has been popularly used as a solvent for CO_2 capture due to its high reactivity with CO_2 and considerably low cost. It is able to absorb CO_2 at a low partial pressure, which is suitable for post-combustion from coal-fired power plants, since the percentage of CO_2 in a typical coal-fired flue gas is usually less than 15% (Chakma, 1995). Moreover, the kinetics of CO_2 absorption using MEA have been shown to be much better than other typical alkanolamines, as indicated from the fact that the rate constant of CO_2-amine reaction was found to be much higher when compared to other alkanolamines, as presented in Table 1.3 (Chakma, 1997).

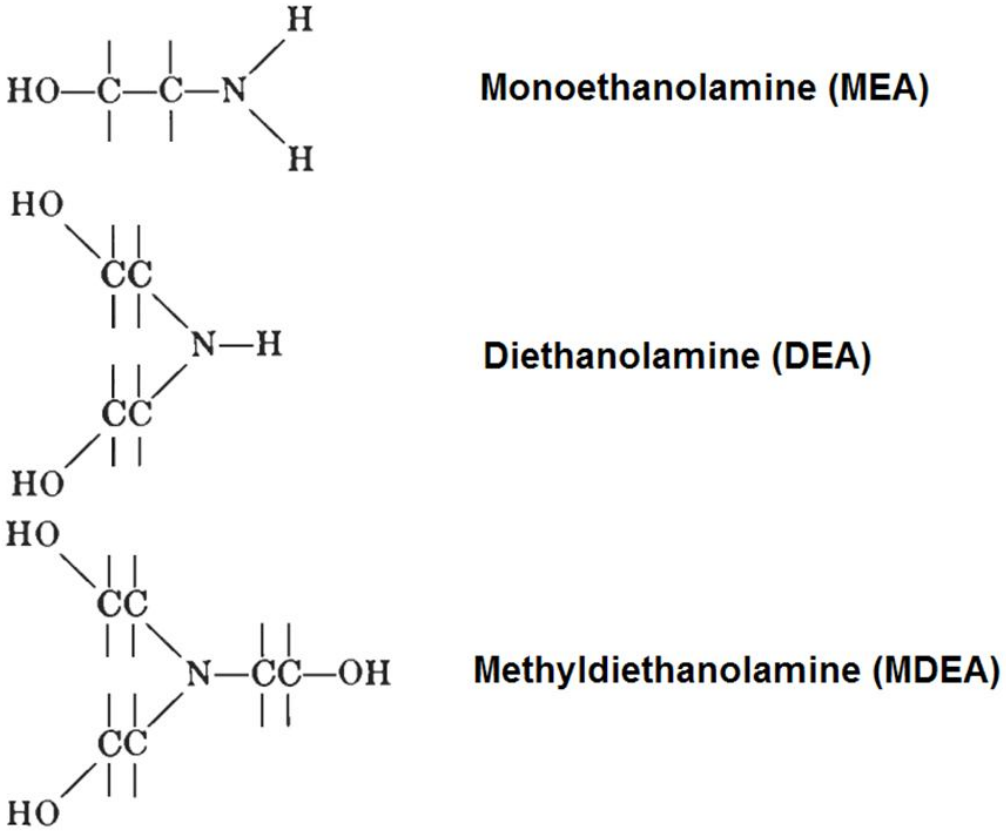

Figure 1.3: Commonly-used alkanolamines in the CO_2 capture process.

Table 1.3: The overall forward rate constant for CO_2-amine reactions. (Chakma, 1997)

Amine type		Reaction rate constant (mol/l·s)
MEA	Primary amine	7600
DEA	Secondary amine	1500
TEA	tertiary amines	16.8
MDEA	tertiary amines	9.2

It should be noted that even though MEA seems to be an ideal candidate based on a reaction rate point of view, its absorption capacity is usually limited by equilibrium stoichiometry at about 0.5 CO_2 loading (mole of CO_2 per mole of amine), in which carbamate is the final product of the reaction (Mandal et al., 2001 and Mofarahi et al., 2008). Moreover, from an energy perspective, MEA is not the most appealing solvent because it requires slightly higher energy consumption in the solvent regeneration process due to higher heat of vapourization compared to other alkanolamines, as shown in Table 1.4 (Chakma, 1997). In addition, if the concentration of MEA is restricted by the equilibrium limit, it directly affects the energy requirement for solvent regeneration because the lower the weight percentage of MEA in aqueous solution, the higher the energy required in the solvent regeneration process (Chakma, 1995).

Ultimately, although MEA is not the ideal solvent for CO_2 capture when considering all the main operational perspectives (reaction rate, absorption capacity, and energy consumption for solvent regeneration), it is still one of the best candidates since it provides high reactivity with CO_2, which leads to many more benefits. For example, capital costs and operating costs are minimized due to the ability to reduce the capture equipment size and solvent requirements and because solvent costs are minimal.

Table 1.4: Heat of vapourization of various alkanolamines. (Chakma, 1997)

Amine type		Heat of vapourization (kJ/kg)
MEA	Primary amine	826
DEA	Secondary amine	670
TEA	tertiary amines	535
MDEA	tertiary amines	550

1.4 Absorption mechanisms in MEA-CO_2-H_2O system

The absorption mechanisms of CO_2 in aqueous MEA solution are expressed as follows (Aboudheir et al., 2003):

Ionization of water:

$$2H_2O \leftrightarrow OH^- + H_3O^+ \quad (1.1)$$

Dissociation of dissolved CO_2 through carbonic acid to bicarbonate:

$$CO_2 + 2H_2O \leftrightarrow HCO_3^- + H_3O^+ \quad (1.2)$$

Bicarbonate formation:

$$CO_2 + OH^- \leftrightarrow HCO_3^- \quad (1.3)$$

Dissociation of bicarbonate:

$$HCO_3^- + H_2O \leftrightarrow CO_3^{2-} + H_3O^+ \quad (1.4)$$

Dissociation of protonated MEA:

$$RNH_3^+ + H_2O \leftrightarrow RNH_2 + H_3O^+ \quad (1.5)$$

Zwitterion formation by the reaction of MEA with CO_2:

$$CO_2 + RNH_2 \leftrightarrow RNH_2^+COO^- \quad (1.6)$$

Carbamate formation by deprotonation of zwitterion:

$$RNH_2^+COO^- + RNH_2 \leftrightarrow RNH_3^+ + RNHCOO^- \quad (1.7)$$

$$RNH_2^+COO^- + H_2O \leftrightarrow H_3O^+ + RNHCOO^- \quad (1.8)$$

$$RNH_2^+COO^- + OH^- \leftrightarrow H_2O + RNHCOO^- \quad (1.9)$$

$$RNH_2^+COO^- + HCO_3^- \leftrightarrow H_2CO_3 + RNHCOO^- \quad (1.10)$$

$$RNH_2^+COO^- + CO_3^{2-} \leftrightarrow HCO_3^- + RNHCOO^- \quad (1.11)$$

Carbamate reversion to bicarbonate:

$$RNHCOO^- + H_2O \leftrightarrow RNH_2 + HCO_3^- \quad (1.12)$$

1.5 Problem statement

This research is focused on CO_2 capture from simulated post-combustion coal-fired flue gas via absorption with MEA solvent, where compounds typically found in flue gases appear to cause two potential problems: solvent degradation and material corrosion. Solvent degradation leads to a number of unwanted effects such as additional solvent cost, waste disposal expense, and corrosion (Chi and Rochelle, 2002). Corrosion problems can directly affect the plant's economic operation, such as causing unplanned down-time or loss of productivity. Since, MEA is an appealing candidate for capture solvent in CO_2 absorption, solvent degradation and corrosion problems in the MEA-based capture process need to be studied in depth in order to find a way to minimize these problems. In addition, MEA itself is corrosive when compared to other typical ethanolamines (Veawab, 2000). Therefore, if the issues of solvent degradation and material corrosion can be minimized, MEA will obviously be one of the best solvents for CO_2 capture from post-combustion coal-fired flue gas.

For the purpose of simultaneously minimizing MEA degradation and material corrosion, the relationship between solvent degradation and corrosion must be understood. Degradation products are often linked to corrosion in that degradation products

normally increase material corrosion. Similarly, corrosion inhibitors, which are mostly heavy metal compounds, have proven to tremendously accelerate MEA degradation (Bello and Idem, 2006; Uyanga and Idem, 2007; and Sexton and Rochelle, 2009). In a typical CO_2 capture plant, MEA degradation and corrosion potentially-severely occur in different capture units. From the process diagram illustrated in Figure 1.2 (Mofarahi et al., 2008), corrosion can be observed in almost every section of a capture plant. However, it is potentially found mostly at the bottom of the absorber and at the top of the stripper column, as the consequences of the presence of rich amine solution and high temperature, respectively (Veawab, 2000 and Soosaiprakasam and Veawab, 2008). Since carbon steel corrosion is more sensitive to CO_2 loading (mol CO_2/mol MEA) than the concentrations of other components, such as dissolved O_2 or MEA (Kladkaew et al., 2011), the rich amine solution leaving the absorber, which contains high CO_2 loading, dramatically increases material corrosion. When the rich amine enters the top of the stripper, where the temperature is typically 120°C (while the temperature of the absorber is normally 55°C in a MEA system), corrosion is accelerated due to the effects of high temperature. On the other hand, MEA degradation mostly occurs in the stripper unit. In contrast with the effect on corrosion, CO_2 appears to inhibit solvent degradation process (Bello and Idem, 2006; Uyanga and Idem, 2007; and Supap et al., 2009). Thus, the absorber, especially at the bottom where high CO_2 loading occurs, is expected to have less MEA degradation than occurs in the stripper column, where most of the CO_2 is released from the solution and leaves the unit. Moreover, the high temperature of the stripper column also accelerates the solvent degradation process. The details on both MEA degradation and material corrosion are discussed thoroughly in Chapters Two and Three.

1.6 Research objectives

As has been mentioned above, this research is focused on simultaneous inhibitions of material corrosion and solvent degradation in the post-combustion CO_2 capture process from simulated coal-fired flue gas by absorption with a chemical solvent (monoethanolamine or MEA). Therefore, flue gas composition needs to be taken into account. Studying the effect of components typically present within a flue gas on both material corrosion and MEA degradation was considered beneficial not only as a way of understanding the level of aggressiveness in material corrosion or solvent degradation caused by a given compound, but also of helping to develop the experimental environment to be as relevant as possible to practical applications in order to perform subsequent inhibition studies. Typical flue gas composition after sulphur dioxide (SO_2) scrubbing was presented in Table 1.5 (Chakma, 1995). Besides CO_2, O_2, and water, of which the effects on corrosion and solvent degradation in MEA-based CO_2 capture processes have been well established, sulphur dioxide (SO_2), sulphur trioxide (SO_3), and nitrogen oxide (NO_x) are compounds of which the effects must be examined. Unfortunately, the actual concentrations of sulphur dioxide (SO_2), sulphur trioxide (SO_3), and nitrogen dioxide (NO_2) dissolved into aqueous solution are difficult to measure; therefore, within this work, sulphurous acid (H_2SO_3), sulphuric acid (H_2SO_4), and nitric acid (HNO_3) were used to represent the solubility of sulphur dioxide (SO_2), sulphur trioxide (SO_3), and nitrogen dioxide (NO_2) in aqueous solutions, respectively. Moreover, what has been seen in the IMC Chemicals Facility in Trona, CA, USA, where a CO_2 capture process from flue gas has been operated since 1978, is that anions, especially chloride ion (Cl^-), which are

frequently found to originate from coal, are presented in significant amounts in both lean MEA and in the reclaimer bottom, as shown in Table 1.6 (Strazisar et al., 2003). Thus, the presence of chloride ion (Cl^-) also needed to be taken into consideration in terms of its effect on both material corrosion and solvent degradation. Chloride exists within coal in different forms, such as neutral salts, inorganic compounds, or acid substances. Based on the data provided in Table 1.6, the sources of chloride within a flue gas were represented by sodium chloride (NaCl), ferrous chloride ($FeCl_2$), and hydrochloric acid (HCl) as a commonly found neutral salt, an inorganic compound, and an acid compound, respectively. In summary, the effects of different types of chlorides (NaCl, $FeCl_2$, HCl), sulphurous acid (H_2SO_3), sulphuric acid (H_2SO_4), and nitric acid (HNO_3) on both corrosion and solvent degradation in MEA-based CO_2 capture from simulated post-combustion coal-fired flue gas were comprehensively studied in order to understand the influence of each compound on either of these processes. Moreover, sodium bisulfite ($NaHSO_3$), sodium sulfite (Na_2SO_3), sodium sulphate (Na_2SO_4), and ferrous sulphate heptahydrate ($FeSO_4 \cdot 7H_2O$) were also selected in the study of material corrosion. In addition, all the systems simulated to practical environments by introducing carbon dioxide (CO_2) and oxygen (O_2), as well as maintaining the appropriate process temperature, to ensure they are as relevant as possible to industry.

Lastly, once the understanding of material corrosion and solvent degradation in the MEA-based CO_2 capture process had been well-established in the initial studies, inhibition studies for the purpose of finding means of minimizing damage caused by degraded solvent and material corrosion were then performed in both corrosion and solvent deg-

radation processes, where the inhibition studies were done by introducing inhibitors. At the conclusion of these studies, an “ultimate” inhibitor that was able to prevent material corrosion while at the same time inhibiting MEA degradation is obtained.

Table 1.5: Typical flue gas composition. (Chakma, 1995)

Composition	Concentration (%mole)
CO_2	7-15
O_2	2-12
N_2	65-75
H_2O	5-15
SO_2	2-400 ppm
SO_3	1-10 ppm
NO_x	1- 400 ppm

* Concentrations were analysed after SO_2 scrubbing

* ppm = mg/l

Table 1.6: Ion concentration (ppm) presented in IMC Chemicals Facility in Trona, CA, USA. (Strazisar et al., 2003)

Ions	Ion concentrations (ppm)	
	Lean MEA	**Reclaimer bottom**
	Cations	
Sodium	80	821
Potassium	2.2	18
Calcium	1.1	1.3
Iron	1.4	1.1
Copper	0.2	0.1
Zinc	0.3	0.2
	Anions	
Fluoride	300	1500
Chloride	1600	49000
Bromide	0.9	80
Sulphate	2200	250
Nitrate	290	3100
Nitrite	130	N/A
Phosphate	7.8	230

CHAPTER TWO

CORROSION IN MEA-BASED CO_2 CAPTURE PROCESS

2.1 Background to corrosion

Corrosion is one of the major problems found within the CO_2 capture process in amine-treated plants. It severely damages plant utilities such as the absorber, stripper, trays, pipelines, and valves and results in reduction of the process efficiency, as well as induces unnecessary maintenance costs. Since this research is focused on the CO_2 capture from simulated post-combustion coal-fired flue gas by absorption with MEA solvent, the information on corrosion mechanisms, corrosion kinetics, and corrosion prevention within the CO_2 capture process using aqueous MEA solution should be well established.

Firstly, the questions of what corrosion is and what types of corrosion can be observed in typical MEA-treatment plants should be answered. Corrosion can be described as "an attack on a metallic material by reaction with its environment" (Roberge, 1999). Even though corrosion can also occur on non-metallic materials, this research mainly is focused on corrosion of metallic-based substances, to be specific, low carbon steel 1020, which is normally used as a capture plant's construction material. Corrosion of metallic materials can be divided into three main categories (Bardal, 2003). First is wet corrosion, whereby the corrosive environment is an aqueous solution with dissolved species. The solution is considered as an electrolyte when the process is typically electrochemical. Second is corrosion in other fluids such as fused salts or molten metals. Lastly is dry corro-

sion, wherein the corrosive environment is a dry gas. Dry corrosion is also frequently called chemical corrosion, and the best-known example is high-temperature corrosion. Since this work focused on metal corrosion occurring in a CO_2 capture process operated with MEA solution, wet corrosion is the only type of corrosion that is emphasized.

In general, six types of corrosion can be observed (Jones, 1996; Roberge, 1999; Veawab, 2000; Bardal, 2003). First is uniform corrosion, which occurs evenly over the entire surface area or a large fraction of the total area. Uniform corrosion is easy to predict, detect, and measure. Significant failure due to this type of corrosion is rarely observed (Veawab, 2000). Second is pitting corrosion, which is usually found in aggressive operating conditions or in dead zones where species can stagnantly accumulate (Jones, 1996). Pitting corrosion causes more severe outcomes than uniform corrosion because it is difficult to predict, detect, or prevent in design. A small narrow pit with minimal overall metal loss can lead to failure of an entire engineering system (Roberge, 1999). The third type of corrosion is galvanic corrosion, also called "dissimilar metal corrosion". It refers to corrosion that occurs when two dissimilar materials are in contact in a corrosive electrolyte. One metal is considered noble and the other is more active in terms of how strongly its ions are bound to the surface. The noble metal tends to gain electrons from the active one, while the electrolyte behaves as a media for ions flow. As a result, the active metal will corrode, while corrosion is prevented in the noble metal (Bardal, 2003). The fourth type is erosion corrosion, which is corrosion accelerated by the flow of the corrosive fluid on a metal surface (Roberge, 1999). The fifth type is stress corrosion or cracking, which is characterized by a crack induced by a combination of tensile stress and

exposure to a corrosive environment (Veawab, 2000). Lastly is inter-granular corrosion. Since the micro-structures of metals are made up of grains, inter-granular corrosion is usually found along the grain boundaries or immediately adjacent to the grain boundaries, while the bulk of the grains remain largely unaffected. This type of corrosion is typically caused by improper heat treatment or welding techniques (Veawab, 2000).

2.2 Corrosion mechanism

Corrosion occurs through electrochemical reactions at the interface between the metal and electrolyte. The process is described sequentially when the oxidizing agents, which are species that are able to take up electrons, move from bulk solution to the metal-solution interface. Then, electrochemical reactions occur through electron transfer where the metal is oxidized and loses its electrons to the oxidizing agents. In other words, the electrons released by the metal are consumed by the oxidizing agents. In addition, the reaction wherein the metal loses its electrons to the oxidizing agents is called an "oxidation reaction" and might also be referred to as an "anodic reaction." In contrast, reactions wherein the oxidizing agents gain electrons released from the metal are called "reduction reactions" and are generally referred as "cathodic reactions." A simplified corrosion process of iron, which is a metallic material, and water, which is a corrosive environment, is presented in Figure 2.1.

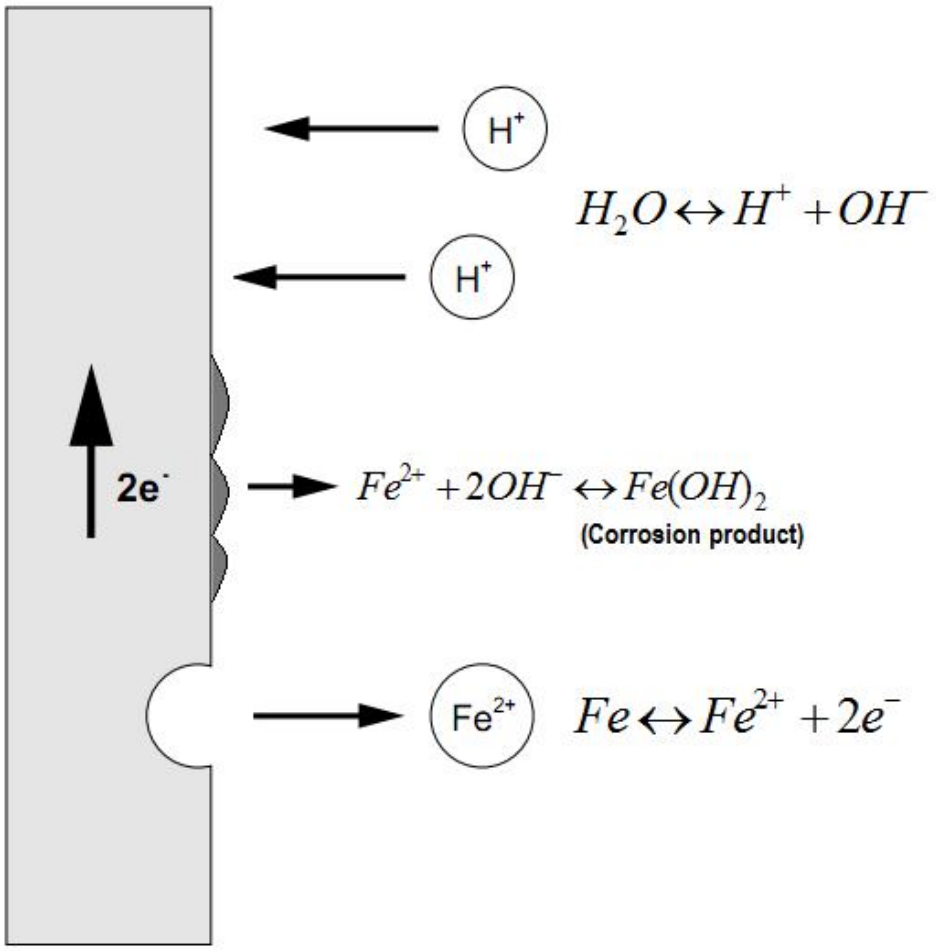

Figure 2.1: A simplified corrosion process involving iron and water.

The corrosion mechanisms in systems containing O_2, CO_2, MEA, and water on carbon steel have been purposed. They consist of a number of oxidation reactions and reduction reactions as presented through equations 2.1 to 2.12 (Veawab and Aroonwilas, 2002).

Dissociation of water:

$$2H_2O \leftrightarrow OH^- + H_3O^+ \tag{2.1}$$

Hydrolysis of carbon dioxide:

$$2H_2O + CO_2 \leftrightarrow H_3O^+ + HCO_3^- \tag{2.2}$$

Dissociation of bicarbonate ion:

$$H_2O + HCO_3^- \leftrightarrow H_3O^+ + CO_3^{2-} \tag{2.3}$$

Dissociation of protonated amine:

$$RNH_3^+ + H_2O \leftrightarrow RNH_2 + H_3O^+ \tag{2.4}$$

Carbamate reversion:

$$RNHCOO^- + H_2O \leftrightarrow RNH_2 + HCO_3^- \tag{2.5}$$

Iron dissolution:

$$Fe \leftrightarrow Fe^{2+} + 2e^- \tag{2.6}$$

Reduction of hydronium ion:

$$2H_3O^+ + 2e^- \leftrightarrow 2H_2O + H_2 \tag{2.7}$$

Reduction of bicarbonate ion:

$$2HCO_3^- + 2e^- \leftrightarrow 2CO_3^{2-} + H_2 \tag{2.8}$$

Reduction of undissociated water:

$$2H_2O + 2e^- \leftrightarrow 2OH^- + H_2 \quad (2.9)$$

Reduction of dissolved O_2:

$$O_2 + 2H_2O + 4e^- \leftrightarrow 4OH^- \quad (2.10)$$

Formation of ferrous hydroxide:

$$Fe^{2+} + 2OH^- \rightarrow Fe(OH)_2 \quad (2.11)$$

Formation of ferrous carbonate:

$$Fe^{2+} + CO_3^{2-} \rightarrow FeCO_3 \quad (2.12)$$

Since ferrous hydroxide ($Fe(OH)_2$), which is one of the corrosion products, is not stable, when it is exposed to O_2 and water, it is oxidized to a trivalent hydrated ferric oxide ($Fe_2O_3 \cdot nH_2O$) or ferric hydroxide ($Fe(OH)_3$), which may be expressed as hydrated ferric oxide ($FeOOH \cdot H_2O$). If exposure to oxygen is strongly limited, iron (II,III) oxide (Fe_3O_4) is potentially formed instead of the trivalent corrosion products (Soosaiprakasam and Veawab, 2008). The formation of an oxide layer usually acts as a protective film covering a metal surface in order to prevent it from further surface reactions is called passivation.

Formation of iron (II,III) oxide or magnetite (Fe_3O_4):

$$3Fe + 4H_2O \rightarrow Fe_3O_4 + 4H_2 \quad (2.13)$$

Formation of ferric oxide or hematite (Fe_2O_3):

$$2Fe_3O_4 + H_2O \rightarrow 3Fe_2O_3 + H_2 \quad (2.14)$$

Another mechanism of carbon steel corrosion in CO_2-containing aqueous solution was reported by Li et al., (2007). Hydrogen ion (H^+) reduction predominantly induced corrosion, especially at a low pH range, because of its high concentration. Hydrogen ion also indirectly assisted the reduction of bicarbonate (HCO_3^-) and carbonic acid (H_2CO_3) because these reactions are preferable in a low pH range. On the other hand, when the pH of the solution increased, the reduction of water began to dominate as the major cathodic reaction. In contrast, the anodic reaction was mainly the dissolution of iron regardless of the pH of the solution. The cathodic and anodic reactions are summarized as the equations presented below.

Anodic reactions:

$$Fe \leftrightarrow Fe^{2+} + 2e^- \tag{2.6}$$

Cathodic reactions:

$$2H^+ + 2e^- \leftrightarrow H_2 \tag{2.15}$$

$$2H_2CO_3 + 2e^- \leftrightarrow 2HCO_3^- + H_2 \tag{2.16}$$

$$2HCO_3^- + 2e^- \leftrightarrow 2CO_3^{2-} + H_2 \tag{2.8}$$

$$2H_2O + 2e^- \leftrightarrow 2OH^- + H_2 \tag{2.9}$$

Formation of ferrous carbonate:

$$Fe^{2+} + CO_3^{2-} \rightarrow FeCO_3 \tag{2.12}$$

$$Fe(HCO_3)_2 \leftrightarrow FeCO_3 + CO_2 + H_2O \tag{2.17}$$

Formation of ferrous bicarbonate:

$$Fe + 2HCO_3^- \rightarrow Fe(HCO_3)_2 \quad (2.18)$$

Banas' et al., (2007) also reported that the main causes of corrosion in iron alloys were the presence of dissolved carbon dioxide (CO_2) and dissolved hydrogen sulphide (H_2S). When CO_2 dissolved in water at isothermal conditions, it resulted in an equilibrium system between water, hydronium ions (H_3O^+), bicarbonate (HCO_3^-), and carbonate (CO_3^{2-}), as illustrated in equations 2.2 and 2.3, in which the hydronium ion can be used to determine the pH of the solution. The anodic reaction was mainly iron dissolution, while the cathodic reactions were the reduction of hydronium ion (H_3O^+), bicarbonate ion (HCO_3^-), and undissociated water (H_2O). In addition, the formation of ferrous carbonate ($FeCO_3$), which is a corrosion product, possibly occurred through several mechanisms, as shown in equations 2.19 and 2.20. Although ferrous carbonate has considerably low solubility in water, in a high pH solution, ferrous carbonate film can be dissolved with the help of bicarbonate ions, resulting in a soluble ferrous-complex compound, as presented in equation 2.21.

Formation of ferrous carbonate:

$$Fe(OH)_2 + H_2CO_3 \rightarrow FeCO_3 + 2H_2O \quad (2.19)$$

$$Fe(OH)_2 + HCO_3^- + H^+ \rightarrow FeCO_3 + 2H_2O \quad (2.20)$$

Formation of soluble ferrous-complex compound:

$$FeCO_3 + HCO_3^- \rightarrow Fe(CO_3)_2^{2-} + H^+ \quad (2.21)$$

Moreover, the formation of other corrosion products was also identified, as presented through equations 2.22 to 2.24.

Formation of ferrous hydroxide:

$$Fe + 2H_2O \rightarrow Fe(OH)_2 + 2H^+ + 2e^- \quad (2.22)$$

Formation of ferrous oxide (FeO):

$$Fe + H_2O \rightarrow FeO + 2H^+ + 2e^- \quad (2.23)$$

Formation of iron (II,III) oxide or magnetite (Fe_3O_4):

$$3FeO + H_2O \rightarrow Fe_3O_4 + 2H^+ + 2e^- \quad (2.24)$$

2.3 Corrosion kinetics

Several techniques have been used to determine corrosion rate. Examples include the weight loss technique, thickness reduction, and electrochemical method (Bardal, 2003). Weight loss technique was commonly used in early studies because it directly quantifies corrosion by weighing a specimen before and after it has been exposed to a corrosion medium. Thickness reduction is widely used as the measurement of most practical significance of corrosion in terms of thickness reduction per unit times, such as, for example, millimetres per year (mm/year), mils (mili-inches) per year (mpy), or inches per year (ipy). Due to corrosion occurring through electrochemical reactions, the electrochemical technique is ideal for the study of the corrosion process. Therefore, corrosion rate determined by electrochemical technique is an effective approach for determining the

corrosion kinetics. In addition, the electrochemical technique is much less time consuming compared to the weight loss or thickness reduction.

2.3.1 Determination of the corrosion rate by using electrochemical technique

Corrosion rate is a rate determined by measuring the state of equilibrium of the opposing electrochemical reactions, the anodic reaction and the cathodic reaction. When these two reactions are in equilibrium, the flow of electrons from each reaction is balanced, or in other words, it is equal to zero (Bardal, 2003). The corrosion rate can be determined by using a Tafel plot, which is a plot between the potential versus the logarithm of the electrical current (Kladkaew et al., 2009), as presented in Figure 2.2. The plot between applied voltage and electrical current, which is driven by a potential difference from its corrosion potential, is generally called a polarization plot. The theoretical current for the anodic and cathodic reactions are shown as dotted lines, while the solid lines are the total current, which is the sum of the anodic and cathodic currents, or the actual current, which is measured when measuring the potential of the metal using a potentiostat (an electronic device used for controlling the potential of a working electrode). The sharp point in the curve is the point where the current changes sign as the reaction changes from the anodic (upper line) to cathodic region (lower line). It is also the point where electrons released form the anodic reaction equal the electrons consumed by the cathodic reaction. In other words, it is the point where the system reaches its equilibrium and the corrosion process actually occurs. The intersection of the currents between the anodic and cathodic Tafel regions is determined by extrapolation, where the current at the intersec-

tion is referred as the corrosion current (i_{corr}) and the potential at the intersection is referred to as the corrosion potential (E_{corr}). Consequently, a corrosion rate can be calculated by using the corrosion current (i_{corr}) that is obtained from the Tafel plot, as presented in equation 2.25 (Bardal, 2003), which it can also be rearranged by combining i_{corr}/A to be I_{CORR} or the so-called corrosion current density.

$$\text{Corrosion rate (mpy)} = \frac{0.13 \cdot i_{corr} \cdot (EW)}{A \cdot d} \qquad (2.25)$$

where: mpy is milli-inches per year

i_{corr} is a corrosion current (μA; microampere)

EW is the equivalent weight of a corrosion specimen (g)

A is the surface area of the corrosion specimen (cm^2)

d is the density of the corrosion specimen (g/cm^3)

0.13 is a constant derived from Faraday's constant (C^{-1}; coulomb)

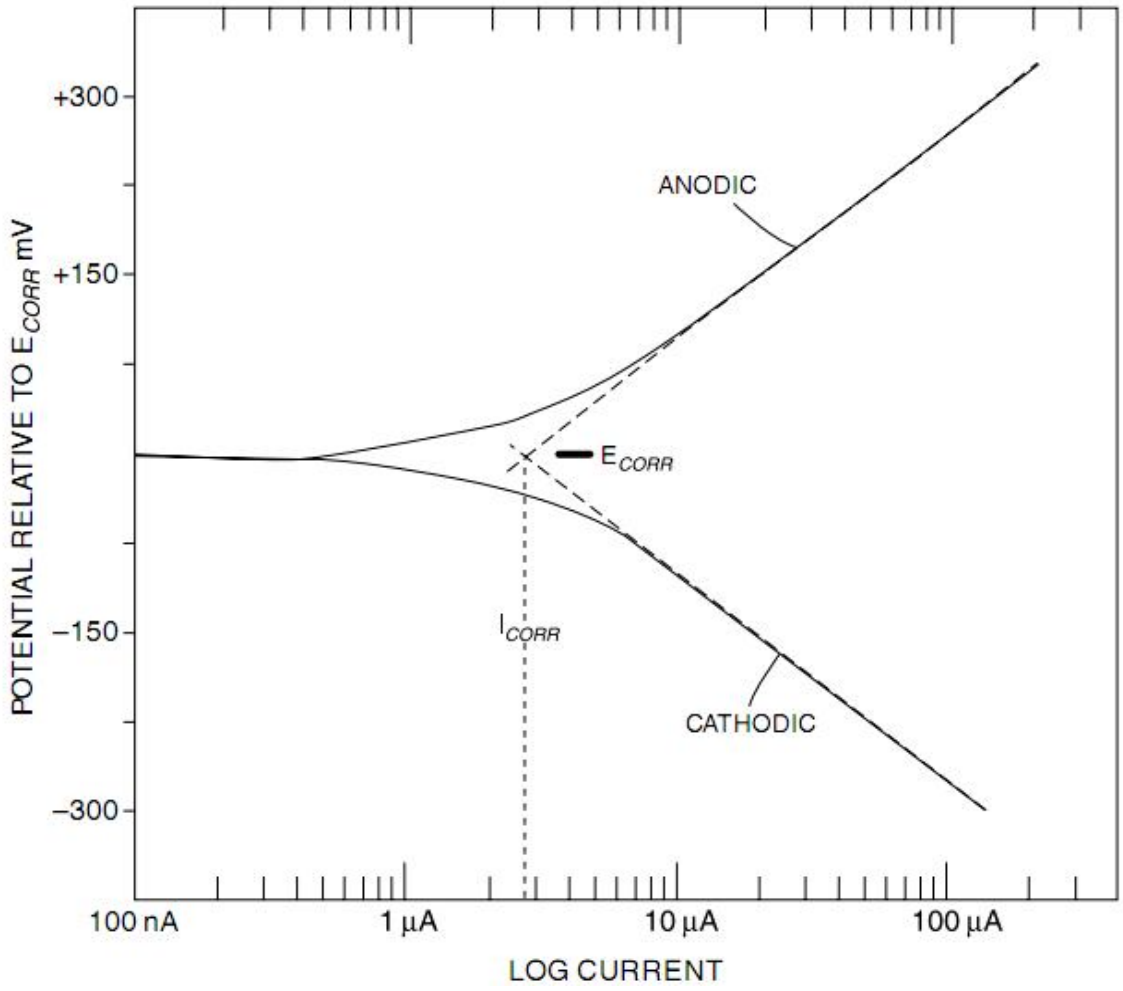

Figure 2.2: Tafel plot. (Bardal, 2003)

2.3.2 Corrosion kinetics in typical MEA-based CO_2 capture process

In the simplified MEA-based CO_2 capture process where a system contains mainly MEA, H_2O, CO_2, and O_2, the effects of concentration of MEA, CO_2, O_2, and the solution temperature on the kinetics of carbon steel corrosion were studied by a number of researchers (Veawab, 2000; Soosaiprakasam and Veawab, 2008; and Kladkaew et al., 2009).

Corrosion rate potentially increased with increasing MEA concentration in which it was more pronounced in the anodic polarization region as indicated from the anodic potential shifting to a more positive value with increasing amine concentration (Veawab, 2000). Passivation, a protective layer of corrosion products, mainly iron oxides, was also found to be weakened as the amine concentration increased, as indicated from the passive current density shifting to a higher value (Kladkaew et al., 2009). Another potential cause of the increase of corrosion rate with increasing MEA concentration was the increase of bicarbonate ions (HCO_3^-). Due to a greater amount of MEA being available to chemically react with CO_2, bicarbonate ion production increased, and the bicarbonate ion is well known to be one of the dominant species in reduction reactions (Soosaiprakasam and Veawab, 2008).

CO_2 loading caused the surface concentration of bicarbonate ions (HCO_3^-) and hydronium ions (H_3O^+) to rise, which led to an increase in the reduction reactions (Soosaiprakasam and Veawab, 2008). Greater CO_2 loading resulted in lower solution pH,

which was a consequence of an increase in hydrogen ion (H^+) concentration. Some results reported that an increase of CO_2 loading mainly affected the cathodic polarization in that it shifted to a greater value when CO_2 concentration increased (Veawab, 2000). On the other hand, some results illustrated that CO_2 loading caused significant effects on both anodic and cathodic polarizations (Kladkaew et al., 2009). In addition, the passivation was weakened as the CO_2 loading increased, as indicated from the shift of the passivation current density to a more positive value (Kladkaew et al., 2009).

Increased dissolved O_2 concentration in a solution led to a higher corrosion rates. It induced an additional reduction reaction of dissolved O_2, which helped accelerate the corrosion process. The additional reaction caused by dissolved O_2 was evidenced by a significant change in the cathodic polarization slope (Kladkaew et al., 2009). By contrast, no significant difference was seen in the slope of the anodic polarization region. Unlike the results that have been discussed so far, the passive region appeared to be stronger in the system containing dissolved O_2 compared to non-dissolved O_2 systems, which was indicated from the shift of the passivation current density to a negative value as the dissolved O_2 concentration increased. This might be because the passive film of iron oxides established on the metal surface was strengthened in the presence of dissolved O_2 due to the fact that the film included species produced by O_2 reduction reactions (Kladkaew et al., 2009).

Corrosion rate appears to obey the Arrhenius equation (Veawab, 2000). Solution temperature changed both anodic and cathodic polarization curves toward the positive

directions, which means that the corrosion rate increased with increasing solution temperature as a power function. One explanation for this is that the pH of the solution was greater at a lower temperature than at a higher temperature. The alkalinity could partly contribute to the lower iron dissolution rate at a lower temperature (Soosaiprakasam and Veawab, 2008). In other words, a higher temperature led to the production of greater amounts of hydrogen ion (H^+), which accelerated the metal corrosion. The passive current density indicated greater passive film protection at lower temperatures. However, some results showed that the passive film at higher temperatures appeared to be more stable than at lower temperatures (Kladkaew et al., 2009). In addition, the difference in anodic Tafel slopes between low and high temperatures suggested different mechanisms of iron dissolution for each temperature range.

The effects of three oxidizing agents, hydronium/hydrogen ions (H_3O^+/H^+), bicarbonate ions (HCO_3^-), and water (H_2O) on the corrosion rate of carbon steel in systems containing various conditions of 1 to 5M MEA, 0 to 0.4 CO_2 loading, and at 30 to 80°C (303 to 353K) were simulated using the FORTRAN-90 program in comparison with the experimental data (Veawab and Aroonwilas, 2002). The best simulation illustrated that the reduction reactions caused by hydronium/hydrogen ions played an insignificant role in inducing carbon steel corrosion due to their low concentration in alkaline systems. On the other hand, although the reduction reaction of water at a metal–solution interface illustrated an extremely low rate, because of its high concentration in the systems, water was shown to be a primary contributor to the carbon steel corrosion. The concentration of bicarbonate ions in the system was much lower compared to water. However, the rate

constant of the reduction reaction of bicarbonate was relatively high, which led to the conclusion that the bicarbonate ion was another primary contributor to the corrosion process in MEA-based systems. In addition, Zhang et al., (2006) investigated the effect of bicarbonate ion concentration on CO_2 corrosion in oil and gas fields under high pressure and high temperature, and the results illustrate that the corrosion rate of steel X65 appeared to decrease with increased bicarbonate ion concentration while pH of the solution increased.

2.4 Corrosion prevention

2.4.1 Brief background of corrosion prevention

There are many ways to prevent corrosion, including, for example, appropriate material selection, suitable design, change of process environment, and application of coating (Bardal, 2003). The choice between these possibilities is usually based on economic considerations. However, material selection, process design, and application of coating are not discussed in this work, since they need to be considered at the beginning of the planning stage. Therefore, a change of process environment is a more appropriate approach to addressing a corrosion problem in a process that is already operating.

One way to change a process environment to prevent material corrosion with minimum interference in the original process operation is to introduce a corrosion inhibitor, which is a chemical compound added to a solution to decrease the corrosion rate. Corro-

sion inhibitors can be classified through several categories. One is by their chemical nature, which categorizes them as either organic inhibitors or inorganic inhibitors. Organic inhibitors are, for example, amines, aldehydes, and carboxylic acids, while inorganic inhibitors are usually crystalized salts of heavy metals. Moreover, typical corrosion inhibitors can prevent corrosion in three different ways (Veawab, 2000):

I. The inhibitor induces formation of corrosion products, which form on the metal surface and behave as a physical barrier to prevent surface reactions.
II. The inhibitor adsorbs as a thin film onto the metal surface and covers the surface in order to prevent it from participating in the surface reactions.
III. The inhibitor prevents corrosion by reacting with the oxidizing agents.

2.4.2 Corrosion inhibitors

Inorganic inhibitors are more popularly used as corrosion inhibitors in the petroleum and petrochemical industries than the organic ones, due to the fact that they usually provide higher inhibition performance (Veawab, 2000). Among inorganic inhibitors, heavy metal-based inhibitors, for example, chromate, cerate, molybdate, borate, vanadate, copper, and cobalt compounds, provide excellent inhibition efficiencies, since they normally induce the formation of dense-insoluble oxide barriers of corrosion products on the metal surface that prevent the surface from participating in further corrosion reactions. However, due to environmental concerns, the use of some of these heavy metal inhibitors is strongly limited, especially the chromates, which have high levels of toxicity due to their carcinogenic effects. Therefore, chromates have been prohibited according to the

Clean Water Act, the Comprehensive Environmental Response, Compensation and Liability Act (CRCLA), and Toxic Substances Control Act (TSCA) (Cook et al., 2005). Therefore, the vanadium compounds, particularly sodium metavanadate ($NaVO_3$), are the most widely used as a corrosion inhibitors in MEA-treating plants, since they have less toxicity compared to chromate compounds (Antonijevic and Petrovic, 2008). Nevertheless, heavy metal-based corrosion inhibitors are not suitable to use in this work, since this thesis is focused on minimizing carbon steel corrosion at the same time as inhibiting oxidative MEA degradation, and heavy metals appear to tremendously accelerate the solvent degradation process (Goff and Rochelle, 2004).

Organic inhibitors normally prevent corrosion by adsorption onto a metal surface and behave as a protective film, where the effectiveness of the organic film layer depends strongly on chemical composition, molecular structure, and affinity for the metal surface. Due to the fact that film formation is an adsorption process, temperature and inhibitor concentration are essential parameters, as the strength of the adsorption bond is also a dominant factor determining the performance of soluble organic inhibitors. The most widely used organic inhibitors for corrosion in the petroleum and petrochemical industries are nitrogen-containing compounds, such as, for example, amines, amides, quaternary ammonium salts. A number of researchers had studied the effects of various amine-based inhibitors on the corrosion process in the presence of carbon dioxide (CO_2). Some organic inhibitors were selected, due to their low toxicities, in one study of inhibitor performance within MEA-based CO_2-saturated systems (Veawab, 2000). Six of the selected inhibitors were amines with different nitrogen functional groups, while the other two

were carboxylic acid and sulfoxide compounds. The results illustrated that the inhibition performances varied from 75 to 92%, depending on the type of inhibitor. Carboxylic acid illustrated the best inhibition performance, followed by sulfoxide, and long-chain aliphatic amines, respectively. The inhibiting efficiency apparently depended on concentration in that a higher concentration led to greater inhibition performance. Moreover, solution temperature also significantly affected the performance of inhibitors in that increasing temperature improved inhibiting efficiency. Another research group showed that thiourea proved to be a superior inhibitor to prevent steel (X70) corrosion when compared to the typical amines in the presence of an acid medium (He et al., 2008). The inhibiting performance of thiourea on X70 steel in saline solution containing CO_2 was investigated, and the study showed that thiourea was an excellent corrosion inhibitor in saline solution containing saturated CO_2. Currently, there are many amine-based corrosion inhibitors commercially available. One of the well-known compounds is imidazoline and its derivatives. Thus, imidazoline-based inhibitors were popularly studied in terms of their performance in corrosion prevention. Lopez et al., (2004) studied the morphology of the corrosion products caused by three different imidazoline-based inhibitors (aminopropylimidazol; API, PC, and QB) in a chloride medium containing saturated CO_2 at pH 4 and a temperature of 40°C. The results showed that imidazoline-based inhibitors were suitable to use in for corrosion prevention of carbon steel. However, the inhibition behaviours varied, depending on the inhibitor structures. API and PC helped to generate ferrous carbonate ($FeCO_3$), which precipitated as a corrosion product onto the metal surface, while QB tended to adsorb onto the metal-solution interface then behave as a protective barrier to prevent the metal surface from participating in the electrochemical reactions. Paolinelli

et al. (2008) also used a commercial imidazoline-based inhibitor to study corrosion prevention of carbon (C)-manganese (Mn) steel in an environment containing sodium chloride (NaCl) solution with saturated CO_2 at pH 6 and a temperature of 40°C. The results illustrated that a protective film was generated after the inhibitor was added to the system and this eventually led to a decrease in the corrosion rate. Moreover, the inhibition efficiencies of different amine-based inhibitors, mercaptobenzothiazoles, on N80 steel in saturated CO_2 solution at 90°C were also studied by using the weight loss technique (Zhang et al., 2007). The inhibitors (N,N'-bis-(2-thionobenzothiazolin-3-yl-methyl)-n-dodecylamine; BTBMDA and N,N'-bis-(2-thionobenzothiazolin-3-yl-methyl)-n-octadecylamine; BTBMOA) appeared to adsorb onto the metal surface, which helped prevent the metal surface from further attack by oxidizing agents.

By introducing a reducing agent, which is a compound that has a tendency to donate electrons to other compounds or is a so-called "electron donor" and is able to react with the oxidizing agents by supplying its own electron to the oxidizing agents instead of the metal, is another way to reduce the corrosion rate because it leads to less oxidizing agents being available to participate in the electrochemical reactions. Consequently, sodium sulfite (Na_2SO_3), which is one of the well-known reducing agents, was studied in terms of steel corrosion at room temperature (Gouda and Sayed, 1973). It provided excellent inhibition performance with steel corrosion by not only behaving as an oxygen scavenger but also satisfactorily tolerating traces of chloride (Cl^-) and sulphate (SO_4^{2-}) ions present in the solution. However, it should be noted that a reducing agent is usually consumed over a course of time, and therefore, it needs to be continually fed into the system in order to maintain the inhibition performance.

CHAPTER THREE

SOLVENT DEGRADATION IN MEA-BASED CO_2 CAPTURE PROCESS

3.1 Background on MEA degradation

Solvent degradation in carbon dioxide (CO_2) capture is typically a consequence of the presence in post-combustion coal-fired flue gas of approximately 10% carbon dioxide (CO_2), 5 to 10% oxygen (O_2), sulphur dioxide (SO_2), sulphur trioxide (SO_3), nitrogen oxides (NO_x), and other components such as fly ash, resulting in significant solvent loss as well as inducing material corrosion. Generally, alkanolamines are subject to three types of degradation (Chi and Rochelle, 2002), which are discussed in detail below.

First is carbamate polymerization. The formation of carbamate is expected to occur in the reaction between CO_2 and MEA, but several other side reactions can be formed and result in irreversible degradation products. Carbamate polymerization can occur throughout the CO_2 capture system due to the fact that it requires only the presence of CO_2 and MEA. However, it tends to occur at a relatively high temperature. Consequently, it is mostly found in the stripper column, which typically operates at a higher temperature (120°C) compared to the absorber column (55°C), and it produces high molecular weight degradation products. Any amines that form carbamate with CO_2 will be degraded according to carbamate polymerization, so this is encountered in a range of applications, such as natural gas treating, ammonia production, and CO_2 capture from flue gas (Goff and Rochelle, 2006).

Second is oxidative degradation, which requires O_2 and is normally catalyzed by the presence of dissolved metals or other catalysts, such as acid compounds. It produces oxidized fragments of the solvent, such as organic acids and ammonia (NH_3). Oxidative degradation is expected to occur in the presence of dissolved O_2 in the liquid holdup at the bottom of the absorber. Due to the fact that O_2 is not usually present in other types of gas treating plants, oxidative degradation is likely limited to CO_2 capture from flue gas applications.

Third is thermal degradation, which apparently occurs at temperatures higher than 200°C and, therefore, should not be a problem in plants for CO_2 capture from coal-fired flue gas, since the typical operating temperature does not exceed 200°C, even in the re-boiler unit.

This research is focused mainly on MEA-based CO_2 capture from simulated post-combustion coal-fired flue gas where oxidative MEA degradation is primary observed. Therefore, throughout this chapter, oxidative MEA degradation will be mainly discussed, since it is the more predominantly cause of solvent degradation compared to thermal degradation (Lepaumier et al., 2011). Also, it was a much more significant source of solvent loss when compared to carbamate polymerization (Strazisar et al., 2003).

3.2 Oxidative MEA degradation mechanism

The oxidative MEA degradation mechanism has been studied by only a handful of researchers, so there remains room for further investigation. There are three primary reasons why the minimizing of oxidative MEA degradation is so important. First is solvent loss. Due to degradation losses, replacement solvent needs to be introduced into the system in order to maintain the same capture capacity, which eventually leads to additional operating cost. Second, some degradation products are considerably toxic, so proper treatment is mandatory, which induces additional cost for proper handling/disposal of these products. Lastly, material corrosion is often linked with degradation products in that these products usually accelerate the corrosion process, which, once again, induces unnecessary additional maintenance costs (Goff and Rochelle, 2004).

Even though oxidative degradation of MEA is a much more significant source of solvent degradation compared to carbamate polymerization (Strazisar et al., 2003), it would be beneficial to understand the carbamate polymerization mechanism since it is directly associated with carbamate, which is a primary product generated from the reaction between MEA and CO_2. The carbamate polymerization mechanism proposed by Strazisar et al. (2003) illustrated that MEA initially reacted with CO_2 at high temperatures, resulting in the formation of 2-oxazolidone. Then, 2-oxazolidone further reacted with another MEA molecule and formed 1-(2-hy droxyethyl)-2-imidazolidinone and N-(2-hydroxyethyl)-ethylenediamine, respectively, as shown in Figure 3.1.

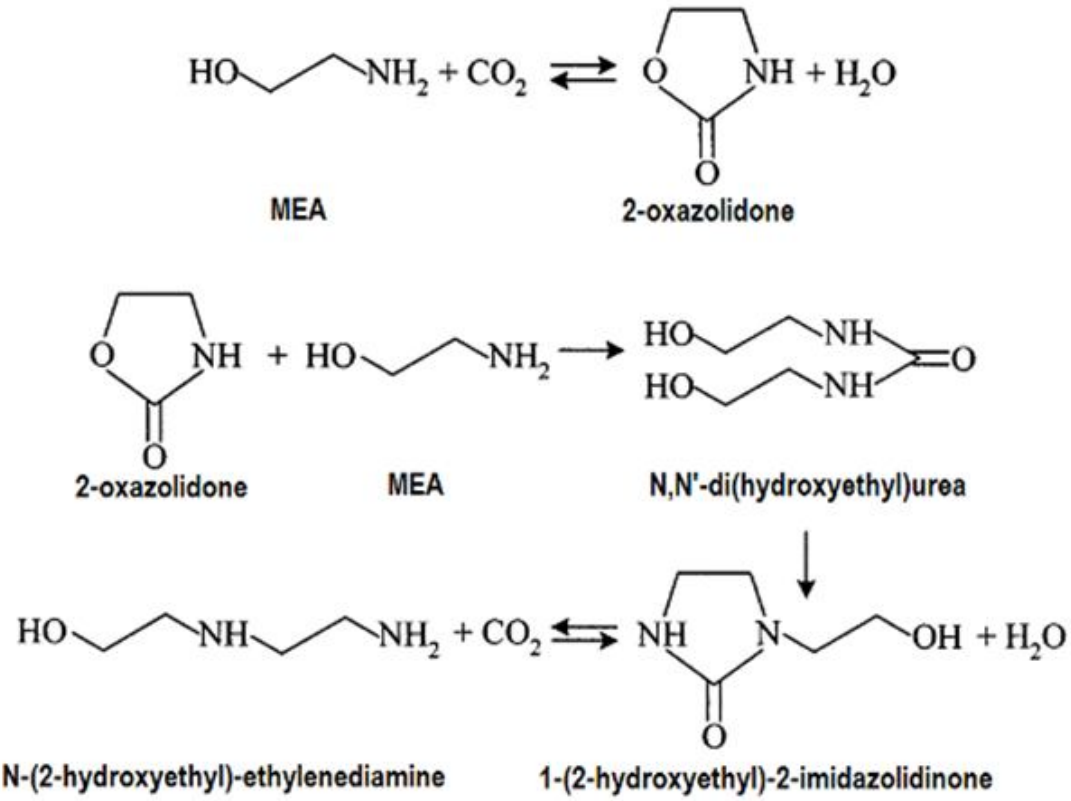

Figure 3.1: Carbamate dimerization of MEA. (Strazisar et al., 2003)

For oxidative MEA degradation, Rooney et al. (1998) proposed a mechanism derived from systems with a presence of O_2, which resulted in the production of carboxylic acids as the final degradation products, as shown in Figure 3.2. These acids potentially reacted with another molecule of MEA, resulting in the formation of heat-stable salts such as acetates, formates, and oxalates. These salts are difficult to regenerate, especially under the typical regenerating conditions in a flue gas treating process. The mechanism began with the MEA molecule decomposing to ammonia and vinyl alcohol, then acetaldehyde was produced, which finally, again, decomposed to acetic acid. Another path was initiated when MEA was degraded to α-amino acetaldehyde, which either reacted with water molecules and generated methylamine and formic acid or decomposed to glycine and produced glycolic acid, glyoxylic acid, and oxalic acid, respectively.

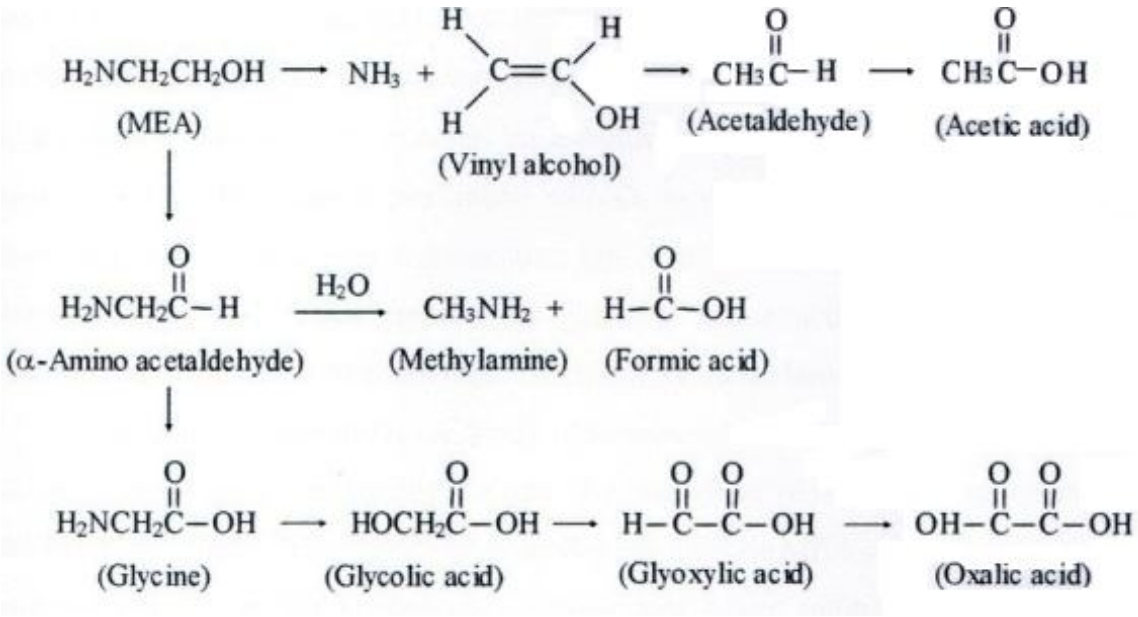

Figure 3.2: Oxidative MEA degradation mechanism. (Rooney et al., 1998)

Strazisar et al., (2003) additionally proposed that acetic acid also reacted with MEA molecules and generated N-acetylethanolamine. In the presence of ferric ions (Fe^{3+}) or hydrogen radicals (·H), N-acetylethanolamine reacted with another MEA molecule to form 2-hydroxyethylamino-N-hydroxyethyl acetamide through a radical mechanism. Then, the acetamide decomposed to a six-member ring by internal elimination of water between the alcohol group and the corresponding amine group to become either 1-hydroxyethyl-2-piperazinone or 4-hydroxyethyl-2-piperizinone, as shown in Figure 3.3.

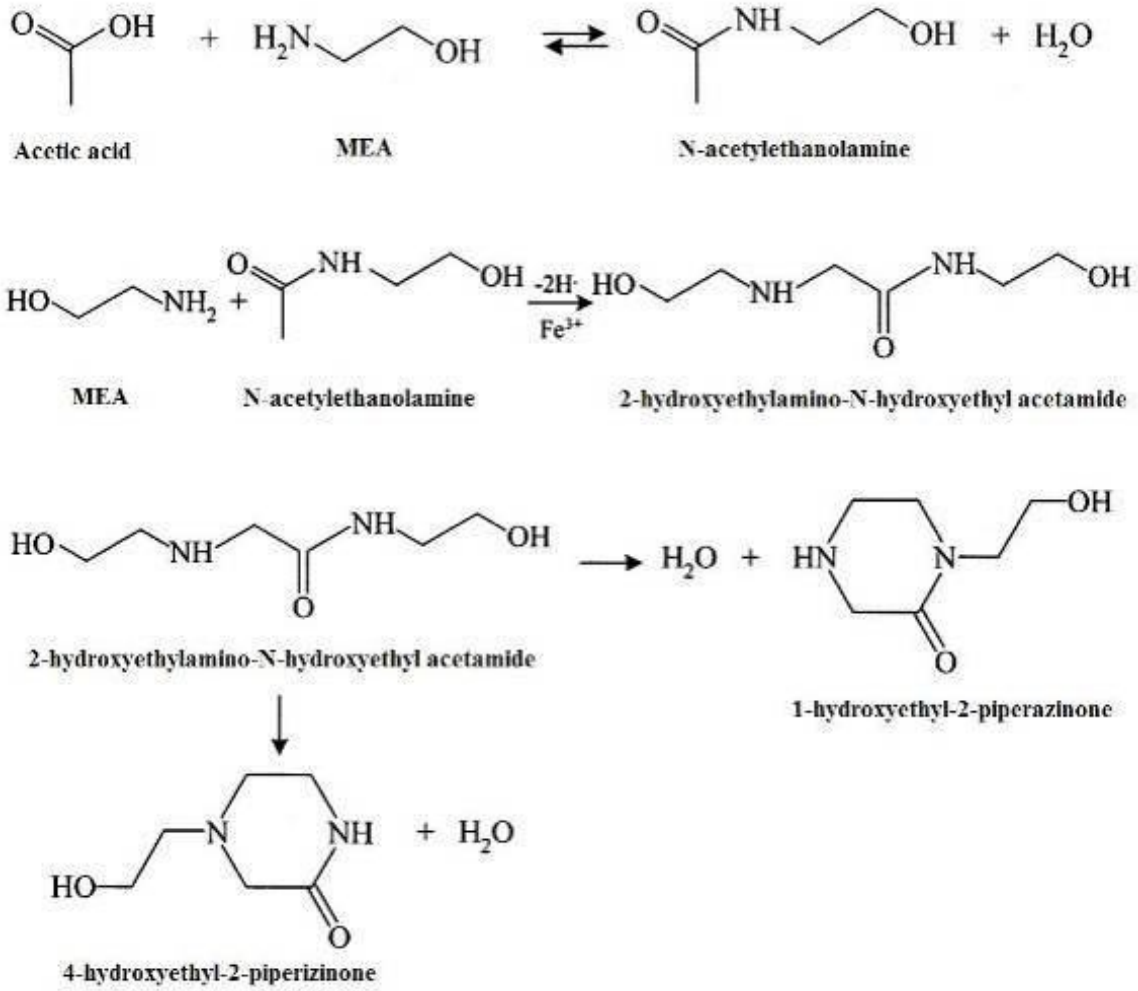

Figure 3.3: Oxidative degradation mechanism through the reaction between MEA and acetic acid. (Strazisar et al., 2003)

There are two additional mechanisms that give the same final degradation products, even though they occurred through different reaction pathways (Goff and Rochelle, 2004; and Chi and Rochelle, 2002). One is the mechanism involving electron abstraction from a lone pair of nitrogen molecules, and the other mechanism involved the abstraction of a hydrogen atom from nitrogen, α-carbon, or β-carbon.

The electron abstraction mechanism is presented in Figure 3.4. MEA decomposed to an aminum radical through a radical-initiated reaction in the presence of ferric ions (Fe^{3+}) or radicals ($R\cdot$), in which a free radical removed an electron from the nitrogen of the amine group. Then, a hydrogen ion (H^{+}) was removed from the aminum radical to produce an imine radical. Next, the imine radical either reacted with O_2 or was decomposed to imine by another free radical. The reaction between the imine radical and O_2 is illustrated within the dashed box in Figure 3.4, where O_2 reacted with the imine radical to form an amino peroxide radical, the peroxide radical then converted into peroxide by reacting with MEA, which finally led to the formation of imine and hydrogen peroxide. On the other hand, formaldehyde and hydroxylacetaldehyde, which each combined with ammonia, were generated through the hydrolysis reaction and the decomposition of imine. The rate limiting step of this mechanism was concluded to be the electron abstraction reaction rather than the hydrogen abstraction step.

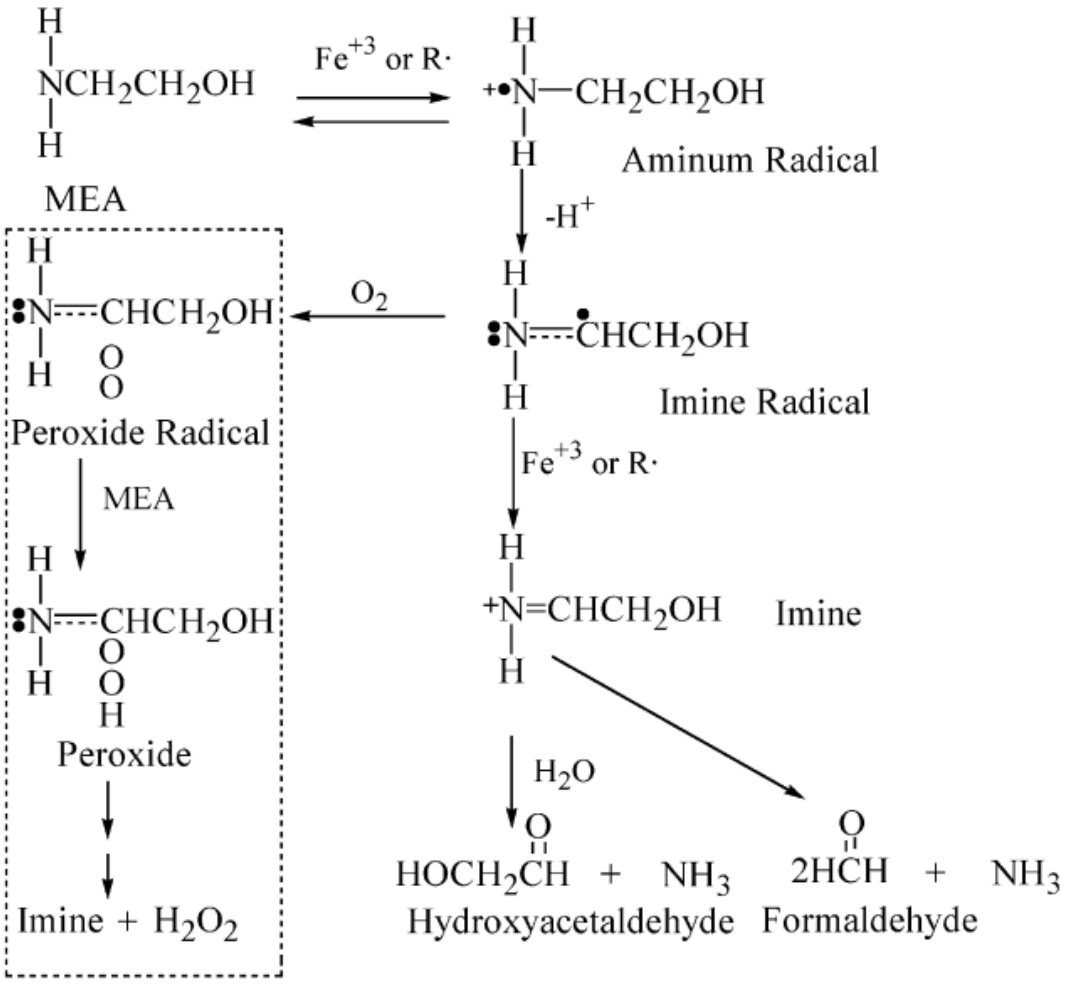

Figure 3.4: Oxidative degradation mechanism through electron abstraction. (Chi and Rochelle, 2002)

The hydrogen abstraction mechanism is presented in Figure 3.5. MEA was degraded by using ionization radiation as an initial step. The radiation generated radicals from the aqueous amine solution, such as hydrogen (H·) and hydroxyl (OH·) radicals. In aqueous solution, MEA decomposed to a five-member cyclic molecule by hydrogen bonding between HN --- O or OH --- N. Free radicals then abstracted a hydrogen atom from the nitrogen, the α-carbon, or the β-carbon. The newly formed amine radical then transferred internally through the ring structure, which ultimately resulted in cleavage of the N --- C bond. The possible degradation products were amines, aldehydes, or aldehyde radicals. Aldehyde radicals acted as an initiator by abstracting hydrogen from a second molecule of MEA, generating an MEA radical and aldehyde. In summary, it was proposed that MEA was more likely to degrade through hydrogen abstraction from one of the carbons than electron abstraction from the nitrogen atom.

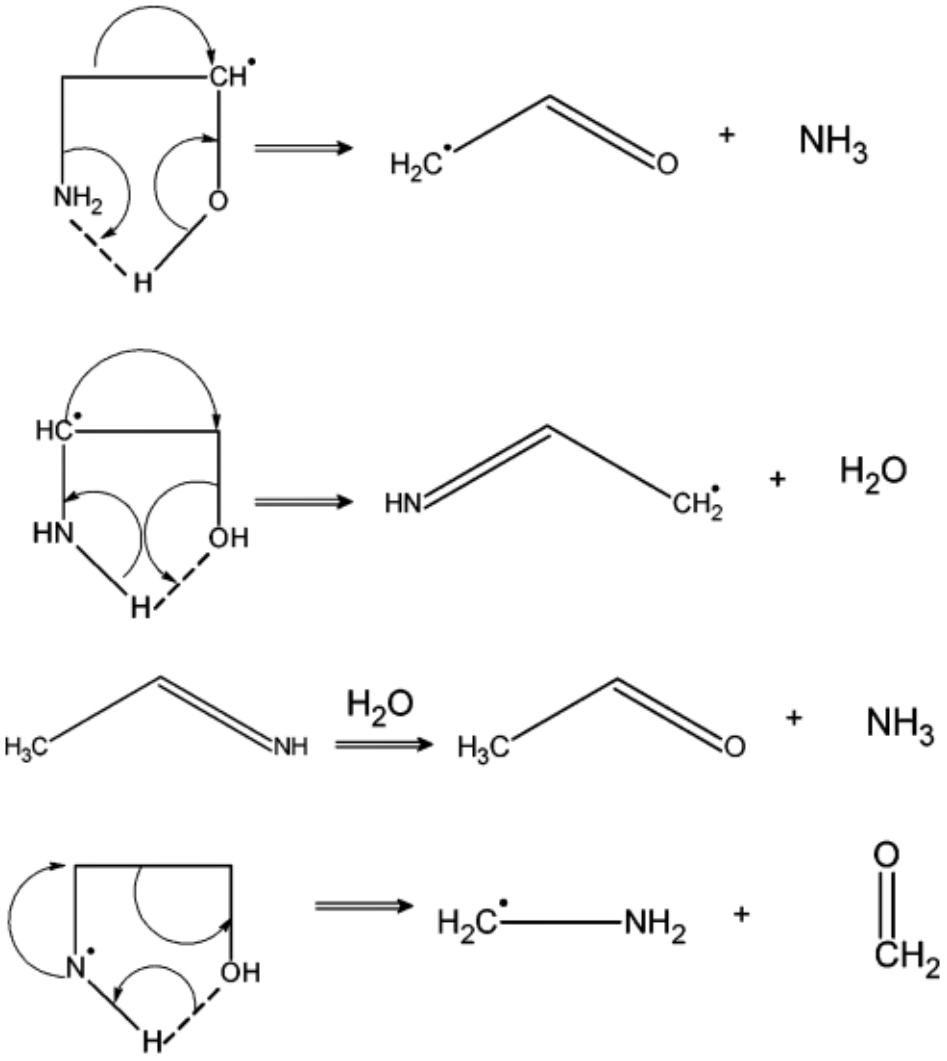

Figure 3.5: Oxidative degradation mechanism through hydrogen abstraction. (Goff and Rochelle, 2004)

3.3 Kinetics of oxidative MEA degradation

Focusing on the reaction of aqueous MEA and O_2, which are the main components in oxidative MEA degradation, it is necessary to understand what physical processes occur and how MEA and O_2 interact. First, O_2 must dissolve into the amine solution so it can react with MEA to form the degradation products. This indicates that the system depends on both the rate of mass transfer of O_2 from a flue gas to the liquid solution, as well as the rate of kinetic interaction of O_2 with MEA. It was reported that MEA concentration played an important role in indicating which physical process was likely to occur; at MEA concentration beyond 7M, mass transfer appeared to be the rate determining step; in contrast, in solutions with MEA concentration below 2M, the rate appeared to be controlled by the kinetics of interaction between MEA and O_2, while solutions of intermediate MEA concentration illustrated the effects of both kinetics and O_2 mass transfer (Goff and Rochelle, 2004).

In typical CO_2 capture systems, amines are normally recycled within the process; and the operating conditions, operation times, and impurities can cause the problem of solvent degradation. Moreover, some of the degradation products possibly reduce the efficiency of CO_2 capture and some might induce serious material corrosion. The oxidative MEA degradation kinetics in systems containing MEA, H_2O, and O_2 at a temperature range between 120 to 170°C were proposed by Supap et al., (2001). The study was conducted in an environment with no presence of CO_2 in order to ensure that the kinetics fully represented the reaction between MEA and O_2. The results illustrated that the rate of

the oxidative MEA degradation was the functions of both MEA and O_2 concentrations. Nevertheless, the kinetic model established that the degradation rate was more sensitive to O_2 concentration than to MEA concentration.

Chi and Rochelle, (2002) studied the kinetics of the oxidative MEA degradation in the presence of iron by measuring the rate of ammonia (NH_3) evolution at CO_2 loading of 0.4 (mol CO_2/mol MEA) and a temperature of 55°C, which is a typical absorber temperature in MEA systems. The results illustrated that the total iron ions (Fe^{2+} and Fe^{3+}), regardless of the oxidation states, had a serious effect on the decomposition of MEA to ammonia. Iron ions with as low of concentration as 1mM increased the decomposition rate by a factor of 5 at 0.4 CO_2 loading. Thus, in order to minimize MEA degradation, iron ion concentration should be kept to less than 0.01mM. However, without the presence of CO_2 and O_2, total iron ions of ferrous ion (Fe^{2+}) and ferric ion (Fe^{3+}) had no effect on the oxidative degradation of MEA. Moreover, a later study of Goff and Rochelle (2004) illustrated that solutions catalyzed by copper ions showed higher degradation rates compared to iron ion-catalyzed solutions. In addition, solutions with lower CO_2 loading (mol CO_2/mol MEA) appeared to degrade faster than solutions with higher CO_2 loading due to the lower O_2 solubility and lower diffusion coefficient, where the accumulation of degradation products did not appear to significantly affect the degradation rate.

Bello and Idem (2006) performed a mechanistic-based kinetic study of oxidative MEA degradation with and without sodium metavanadate ($NaVO_3$), which is a conventional corrosion inhibitor, under experimental conditions of 11.4 and 17.9 mol percent

(%mol) of MEA, 250 and 350 kPa O_2, 0 to 0.44 CO_2 loading (mol CO_2/mol MEA), and temperature of 55 to 120°C. The results showed that the degradation rates increased with increasing MEA concentration, O_2 concentration, sodium metavanadate concentration, and temperature. MEA was more likely to degrade in the presence of O_2 rather than CO_2. In contrast, CO_2 actually slowed down the degradation rate due to it reduced O_2 solubility in the aqueous MEA solution, which resulted in the reduction of degraded MEA. Thus, CO_2 appeared to be a degradation inhibitor, which helped retard MEA decomposition.

In a CO_2 capture process containing MEA, H_2O, CO_2, O_2, and SO_2, not only can O_2 induce MEA degradation, but SO_2 is also able to react with MEA. Kinetic studies of MEA-H_2O-CO_2-O_2-SO_2 systems were done by Uyanga and Idem (2007) and Supap et al. (2009). Both studies consistently concluded that MEA degradation was affected by a number of factors such as temperature and the concentrations of MEA, O_2, CO_2, and SO_2. The degradation rates increased with increasing MEA concentration, O_2 concentration, SO_2 concentration, and temperature. In contrast, CO_2 behaved as a degradation inhibitor in both studies. Moreover, both studies established the correlations of MEA degradation kinetics in which the rate expressions showed that the rates were most sensitive to the presence of SO_2 compared to the presence of MEA, CO_2, or O_2. Uyanga and Idem, (2007) studied systems containing MEA, H_2O, CO_2, O_2, SO_2, and a corrosion inhibitor ($NaVO_3$). The results showed that SO_2 and O_2 strongly induced MEA degradation. Sodium metavanadate also accelerated the MEA degradation process, whereas CO_2 had the opposite effect. It behaved as a degradation inhibitor, which helped to slow down degradation due to the salting-out phenomenon, where dissolved CO_2 inhibited the O_2 and SO_2

solubility, thereby minimizing their effectiveness in MEA degradation. Consequently, it was suggested that lean MEA was more prone to degrade compared to loaded MEA. However, a tremendous corrosive effect due to dissolved CO_2 must be taken into account, since aqueous solution containing CO_2 is well-known to induce severe corrosion. The rate of MEA degradation was also accelerated in the presence of sodium metavanadate, which is known as a corrosion inhibitor, due to sodium metavanadate behaving as a catalyst in the degradation process. Moreover, an increase in temperature resulted in a higher degradation rate; thus, the oxidative MEA degradation in a typical CO_2 capture process would be expected to be greater in the regenerator unit (120°C) than in the absorber (55°C) unit. Lastly, MEA itself caused degradation, as indicated from the fact that the rate of MEA degradation increased with increasing MEA concentration. In summary, the kinetic correlation of oxidative MEA degradation in systems containing MEA, H_2O, CO_2, O_2, and SO_2 was shown in equation 3.31, which was derived in order to compensate for an absence of either O_2 or SO_2.

$$-r_{MEA} = 0.00745 \exp\left(\frac{45258}{RT}\right)[MEA]^{1.9}[CO_2]^{-0.3}([O_2]^{2.8} + [SO_2]^{3.4}) \qquad (3.1)$$

Supap et al. (2009) also proposed a kinetic model of oxidative MEA degradation, as presented in equation 3.2, in which the same trend was found as illustrated by Uyanga and Idem (2007), which was that increasing temperature and concentrations of O_2 and SO_2 accelerated MEA degradation. Increasing CO_2 concentration slowed down the degradation process by reducing the aqueous solubility of O_2 and SO_2 in MEA solution, minimizing intimate contact of O_2 and SO_2 with MEA. The rate model for this study provided an

improvement in that any of the parameters of O_2, SO_2, and CO_2 concentration can be removed without affecting the usability of the model.

$$-r_{MEA} = \frac{\left\{6.74 \times 10^{9} \exp\left(\frac{-29403}{RT}\right)[MEA]^{0.02}([O_2]^{2.91} + [SO_2]^{3.52})\right\}}{(1 + 1.18[CO_2]^{0.18})} \quad (3.2)$$

3.4 Oxidative MEA degradation prevention

Since oxygen (O_2) is a primary contributor to oxidative solvent degradation, there are several options to inhibit the degradation process associated with minimization of oxygen species. First, an oxygen scavenger and/or reaction inhibitor can be introduced to the system to either react with dissolved O_2 or its intermediates, where the scavenger must react faster with O_2 and/or intermediates than the MEA molecule. Second, a chelating agent is added to bind with dissolved metals to prevent them from catalyzing O_2 to the more active species, such as oxygen containing free radicals, which will accelerate the solvent degradation process. Lastly, salting out phenomena is introduced to the system. Due to the fact that gas generally decreases in aqueous solubility as the ionic strength of the solution increases, adding stable salt will reduce O_2 solubility, which eventually leads to the reduction of oxidative solvent degradation (Goff and Rochelle, 2006).

3.4.1 Oxygen scavengers and/or reaction inhibitors

Goff and Rochelle (2006) studied the effects of different types of oxygen scavengers (sodium sulfite; Na_2SO_3, formaldehyde, hydroquinone, and ascorbic acid) and a reaction inhibitor (Inhibitor A) on oxidative MEA degradation in systems containing O_2, CO_2, iron ions, and copper ions. By measuring the amount of ammonia (NH_3) produced in the degradation process, the degradation rate was determined. Inhibitor A is an inorganic compound that proved to effectively inhibit oxidative MEA degradation by behaving as a reaction inhibitor rather than an oxygen scavenger. When the concentration of Inhibitor A increased, the ammonia production decreased in both rich (0.4 mol CO_2/mol MEA) and lean (0.15 mol CO_2/mol MEA) solutions. However, the rich solution showed lower ammonia production when it was added with Inhibitor A, which meant that it was more easily inhibited than the lean one. Since, copper-based and iron-based inhibitors are normally introduced to the CO_2 capture process to prevent corrosion, the presence of copper ions and iron ions needed to be taken in to consideration. The results illustrated that a solution containing dissolved copper showed higher degradation rates than a solution containing dissolved iron, and it was able to be inhibited more easily by Inhibitor A than the solution containing dissolved iron. Inhibitor A appeared to be less effective in a system containing mixed types of ions (iron and copper ions). Nevertheless, Inhibitor A still provided satisfactory inhibiting efficiency by significantly reducing oxidative MEA degradation. Moreover, Inhibitor A was not expected to degrade; thus, it did not need to be continuously fed to the system in order to maintain efficiency.

On the other hand, the major disadvantage of using oxygen scavengers is that they were consumed stoichiometrically over a course of time. Thus, they needed to be constantly fed to the system in order to maintain the inhibition efficiencies, which eventually led to an increase in operating costs. Additionally, they formed oxidized degradation products that accumulated in the system and needed to be disposed. Sodium sulfite (Na_2SO_3) is a known oxygen scavenger. It inhibits oxidative solvent degradation by reacting with O_2 then reduces O_2 concentration in a solution, resulting in the reduction of degradation rates. However, the effective range of sodium sulfite concentration appears to be below 100 mM; whenever concentration was beyond the optimum range, O_2 mass transfer was enhanced, leading to an increase in oxidative MEA degradation. Formaldehyde is considered to be one of the intermediates in oxidative MEA degradation, and it potentially behaves as an oxygen scavenger by reacting with O_2 and thereby reduces the rate of oxidative solvent degradation. Aldehydes are easily oxidized to carboxylic acids and usually end up as heat stable salts, such as, for example, formate, acetate, and glycolate. These were strongly required to be removed from the system due to the fact that they lower the performance of CO_2 capture of MEA solution by binding with MEA molecules, resulting in unreactive MEA for CO_2 absorption. On the other hand, hydroquinone and ascorbic acid behave differently. Although they are both known as oxygen scavengers, they accelerated oxidative MEA degradation because of the formation of radical intermediates. Since, oxidative solvent degradation is normally initiated by free radicals, the presences of radical intermediates will definitely promote the solvent degradation process.

3.4.2 Chelating agents

A chelating agent is a compound that chemically bonds with dissolved metals. An effective chelating agent for oxidation inhibition would result in an inactive metal catalyst. Three types of chelating agents, one organic (ethylene-diamine-tetraacetic acid; EDTA) and two inorganics (trisodium phosphate; Na_3PO_4 and sodium tetrasulfide; Na_2S_4), were studied in terms of their efficiency in oxidative MEA degradation inhibition in the presences of dissolved transition metals (copper and iron). The results illustrated that EDTA was clearly a more effective inhibitor than trisodium phosphate; however, the performance of EDTA declined over the course of time due to the fact that it was consumed as the process proceeded, while trisodium phosphate did not degrade, so it was more stable. Since sodium tetrasulfide is known as compound for precipitating metal ions, it decreased the oxidative degradation rates yet eliminated the corrosion inhibitor due to the fact that most of the corrosion inhibitors were heavy metal-based compounds. Consequently, chelating agents were not suitable inhibitors for oxidative solvent degradation within MEA-based CO_2 capture processes where material corrosion is one of the major problems.

3.4.3 Stable salts

Neutral salts are known to increase the rate constants in reactions involving charged intermediates, however, they also known to increase the ionic strength of a solution and generally decrease gas solubility in the solution. The effects of three stable salts

(potassium chloride; KCl, potassium bromide; KBr, and potassium formate; KCOOH) on the inhibition of oxidative MEA degradation were investigated. Potassium chloride appeared to increase the rates of solvent degradation due to the fact that the increase in kinetics was larger than the decrease in the aqueous solubility of O_2. On the other hand, both potassium formate and potassium bromide led to slight decreases in the degradation rates due to the fact that the reduction of O_2 solubility was dominant over the increase of the kinetics. Nevertheless, potassium formate and potassium bromide were still very weak inhibitors compared to oxygen scavengers and a reaction inhibitor.

CHAPTER FOUR

EXPERIMENTAL APPARATUS AND PROCEDURES

4.1 List of chemicals and gases

A full list of chemicals and gases used in this work along with their purities and suppliers are presented in Table 4.1. A chemical list was combined of the chemicals associated in the studies of the effects of simulated flue gas compositions on carbon steel corrosion and oxidative MEA degradation, the standard chemicals used in the verification of the corrosion and solvent degradation products, the chemicals used in the inhibition study of carbon steel corrosion and oxidative MEA degradation, and the chemicals associated with the analytical techniques. And a gas list was mainly 100% Nitrogen (N_2), 100% Carbon dioxide (CO_2), 6% Oxygen (O_2) balanced with 94% Nitrogen (N_2), and ultra-high purity Helium (He).

Table 4.1: A full list of chemicals and gases.

Chemicals		
Chemical	**Supplier**	**Purity**
Monoethanolamine (MEA)	Fisher chemical, CA	99%wt
Sodium chloride (NaCl)	Sigma-Aldrich, CA	99%wt
Ferrous chloride ($FeCl_2$)	Sigma-Aldrich, CA	98%wt
Hydrochloric acid (HCl)	Fisher chemical, CA	1M
Sodium sulphate (Na_2SO_4)	Sigma-Aldrich, CA	98%wt
Ferrous sulphate heptahydrate ($FeSO_4 \cdot 7H_2O$)	Sigma-Aldrich, CA	99%wt
Sulphuric acid (H_2SO_4)	Fluka	95% - 97% in water
Sulphuric acid (H_2SO_4)	Fluka	1M
Sodium sulfite (Na_2SO_3)	Sigma-Aldrich, CA	98%wt
Sodium bisulfite ($NaHSO_3$)	Sigma-Aldrich, CA	99%wt
Sulphurous acid (H_2SO_3)	Fluka	4.5% - 5.5% in water
Nitric acid (HNO_3)	Sigma-Aldrich, CA	1M
3-methylpyridine (3-$CH_3C_5H_4N$)	Sigma-Aldrich, CA	99%wt
Glycine anhydride ($C_4H_6N_2O_2$)	Sigma-Aldrich, CA	99%wt
N-acetylethanolamine ($CH_3CONHCH_2CH_2OH$)	Sigma-Aldrich, CA	90%wt (Technical grade)
2-oxazolidone ($C_3H_5NO_2$)	Sigma-Aldrich, CA	98%wt
N-methyl caprolactam ($C_7H_{13}NO$)	Sigma-Aldrich, CA	99%wt
1-2-hydroxyethyl-2-imidazolidinone	Sigma-Aldrich, CA	75% in water

($C_5H_{10}N_2O_2$)		
Diethyl fumarate ($C_2H_5OCOCH=CHCOOC_2H_5$)	Sigma-Aldrich, CA	98%wt
Ferric oxide (Fe_2O_3)	Sigma-Aldrich, CA	99%wt
Iron (II,III) oxide (Fe_3O_4)	Sigma-Aldrich, CA	98%wt
Ferrous oxide (FeO)	Sigma-Aldrich, CA	99%wt
Goethite (FeOOH)	Sigma-Aldrich, CA	35%wt Fe
Inhibitor A	Sigma-Aldrich, CA	97%wt
Inhibitor B	Sigma-Aldrich, CA	99%wt
Inhibitor C	Sigma-Aldrich, CA	99%wt
Methyl orange ($C_{14}H_{14}N_3NaO_3S$)	Sigma-Aldrich, CA	0.1%wt
Phosphoric acid (H_3PO_4)	Sigma-Aldrich, CA	85%wt
Potassium dihydrogen phosphate (KH_2PO_4)	Sigma-Aldrich, CA	99%wt
Acetonitrile (CH_3CN)	Sigma-Aldrich, CA	99.9%wt
Trimellitic acid ($C_6H_3(CO_2H)_3$)	Sigma-Aldrich, CA	99.9%wt
polyvinyl alcohol ($[-CH_2CHOH-]_n$)	Sigma-Aldrich, CA	98%mol in water
trizma base ($NH_2C(CH_2OH)_3$)	Sigma-Aldrich, CA	99.8%wt
Hexadimethrine bromide	Sigma-Aldrich, CA	>95%wt
Sodium hydroxide (NaOH)	Hewlett-Packard Canada LTD., CA	1M and 0.1M
Ethylene glycol ($HOCH_2CH_2OH$)	Cole-Parmer Canada Inc.	1:1 (Ethylene glycol:water)

Gases		
100% Nitrogen (N_2)	Praxair, Regina, CA	Industrial grade
100% Carbon dioxide (CO_2)	Praxair, Regina, CA	Grade 4.8
6% oxygen (O_2) balanced with 94% Nitrogen (N_2)	Praxair, Regina, CA	Premixed grade
100% Helium (He)	Praxair, Regina, CA	Ultra-high purity grade

4.2 Solvent preparation

Solvent preparation was done by diluting monoethanolamine (MEA) with deionized water to a desired concentration (5M) by using a volumetric flask. The concentration was then measured for its accuracy by titration with a standard solution of 1M hydrochloric acid (HCl) by using 0.1%wt methyl orange solution as an indicator. The prepared solution was then mixed with the additives which varied depending on the studied system before being loaded with carbon dioxide (CO_2). The loading of CO_2 was done by purging 100% CO_2 gas into the solution, where the CO_2 content was measured by a standard procedure provided by the Association of Official Analytical Chemists (AOAC) (Horowitz, 1975). The method was based on an acidification technique where a CO_2 loading (mol of CO_2/mol of MEA) was determined from the titration-based calculation. The MEA concentration was able to be determined directly from the titration of the solution with 0.1% methyl orange, while, the amount of CO_2 dissolved in the solution was calculated from the evolved gas collected in a precision gas burette containing a displacement solution in which an excess 1M HCl was added to the loaded solution in order to ensure all the CO_2 had been evolved. Finally, the CO_2 loading was calculated as a ratio between the moles of CO_2 evolved and the moles of amine in the sample (mol of CO_2/mol of MEA), where the CO_2 loading was kept constant in all the experiments at 0.5 mol of CO_2/mol of MEA.

4.3 Corrosion experiment

The corrosion experiment was carried out using electrochemical technique. This technique basically measured an electrical current produced between metal and electrolyte and then converted it into a corrosion rate. The technique has been widely used due to the fact that it provides reproducible data and is not time consuming when compared to other corrosion measurement techniques, such as for example, weight loss technique and thickness reduction.

4.3.1 Specimen preparation

Carbon steel 1020 (Metal Samples, Alabama, USA), which is commonly found as a construction material in many amine treatment plants, was selected to use as a corrosion specimen. Its composition is presented in Table 4.2. A specimen was shaped into a cylindrical element with a 3/8 in (9.5 mm) diameter and 1/2 in (12.7 mm) length, and it drilled in one end to a depth of 1/4 in (6.4 mm) in order to accommodate a 3-48 UNC-2A thread. Prior to use, the specimen was prepared by wet grinding with 240 grit silicon carbide paper, then polishing with 600 grit silicon carbide paper, rinsed with deionized water, and air dried in order to clean up the surface. To remove any remaining grease, the specimen was then rinsed with methanol, followed by being air dried and kept in a desiccator until ready to be used.

Table 4.2: The composition of carbon steel 1020 (Metal Samples, Alabama, USA).

Composition	**%wt**
Fe	99.188
C	0.019
Mn	0.580
Si	0.200
S	0.006
P	0.007

4.3.2 Experimental apparatus

The electrochemical experimental apparatus is presented in Figure 4.1,

The corrosion cell model K47 (Princeton Applied Research, NJ, USA) consisted of a one litre flat bottom glass vessel equipped with one working electrode, which was mounted to a specimen, two high density carbon graphite counter electrodes, a mercury-mercurous sulphate reference electrode (MSE), a salt bridge tube attached with vycor frit at one end and a purge tube for inlet and outlet gases, as illustrated in Figure 4.2. In addition, a condenser was also equipped with the corrosion cell through the outlet of the purge tube in ordered to prevent any change in the solution concentration due to evaporation during the process.

The water bath was equipped with a temperature controller in order to maintain the operating temperature. The temperature was also monitored using a 0 to 100°C thermometer where its accuracy was confirmed to be ±1°C. Since, the water bath was in an open system, heat loss was minimized by covering the water surface with hollow balls.

A potentiostat model 273A (Princeton Applied Research, NJ, USA), which is an electronic device used in controlling the potential of a working electrode through an electrometer, was used to measure the electrical current produced due to the system's polarization (change in potential). The potentiostat was periodically hard-reset and calibrated every three months using the built-in functions in order to ensure its accuracy.

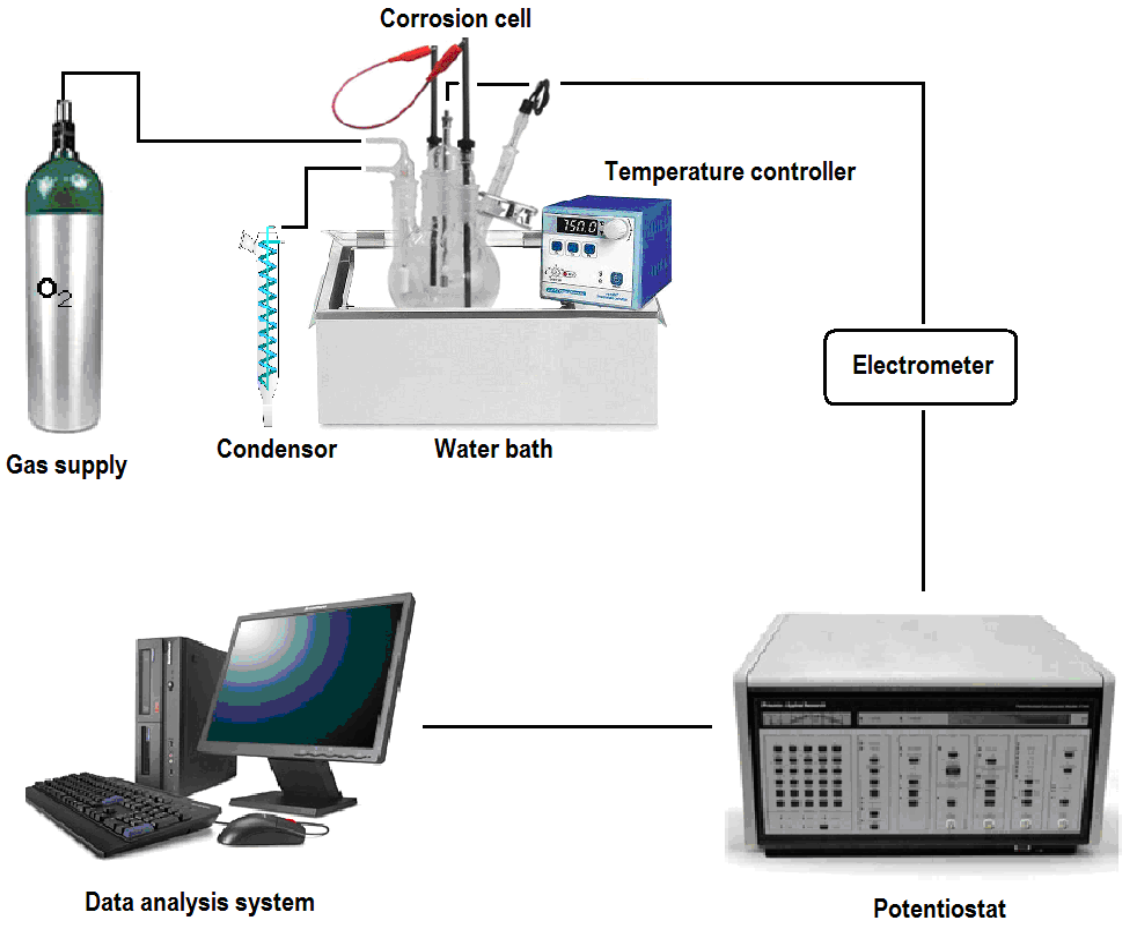

Figure 4.1: Electrochemical apparatus for a corrosion experiment. (Original in colour)

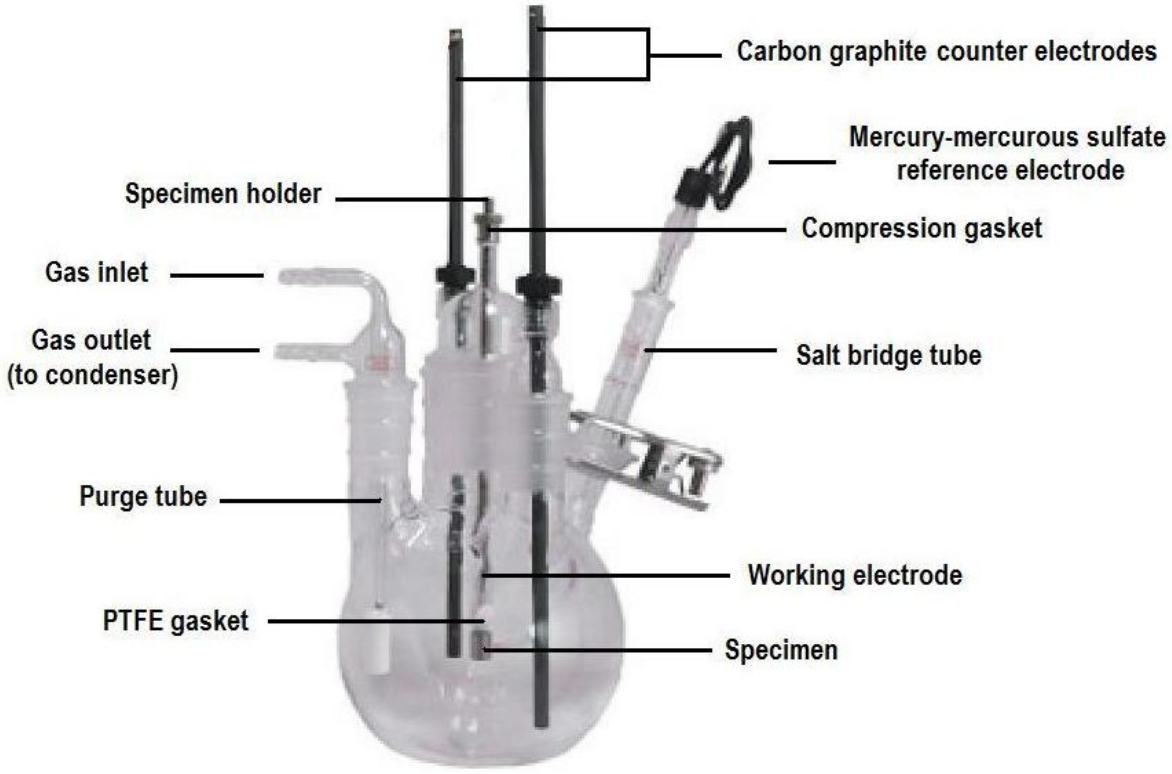

Figure 4.2: A corrosion cell.

The data acquisition system consisted of PowerCORR software version 2.47 (Princeton Applied Research, NJ, USA), which acquired and analyzed the data sent and/or received by the potentiostat using a compatible computer.

The gas supply was mainly 6% O_2 balanced with 94% N_2 and 100% N_2 (only used in the equipment validation). The gas was introduced to a corrosion cell at a constant flow rate (150 ml/min) through a series of gas flow meters. Since the corrosion experiments were performed at specific temperatures and pressure (atmospheric pressure; 0.101325MPa) that varied depending on the system, the O_2 concentration dissolved in aqueous alkanolamine solution was calculated using the following equation (Rooney and Daniels, 1998), where the equation was also used to calculate the dissolved O_2 concentration for the oxidative MEA degradation study.

Oxygen solubility in aqueous alkanolamine solution:

$$[O_2](mol/m^3) = -2.545 + 0.807\times10^{-2}T - 84.14p + 2.096\times10^{-4}pT^2 + \frac{2.322\times10^4 p}{T} + 1.027p^2 - \frac{3.911\times10^2 p^2}{T} \quad (4.1)$$

where: T = temperature (K)

p = pressure (MPa)

4.3.3 Experimental procedures

First, the corrosion apparatus was validated according to ASTM G5-94 (2004) in order to ensure its accuracy by performing a potentiodynamic scan with 1M sulphuric acid solution at 30°C in the presence of 100% N_2 gas by using stainless steel 430 as a corrosion specimen. Then, an actual corrosion experiment was carried out at atmospheric pressure by immersing a corrosion cell equipped with a working electrode, two counter electrodes, and a purge tube, in which the cell containing 900 ml of a test solution in a temperature-controlled water bath where the temperature was set by a controller and monitored to be ±1°C by a thermometer. The operating temperature in the corrosion experiment was kept below the boiling point (100°C) of a heating medium (water) where the maximum operating temperature was set at 80°C in order to prevent rapid evaporation of water. Then, 6% O_2 balanced with 94% N_2 gas was introduced to the corrosion cell through a purge tube at a rate of 150 ml/min for one hour, which was the same in every corrosion experiment. After that, a salt bridge was filled with a test solution and placed into the corrosion cell along with the mercury-mercurous sulphate reference electrode (MSE). The bridge's tip was adjusted to be roughly 3 to 4 mm away from the specimen surface, and this position was maintained by using a socket clamp. Finally, the corrosion cell and the potentiostat were fully equipped by connecting all the electrical lines. The corrosion potential (E_{corr}), which was measured with respect to the MSE reference electrode, was monitored for an hour in order to ensure the system stability had been achieved, which was indicated once E_{corr} remained constant. Then, the potentiodynamic polarization was initiated with a scanning rate of 0.166 mV/s. The process continually

applied electrical potentials and measured the electrical currents produced by the system. Both the potentials and currents were recorded through the potentiostat linked to the computer software in order to perform a polarization plot that provided information on the corrosion behaviour.

4.3.4 Corrosion rate calculation

Corrosion rate was calculated using data provided by a Tafel plot, which is a plot obtained from the potentiodynamic scan, usually at ±0.25V from the corrosion potential (E_{corr}). The scan data were plotted as the applied potentials versus the logarithms of the electrical currents, as presented in Figure 4.3. The corrosion current (i_{corr}) was found at the intersection of the extrapolations of the currents between the anodic and cathodic Tafel regions. Even though a corrosion rate was able to automatically be calculated by using a built-in function in the PowerCORR software, it should be noted that the calculation was based on equation 4.2.

$$\text{Corrosion rate (mpy)} = \frac{0.13 \cdot i_{corr} \cdot (EW)}{A \cdot d} \qquad (4.2)$$

where: mpy is milli-inches per year

i_{corr} is the corrosion current (μA; microampere)

EW is the equivalent weight of a corrosion specimen (g)

A is the surface area of a corrosion specimen (cm^2)

d is the density of a corrosion specimen (g/cm^3)

0.13 is the constant derived from Faraday's constant (C^{-1}; coulomb or $(A \cdot s)^{-1}$)

Moreover, equation 4.2 can be rearranged by combining i_{corr}/A to be I_{CORR} or so-called corrosion current density ($\mu A/cm^2$). In addition, in this work, EW, A, and d were calculated to be 27.82 g, 5.1 cm^2, and 7.87g/cm^3, respectively.

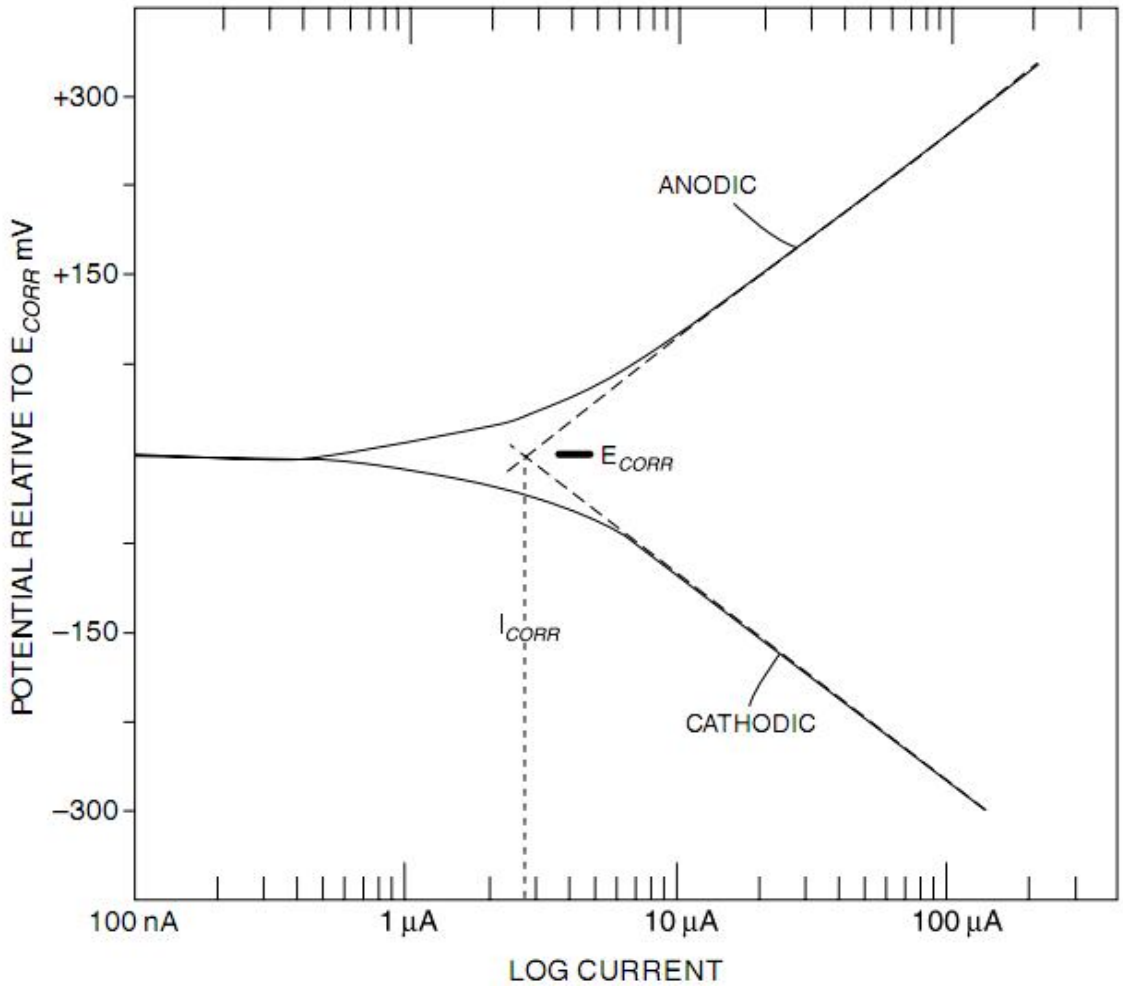

Figure 4.3: A Tafel plot. (Bardal, 2003)

4.4 Oxidative MEA degradation experiment

The solvent degradation experiments were carried out in a high pressure compact bench-top lab reactor model 5523 (Parr Instrument Company, IL, USA) equipped with a programmable temperature controller model 4836 with a tachometer display module (Parr Instrument Company, IL, USA). The reactor specifications are presented in Table 4.3, along with the images of a fully equipped reactor and a reactor head presented in Figures 4.4 and 4.5, respectively. The reactor was also equipped with a magnetic drive stirrer with a variable speed motor at 1.17 hp and an aluminum block heater with a heat power of 1000 watts, which required an electrical supply of 115 volts. The oxidative MEA degradation experiments were done by assembling the reactor containing 450 ml of a test solution into a block heater, connecting the stirring system through the magnetic drive, attaching a temperature controller by plugging in the thermocouple, connecting the cooling solution (50%wt ethylene glycol in water) through the cooling loop, introducing a gas line, and ensuring closure of all valves. The solution was continually stirred at about 500 rpm while it was heated to a desired temperature, and half an hour was allowed to stabilize the system at the required temperature. When the temperature was reached, there was some vapour produced within the reactor, mainly due to water vaporization, which could be observed through the pressure gauge, since the reactor was a leak-free system. Then, an additional 350 kPa (51 psi) of 6% O_2 balanced with 94% N_2, where the O_2 solubility in the aqueous alkanolamine solution can be calculated from equation 4.1, was introduced to the system through a gas inlet valve, which finally brought the system's pressure to about 760 kPa (110 psi), and the system was kept constantly at this

pressure throughout the process. Due to the fact that solvent degradation takes months to proceed, the oxidative MEA degradation experiment was performed at an elevated pressure of 760 kPa (110 psi) in order to accelerate the reaction process to be able to observe the solvent degradation within about two to three weeks. A solution sample of 4 ml was collected daily. It was immediately run over by cold water to quench the reaction and quickly put into a refrigerator maintained at 4°C in order to stop the degradation process. The samples were kept until the run was finished, which normally took about two to three weeks, and they were then tested for the concentrations of MEA at different times by using high performance liquid chromatography (HPLC). Since MEA had been degraded over the course of times, the concentration reduced accordingly; therefore, the oxidative MEA degradation rates were calculated as the reduction of MEA concentration over time (kmol of MEA/$m^3 \cdot$hr). In addition, even though the solution samples were kept in a refrigerator until the run was finished, no change in the MEA concentrations was observed over that time. This was demonstrated by randomly selecting solution samples and testing for the MEA concentration of the same sample at different times (half an hour, a day, a week, and two weeks). The results showed that the MEA concentrations in the sample were the same regardless of storage time in the refrigerator.

Table 4.3: Parr reactor model 5523 specifications.

Parr reactor model 5523	
Size	600 ml
Material	Stainless steel T316
Reactor mounting	Compact bench top
Reactor's width (without controller)	8.3 in
Reactor's depth	9.5 in
Reactor's height	25.4 in
Reactor's weight	30 pounds
Vessel style	Movable
Vessel's inside diameter	2.5 in
Vessel's inside depth	8 in
Vessel's weight	17 pounds
Maximum pressure	3000 psi (200 bar)
Maximum temperature (with PTFE flat gasket)	350 °C
Valve connections	1/8 in male NPT
Maximum torque	2.5 inch-pound (0.28 Nm)
Impeller (4-blade)	2 impellers (1.38 in diameter)
Pressure gauge	0 to 300 psi
Pressure gauge size	3.5 in
Temperature measurement	Fixed thermocouple
Cooling coil	Single loop

Figure 4.4: A fully equipped reactor. (Original in colour)

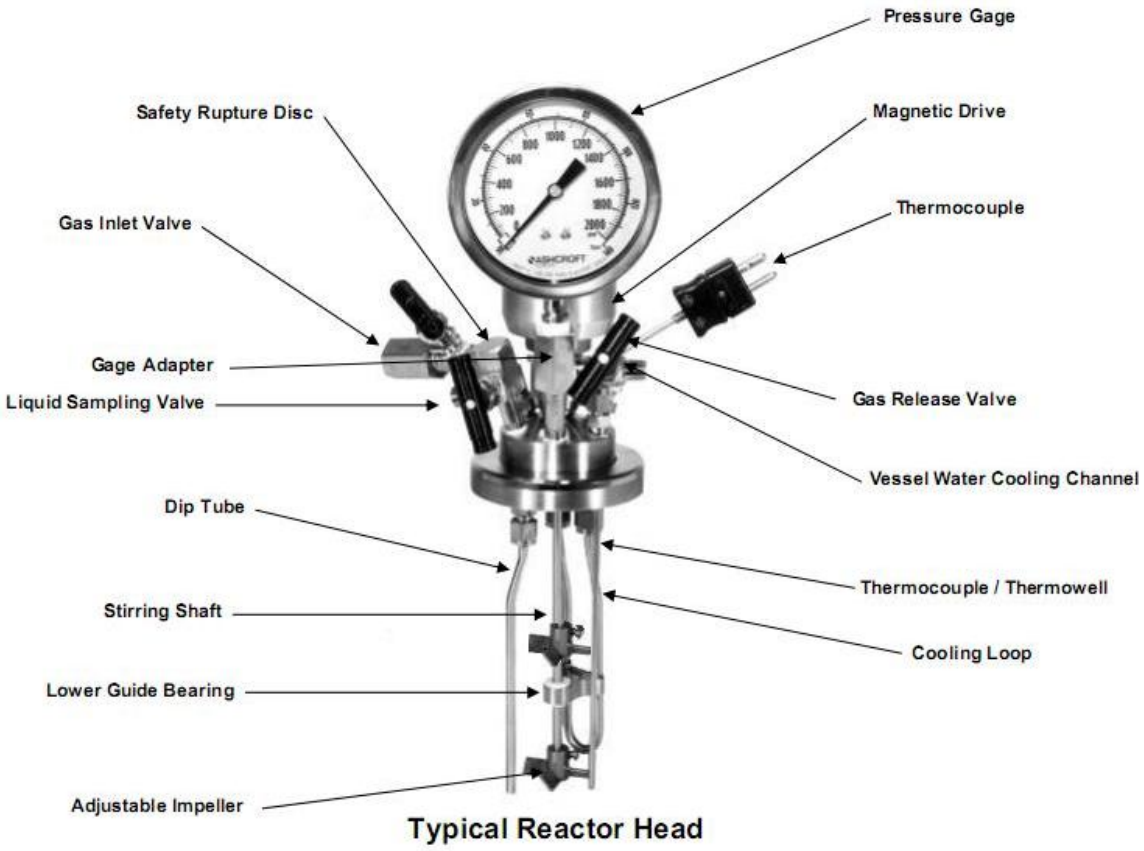

Figure 4.5: Reactor's head. (Original in colour)

4.5 Analytical techniques

Gas chromatography with mass spectrometry (GC-MS), high performance liquid chromatography with refractive index detection **(**HPLC-RID**),** capillary electrophoresis with diode array detection **(**CE-DAD**),** inductively coupled plasma with mass spectrometry (ICP-MS), and scanning electron microscopy with x-ray microanalysis (SEM-EDS) were used in the analyses of the liquid samples and the solid corrosion products.

4.5.1 Gas chromatography with mass spectrometry (GC-MS)

Gas chromatography with mass spectrometry (GC-MS) model 6890-5073 supplied by Hewlett-Packard Canada Ltd., Quebec, CA, with HP-Innowax having polyethylene glycol crosslink as a high polar stationary phase, was used to determine compounds presented in the liquid samples in both corrosion and solvent degradation experiments in which the samples could be vapourized. The column had an inside diameter of 0.25 mm, a thickness of 0.25 μm, and a length of 30 m (Hewlett-Packard Canada Ltd., Quebec, CA).

First, the liquid samples were filtered with 0.2 μm nylon membrane filter in order to remove solid particles and were then stored in standard GC vials (Agilent Technologies Canada, Ontario, CA). The samples were auto-injected by autosampler/autoinjector model 7683 (Hewlett-Packard Canada Ltd., Quebec, CA) at a volume of 1μl (±0.3% error) through the GC inlet using a split injection mode with a split ratio of 30:1 at an inlet

temperature of 250°C, and each sample was analyzed twice in order to ensure reproducibility. The oven temperature was initially set at 70°C then increased to 240°C at a rate of 7°C/min and held at 240°C for another 10 minutes to allow sufficient time for the separation process (Supap et al., 2006), where ultra-high purity grade helium (He) was used as a carrier gas with a flow rate of 1 ml/min. The MS scan mode had a mass range from 10 to 300 u (Da). Compounds were identified by matching their mass spectra with the commercial mass spectra database provided by the National Institute of Standards and Technology (NIST) version 1998 and also with the mass spectra of the standard chemicals.

4.5.2 High performance liquid chromatography with refractive index detection (HPLC-RID)

High performance liquid chromatography with refractive index detection (HPLC-RID) was used in determining MEA concentration by using a standard calibration curve where peak areas were plotted relatively with their standard concentrations (0 to 6M). An HPLC model 1100 was equipped with a RID model G1315B and an online degasser model G1322A (Agilent Technologies, Mississauga, Canada, Ontario, CA). The HPLC column was Nucleosil 100-5 SA containing a strong sulphonic acid cationic exchanger with a length of 250 mm and a 4.6 mm inside diameter (Macherey-Nagel, Germany).

HPLC mobile phase preparation was done by adjusting the pH of 0.05M potassium dihydrogen phosphate solution (KH_2PO_4) to be 2.6 by using 85%wt phosphoric acid

(H_2PO_4). The solution was left to degas in an ultrasonic bath for at least 3 hours and then filtered under vacuum with a 0.2 μm nylon filter prior to use.

The sample preparation was done by diluting a test solution to a 1:40 volume-based dilution with nanopure water (200 μl of a test solution in 8 ml of nanopure water) and then filtered with a 0.2 μm nylon membrane filter and stored in a standard screw top vial (Agilent Technologies, Mississauga, Canada, Ontario, CA) until ready to be analysed.

Before performing an analysis, all lines in the system had to be cleaned with nanopure water. Then, the column was installed and the entire machine was again rinsed with nanopure water until the system's steady line was reached. Then, the system was rinsed with mobile phase until it was again stabilized. The samples were injected by the autosampler model G1313A (Agilent Technologies Canada, Ontario, CA) at a volume of 8 μl and then passed through a RID detector. The system was kept at a constant temperature (30°C), while the mobile phase continually flowed at a rate of 1 ml/min. When the analysis was finished, the system and the column were cleaned with nanopure water and stored with acetonitrile. Then, the column was taken out of the machine, closed at both ends, and kept at room temperature. In addition, a calibration curve using standard MEA concentrations was performed prior to every analysis in order to ensure accuracy.

4.5.3 Capillary electrophoresis with diode array detection (CE-DAD)

A capillary electrophoresis (CE) model HP 3D CE equipped with diode array detection (DAD) (Hewlett-Packard Canada LTD., Montreal, Quebec, CA) was used in determining organic and inorganic anions. A fused silica capillary column with a 75 μm inside diameter and 720 mm effective length **(**Agilent Technologies, Mississauga, Canada, Ontario, CA**)** was used.

The background electrolyte (BGE) preparation was done by mixing 0.4203g of trimellitic acid, 0.2g of polyvinyl alcohol, and 4.844g of trizma base, with 200g of nanopure water. A bromide solution was prepared as 10%wt/wt of hexadimethrine bromide in nanopure water (Bord et al., 2005). Both solutions were stored in a refrigerator at 4°C and filtered with a 0.2 μm nylon membrane syringe filter prior to use. The liquid sample preparation was done by diluting the samples to 1:10 volume-based dilution with nanopure water not only to minimize the effects of high concentration compounds (MEA and CO_2) that might interfere with the detecting sensitivity but also to accommodate a suitable DAD detection range (50 – 10000 ppm).

The machine was calibrated and initialized before performing the analysis. The capillary was preconditioned by flushing with 1M sodium hydroxide (NaOH) for 30 minutes, coating with bromide solution for another 30 minutes, washing with 0.1M sodium hydroxide (NaOH) for 15 minutes, and cleaning with high-purity water for 15 minutes at a constant pressure of 1 bar. Then, the capillary was flushed with the BGE at

least 30 minutes or until a steady signal was achieved, and it was finally conditioned under minus 30kV for another 10 minutes. Before each injection, the capillary was again preconditioned with BGE for 5 minutes and then the analysis was performed at a wavelength of 240 nm, while the capillary was kept at a constant temperature of 30°C throughout the process. After the analysis, the capillary was cleaned by flushing with 1M NaOH for 30 minutes, followed by flushing with high-purity water for another 30 minutes, and the entire system was stored in high-purity water.

4.5.4 Inductively coupled plasma with mass spectrometry (ICP-MS)

The Varian ICP-MS (Varian, Inc., Mississauga, ON, CA; first generation) was used in determining total iron ions (Fe^{2+} and Fe^{3+}) concentration in a test solution. The instrument was tuned daily to maintain the system's stability and performance. The sample preparation was done by putting approximately 1 to 2 ml of liquid sample into a Teflon beaker for digestion. One part of the sample was digested with two parts of 2 ml OMNI trace nitric acid (HNO_3) and then heated on a hot plate until the volume was reduced to approximately 1 ml. The sample was then diluted with deionized water in order to accommodate the ICP-MS analysis, where the total iron ions concentration range was varied from 0 to 500 ppm and the Fe intensity was monitored at mass 57.

4.5.5 Scanning electron microscopy with x-ray microanalysis (SEM-EDS)

A SEM model JSM-5600 (JEOL USA, Inc., Peabody, MA, USA) equipped with EDS model EDAX Genesis 7000 (EDAX, Inc., Mahwah, NJ, USA) was used to capture images of the corrosion products on a specimen surface and also characterize elements presented in the product layers. A solid sample, a corrosion specimen, was prepared in a sample stub and placed directly into the sample holders inside the SEM analysis chamber, where no sputter coating was required. At each location, images at 100x, 250x, 800x, and 1500x magnifications were collected at 20kV energy level with approximately 8 to 9 mm of working distance. The spot size varied depending on the image but was usually set to around 30. After images were collected, the EDS scans were run at 200 and 3600 seconds at a working distance of approximately of 17 mm and a spot size of 40, while the energy level remained the same at 20kV. It should be noted that the EDS was not able to detect elements of hydrogen (H), helium (He), lithium (Li), or beryllium (Be), since the smallest element that can be detected by using EDS is boron (B). In addition, prior to the analysis, background scans of the carbon tape and aluminum sample stub were performed in order to ensure that elements on the sample stub would not be presented in the final results.

CHAPTER FIVE

RESULTS AND DISCUSSION OF CARBON STEEL (1020) CORROSION

5.1 Experimental conditions

The corrosion study was conducted by varying additives along with their concentrations under the base-case conditions. All the experiments on carbon steel (C1020) corrosion were performed under the conditions presented in Table 5.1 except for the study of temperature effects, where two additional temperatures (30 and 60°C) were introduced. Nevertheless, it should be noted that the operating temperatures in the corrosion experiments were set to be below the boiling point (100°C) of a heating medium (water) in order to prevent rapid evaporation of the medium. The selection of the additives aimed to represent various species typically found in a flue gas. So, two types of chlorides (sodium chloride; NaCl and ferrous chloride; $FeCl_2$) and hydrochloric acid (HCl) were selected to represent various sources of chlorides in a flue gas in which sodium chloride (NaCl) represented a commonly found salt, hydrochloric acid (HCl) represented a mineral acid, and ferrous chloride ($FeCl_2$) represented an inorganic compound. The reason sodium-base and iron-base compounds were selected is they are cations with a significant presence within the CO_2 capture process (Strazisar et al., 2003). Moreover, two different sulphate compounds (sodium sulphate; Na_2SO_4 and ferrous sulphate; $FeSO_4 \cdot 7H_2O$) and sulphuric acid (H_2SO_4) were also selected to study their effects on carbon steel corrosion where sodium sulphate (Na_2SO_4) represented a commonly found sulphate salt, ferrous sulphate ($FeSO_4 \cdot 7H_2O$) represented an inorganic compound, and sulphuric acid (H_2SO_4) repre-

sented aqueous solution of sulphur trioxide (SO_3). Sulphurous acid (H_2SO_3) was also chosen as a representative of sulphur dioxide (SO_2) in aqueous solution where sodium sulfite (Na_2SO_3) and sodium bisulfite ($NaHSO_3$) were studied additionally to identify the effects of sulfite and bisulfite anions on corrosion. Lastly, nitric acid (HNO_3) was also selected to represent nitrogen dioxide (NO_2) in an aqueous solution. The concentration ranges of each additive chosen in the study are presented in Table 5.2.

There are two reasons that the aqueous acid solutions (H_2SO_4, H_2SO_3, and HNO_3) were used instead of the actual acid gas components (SO_3, SO_2, and NO_2) present in a flue gas. First, this work focused on the study of carbon steel (C1020) corrosion by the reactions occurring in aqueous phase within the CO_2 capture process. Unfortunately, the method to determine an amount of acid gas dissolved into an aqueous solution has not been well-established, so the acid solutions (H_2SO_4, H_2SO_3, and HNO_3) were chosen to represent the dissolved acid gases (SO_3, SO_2, and NO_2) in aqueous solution in order to avoid the difficulty in making a concentration determination of the solubility of the actual gases. To simplify the calculation, this work assumed that the concentrations of the aqueous acid solutions (H_2SO_4, H_2SO_3, and HNO_3) were equal to the concentrations of the acid gases (SO_3, SO_2, and NO_2) present in a flue gas. Table 5.3 illustrates the actual acid gases concentrations present in a flue gas, the calculated dissolved-gases concentrations in which they were calculated based on the assumption that all the gases are fully dissolved into aqueous solution, and the experimental concentrations of the aqueous acid solutions that were used in this study. Secondly, the acid gases (SO_3, SO_2, and NO_2) are considerably toxic. Therefore, there are limitations due to safety regulations in the con-

centration ranges allowed to be used in a laboratory workplace. The allowable concentrations of the gases were well below the concentrations that are typically found in a flue gas. Therefore, using the acid solutions (H_2SO_4, H_2SO_3, and HNO_3) to represent the aqueous solutions of the acid gases (SO_3, SO_2, and NO_2) allowed the experimental conditions to reach the concentrations relevant to those present within a flue gas.

Table 5.1: The base-case conditions (no additive) of carbon steel (C1020) corrosion.

Component	Condition
MEA concentration	5M (0.9% error)
CO_2 loading	0.5 mol CO_2/mol MEA (2.3% error)
O_2 concentration	0.000351M (at 80°C)
Temperature	80°C (±1°C)
Pressure	Atmospheric pressure (1 atm)
The rate of reaction	**166.35 mpy** (6.3% error)

Table 5.2: The concentration ranges of additives in the carbon steel (C1020) corrosion study.

Additive	Concentration
Sodium chloride (NaCl)	0 - 2000 ppm
Ferrous chloride ($FeCl_2$)	
Hydrochloric acid (HCl)	
Sodium sulphate (Na_2SO_4)	0 - 12 ppm
Ferrous sulphate heptahydrate ($FeSO_4 \cdot 7H_2O$)	
Sulphuric acid (H_2SO_4)	
Sulphurous acid (H_2SO_3)	0 - 400 ppm
Sodium sulfite (Na_2SO_3)	
Sodium bisulfite ($NaHSO_3$)	
Nitric acid (HNO_3)	0 - 400 ppm

Table 5.3: The concentration ranges of the acid gas typically present in a flue gas, the calculated dissolved-gas concentration in aqueous solution, and the experimental concentration of the aqueous acid solution that were used in this work.

Typical flue gas	**Calculated dissolved-gas concentration in aqueous solution***	**Experimental concentration of the aqueous acid solution**
$SO_3 \leq 12$ ppm	$H_2SO_4 \leq 15$ ppm	H_2SO_4 0 – 12 ppm
$SO_2 \leq 400$ ppm	$H_2SO_3 \leq 512$ ppm	H_2SO_3 0 – 400 ppm
$NO_2 \leq 400$ ppm	$HNO_3 \leq 365$ ppm	HNO_3 0 – 400 ppm

*Calculated based on the assumption that all the gases are fully dissolved into aqueous solution.

5.2 The effects of different types of chloride compounds on carbon steel (1020) corrosion

Three different chloride compounds were studied in their effects on carbon steel (1020) corrosion: sodium chloride (NaCl) represented a commonly found salt, hydrochloric acid (HCl) represented a mineral acid, and ferrous chloride ($FeCl_2$) represented an inorganic compound. The corrosion rate graphs of these systems are illustrated in Figure 5.1.

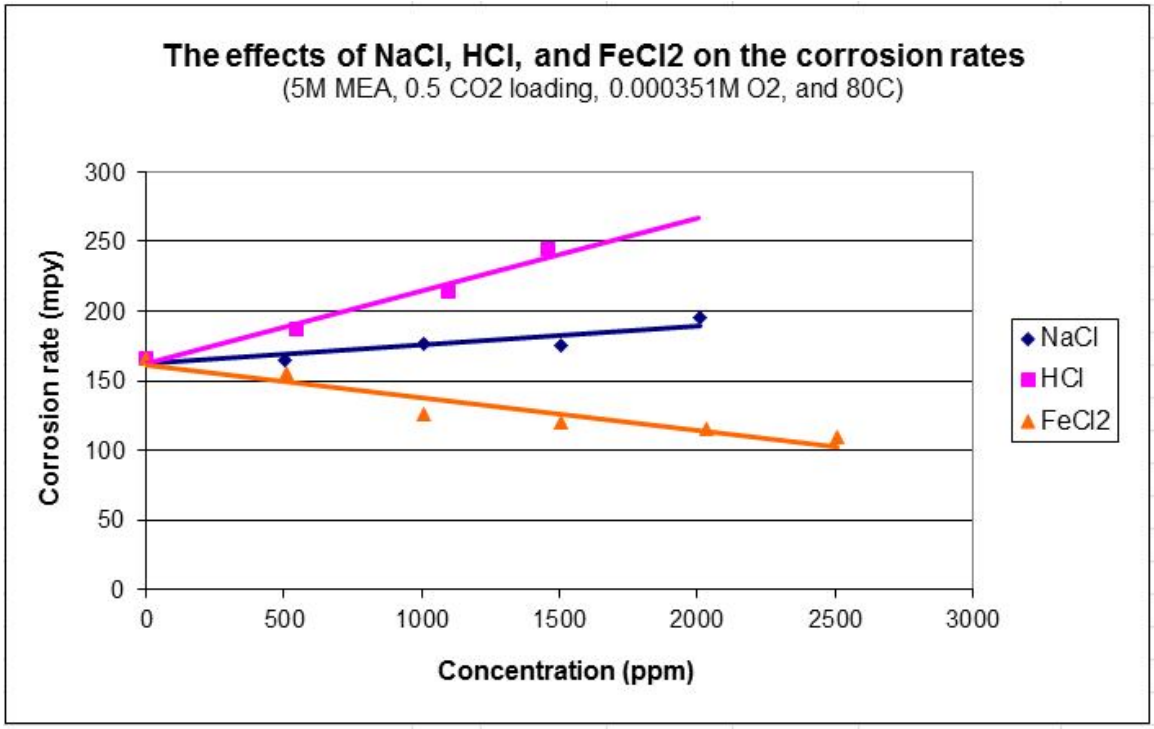

Figure 5.1: The effects of different types of chloride compounds on the corrosion rates of carbon steel 1020 (%error: 5.8%, 4.5%, and 3.9% in NaCl, HCl, and $FeCl_2$ systems, respectively). (Original in colour)

5.2.1 The effect of sodium chloride (NaCl) on the corrosion rate

The corrosion rates slightly increased as NaCl concentrations increased, which was mostly due to the influence of chloride ion (Cl^-) alone. Since, the sodium ion (Na^+) has a much lower standard electrode potential (E_0^0 = -2.71 V) compared to the ferrous ion (Fe^{2+}; E_0^0 = -0.44 V), as shown in Table 5.4, which indicates that the sodium ion hardly gained any electrons released by the metal surface. Therefore, the sodium ion was considered to have a negligible effect on increasing the corrosion rate due to the fact that it did not appear to behave as an oxidizing agent in the corrosion reaction of carbon steel. On the other hand, the chloride ion played an important role in increasing the corrosion rates. Along with other oxidizing agents, the chloride ion combined with the ferrous ion released by the metal surface. This formed an unstable film of ferrous chloride ($FeCl_2$), which was more soluble compared to other ferrous compounds (corrosion products). Ferrous chloride helped to stimulate further iron dissolution by dissolving back into the solution, leaving the metal surface open for another attack by the oxidizing agents, which eventually led to more metal corrosion. The possible reaction schemes are illustrated, as presented in equations 5.1 to 5.17, along with their standard electrode potentials (E_0^0) for a half cell reduction reaction at 25°C (Bardal, 2003). A standard potential is an indication of a reaction likely to be cathodic, and if a standard electrode potential (E_0^0) for a half cell reduction reaction of any reaction was higher than the standard electrode potential of a half cell reduction reaction of the iron dissolution, that reaction was likely to be a cathodic reaction.

Dissociation of water:

$$2H_2O \leftrightarrow H_3O^+ + OH^- \quad (5.1)$$

Carbonic acid formation:

$$CO_2 + H_2O \leftrightarrow H_2CO_3 \quad (5.2)$$

Dissociation of carbonic acid:

$$H_2CO_3 + H_2O \leftrightarrow H_3O^+ + HCO_3^- \quad (5.3)$$

Dissociation of bicarbonate ion:

$$HCO_3^- + H_2O \leftrightarrow H_3O^+ + CO_3^{2-} \quad (5.4)$$

Anodic reaction

Iron dissolution:

$$Fe \rightarrow Fe^{2+} + 2e^- \quad (5.5)$$

(Standard electrode potential (E_0^0) is -0.44 V for a half cell *reduction* reaction.)

Cathodic reactions

Reduction of hydrogen ion:

$$2H^+ + 2e^- \rightarrow H_2 \quad (5.6)$$

(Standard electrode potential (E_0^0) is 0 V.)

Reduction of hydronium ion:

$$2H_3O^+ + 2e^- \leftrightarrow 2H_2O + H_2 \quad (5.7)$$

Reduction of bicarbonate ion:

$$2HCO_3^- + 2e^- \leftrightarrow 2CO_3^{2-} + H_2 \quad (5.8)$$

(Standard electrode potential (E_0^0) is -0.20 V.)

Reduction of dissolved O_2:

$$O_2 + 2H_2O + 4e^- \leftrightarrow 4OH^- \quad (5.9)$$

(Standard electrode potential (E_0^0) is 0.4 V.)

$$O_2 + 4H^+ + 4e^- \leftrightarrow 2H_2O \quad (5.10)$$

(Standard electrode potential (E_0^0) is 1.23 V.)

Reduction of iron (II,III) oxide (a corrosion product):

$$Fe_3O_4 + 8H^+ + 2e^- \leftrightarrow 3Fe^{2+} + 4H_2O \quad (5.11)$$

(Standard electrode potential (E_0^0) is 0.98 V.)

Corrosion products

Formation of ferrous hydroxide:

$$Fe^{2+} + 2OH^- \leftrightarrow Fe(OH)_2 \quad (5.12)$$

Formation of ferric hydroxide:

$$2Fe(OH)_2 + H_2O + \frac{1}{2}O_2 \rightarrow 2Fe(OH)_3 \quad (5.13)$$

Formation of ferrous carbonate:

$$Fe^{2+} + CO_3^{2-} \rightarrow FeCO_3 \quad (5.14)$$

Formation of ferrous bicarbonate:

$$Fe^{2+} + 2HCO_3^- \rightarrow Fe(HCO_3)_2 \tag{5.15}$$

Formation of iron (II,III) oxide or magnetite (Fe_3O_4):

$$3Fe + 4H_2O \rightarrow Fe_3O_4 + 4H_2 \tag{5.16}$$

Formation of ferrous chloride:

$$Fe^{2+} + 2Cl^- \rightarrow FeCl_2 \tag{5.17}$$

Table 5.4: Standard electrode potential (E_0^0) at 25°C. (Bardal, 2003)

Standard electrode potential E_0^0 at 25°C	
Electrode reaction	**E_0^0 (V)**
$O_2 + 4H^+ + 4e^- \rightarrow 2H_2O$	1.23
$Fe_3O_4 + 8H^+ + 2e^- \rightarrow 3Fe^{2+} + 4H_2O$	0.98
$NO_3^- + 4H^+ + 3e^- \rightarrow NO + 2H_2O$	0.96
$NO_3^- + 3H^+ + 2e^- \rightarrow HNO_2 + H_2O$	0.94
$NO_3^- + 10H^+ + 8e^- \rightarrow NH_4^+ + 3H_2O$	0.88
$NO_3^- + 2H^+ + e^- \rightarrow NO_2 + H_2O$	0.80
$Fe^{3+} + e^- \rightarrow Fe^{2+}$	0.77
$O_2 + 2H^+ + 2e^- \rightarrow H_2O_2$	0.69
$H_2SO_3 + 4H^+ + 4e^- \rightarrow S + 3H_2O$	0.45
$2H_2SO_3 + 2H^+ + 4e^- \rightarrow S_2O_3^{2-} + 3H_2O$	0.40
$O_2 + 2H_2O + 4e^- \rightarrow 4OH^-$	0.40
$SO_4^{2-} + 4H^+ + 2e^- \rightarrow H_2SO_3 + H_2O$	0.17
$2H^+ + 2e^- \rightarrow H_2$	0
$Fe_3O_4 + 8H^+ + 8e^- \rightarrow 3Fe + 4H_2O$	-0.085
$2HCO_3^- + 2e^- \rightarrow 2CO_3^{2-} + H_2$	-0.20
$Fe^{2+} + 2e^- \rightarrow Fe$	-0.44
$2H_2O + 2e^- \rightarrow 2OH^- + H_2$	-0.83
$Fe(OH)_2 + 2e^- \rightarrow Fe + 2OH^-$	-0.88
$Na^+ + e^- \rightarrow Na$	-2.71

5.2.2 The effect of hydrochloric acid (HCl) on the corrosion rate

Hydrochloric acid (HCl) strongly accelerated the corrosion process due to the fact that the hydrogen ion (H^+) has a higher standard electrode potential (E_0^0 = 0 V) compared to the ferrous ion (Fe^{2+}; E_0^0 = -0.44 V). Consequently, it behaved as an oxidizing agent to accelerate the corrosion process by stimulating the iron dissolution reaction. The chloride ion (Cl^-) also accelerated corrosion by combining with ferrous ion (Fe^{2+}), generating ferrous chloride ($FeCl_2$), which helped in stimulating further iron dissolution by dissolving back into the solution and leaving the metal surface open for more attacks from the oxidizing agents. Moreover, the effects of hydrochloric acid (HCl) and sodium chloride (NaCl) on carbon steel corrosion were compared, and the results showed that hydrochloric acid significantly induced more corrosion compared to sodium chloride, as illustrated in Figure 5.1, even though both of them have a single valent of the chloride ion in their compositions and should, therefore, have the same chloride effect. However, the hydrochloric acid systems resulted in higher corrosion rates because the hydrogen ion (H^+) is a much stronger oxidizing agent in corrosion compared to the sodium ion (Na^+) due to a much higher standard electrode potential, as illustrated in Table 5.4. The effect of hydrogen ion as the oxidizing agent was more dominant in inducing corrosion than the effect of the chloride ion, which is why hydrochloric acid induced more corrosion when compared to sodium chloride.

5.2.3 The effect of ferrous chloride ($FeCl_2$) on the corrosion rate

Firstly, when ferrous chloride ($FeCl_2$) mixed with MEA solution, a light-weight reddish-brown precipitated particle was generated. By physical appearance (colour), it appeared to be ferric oxide (Fe_2O_3). Ferrous hydroxide ($Fe(OH)_2$) was first generated from the reaction shown in equation 5.18. However, it was not stable. With accesses to oxygen (O_2) and water, it was oxidized to a trivalent hydrated iron oxide (ferric oxide; Fe_2O_3; reddish-brown) (Soosaiprakasam and Veawab, 2008).

$$FeCl_2 + 2[R-NH_2] \xrightarrow{2H_2O} 2[R-NH_3^+Cl^-] + Fe(OH)_{2(solid)} \qquad (5.18)$$

The solution was tested with ICP-MS and showed that the total iron ions (Fe^{2+} and Fe^{3+}) concentration decreased from the initial stage after it was mixed with MEA, which essentially ensured that the precipitate particle must be some kind of iron-combining compound. However, after the solution was loaded with 0.5 CO_2 loading (mol CO_2 per mol MEA), the total iron ions concentration was higher compared to the concentration before loading with the CO_2, which indicated that the iron-combining compound dissolved back into the solution when the acidity of the solution was increased.

Ferrous chloride ($FeCl_2$) showed negative effects on carbon steel corrosion. As discussed earlier, the chloride ion (Cl^-) appeared to accelerate the corrosion process. However, ferrous chloride was shown to slow down the metal corrosion, even though it has two valents of chloride ions in its composition. One reason why adding ferrous chlo-

ride decreased the corrosion rate was that the anodic reaction was mainly the iron dissolution; thus, if there was a ferrous ion (Fe^{2+}) already present in a solution due to the addition of ferrous chloride, it would inhibit any ferrous ion being released from the metal surface, resulting in the reduction of the corrosion rates. Moreover, the ferrous ion also partly reacted with dissolved oxygen (O_2) and precipitated some iron oxide (Fe-O) compounds out of the solution. By using SEM-EDS techniques, the precipitated particle was confirmed to contain mainly Fe and O elements, as presented in Figure 5.2 and Table 5.5. Therefore, O_2, which was one of the major oxidizing agents in the Re-Dox reactions, partly reacted with ferrous ion before it reached the metal surface. This, to some extent, led to the decrease in corrosion rates.

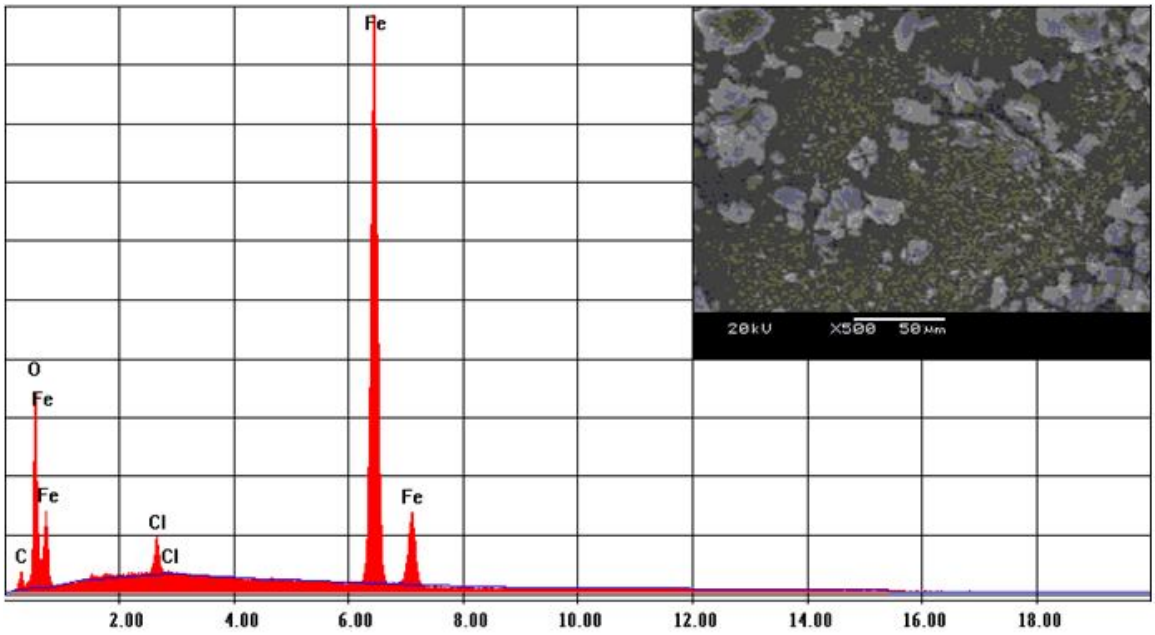

Figure 5.2: SEM-EDS scanning result for iron oxide (Fe-O) compound. (Original in colour)

Table 5.5: EDS elemental analysis for iron oxide (Fe-O) compound.

Element	Relative %Wt.
C	6.92
O	12.88
Cl	1.61
Fe	78.59
Total:	100.00

5.2.4 Summary of the effects of cations (Na^+, H^+, and Fe^{2+}) and chloride ion (Cl^-) on the corrosion rates

In the study of the effects of three different types of chloride compounds (NaCl, HCl, and $FeCl_2$) on carbon steel (1020) corrosion, there were three cations (Na^+, H^+, and Fe^{2+}) introduced to the system and each of them provided different levels of contribution to carbon steel corrosion. Sodium ion (Na^+) did not appeared to accelerate carbon steel corrosion due to having a lower standard electrode potential (E_0^0 = -2.71 V) than the metal itself (E_0^0 = -0.44 V), so it was not able to gain any electrons released from the metal. Therefore, it was considered to have a negligible effect on increasing the corrosion rate. On the other hand, the hydrogen ion (H^+) strongly accelerated the corrosion process since it has a higher standard electrode potential (E_0^0 = 0 V) compared to the metal, so it behaved as an oxidizing agent and accelerated the corrosion reactions. Comparatively, the ferrous ion (Fe^{2+}) tended to slow down the metal corrosion since it inhibited ferrous ion from being released from the metal surface due ferrous ion already being present in the solution by the addition of ferrous chloride.

The role of the chloride ion (Cl^-) in carbon steel corrosion is that it helped accelerate corrosion by combining with ferrous ion released by the metal surface and forming a soluble film of ferrous chloride ($FeCl_2$). Ferrous chloride then helped to stimulate further iron dissolution by dissolving back into the solution, leaving the metal surface open for another attack by the oxidizing agents, which eventually led to increased metal corrosion.

5.3 The effects of different types of sulphate compounds on carbon steel (1020) corrosion

Two different sulphate compounds (sodium sulphate; Na_2SO_4 and ferrous sulphate; $FeSO_4 \cdot 7H_2O$) and sulphuric acid (H_2SO_4) were used to study their effects on carbon steel (1020) corrosion: sodium sulphate (Na_2SO_4) represented a commonly-found sulphate salt, ferrous sulphate ($FeSO_4 \cdot 7H_2O$) represented an inorganic compound, and sulphuric acid (H_2SO_4) represented an aqueous solution of sulphur trioxide (SO_3).

The corrosion results of the different sulphate compounds are illustrated in Figure 5.3, which shows the addition of sodium sulphate (Na_2SO_4), sulphuric acid (H_2SO_4), and ferrous sulphate ($FeSO_4 \cdot 7H_2O$) all increased the corrosion rates. However, no significant difference in the rates between each compound was found. This was because cations (H^+, Na^+, Fe^{2+}) in the compounds had an insignificant effect on the increase of corrosion rates when compared to the effect of sulphate ion (SO_4^{2-}). In other words, the increase of the rates was primarily due to the presence of the sulphate ion. There were two major roles of the sulphate ion (SO_4^{2-}) in accelerating the corrosion process. Firstly, the sulphate ion behaved as an oxidizing agent by accepting electrons released by the metal surface due to the sulphate ion having a higher standard electrode potential (E_0^0 = 0.17 V) when compared to the potential of the iron dissolution reaction (E_0^0 = -0.44 V), which indicated that the sulphate ion promoted corrosion by accelerating the rate of iron oxidation. Secondly, the sulphate ion potentially led to the formation of ferrous sulphate ($FeSO_4$), which was able to be hydrolyzed by water and/or oxygen (O_2) and liberated the sulphate

ion back into the solution to again stimulate iron dissolution, as presented in equations 5.22 and 5.23 (Roberge, 1999). Moreover, the hydrogen ion (H^+) released by these reactions also helped in increasing the corrosion rates by behaving as an additional oxidizing agent. However, this effect was likely to be of secondary importance. The possible reaction schemes of sulphate-involved reactions are expressed as follows:

Iron dissolution:

$$Fe \rightarrow Fe^{2+} + 2e^- \tag{5.5}$$

(Standard electrode potential (E_0^0) is -0.44 V for a half cell *reduction* reaction.)

Reduction of sulphate ion:

$$SO_4^{2-} + 4H^+ + 2e^- \leftrightarrow H_2SO_3 + H_2O \tag{5.19}$$

(Standard electrode potential (E_0^0) is 0.17 V.)

Ferrous sulphate formation:

$$Fe^{2+} + SO_4^{2-} \leftrightarrow FeSO_4 \tag{5.20}$$

$$Fe(OH)_2 + SO_4^{2-} + 2H^+ \leftrightarrow FeSO_4 + 2H_2O \tag{5.21}$$

Sulphate ion liberation by water and/or oxygen:

$$FeSO_4 + 2H_2O \leftrightarrow FeOOH + SO_4^{2-} + 3H^+ + e^- \tag{5.22}$$

$$FeSO_4 + \frac{1}{2}O_2 + H_2O + e^- \leftrightarrow FeOOH + SO_4^{2-} + H^+ \tag{5.23}$$

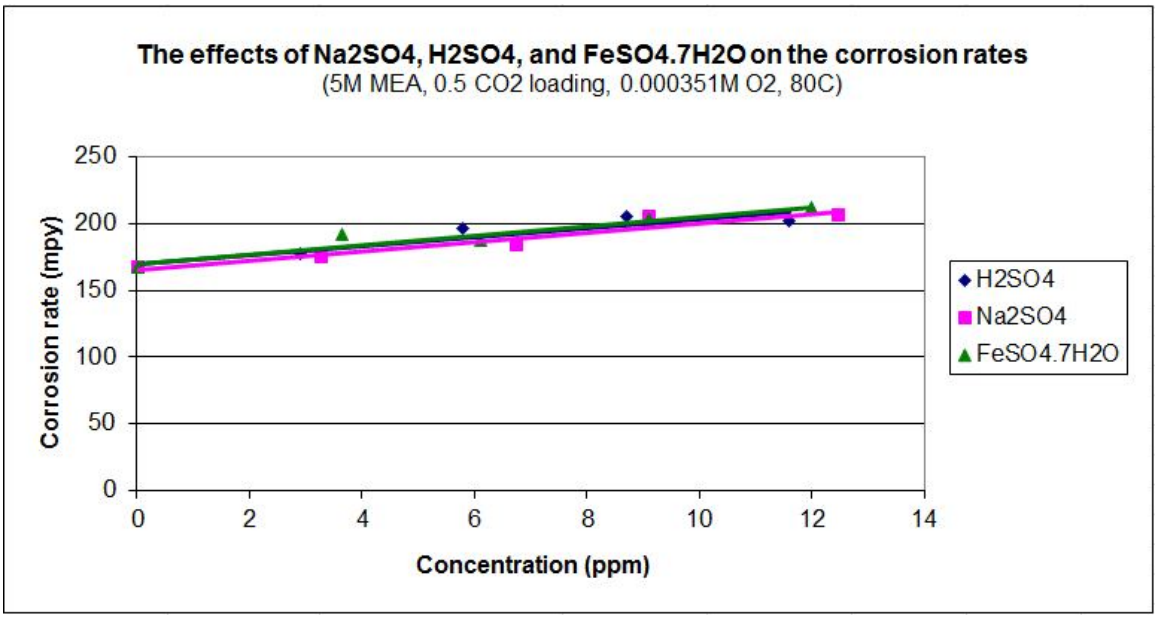

Figure 5.3: The effects of different types of sulphate compounds on the corrosion rates of carbon steel 1020 (%error: 5.9%, 5.0%, and 3.9% in Na_2SO_4, H_2SO_4, and $FeSO_4 \cdot 7H_2O$ systems, respectively). (Original in colour)

5.4 The effect of sulphurous acid (H_2SO_3) on carbon steel (1020) corrosion

Sulphurous acid (H_2SO_3) was used as a representative of sulphur dioxide (SO_2) in aqueous solution. Since it is a weak acid, when it dissolves in water, bisulfite (HSO_3^-) and sulfite (SO_3^{2-}) ions are formed as expressed in the reactions shown below:

Sulphurous acid formation:

$$SO_2 + H_2O \leftrightarrow H_2SO_3 \tag{5.24}$$

Hydrolysis of sulphurous acid:

$$H_2SO_3 + H_2O \leftrightarrow HSO_3^- + H_3O^+ \tag{5.25}$$

Hydrolysis of bisulfite ion:

$$HSO_3^- + H_2O \leftrightarrow SO_3^{2-} + H_3O^+ \tag{5.26}$$

Since, sulfite (SO_3^{2-}) and bisulfite (HSO_3^-) ions are generated when sulphurous acid (H_2SO_3) dissolves in water, the effects of these anions on carbon steel corrosion needed to be studied. As discussed earlier, sodium ion (Na^+) had a negligible effect on increasing the corrosion rates. Therefore, sodium salts of sulfite (SO_3^{2-}) and bisulfite (HSO_3^-) were selected to study their effects on carbon steel corrosion to ensure that the corrosion was primary a consequence of either sulfite or bisulfite ions. Consequently, sodium sulfite (Na_2SO_3) and sodium bisulfite ($NaHSO_3$) were additionally introduced to the study of their effects on carbon steel corrosion.

5.4.1 The effect of sulphurous acid (H_2SO_3) on the corrosion rate

In order to discuss the effect of sulphurous acid (H_2SO_3) on the corrosion rate, the corrosion behaviour of the acid was, hereafter, divided into three regions, as presented in Figure 5.4. The first region was at acid concentrations below 15 ppm, the second region was at acid concentrations between 15 to 75 ppm, and the third region was at acid concentrations of 75 to 400 ppm.

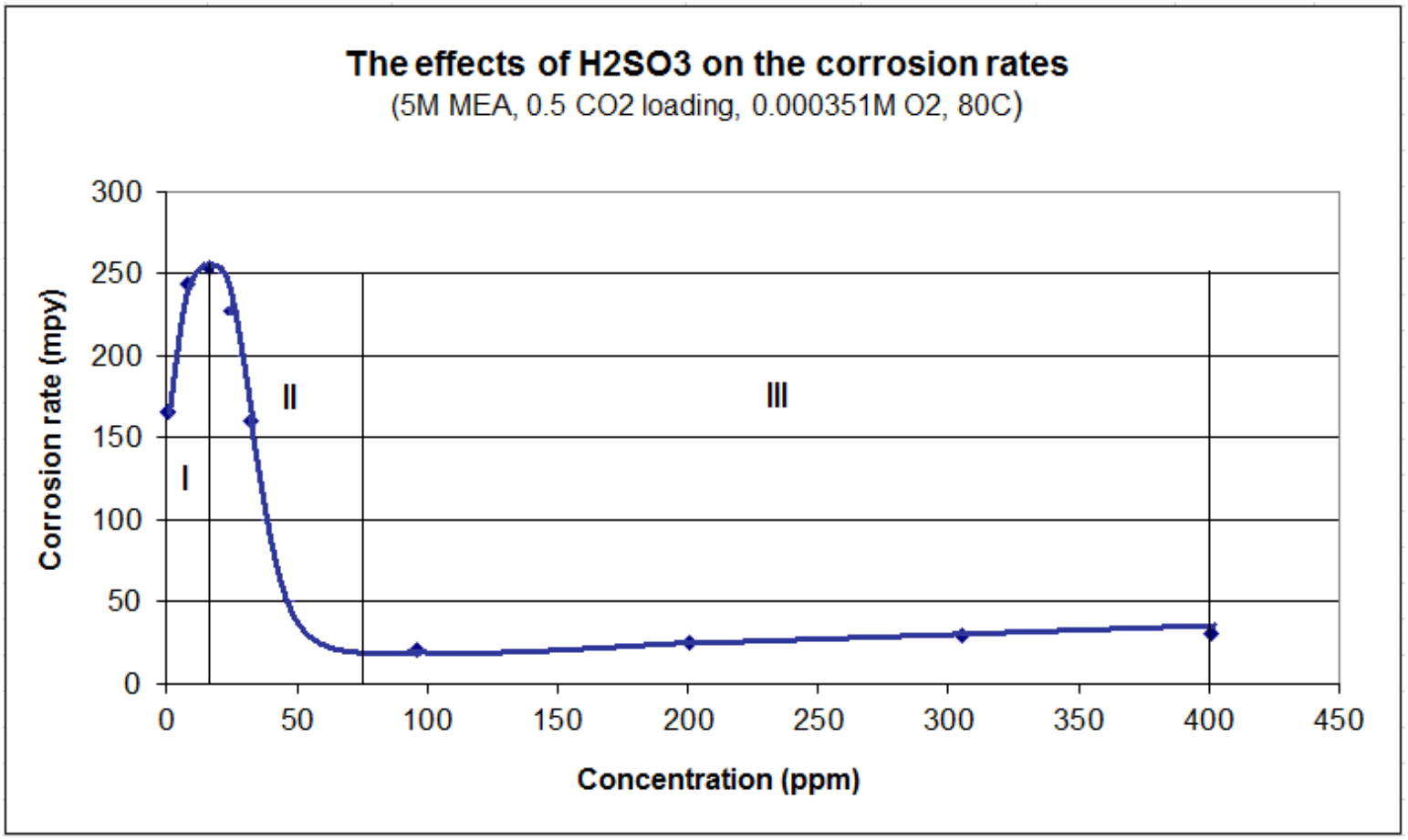

Figure 5.4: The corrosion behaviour of H_2SO_3 on carbon steel 1020 (5.5 %error). (Original in colour)

In the first region, the corrosion rates strongly increased with small acid concentration increases, which was mainly due to the hydrolysis reactions of sulphurous acid (H_2SO_3) and bisulfite ion (HSO_3^-) where sulphurous acid (H_2SO_3) itself and hydronium ion (H_3O^+) produced from these reactions behaved as oxidizing agents to accelerate the corrosion process. However, it should be noted that even though there was some dissolved oxygen in the solution, with a very low concentration of acid in this region, the hydrolysis reactions were likely to be the primary cause of the corrosion instead of the reactions of oxygen (O_2) with sulfite and/or bisulfite ions.

Hydrolysis of sulphurous acid:

$$H_2SO_3 + H_2O \leftrightarrow HSO_3^- + H_3O^+ \tag{5.25}$$

Hydrolysis of bisulfite ion:

$$HSO_3^- + H_2O \leftrightarrow SO_3^{2-} + H_3O^+ \tag{5.26}$$

Iron dissolution:

$$Fe \rightarrow Fe^{2+} + 2e^- \tag{5.5}$$

(Standard electrode potential (E_0^0) is -0.44 V for a half cell *reduction* reaction.)

Reduction of hydrogen ion:

$$2H^+ + 2e^- \rightarrow H_2 \tag{5.6}$$

(Standard electrode potential (E_0^0) is 0 V.)

Reduction of hydronium ion:

$$2H_3O^+ + 2e^- \leftrightarrow 2H_2O + H_2 \tag{5.7}$$

Reduction of sulphurous acid:

$$H_2SO_3 + 2H^+ + 4e^- \leftrightarrow S_2O_3^{2-} + 3H_2O \qquad (5.27)$$

(Standard electrode potential (E_0^0) is 0.40 V.)

In the second region, the corrosion rates reduced sharply with increasing sulphurous acid concentrations. This was a consequence of a cathodic protection primarily due to the reactions between bisulfite ion and/or sulfite ion with dissolved oxygen (O_2). By adding sulphurous acid, bisulfite and sulfite ions were generated and behaved as corrosion reducing agents in that they supplied their own electrons to the oxidizing agents, primarily to dissolved oxygen. It is indicated from the corrosion potentials (E_{corr}) in the Tafel plot, presented in Figure 5.5, that the potentials shifted to lower values when the acid concentrations increased, where the difference in the polarization plot was more pronounce in the cathodic region. In other words, dissolved oxygen, which is well-known to be one of the oxidizing agents that cause corrosion, in sulphurous acid systems, it reacted with bisulfite and sulfite ions in the solution. Thus, the bisulfite and sulfite ions behaved as oxygen scavengers and reduced oxygen concentration in the solution, which resulted in the reduction of the corrosion rates due to less oxidizing agent being available to participate in the electrochemical reactions.

Reaction of sulfite ion with dissolved oxygen:

$$SO_3^{2-} + \frac{1}{2}O_2 \leftrightarrow SO_4^{2-} \qquad (5.28)$$

Reaction of bisulfite ion with dissolved oxygen:

$$HSO_3^- + \frac{1}{2}O_2 \leftrightarrow SO_4^{2-} + H^+ \qquad (5.29)$$

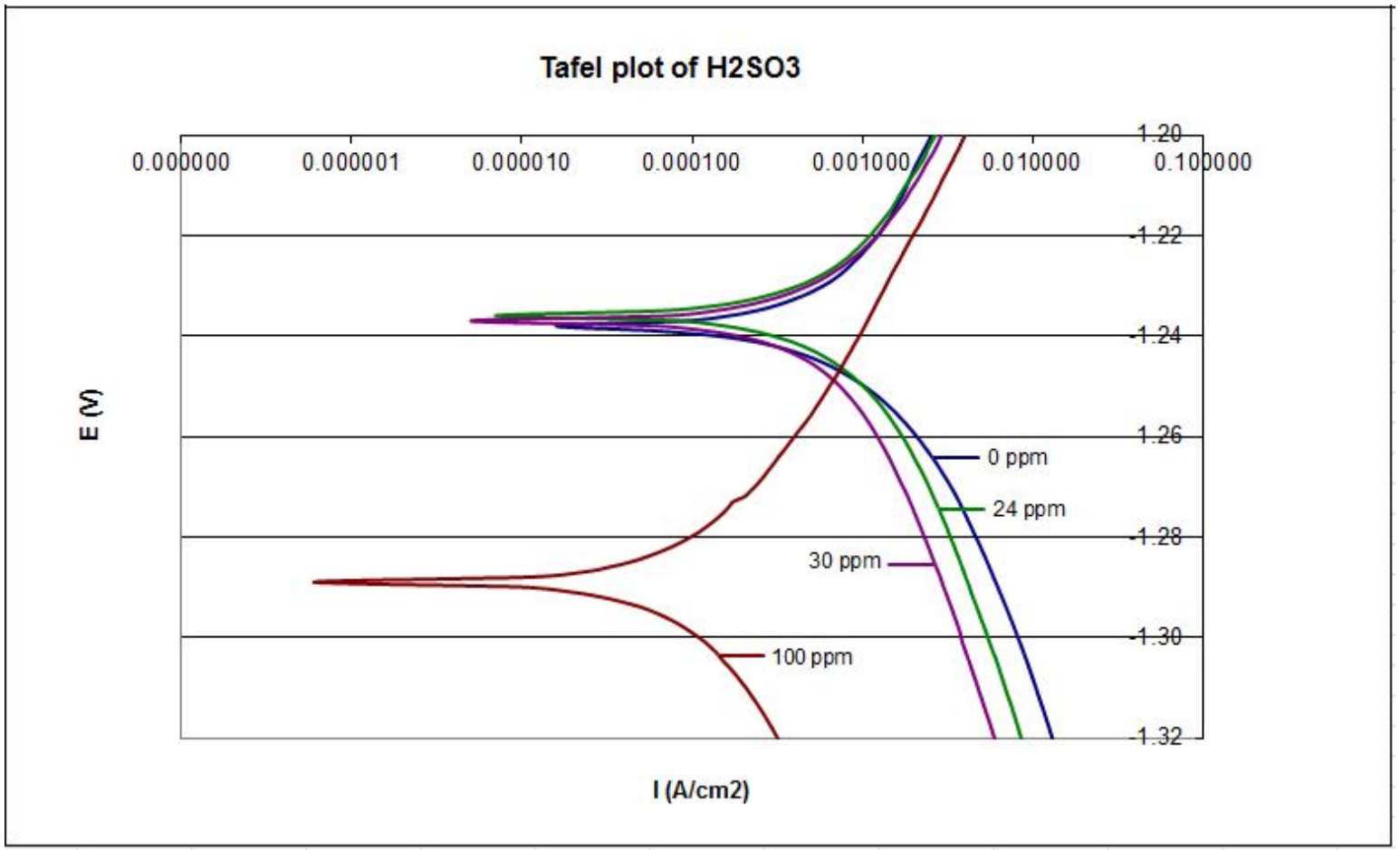

Figure 5.5: Tafel plots of 0 (no H_2SO_3), 24, 30, and 100 ppm H_2SO_3. (Original in colour)

In the third region, the corrosion rates were still inhibited by the oxygen scavenging behaviours of bisulfite and sulfite ions, which was indicated from the corrosion potentials (E_{corr}) continually shifting to the lower negative values as the acid concentrations increased, as presented in Figure 5.6. However, there were slight increases of the corrosion rates with increasing acid concentrations. This was because the reactions between bisulfite and sulfite ions with dissolved oxygen increased as acid concentrations increased but the sulphate ion, which was produced simultaneously with the oxygen scavenging reactions, appeared to slightly accelerate the corrosion process by either behaving as an oxidizing agent or by combining with ferrous ion (Fe^{2+}), which helped to stimulate another ion dissolution. Therefore, when the acid concentration went beyond a certain point (75 ppm), the presence of the sulphate ion started to have the above effect, resulting in the slight increases of the corrosion rates that was seen.

Reduction of sulphate ion:

$$SO_4^{2-} + 4H^+ + 2e^- \leftrightarrow H_2SO_3 + H_2O \qquad (5.19)$$

(Standard electrode potential (E_0^0) is 0.17 V.)

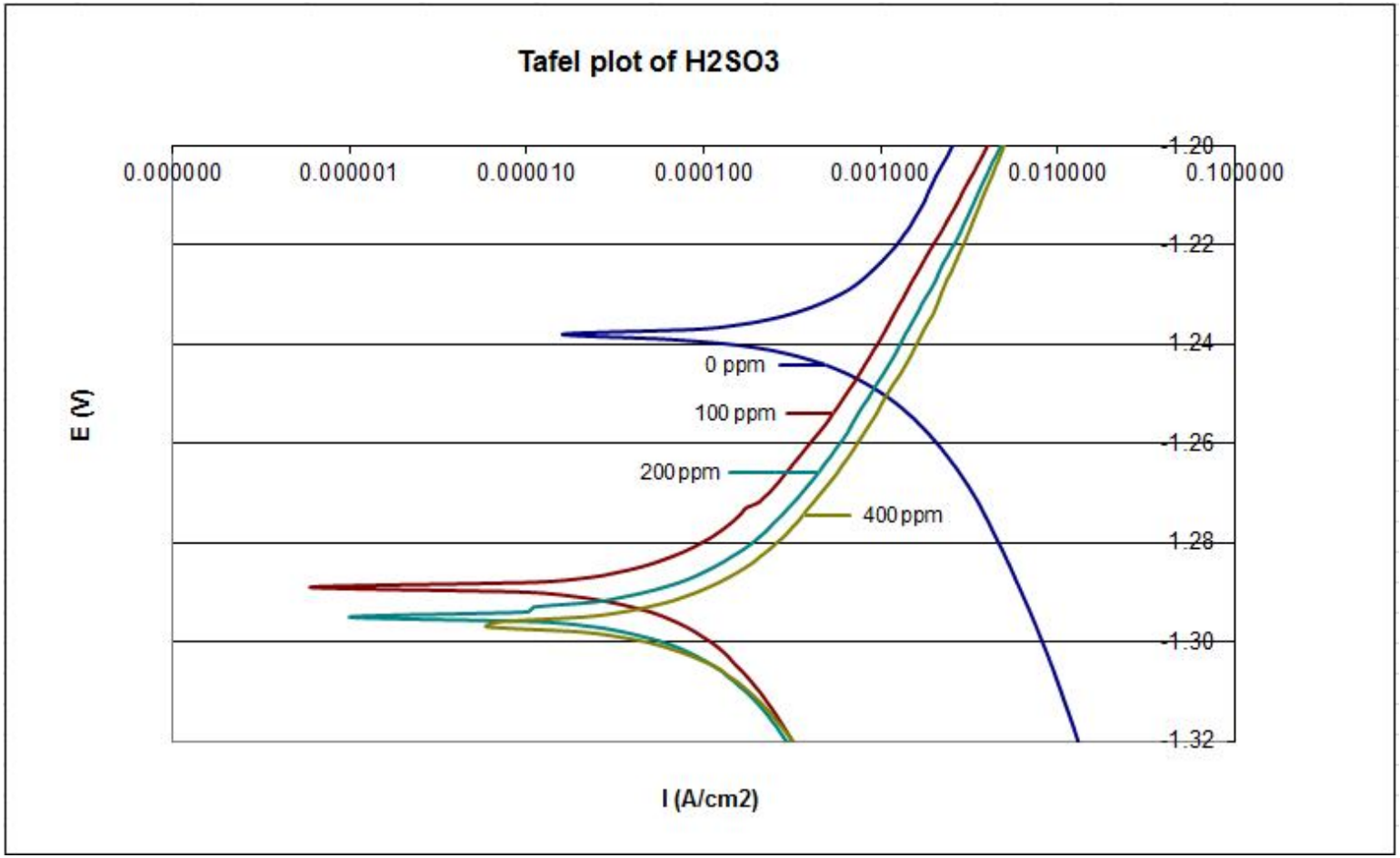

Figure 5.6: Tafel plots of 0 (no H_2SO_3), 100, 200, and 400 ppm H_2SO_3. (Original in colour)

5.4.2 The influences of sulfite (SO_3^{2-}) and bisulfite (HSO_3^-) ions on the corrosion behaviour of sulphurous acid (H_2SO_3)

In sodium sulfite (Na_2SO_3) and sodium bisulfite ($NaHSO_3$) systems, the three regions of corrosion behaviour observed in the sulphurous acid (H_2SO_3) system were also found, as presented in Figure 5.7. The first region was at sodium sulfite concentrations below 25 ppm and sodium bisulfite concentrations below 12 ppm, where the corrosion rates increased with increasing salt concentrations, mainly due to the hydrolysis reactions of sulphurous acid (H_2SO_3) and the bisulfite ion (HSO_3^-). The second region was at sodium sulfite concentrations from 25 to 80 ppm and sodium bisulfite concentrations from 12 to 50 ppm, where the corrosion rates decreased with increasing salt concentrations, which were a consequence of the oxygen scavenging behaviours of sulfite and bisulfite ions. The last region was found at sodium sulfite concentrations 80 to 400 ppm and sodium bisulfite concentrations from 50 to 400 ppm, where the corrosion rates were still inhibited by the cathodic protection, but small increments of corrosion rate increase were found due to the production of sulphate ion.

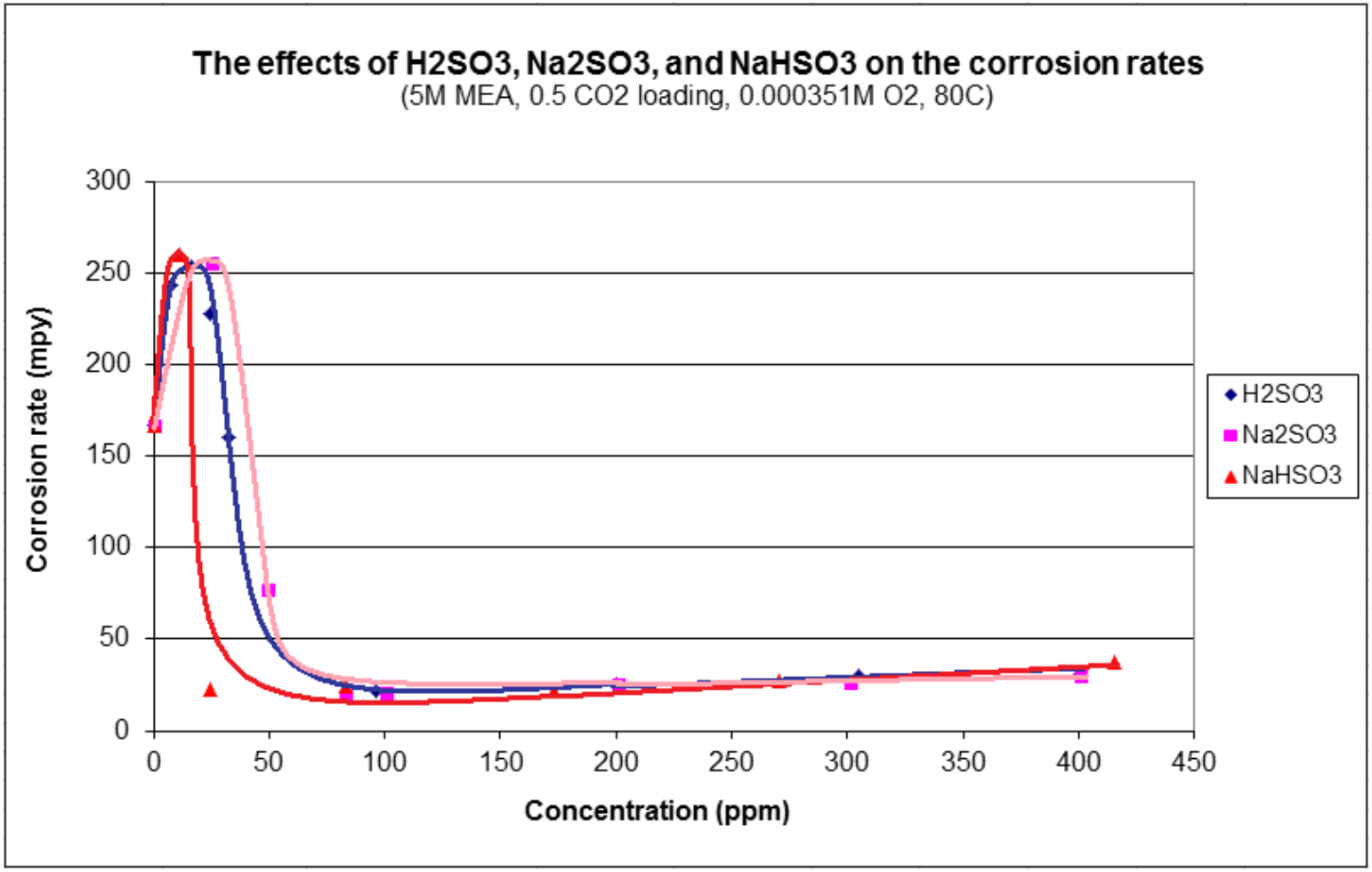

Figure 5.7: The corrosion behaviours of Na_2SO_3, $NaHSO_3$, and H_2SO_3 systems on carbon steel 1020 (%error: 6.3%, 3.2%, and 5.5% in Na_2SO_3, $NaHSO_3$, and H_2SO_3 systems, respectively). (Original in colour)

The influences of sulfite (SO_3^{2-}) and bisulfite (HSO_3^-) ions on corrosion were studied by comparing between the systems with sodium sulfite (Na_2SO_3) and sodium bisulfite ($NaHSO_3$) added. Within the corrosion-accelerated region, the first region, the same corrosion rate was reached at a lower salt concentration in the bisulfite system compared to the sulfite system, which indicated that the bisulfite ion induced more corrosion when compared to the sulfite ion at the same salt concentration. On the other hand, within the corrosion-inhibited region, the second region, the opposite trend was observed. The bisulfite system showed better inhibition performance, as indicated by the fact that at the same salt concentration, corrosion rate was lower in the bisulfite system compared to the sulfite system. In addition, sulphurous acid (H_2SO_3), which can be hydrolyzed to both sulfite (SO_3^{2-}) and bisulfite (HSO_3^-) ions, showed corrosion behaviour somewhere in between the sodium sulfite (Na_2SO_3) and sodium bisulfite ($NaHSO_3$) systems throughout the concentrations used in the study.

5.5 The effect of nitric acid (HNO_3) on carbon steel (1020) corrosion

Nitrogen dioxide (NO_2) is one of the major toxic gases present in coal-fired flue gas. When nitrogen dioxide dissolves in water, nitric acid (HNO_3) is generated. Thus, in this study, nitric acid was used to represent nitrogen dioxide in an aqueous solution. The corrosion behaviour of nitric acid on carbon steel 1020 is presented in Figure 5.8. For nitric acid concentrations of 0 to 100 ppm, the corrosion rates rapidly increased with increasing acid concentration. Since nitric acid is a very strong acid, as soon as it dissolved in water, hydrogen ion (H^+) and nitrate ion (NO_3^-) was formed. Hydrogen ion has known to behave as the oxidizing agent. The nitrate ion either behaved as an oxidizing agent to accelerate the iron dissolution and induced corrosion through several possible reduction reactions, as presented in equation 5.30 to 5.33, where the standard electrode potentials of the reductions of the nitrate ion appear to be well above the standard potential of the iron dissolution; or the nitrate ion possibly competed with other oxidizing agents to combine with ferrous ion (Fe^{2+}) and formed iron nitrate ($Fe(NO_3)_2$), which has a high solubility in an aqueous solution. The ferrous nitrate then dissolved back into the solution, leaving the metal surface open for further attack by the oxidizing agents. This was confirmed by using SEM-EDS techniques, as presented in Figure 5.9. No nitrogen element was found in the corrosion products due to all iron nitrate possibly being dissolved back into the solution.

Iron dissolution:

$$Fe \rightarrow Fe^{2+} + 2e^- \qquad (5.5)$$

(Standard electrode potential (E_0^0) is -0.44 V for a half cell *reduction* reaction.)

Reductions of nitrate ion:

$$NO_3^- + 2H^+ + e^- \rightarrow NO_2 + H_2O \quad (5.30)$$

(Standard electrode potential (E_0^0) is 0.80 V.)

$$NO_3^- + 10H^+ + 8e^- \rightarrow NH_4^+ + 3H_2O \quad (5.31)$$

(Standard electrode potential (E_0^0) is 0.88 V.)

$$NO_3^- + 3H^+ + 2e^- \rightarrow HNO_2 + H_2O \quad (5.32)$$

(Standard electrode potential (E_0^0) is 0.94 V.)

$$NO_3^- + 4H^+ + 3e^- \rightarrow NO + 2H_2O \quad (5.33)$$

(Standard electrode potential (E_0^0) is 0.96 V.)

However, when nitric acid concentration exceeded 100 ppm, the slope of the increase of corrosion rate was reduced, which possibly occurred because a passive layer had already been formed on the metal surface, which helped retard the surface reaction of the reduction of nitrate ion.

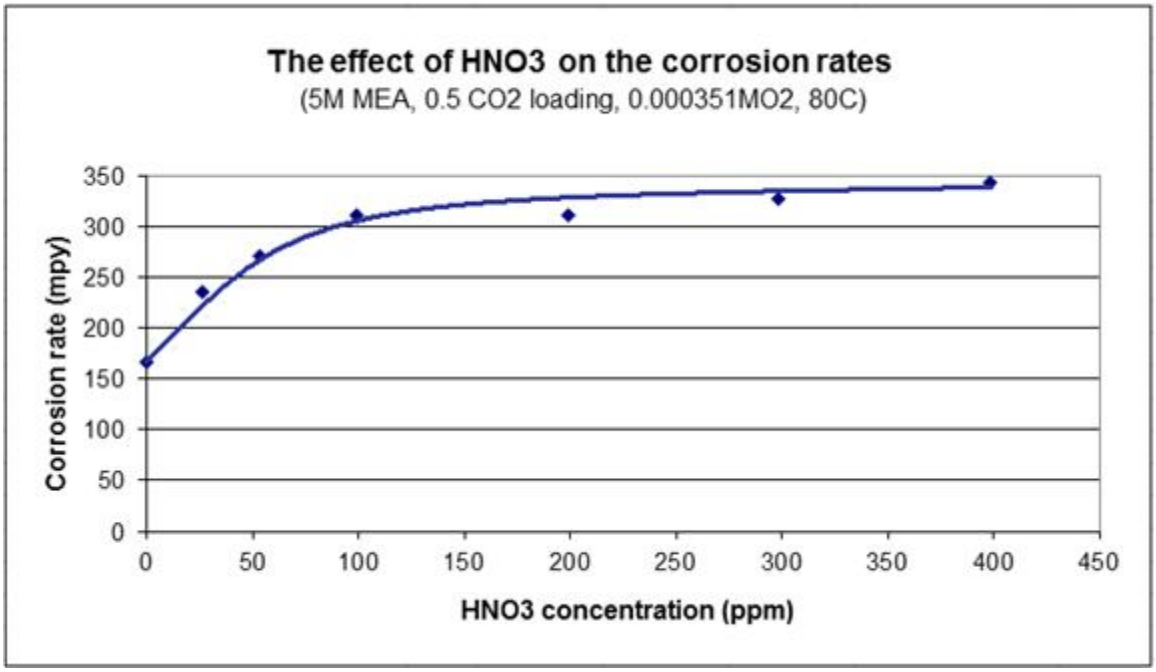

Figure 5.8: The corrosion behaviour of HNO_3 system on carbon steel 1020 (1.6 %error).

(Original in colour)

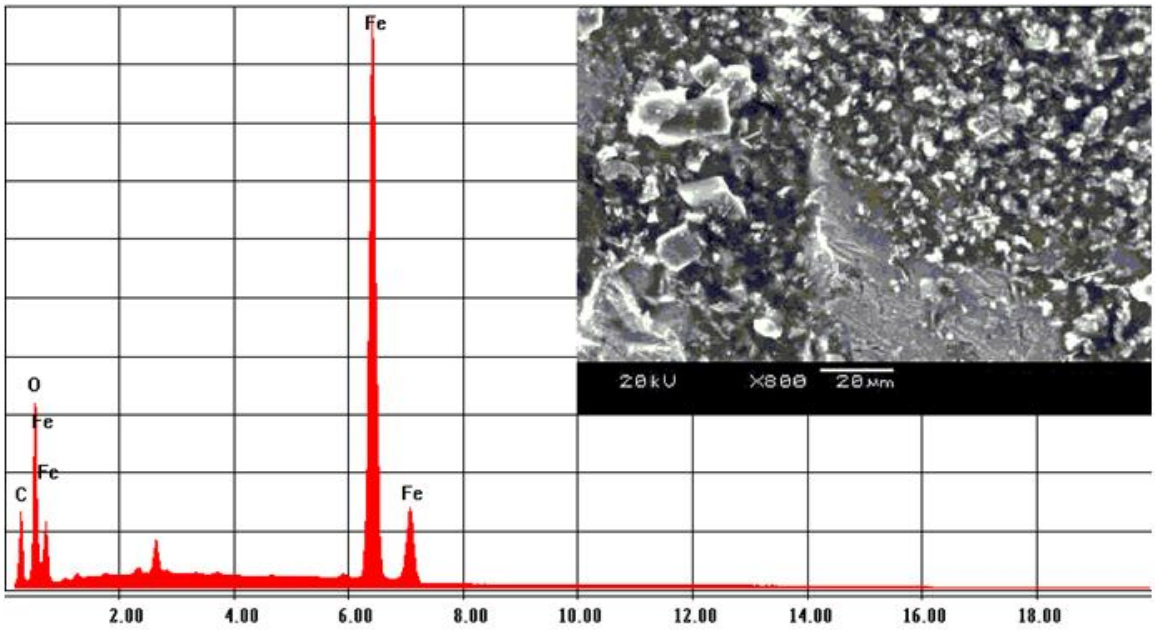

Figure 5.9: SEM-EDS scan for the corrosion product in HNO_3 system. (Original in colour)

5.6 The products of carbon steel (1020) corrosion in systems containing various additives (NaCl, HCl, $FeCl_2$, Na_2SO_4, H_2SO_4, $FeSO_4{\cdot}7H_2O$, Na_2SO_3, H_2SO_3, and HNO_3) under the base-case conditions

A corrosion specimen, carbon steel 1020, was tested for corrosion products using SEM-EDS techniques. The SEM was primarily used to capture images of the products, while the EDS scan was performed in order to characterize the elements present on the product layer. Since the EDS scan was able to distinguish only the chemical elements associated with the corrosion products, product determination was accomplished by comparing the results of the EDS scans of the product layers with the scans obtained from the standard chemicals of iron oxides because the corrosion products of carbon steel are well known to consist mainly of iron oxide compounds. Therefore, four types of iron oxides, ferric oxide (Fe_2O_3), iron (II,III) oxide (Fe_3O_4), ferrous oxide (FeO), and goethite (FeOOH)), and ferrous sulphate heptahydrate ($FeSO_4{\cdot}7H_2O$), which are commonly-found as typical corrosion products, were selected to be the standard chemicals for the EDS scans, and a ratio between %wt of iron (Fe) and %wt oxygen (O) elements was chosen to be a preliminary characterization to determine what chemical species potentially existed in the product layers by comparing the ratios of the products with the standard chemicals. The results of the EDS scans of the products in all the corrosion systems are presented in Table 5.6, and a relative %wt of elements present in the product layers is illustrated, along with the %wt of elements present in the standard iron oxides and iron sulphate.

Table 5.6: The EDS scans of the corrosion products in the systems containing various additives under the base-case conditions and the standard iron compounds.

Compound	Relative %wt. of element									Fe/O ratio
	C	Fe	O	Na	Cl	S	N	Others	%Total	
Base case	12.21	76.16	11.63						100	**6.55**
NaCl	14.42	60.96	21.21	2.16	0.54			0.71	100	**2.87**
HCl	8.63	71.69	15.69		2.11			1.88	100	**4.57**
$FeCl_2$	12.75	70.1	12.53		1.42			3.2	100	**5.59**
Na_2SO_4	66.41	18.39	11.05			1.36		2.79	100	**1.66**
H_2SO_4	60	30	7.03			0.53		2.44	100	**4.27**
$FeSO_4 \cdot 7H_2O$	17.17	71.35	10.13					1.35	100	**7.04**
Na_2SO_3	22.16	56.06	20.86			0.53		0.39	100	**2.69**
H_2SO_3	34.2	39	17.73			0.49		8.58	100	**2.20**
HNO_3	18.6	68.1	11.65					1.65	100	**5.85**
Standard Compound	**Relative %wt. of element**									**Fe/O ratio**
	C	**Fe**	**O**	**Na**	**Cl**	**S**	**N**	**Other**	**%Total**	
Fe_3O_4 (greyish-black)	5.12	82.26	12.32					0.30	100	**6.68**
Fe_2O_3 (reddish-brown)	12.70	63.68	23.62						100	**2.70**
FeO (black)		87.16	11.66					1.18	100	**7.48**
FeOOH (yellow-brown)	7.82	59.59	19.07					13.52	100	**3.12**
$FeSO_4 \cdot 7H_2O$ (green)	16.31	8.13	62.60			8.72		4.24	100	**0.13**

Unfortunately, the Fe/O ratio was not sufficient to confidently conclude which of the iron compounds represented the corrosion products in the tested systems due to the fact that the Fe/O ratios of the products were varied yet seemed to be in the range of most of the standard iron oxides. However, by physical appearance, the products tended to be a combination of goethite (FeOOH; yellow-brown) and iron (II,III) oxide (Fe_3O_4; greyish-black) based on the products' colours. Since, ferrous hydroxide ($Fe(OH)_2$), which was one of the primary corrosion products generated by the reaction between ferrous ion (Fe^{2+}) and hydroxide ion (OH^-), was not stable, as with the access to oxygen (O_2) and water, it potentially oxidized to a trivalent hydrated iron oxide (ferric oxide; Fe_2O_3; reddish-brown) or an iron hydroxide (goethite; FeOOH; yellow-brown), or, if the access to oxygen was greatly limited, iron (II,III) oxide (Fe_3O_4; greyish-black) was formed instead of the trivalent corrosion product (Soosaiprakasam and Veawab, 2008). The possible reaction schemes of the corrosion product formations are presented in the equations shown on the following page below. Therefore, from visual observation, where the corrosion products were a combination of yellow-brown and/or greyish-black colour compounds, goethite (FeOOH; yellow-brown) and iron (II,III) oxide (Fe_3O_4; greyish-black) were potentially the products of the carbon steel (1020) corrosion that occurred in the presence of various additives under the base-case conditions. Even though the Fe/O ratio was not able to confidently determine the species of the corrosion products, it may be use to confirm that there was a possibility for the corrosion products to be a combination of goethite and iron (II,III) oxide due to the fact that the Fe/O ratios of both compounds were in the range of most of the corrosion products found in the study systems. In addition, total iron ions concentration (Fe^{2+} and Fe^{3+}) after performing the corrosion experiments was determined

by ICP-MS, from which the concentration appeared to vary between 3.4 to 7.3 ppm throughout the study systems, as presented in Table 5.7. The SEM images and EDS scanning images of all the systems are shown in Figures 5.9 to 5.13.

Formation of ferrous hydroxide:

$$Fe^{2+} + 2OH^{-} \leftrightarrow Fe(OH)_2 \tag{5.12}$$

Formation of goethite:

$$2Fe^{2+} + \frac{1}{2}O_2 + 3H_2O \leftrightarrow 2FeOOH + 4H^{+} \tag{5.34}$$

$$2Fe(OH)_2 + \frac{1}{2}O_2 \leftrightarrow 2FeOOH + H_2O \tag{5.35}$$

Formation of iron (II,III) oxide or magnetite (Fe_3O_4):

$$3Fe + 4H_2O \rightarrow Fe_3O_4 + 4H_2 \tag{5.16}$$

$$Fe(OH)_2 + 2FeOOH \leftrightarrow Fe_3O_4 + 2H_2O \tag{5.36}$$

Table 5.7: Total iron ions (Fe^{2+} and Fe^{3+}) concentrations after performing the corrosion experiments in systems containing various additives under the base-case conditions.

System name	Total iron ions concentration (Fe^{2+} and Fe^{3+}; ppm)
5M MEA (before corrosion)	<MDL
5M MEA	3.4
2000 ppm NaCl	5.0
1500 ppm HCl	5.5
2000 ppm HCl	5.4
1000 ppm $FeCl_2$ (before corrosion)	360.4
1000 ppm $FeCl_2$	4.4
2000 ppm $FeCl_2$	7.3
9 ppm Na_2SO_4	5.2
12 ppm Na_2SO_4	5.5
9 ppm H_2SO_4	4.2
12 ppm H_2SO_4	4.5
9 ppm $FeSO_4.7H_2O$	6.7
12 ppm $FeSO_4.7H_2O$	6.8
100 ppm H_2SO_3	4.7
200 ppm H_2SO_3	4.6
400 ppm H_2SO_3 (before corrosion)	<MDL
400 ppm H_2SO_3	4.5
300 ppm Na_2SO_3	5
400 ppm Na_2SO_3	5.1
400 ppm HNO_3	5.3

**MDL is method detection limit*

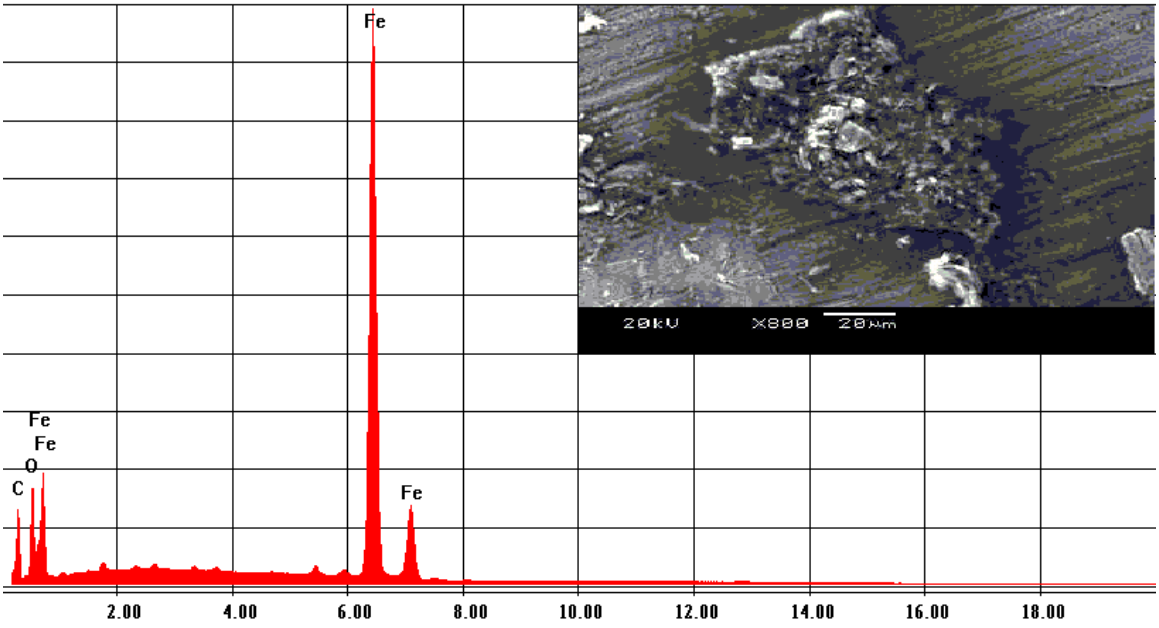

Figure 5.10: SEM-EDS scan for a base-case system. (Original in colour)

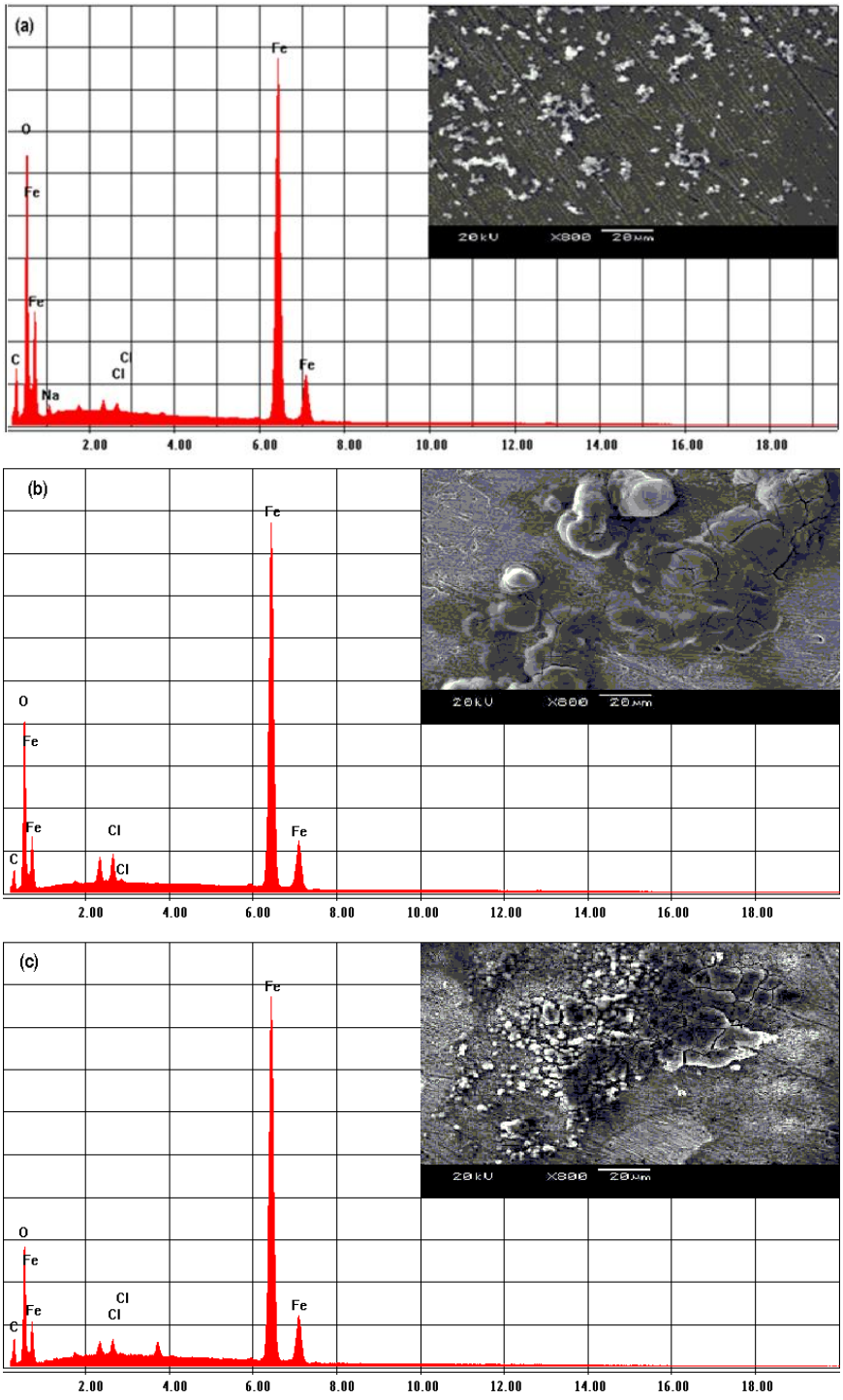

Figure 5.11: SEM-EDS scans for (a) NaCl system, (b) HCl system, and (c) $FeCl_2$ system. (Original in colour)

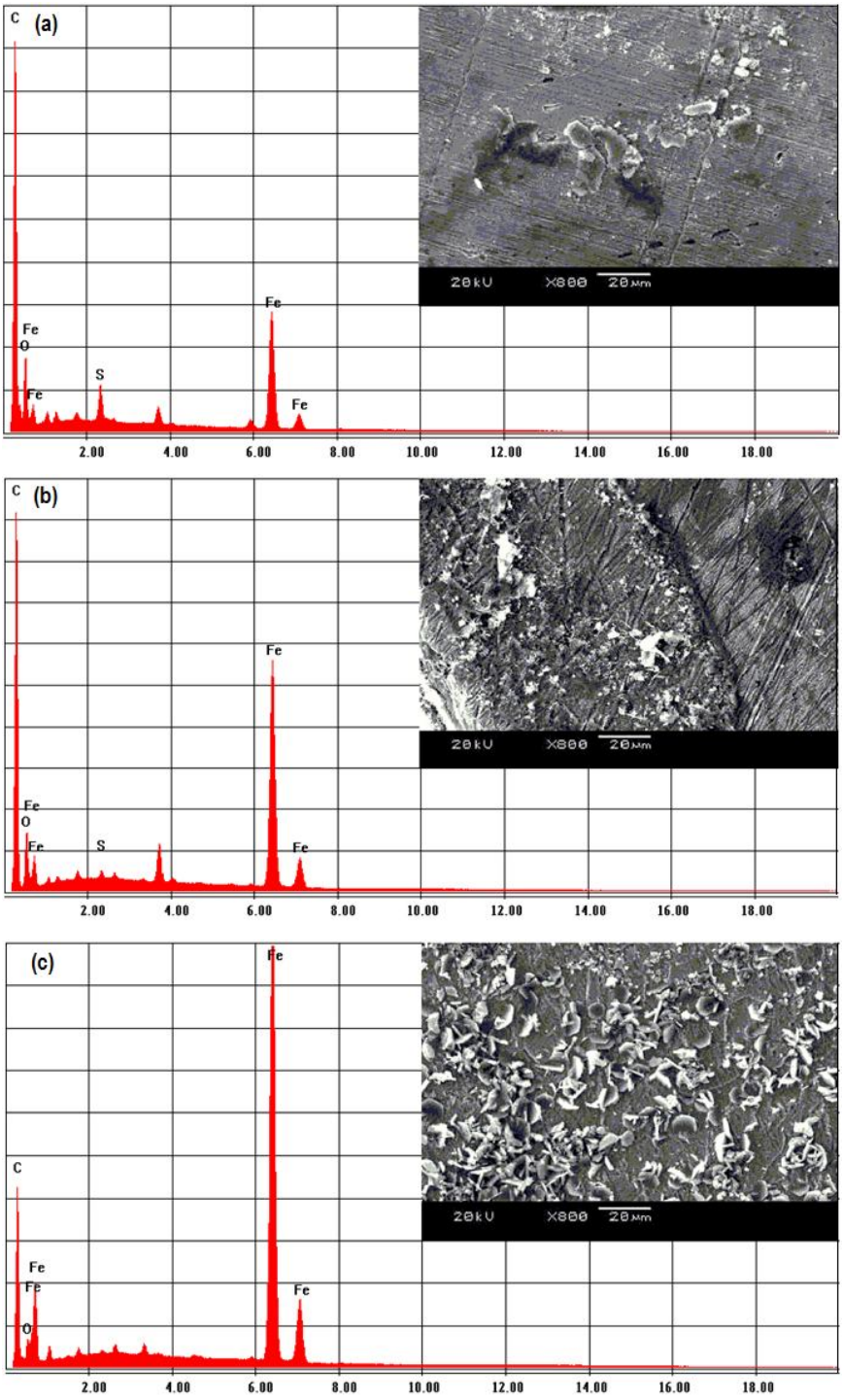

Figure 5.12: SEM-EDS scans for (a) Na_2SO_4 system, (b) H_2SO_4 system, and (c) $FeSO_4 \cdot 7H_2O$ system. (Original in colour)

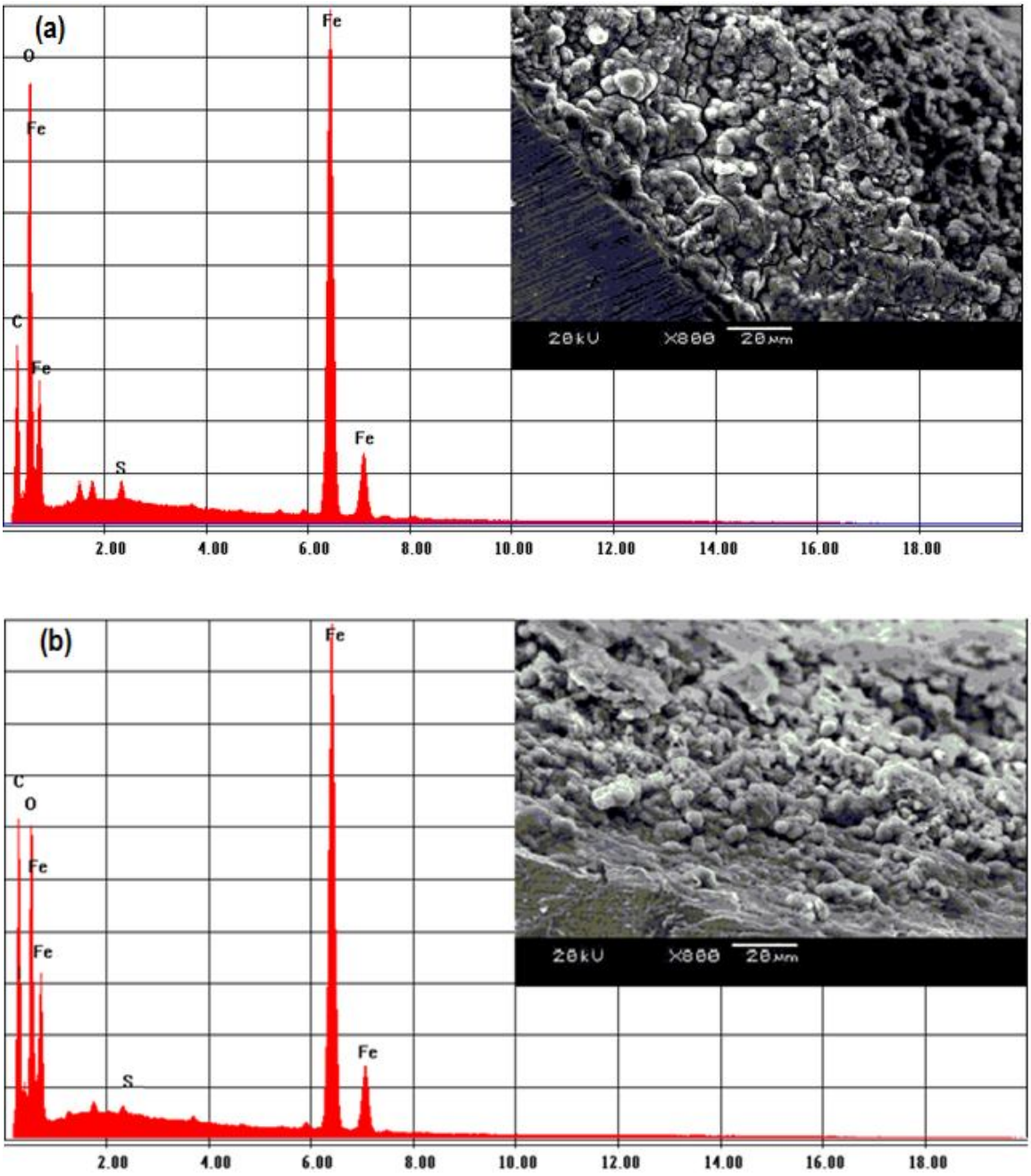

Figure 5.13: SEM-EDS scans for (a) Na_2SO_3 system and (b) H_2SO_3 system. (Original in colour)

5.7 Kinetic study of mixed additives on carbon steel (1020) corrosion

In the kinetic study of the mixed additives on carbon steel (1020) corrosion, hydrochloric acid (HCl), sulphurous acid (H_2SO_3), sulfuric acid (H_2SO_4), and nitric acid (HNO_3) were selected to represent a source of chloride compound and the aqueous solutions of sulphur dioxide (SO_2), sulphur trioxide (SO_3), and nitrogen dioxide (NO_2), respectively. All the experiments in the kinetic study were performed under the base-case conditions except for one system where two additional temperatures (30°C and 60°C) were introduced in order to study the effects of temperature. The concentrations of the additives were selected based on their positive effects on the corrosion rates as discussed previously in the single additive systems studies. The experimental conditions of the kinetics study of the mixed additives on carbon steel (1020) corrosion are illustrated in Table 5.8. MEA, CO_2 loading, and O_2 concentration were kept constant throughout the corrosion study, and the concentrations of the additives were varied between 0 to 2000 ppm of HCl, 0 to 16 of H_2SO_3, 0 to 12 ppm of H_2SO_4, and 0 to 400 ppm of HNO_3.

Table 5.8: The experimental conditions of the kinetic study of the mixed additives on carbon steel (C1020) corrosion.

Component	Condition
MEA concentration	5M (0.9% error)
CO_2 loading	0.5 mol CO_2/mol MEA (2.3% error)
O_2 concentration	0.000351M (at 80°C)
Temperature	80°C (±1°C)
Pressure	Atmospheric pressure (1 atm)
HCl concentration	0 to 2000 ppm
H_2SO_3 concentration	0 to 16 ppm
H_2SO_4 concentration	0 to 12 ppm
HNO_3 concentration	0 to 400 ppm

Kinetics studies are essential to understanding the level of material corrosiveness caused by a given compound. One of the well-known fundamental kinetic correlations is the power law model. In the mixed additives, the power law model was expressed as:

$$r_{corrosion} = k_0 \cdot e^{\frac{-E}{RT}} \cdot [MEA]^a \cdot [O_2]^b \cdot [CO_2]^c \cdot [HCl]^d \cdot [H_2SO_3]^e \cdot [H_2SO_4]^f \cdot [HNO_3]^g \quad (5.37)$$

where: r is the corrosion rate (mpy)

k_0 is the pre-exponential factor or collision constant

E is the activation energy (J/mol)

R is the gas constant (8.314 J/(mol·K))

T is the system temperature (K)

[ ] is the concentration (M)

Since the carbon steel corrosion study focused only the reactions in the liquid phase, a temperature dependence term in the power law model ($k_0 \cdot e^{\frac{-E}{RT}}$) did not accurately represent the study system due to the fact that R is a gas constant. Consequently, it was replaced by a different temperature dependence term ($k_0 \cdot e^{\frac{-H_T}{T}}$) derived based on the system's enthalpy (H; J/mol), which suitably represented the temperature dependence in a liquid phase and which also was a function of temperature. Consequently, equation 5.37 was rearranged into equation 5.38:

$$r_{corrosion} = k_0 \cdot e^{\frac{-H_T}{T}} \cdot [MEA]^a \cdot [O_2]^b \cdot [CO_2]^c \cdot [HCl]^d \cdot [H_2SO_3]^e \cdot [H_2SO_4]^f \cdot [HNO_3]^g \quad (5.38)$$

where: H_T is the temperature sensitivity constant in liquid phase (K)

Moreover, MEA concentration (5M), O_2 concentration (0.000351M), and CO_2 loading (0.5 mol CO_2 per mol MEA) were kept constant in all the experiments, so equation 5.38 was again rearranged to:

$$r_{corrosion} = k \cdot e^{\frac{-H_T}{T}} \cdot [HCl]^d \cdot [H_2SO_3]^e \cdot [H_2SO_4]^f \cdot [HNO_3]^g \quad (5.39)$$

where: k is the rate constant

In order to distinctively signify the effects of either cation, which was mainly hydrogen ion (H^+), or anions (Cl^-, HSO_3^-, SO_3^{2-}, SO_4^{2-}, and NO_3^-) on the corrosion rates, and also to compensate for the absence of any additives in the rate equation, the power law model expressed in equation 5.39 was rearranged to a modified power law model, as presented in equation 5.40:

$$r_{corrosion} = k \cdot e^{\frac{-H_T}{T}} \cdot [H^+]^d \cdot ([Cl^-]^e + [HSO_3^-]^f + [SO_3^{2-}]^g + [SO_4^{2-}]^h + [NO_3^-]^i) \quad (5.40)$$

where: k is the rate constant

To obtain a reliable rate expression, variables should be varied a minimum of three times, and the number of variables should at least equal the number of parameters minus one. Thus, there were seven variables (the concentrations of H^+, Cl^-, HSO_3^-, SO_3^{2-}, SO_4^{2-}, NO_3^-, and T) in the mixed-additives systems that were changed at least three times in order to determine eight parameters expressed as k, d, e, f, g, h, i and H_T, which demonstrated a rate constant, the order of reactions, and a temperature sensitivity constant. By performing multiple non-linear regressions with the non-linear regression package (NLREG), the modified power law rate equation for the systems containing all four additives (HCl, H_2SO_3, H_2SO_4, and HNO_3) are illustrated in equation 5.41, which provides an acceptable percentage of average absolute deviation (%AAD) of 8.6%.

$$r_{corrosion} = (8.922E+09)\cdot e^{\frac{-6430}{T}} \cdot [H^+]^{0.118} \cdot ([Cl^-]^{0.106} + [HSO_3^-]^{0.007} + [SO_3^{2-}]^{0.006} + [SO_4^{2-}]^{0.006} + [NO_3^-]^{0.102}) \tag{5.41}$$

where the percentage of average absolute deviations (%AAD) was calculated by equation 5.42:

$$\frac{\sum_{i=1}^{n} \left| \frac{r_{Exp} - r_{\Pr edicted}}{r_{Exp}} \right|}{n} \times 100 \tag{5.42}$$

where: r_{Exp} is the experimental corrosion rate (mpy)

$r_{\Pr edicted}$ is the predicted corrosion rate (mpy).

It should be noted that the modified power law rate expression illustrated in equation 5.41 only effectively represented the systems in which all the additives (HCl, H_2SO_3, H_2SO_4, and HNO_3) were presented. Even though this work focused mainly on the systems containing all four additives, which represented four different components in a flue gas, it was considered beneficial to have some generalized rate equations for the systems containing fewer additives. Therefore, the generalized modified power law rate equations of single, binary, and tertiary additive systems are presented in Table 5.9, along with their percentage of average absolute deviations (%AAD), where the orders of reaction were kept the same but were different in terms of the rate constant.

Table 5.9: The modified power law rate equations of single, binary, tertiary, and four additives systems.

Run no.	Temperature (K)	Concentration (M)						Experimental corrosion rate (mpy)	Predicted rate (mpy)	%AAD
		H^+	Cl^-	HSO_3^-	SO_3^{2-}	SO_4^{2-}	NO_3^-			
1	353	0	0	0	0	0	0	166.35		
Single additive										
2	353	0.01500	0.015	0	0	0	0	187.37	199.08	**31.1**
3	353	0.03000	0.030	0	0	0	0	214.45	232.55	
4	353	0.04000	0.040	0	0	0	0	244.30	248.04	
5	353	0.00007	0	0.00004	0.000013	0	0	243.60	307.62	
6	353	0.00014	0	0.00008	0.000028	0	0	253.55	336.75	
7	353	0.00006	0	0	0	0.00003	0	177.00	152.33	
8	353	0.00012	0	0	0	0.00006	0	195.70	165.98	
9	353	0.00018	0	0	0	0.00009	0	204.35	174.52	
10	353	0.00024	0	0	0	0.00012	0	201.30	180.85	
11	353	0.00042	0	0	0	0	0.0004	235.50	92.80	
12	353	0.00084	0	0	0	0	0.0008	272.10	108.02	
13	353	0.00158	0	0	0	0	0.0016	312.05	123.97	
14	353	0.00315	0	0	0	0	0.0031	311.15	144.27	
15	353	0.00471	0	0	0	0	0.0047	327.10	157.63	
16	353	0.00628	0	0	0	0	0.0063	344.40	167.84	

$$r_{corrosion} = (4.162\,E+10)\cdot e^{\frac{-6430}{T}} \cdot [H^+]^{0.118} \cdot ([Cl^-]^{0.106} + [HSO_3^-]^{0.007} + [SO_3^{2-}]^{0.006} + [SO_4^{2-}]^{0.006} + [NO_3^-]^{0.102}) \quad (5.43)$$

Binary additives										
17	353	0.01503	0.015	0.00002	0.000007	0	0	182.60	283.87	
18	353	0.03006	0.030	0.00004	0.000013	0	0	225.70	314.97	
19	353	0.04009	0.040	0.00006	0.000020	0	0	239.10	329.15	
20	353	0.05512	0.055	0.00008	0.000026	0	0	259.10	345.36	
21	353	0.01506	0.015	0	0	0.00003	0	178.40	179.19	
22	353	0.03011	0.030	0	0	0.00006	0	195.40	200.89	
23	353	0.04019	0.040	0	0	0.00009	0	206.30	210.93	
24	353	0.05524	0.055	0	0	0.00012	0	226.30	222.42	
25	353	0.01657	0.015	0	0	0	0.0016	203.10	133.11	
26	353	0.03309	0.030	0	0	0	0.0032	253.70	155.20	
27	353	0.04459	0.040	0	0	0	0.0048	311.70	166.50	
28	353	0.06092	0.055	0	0	0	0.0063	368.00	178.16	
29	353	0.00010	0	0.00002	0.000007	0.00003	0	183.30	175.27	**26.9**
30	353	0.00018	0	0.00004	0.000013	0.00006	0	196.50	189.63	
31	353	0.00029	0	0.00006	0.000020	0.00009	0	224.60	200.91	
32	353	0.00039	0	0.00008	0.000027	0.00013	0	256.60	208.82	
33	353	0.00164	0	0.00002	0.000007	0	0.0016	240.70	208.28	
34	353	0.00327	0	0.00004	0.000013	0	0.0032	265.30	230.24	
35	353	0.00490	0	0.00006	0.000020	0	0.0048	335.20	244.23	
36	353	0.00676	0	0.00008	0.000027	0	0.0066	376.30	256.01	
37	353	0.00167	0	0	0	0.00003	0.0016	199.20	127.82	
38	353	0.00332	0	0	0	0.00006	0.0032	256.40	142.56	
39	353	0.00499	0	0	0	0.00009	0.0048	284.80	152.19	
40	353	0.00654	0	0	0	0.00012	0.0063	330.50	158.93	

$$r_{corrosion} = (1.517\,E + 10) \cdot e^{\frac{-6430}{T}} \cdot [H^+]^{0.118} \cdot ([Cl^-]^{0.106} + [HSO_3^-]^{0.007} + [SO_3^{2-}]^{0.006} + [SO_4^{2-}]^{0.006} + [NO_3^-]^{0.102}) \quad (5.44)$$

Tertiary additives										
41	353	0.01509	0.015	0.00002	0.000007	0.00003	0	181.30	310.15	
42	353	0.03018	0.030	0.00004	0.000013	0.00006	0	210.30	342.39	
43	353	0.04028	0.040	0.00006	0.000020	0.00009	0	211.40	357.17	
44	353	0.05536	0.055	0.00008	0.000026	0.00012	0	242.50	373.84	
45	353	0.01661	0.015	0.00002	0.000007	0	0.0016	248.20	275.45	
46	353	0.03316	0.030	0.00004	0.000013	0	0.0032	305.70	308.14	
47	353	0.04468	0.040	0.00006	0.000020	0	0.0048	322.50	324.20	**24.5**
48	353	0.06103	0.055	0.00008	0.000025	0	0.0063	387.50	340.95	
49	353	0.00170	0	0.00002	0.000007	0.00003	0.0016	225.10	231.55	
50	353	0.00339	0	0.00004	0.000013	0.00006	0.0032	282.20	254.81	
51	353	0.00509	0	0.00006	0.000020	0.00009	0.0048	355.10	269.77	
52	353	0.00666	0	0.00008	0.000026	0.00012	0.0063	378.40	280.17	
53	353	0.01663	0.015	0	0	0.00003	0.0016	215.10	191.36	
54	353	0.03321	0.030	0	0	0.00006	0.0032	235.70	216.51	
55	353	0.04477	0.040	0	0	0.00009	0.0048	260.10	229.14	
56	353	0.06116	0.055	0	0	0.00012	0.0063	294.40	242.17	

$$r_{corrosion} = (1.205\,E + 10)\cdot e^{\frac{-6430}{T}} \cdot [H^+]^{0.118} \cdot ([Cl^-]^{0.106} + [HSO_3^-]^{0.007} + [SO_3^{2-}]^{0.006} + [SO_4^{2-}]^{0.006} + [NO_3^-]^{0.102}) \quad (5.45)$$

Four additives										
57	353	0.01667	0.015	0.00002	0.000007	0.00003	0.0016	251.00	267.50	
58	353	0.03327	0.030	0.00004	0.000013	0.00006	0.0032	298.60	297.35	
59	353	0.04486	0.040	0.00006	0.000020	0.00009	0.0048	358.90	311.97	**8.6**
60	353	0.06127	0.055	0.00008	0.000025	0.00012	0.0063	391.60	327.18	
61	303	0.06127	0.055	0.00008	0.000025	0.00012	0.0063	14.57	16.19	
62	333	0.06127	0.055	0.00008	0.000025	0.00012	0.0063	114.10	109.55	

$$r_{corrosion} = (8.922\,E+09)\cdot e^{\frac{-6430}{T}}\cdot[H^+]^{0.118}\cdot([Cl^-]^{0.106}+[HSO_3^-]^{0.007}+[SO_3^{2-}]^{0.006}+[SO_4^{2-}]^{0.006}+[NO_3^-]^{0.102}) \quad (5.41)$$

CHAPTER SIX

RESULTS AND DISCUSSION OF OXIDATIVE MEA DEGRADATION

6.1 Experimental conditions

The oxidative MEA degradation study was done by varying additives along with their concentrations under the base-case conditions. All the experiments in oxidative MEA degradation were performed under the conditions presented in Table 6.1 except for the study of the temperature effects, wherein two additional temperatures (40°C and 80°C) were introduced. Since solvent degradation takes months to proceed, the solvent degradation study was operated at elevated pressure (760 kPa; 110 psi) in order to accelerate the reaction. The selection of the additives aimed to represent various species typically present in a flue gas. Thus, two types of chlorides and hydrochloric acid (HCl) were selected to represent various sources of chlorides in a flue gas in which sodium chloride (NaCl) represented a commonly found salt, hydrochloric acid (HCl) represented a mineral acid, and ferrous chloride ($FeCl_2$) represented an inorganic compound. One reason why sodium-base and iron-base compounds were selected was that they are cations that are significantly present in a CO_2 capture process (Strazisar et al., 2003). Moreover, sulphurous acid (H_2SO_3), sulphuric acid (H_2SO_4), and nitric acid (HNO_3) were also selected as representatives of sulphur dioxide (SO_2), sulphur trioxide (SO_3), and nitrogen dioxide (NO_2) in aqueous solutions, respectively. The concentration range of each additive used in the study of oxidative MEA degradation is presented in Table 6.2.

Table 6.1: The base-case conditions (no additive) of oxidative MEA degradation.

Component	Condition
MEA concentration	5M (1.2% error)
CO_2 loading	0.5 mol CO_2/mol MEA (3.2% error)
O_2 concentration	0.00078M (at 120°C)
Temperature	120°C (±1°C)
Pressure	760 kPa (110 psi)
The rate of reaction	**0.00142 kmol/m^3·hr** (1.6% error)

Table 6.2: The concentration ranges of additives in oxidative MEA degradation study.

Additive	Concentration
Sodium chloride (NaCl)	0 - 2000 ppm
Ferrous chloride ($FeCl_2$)	
Hydrochloric acid (HCl)	
Sulphurous acid (H_2SO_3)	0 - 400 ppm
Sulphuric acid (H_2SO_4)	0 - 12 ppm
Nitric acid (HNO_3)	0 - 400 ppm

There were two reasons that the aqueous acid solutions (H_2SO_4, H_2SO_3, and HNO_3) were used instead of the actual acid gas components (SO_3, SO_2, and NO_2) that are typically present in a flue gas. First, this work focused on the study of oxidative MEA degradation by the reactions in a liquid phase within the CO_2 capture process. Unfortunately, a method to determine an amount of acid gas dissolved into an aqueous solution has not been well-established, so the acid solutions (H_2SO_4, H_2SO_3, and HNO_3) were chosen to represent the dissolved acid gases (SO_3, SO_2, and NO_2) in aqueous solution in order to avoid difficulty in concentration determination of the aqueous solubility of the actual gases. Secondly, the acid gases (SO_3, SO_2, and NO_2) are considerably toxic; therefore, there are limitations due to safety regulations in terms of the concentration ranges allowed to be used in a laboratory workplace. The allowable concentrations of the gases are well below the concentrations that are typically present in a flue gas, so, using the acid solutions (H_2SO_4, H_2SO_3, and HNO_3), which represented the aqueous solutions of the acid gases (SO_3, SO_2, and NO_2), allowed the experimental conditions to reach the relevant concentrations present in a typical flue gas.

6.2 The effects of different types of chloride compounds on oxidative MEA degradation

Two different chloride compounds (sodium chloride; NaCl and ferrous chloride; $FeCl_2$) and hydrochloric acid (HCl), were studied in terms of their effects on oxidative MEA degradation: sodium chloride (NaCl) represented a commonly found salt, hydrochloric acid (HCl) represented a mineral acid, and ferrous chloride ($FeCl_2$) represented an inorganic compound.

6.2.1 The effect of sodium chloride (NaCl) on the degradation rate

The effect of sodium chloride (NaCl) on degradation rate is illustrated in Figure 6.1, which shows that increasing sodium chloride concentration reduced the degradation rates. This was because increased salt concentration enhanced the ionic strength of a given solution, which resulted in a reduction of gas solubility in the solution. Since solvent molecules, which were mainly water molecules, had been bound by dissolved sodium chloride salt, which led to increased difficulty for a gas to dissolve. In other words, the higher sodium chloride concentration in a solution, the less oxygen (O_2), which is a primary contributor to oxidative solvent degradation, can be dissolved, which leads to the less oxidative solvent degradation. Moreover, when the systems had higher sodium chloride concentrations, the degradation rates seemed to be more independent of the operating times. Only systems containing 500 ppm sodium chloride concentration had degradation rates that decreased accordingly, which was a similar trend as obtained from the base-

case system (no additives). Unfortunately, the reason for this remains still unclear. In addition, by adding sodium chloride to the system, the initial MEA degradation rates decreased when compared to the base-case, in which there was no additive, because of the reaction between the chloride ion (Cl^-) and protonated MEA ($R\text{-}NH_3^+$), as expressed in equation 6.1. The reaction led to less initial amine being available to participate in the degradation process. However, it should be noted that the reductions of the initial MEA concentrations when compared to the base-case did not determine the overall degradation rates because there were still many mechanisms associated with the process reactions.

$$Cl^- + R - NH_3^+ \longrightarrow R - NH_3^+ Cl^- \qquad (6.1)$$

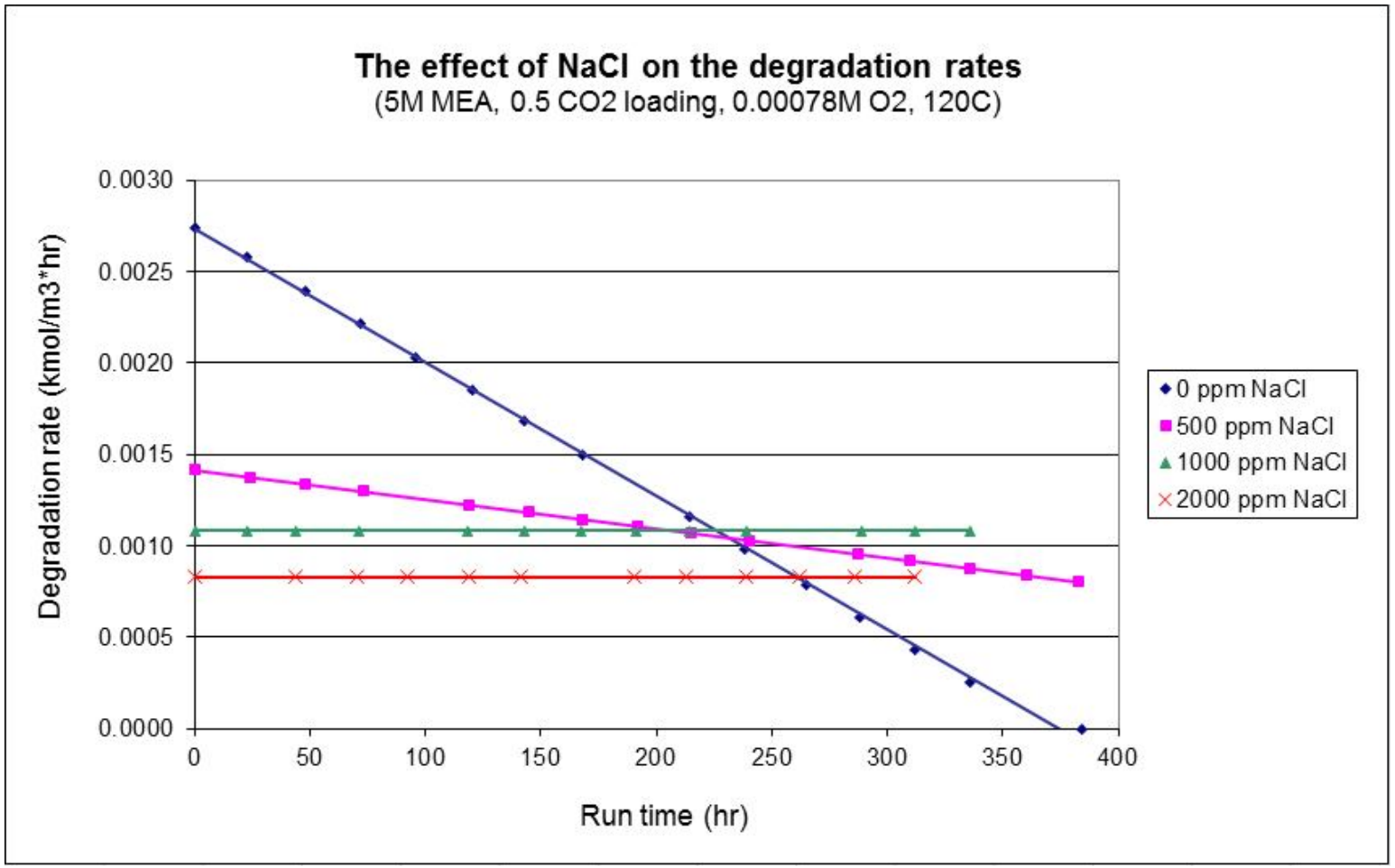

Figure 6.1: The effect of sodium chloride (NaCl) on the oxidative MEA degradation rates (%error: 1.0%, 1.1%, 2.5% in 500, 1000, and 2000 ppm NaCl systems, respectively). (Original in colour)

6.2.2 The effect of hydrochloric acid (HCl) on the degradation rate

The effect of hydrochloric acid (HCl) on the degradation rate is illustrated in Figure 6.2, which shows that increasing acid concentration increased the solvent degradation rate because the hydrogen ion (H^+) helped to initiate the degradation mechanism by behaving as a catalyst in the degradation reactions. With only a small amount of acid introduced to a solution, amine was easily decomposed to different compounds with the help of hydrogen ion. In addition, when compared to the base-case, the initial MEA degradation rates were reduced when acid was added to the system due to the reaction between chloride ion (Cl^-) and protonated MEA ($R\text{-}NH_3^+$), as expressed in equation 6.1. However, it should be noted that the reductions of the initial MEA concentrations compared to the base-case did not determine the overall degradation rates because there were still many mechanisms associated with the process reactions.

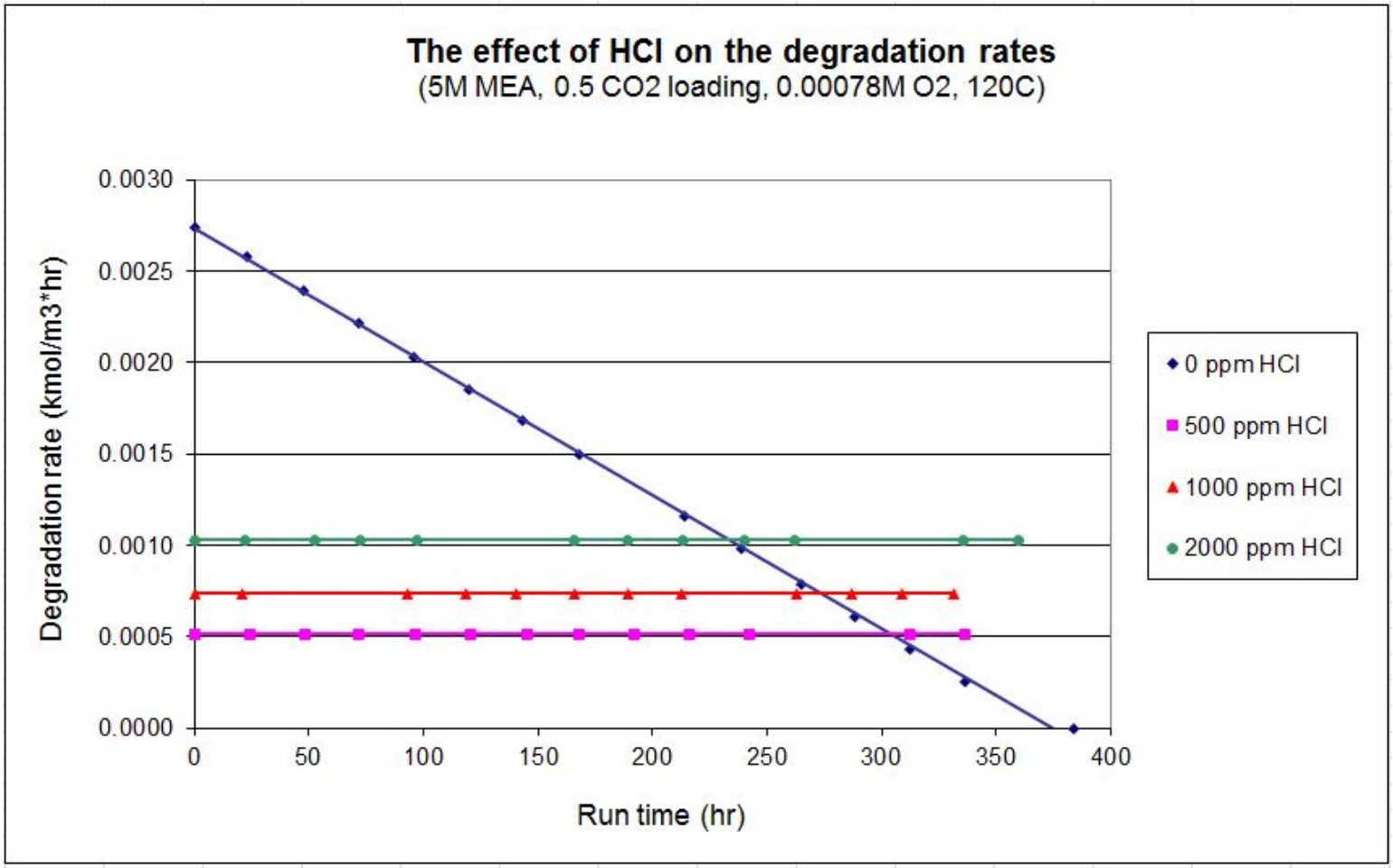

Figure 6.2: The effect of hydrochloric acid (HCl) on the oxidative MEA degradation rates (%error: 3.4%, 2.7%, 2.1% in 500, 1000, and 2000 ppm HCl systems, respectively). (Original in colour)

6.2.3 The effect of ferrous chloride ($FeCl_2$) on the degradation rate

Firstly, when ferrous chloride ($FeCl_2$) mixed with MEA solution, light-weight reddish-brown precipitated particles were generated. Initially ferrous hydroxide ($Fe(OH)_2$) was produced, as expressed in equation 6.2. However, it was not stable, as, with the access of oxygen (O_2) and water, it was oxidized to a trivalent hydrated iron oxide (ferric oxide; Fe_2O_3; reddish-brown) (Soosaiprakasam and Veawab, 2008). Moreover, the formation of ferric oxide was supported by physical appearance (colour) and SEM-EDS techniques, due to that fact that it was reddish-brown in colour and consisted of mainly iron oxide, as illustrated in the SEM-EDS scan presented in Figure 6.3.

$$FeCl_2 + 2[R-NH_2] \xrightarrow{2H_2O} 2[R-NH_3^+Cl^-] + Fe(OH)_{2(solid)} \qquad (6.2)$$

The solution was then tested with ICP-MS technique, which showed that the total iron ions (Fe^{2+} and Fe^{3+}) concentration after it was mixed with MEA decreased from its initial stage, which basically ensured that the precipitate particle must be some type of iron-combining compound. However, after the solution was loaded with 0.5 CO_2 loading (mol CO_2 per mol MEA), the total iron ions concentration was higher compared to the concentration before loading with CO_2, which indicated that the iron-combining compound dissolved back into the solution when the acidity of the solution was increased.

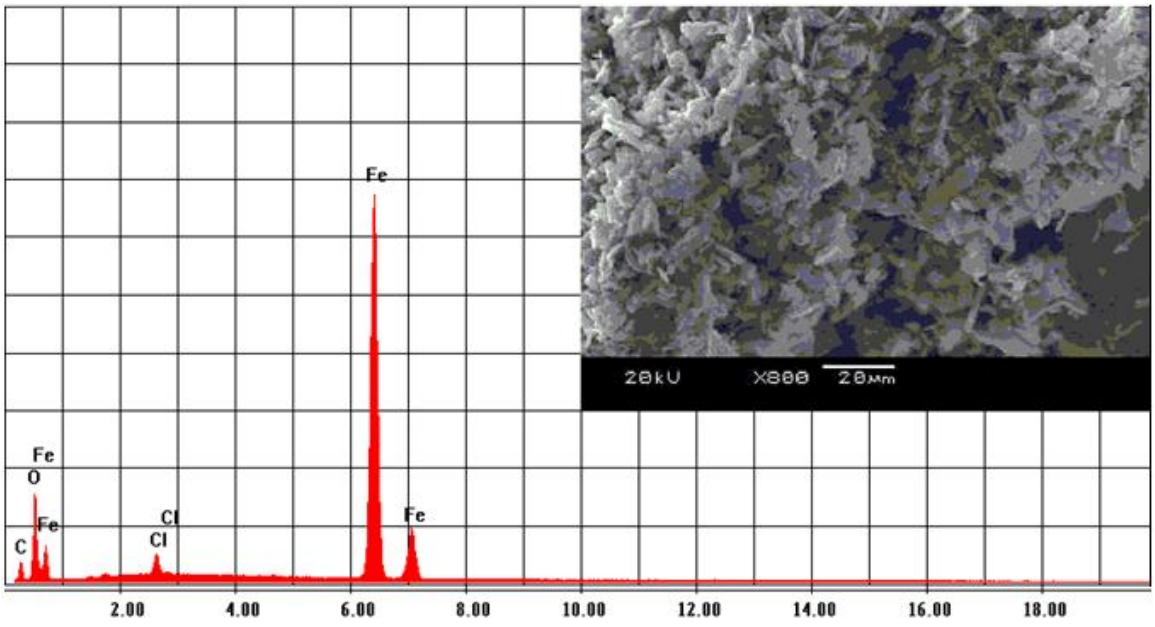

Figure 6.3: SEM-EDS scan for particle generated when mixing $FeCl_2$ and 5M MEA. (Original in colour)

The effect of ferrous chloride ($FeCl_2$) on the oxidative MEA degradation was that the degradation rates increased with increasing ferrous chloride concentrations, as illustrated in Figure 6.4. In the presence of oxygen (O_2), ferrous ion (Fe^{2+}) helped to elevate oxygen to more active species, such as superoxide ($\cdot O_2^-$) and hydroxyl ($\cdot OH$) radicals. These reactive oxygen species (ROS) then accelerated the oxidative MEA degradation due to the fact that the solvent degradation process includes radical initiating reactions, especially with the hydroxyl radical ($\cdot OH$), which had the highest reaction rate with amines, as shown in Table 6.3 (Bedell, 2011). In addition, the results obtained from ICP-MS techniques showed that the total iron ions (Fe^{2+} and Fe^{3+}) concentration in the solution reduced as the process proceeded. Total iron ions concentration was reduced to about 92.5% after 336 hours of run time. It was also associated with the fact that there were some precipitated particles found at the bottom of the reactor after the experiment, which were later identified, using SEM-EDS techniques, to be iron-based compounds, as illustrated Table 6.4 and the SEM image illustrated in Figure 6.5.

Formation of reactive oxygen species (ROS) catalyzed by ferrous ion (Bedell, 2011):

$$Fe^{2+} + O_2 \rightarrow Fe^{3+} + \bullet O_2^- \quad (6.3)$$

$$Fe^{2+} + 2H^+ + \bullet O_2^- \rightarrow Fe^{3+} + H_2O_2 \quad (6.4)$$

$$Fe^{2+} + H^+ + H_2O_2 \rightarrow Fe^{3+} + H_2O + \bullet OH \quad (6.5)$$

$$Fe^{2+} + H^+ + \bullet OH \rightarrow Fe^{3+} + H_2O \quad (6.6)$$

Overall: $4Fe^{2+} + O_2 + 4H^+ \rightarrow 4Fe^{3+} + 2H_2O$ (6.7)

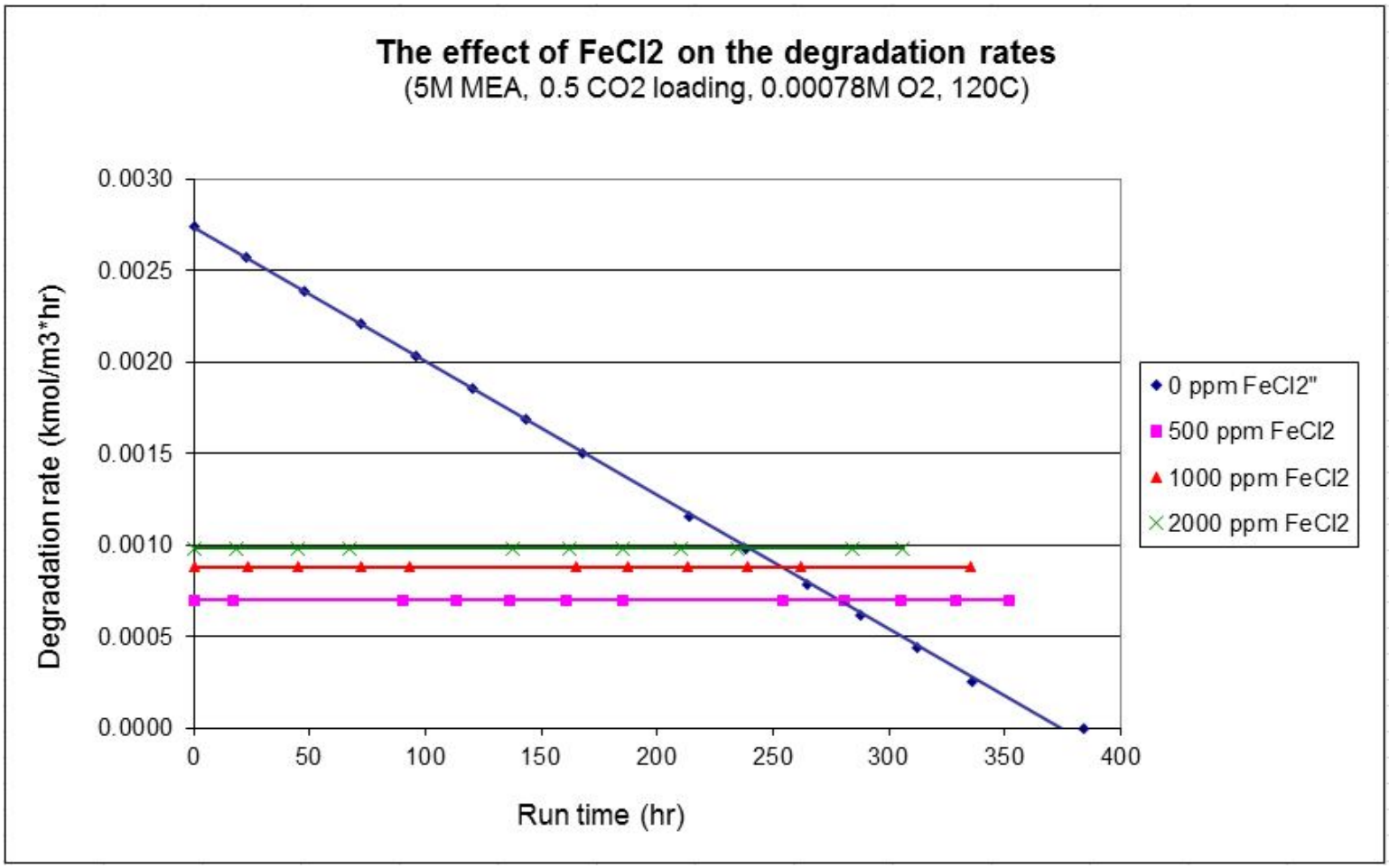

Figure 6.4: The effect of ferrous chloride ($FeCl_2$) on the oxidative MEA degradation rates (%error: 2.94%, 2.85%, 2.44% in 500, 1000, and 2000 ppm $FeCl_2$ systems, respectively). (Original in colour)

Table 6.3: The rate constants of the reactions of oxygen intermediates with amines at 25°C. (Bedell, 2011)

Reactions	Reaction rates ($L \cdot mol^{-1} \cdot s^{-1}$)
Oxygen: $RH + O_2 \rightarrow products$	< 0.002
Superoxide: $RH + O_2^- \rightarrow \bullet R + HO_2^-$	< 50
Peroxide: $RH + HO_2^- \rightarrow \bullet R + \bullet OH + H_2O$	Slow
Hydroxyl: $RH + \bullet OH \rightarrow \bullet R + H_2O$	10^8 - 10^{10}

Table 6.4: The EDS scan for the precipitate particles found after performing an oxidative MEA degradation experiment.

Element	Relative %Wt.
C	6.49
O	19.26
Fe	69.25
Others	5.00
Total:	100.00

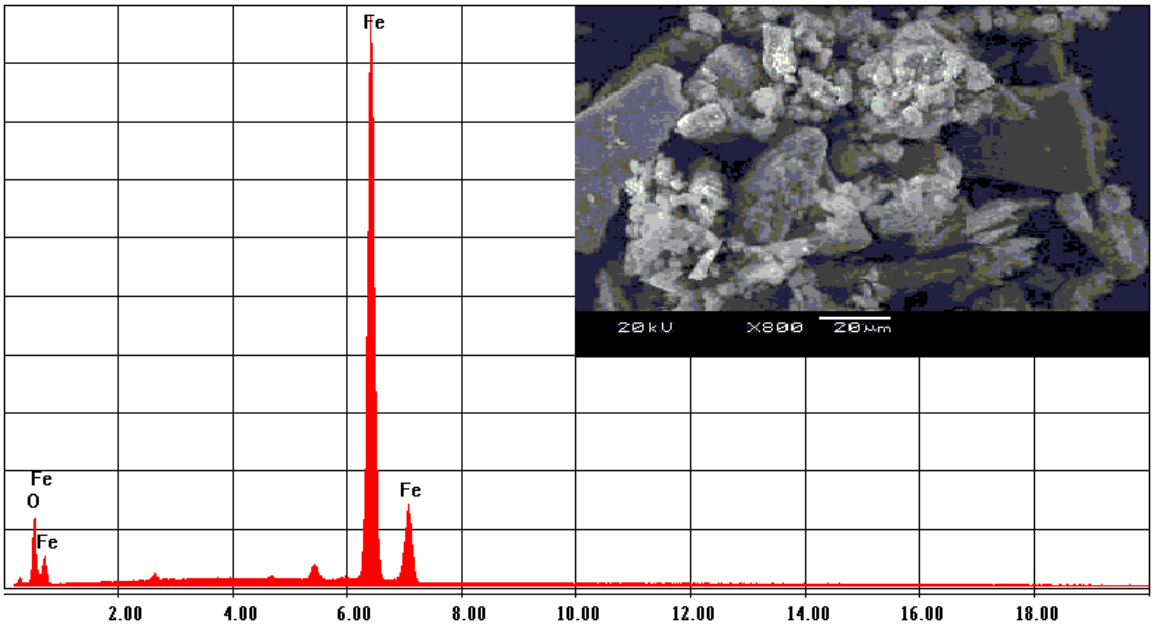

Figure 6.5: SEM-EDS scan for the precipitate particles found after performing an oxidative MEA degradation experiment. (Original in colour)

In addition, when compared to the base-case, the initial MEA degradation rates were reduced when ferrous chloride was added to the system, due to the reaction of chloride ion (Cl^-) with protonated MEA ($R\text{-}NH_3^+$). However, it should be noted that the reductions of the initial MEA concentrations, when compared to the base-case system, did not determine the overall degradation rates because there were still many mechanisms associated with the process reactions.

6.2.4 The summary of the effects of cations (Na^+, H^+, and Fe^{2+}) and chloride ion (Cl^-) on the oxidative MEA degradation rates

In the study of the effects of three different types of chloride compounds (NaCl, HCl, and $FeCl_2$) on oxidative MEA degradation, there were three cations (Na^+, H^+, and Fe^{2+}) introduced to the systems, and each provided different levels of contribution to oxidative MEA degradation. Even though the effect of sodium ion (Na^+) on solvent degradation is still unclear, hydrogen ion (H^+) proved to strongly accelerate the degradation process by behaving as a catalyst that helped to initiate the degradation reactions. Ferrous ion (Fe^{2+}) also proved to speed up the oxidative MEA degradation by elevating oxygen (O_2) to more active species, such as superoxide ($\cdot O_2^-$) and hydroxyl ($\cdot OH$) radicals. Then, these reactive oxygen species (ROS) helped to accelerate the oxidative degradation due to the fact that the solvent degradation process is considerably radical initiating.

Moreover, the primary role of chloride ion (Cl^-) in oxidative MEA degradation was that it helped to reduce the initial degradation rates when compared to the base-case system by binding with protonated MEA ($R\text{-}NH_3^+$), as presented in equation 6.1. Thus, when MEA had been partly occupied by chloride ion, it resulted in less MEA remaining to participate in the degradation reactions, which led to the reduction of the initial degradation rates when compared to the base-case where no additive was added. However, it should be noted that the reduction of the initial MEA concentrations did not determine the overall degradation rates because there were still many mechanisms associated with the process reactions. In addition, the initial MEA concentrations were determined in each chloride additive, as shown in Table 6.5. The table demonstrated that MEA concentrations reduced after chloride compounds were introduced to the systems, which corresponded to the initial rate data.

$$Cl^- + R - NH_3^+ \longrightarrow R - NH_3^+Cl^- \qquad (6.1)$$

Table 6.5: Initial MEA concentrations in different chlorides systems.

System name	Chloride concentration (ppm)	MEA Concentration (M; mol/l)	% MEA concentration reduction compared to the base-case system
Base-case (no additive)	0	4.944	
Sodium chloride (NaCl)	620	4.934	0.20
	1220	4.925	0.30
	2280	4.911	0.66
Ferrous chloride ($FeCl_2$)	620	4.917	0.55
	1160	4.919	0.50
	2100	4.925	0.38
Hydrochloric acid (HCl)	510	4.846	1.98
	1021	4.795	3.01
	1969	4.680	5.33

6.3 The effect of sulphuric acid (H_2SO_4) on oxidative MEA degradation

Sulphuric acid (H_2SO_4) was used to represent sulphur trioxide (SO_3) in an aqueous solution, and the oxidative MEA degradation rates of the systems containing different concentrations of sulphuric acid are presented in Figure 6.6, which shows that the degradation rates increased with increasing acid concentrations. The increase of the rates was because sulphuric acid is a strong acid, so as soon as it dissolved in water, hydrogen ion (H^+) and sulphate ion (SO_4^{2-}) were formed. The hydrogen ion and sulphate ion generated helped to initiate degradation mechanisms in that they behaved as the catalysts in the oxidative MEA degradation reactions and accelerated the degradation process. Hydrogen ion potentially behaved as a catalyst to assist amine to easily decompose into different compounds, while sulphate ion possibly converted into sulphate radical ($SO_4^{\bullet -}$) in the presence of free radicals (Shen and Rochelle, 1998), thereby setting up a chain reaction of oxidative MEA degradation.

In addition, when compared to the base-case system, the initial MEA degradation rates reduced when acid was added to the systems due to the protonated MEA being bound with a free acid in a solution by electrostatic interaction to form an amine sulphate ($(RNH_3)_2SO_4$) (Li et al., 2011 in press), as expressed in equation 6.8. Therefore, MEA concentration was decreased after a solution was added with sulphuric acid, leading to less MEA being available to participate in the degradation reactions, which resulted in the reduction of the initial degradation rates when compared to the base-case system. Nevertheless, it should be noted that the reductions of the initial MEA concentrations did not

determine the overall degradation rates because there were still many mechanisms associated with the degradation process.

$$SO_4^{2-} + 2R - NH_3^+ \longrightarrow (R - NH_3^+)_2 SO_4^{2-} \tag{6.8}$$

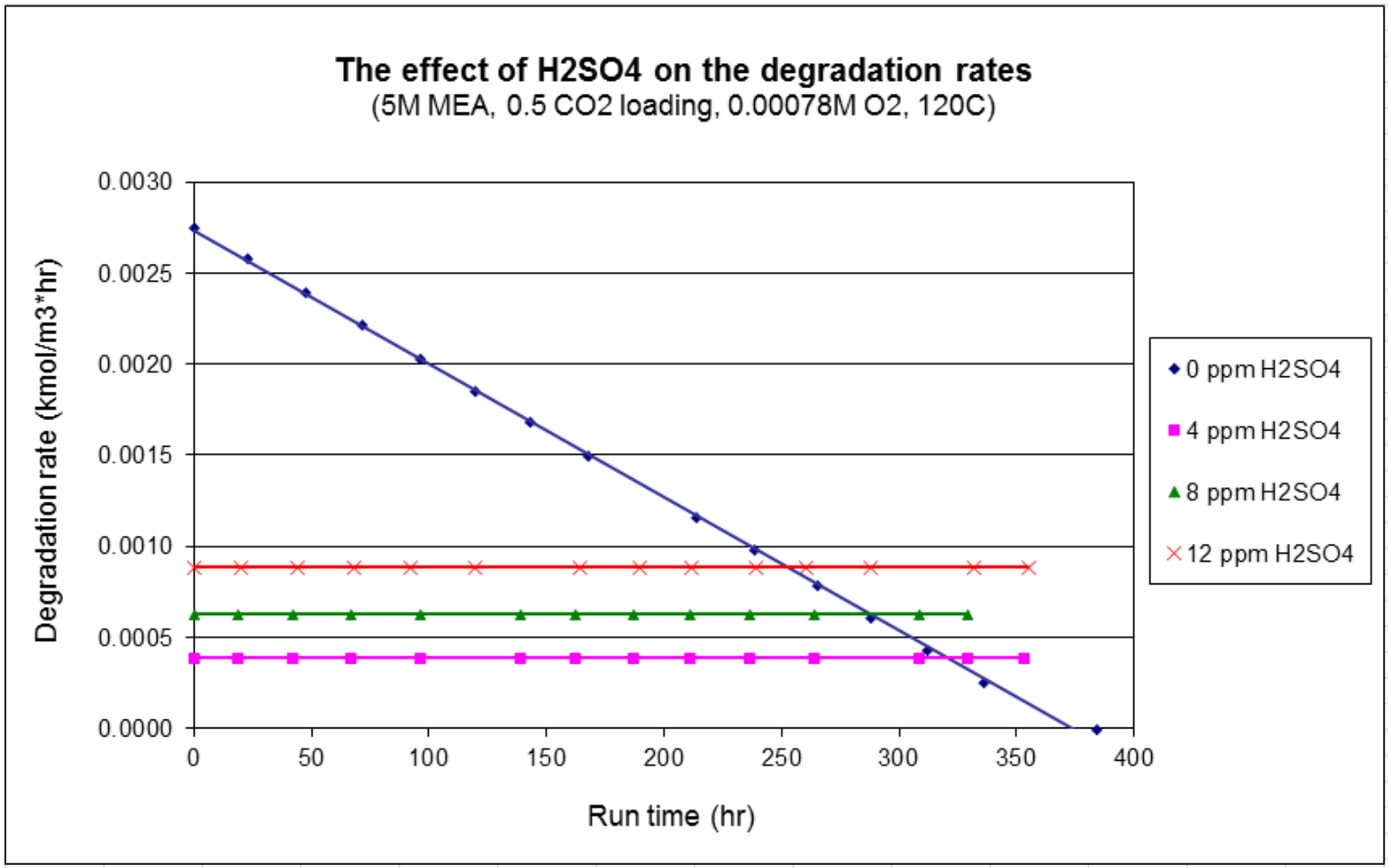

Figure 6.6: The effect of sulphuric acid (H_2SO_4) on the oxidative MEA degradation rates (%error: 4.08%, 2.11%, and 2.76% in 4, 8, and 12 ppm H_2SO_4 systems, respectively). (Original in colour)

6.4 The effect of sulphurous acid (H_2SO_3) on oxidative MEA degradation

Sulphurous acid (H_2SO_3) was used as a representative of sulphur dioxide (SO_2) in aqueous solution. Since it is a weak acid, when it dissolves in water bisulfite (HSO_3^-) and sulfite (SO_3^{2-}), ions are formed as expressed in the reactions below:

Sulphurous acid formation:

$$SO_2 + H_2O \leftrightarrow H_2SO_3 \tag{6.9}$$

Hydrolysis of sulphurous acid:

$$H_2SO_3 + H_2O \leftrightarrow HSO_3^- + H_3O^+ \tag{6.10}$$

Hydrolysis of bisulfite ion:

$$HSO_3^- + H_2O \leftrightarrow SO_3^{2-} + H_3O^+ \tag{6.11}$$

Increasing sulphurous acid (H_2SO_3) concentration continually reduced the oxidative MEA degradation rates. However, when the acid concentration went beyond 250 ppm, the degradation rates tended to increase, as illustrated in Figure 6.7. This was because sulphurous acid reacted easily with dissolved oxygen (O_2), thus, it behaved as an oxygen scavenger. When oxygen concentration in a solution was reduced, the oxidative MEA degradation also reduced accordingly because oxygen was a primary contributor to oxidative solvent degradation. The reaction of sulphurous acid with dissolved oxygen occurred through the reactions between bisulfite (HSO_3^-) and sulfite (SO_3^{2-}) ions with dissolved oxygen, as shown in equations 6.12 and 6.13. Moreover, a compound combined between MEA and sulphurous acid itself was also able to react with oxygen and helped

reduce oxygen concentration in the solution by generating a complex compound of protonated MEA and sulphate ion (Cho et al., 2001), as presented in equations 6.14 and 6.15. In contrast, due to the higher concentrations of hydrogen ion (H^+) and sulphate ion (SO_4^{2-}) produced by the oxidation reactions of bisulfite and sulfite ions, when the acid concentration went beyond 250 ppm, the presence of hydrogen and sulphate ions began to dominate the reactions, instead of the reactions with dissolved oxygen, which eventually led to the increase of the degradation rates, as hydrogen and sulphate ions helped to accelerate the degradation reactions.

Reaction of bisulfite ion with dissolved oxygen:

$$HSO_3^- + \frac{1}{2}O_2 \leftrightarrow SO_4^{2-} + H^+ \tag{6.12}$$

Reaction of sulfite ion with dissolved oxygen:

$$SO_3^{2-} + \frac{1}{2}O_2 \leftrightarrow SO_4^{2-} \tag{6.13}$$

Formation of complex compound of protonated MEA and sulphurous acid (Cho et al., 2001):

$$2[R-NH_2] + H_2SO_3 \rightarrow [R-NH_3^+]_2 SO_3^{2-} \tag{6.14}$$

Formation of complex compound of protonated MEA and sulphate (Cho et al., 2001):

$$[R-NH_3^+]_2 SO_3^{2-} + \frac{1}{2}O_2 \rightarrow [R-NH_3^+]_2 SO_4^{2-} \tag{6.15}$$

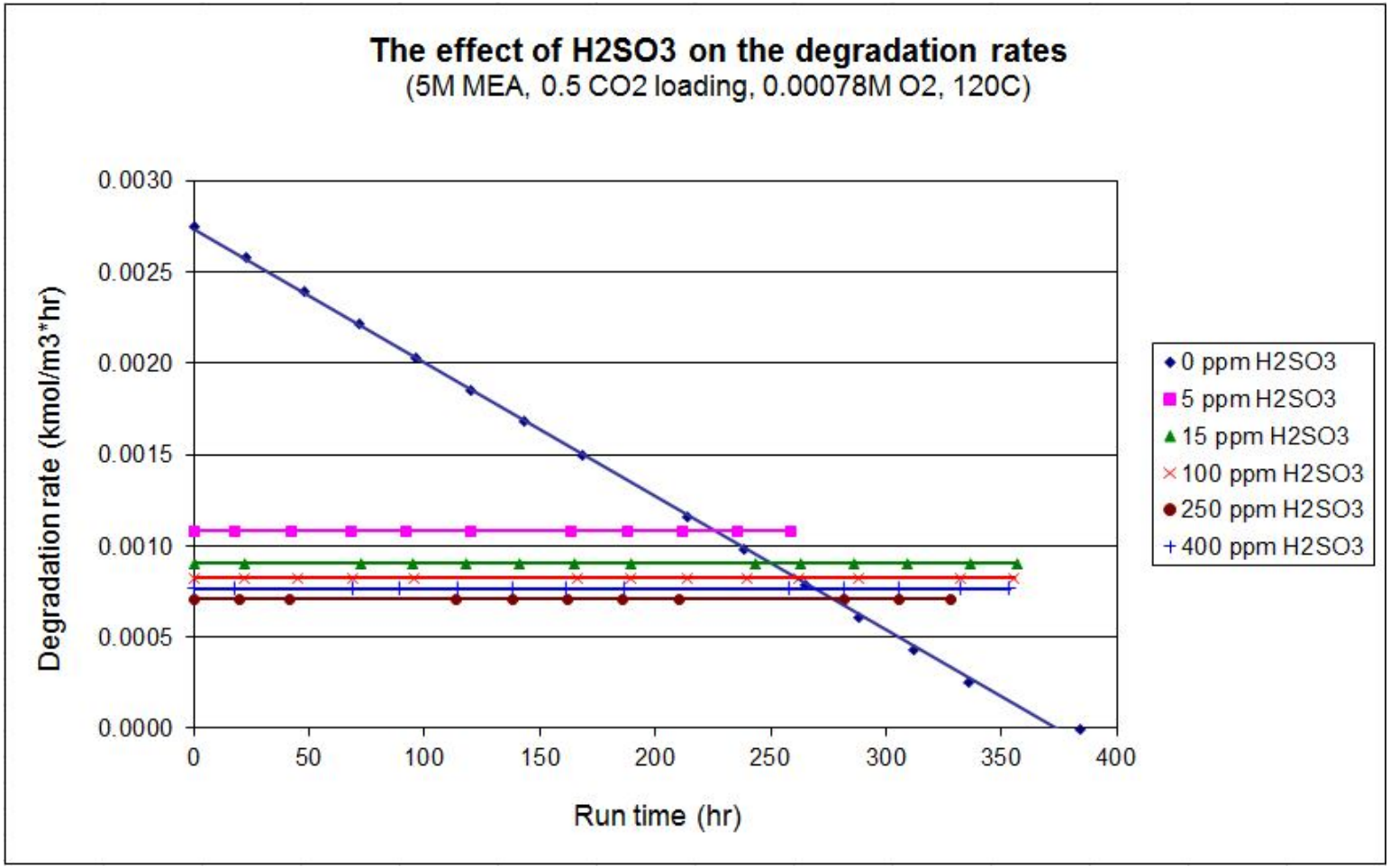

Figure 6.7: The effect of sulphurous acid (H_2SO_3) on the oxidative MEA degradation rates (%error: 1.29%, 1.42%, 1.90%, 3.15%, 2.32% in 5, 15, 100, 250, and 400 ppm H_2SO_3 systems, respectively). (Original in colour)

The initial degradation rate of the base-case system appeared to be higher than all the initial degradation rates of the systems containing various concentrations of sulphurous acid. Since, MEA was partly occupied by sulphurous acid in that it combined with sulphurous acid and formed a complex compound of protonated amine and sulfite ion, as presented in equation 6.14, which led to less MEA being available in the solution to participate in the degradation reaction. In addition, the initial MEA concentrations had been determined in the systems containing various concentrations of sulphurous acid, as presented in Table 6.6, and this showed that the MEA concentrations reduced after acid was added to the system, which corresponded to the initial rate data. However, it should be noted that the reductions of the initial MEA concentrations did not determine the overall degradation rates because there were still many mechanisms associated with the process reactions.

Table 6.6: Initial MEA concentrations in the systems containing various concentrations of H_2SO_3.

H_2SO_3 concentration (ppm)	**MEA Concentration (M; mol/l)**	**% MEA concentration reduction compared to the base-case system**
0 (base-case)	4.944	
15	4.942	0.05
49	4.937	0.15
99	4.927	0.34
394	4.883	1.23

6.5 The effect of nitric acid (HNO_3) on oxidative MEA degradation

Nitrogen dioxide (NO_2) is one of the major toxic gases present in a coal-fired flue gas. When nitrogen dioxide dissolves in water, nitric acid (HNO_3) is generated. Thus, in this study, nitric acid was used to represent nitrogen dioxide in an aqueous solution. The oxidative MEA degradation rates in various nitric acid concentrations are illustrated in Figure 6.8. The figure shows that the degradation rates increased with increasing acid concentrations, with the increase of the rates being due to the fact that nitric acid is a strong acid so it forms hydrogen ion (H^+) and nitrate ion (NO_3^-) simultaneously when it dissolves in aqueous solution. The hydrogen ion and nitrate ion then helped to accelerate the degradation mechanisms in that they behaved as catalysts in the oxidative MEA degradation reactions. Hydrogen ion potentially behaved as a catalyst to assist amine to easily decompose into different compounds, while nitrate ion possibly converted into nitrate radicals ($\bullet NO_3$) in the presence of free radicals (Wayne et al., 1991), thereby setting up a chain reaction of the oxidative MEA degradation process. The initial degradation rates again reduced when acid was added to the system, when compared to the base-case system, due to the protonated MEA partly combining with nitrate ion and generating an amine nitrate (RNH_3NO_3) (Xing et al., 2011), as expressed in equation 6.16. Since MEA was previously occupied, it resulted in less MEA being available to participate in the degradation reactions. In addition, the initial MEA concentrations were measured in systems containing various concentrations of nitric acid, as shown in Table 6.7, The results show that MEA concentrations reduced after acid was added to the systems, which corresponds to the initial rate data. Once again, it should be noted that the reductions of the initial

MEA concentrations did not determine the overall degradation rates since there were still many mechanisms associated with the process reactions.

$$NO_3^- + R - NH_3^+ \longrightarrow R - NH_3^+ NO_3^- \qquad (6.16)$$

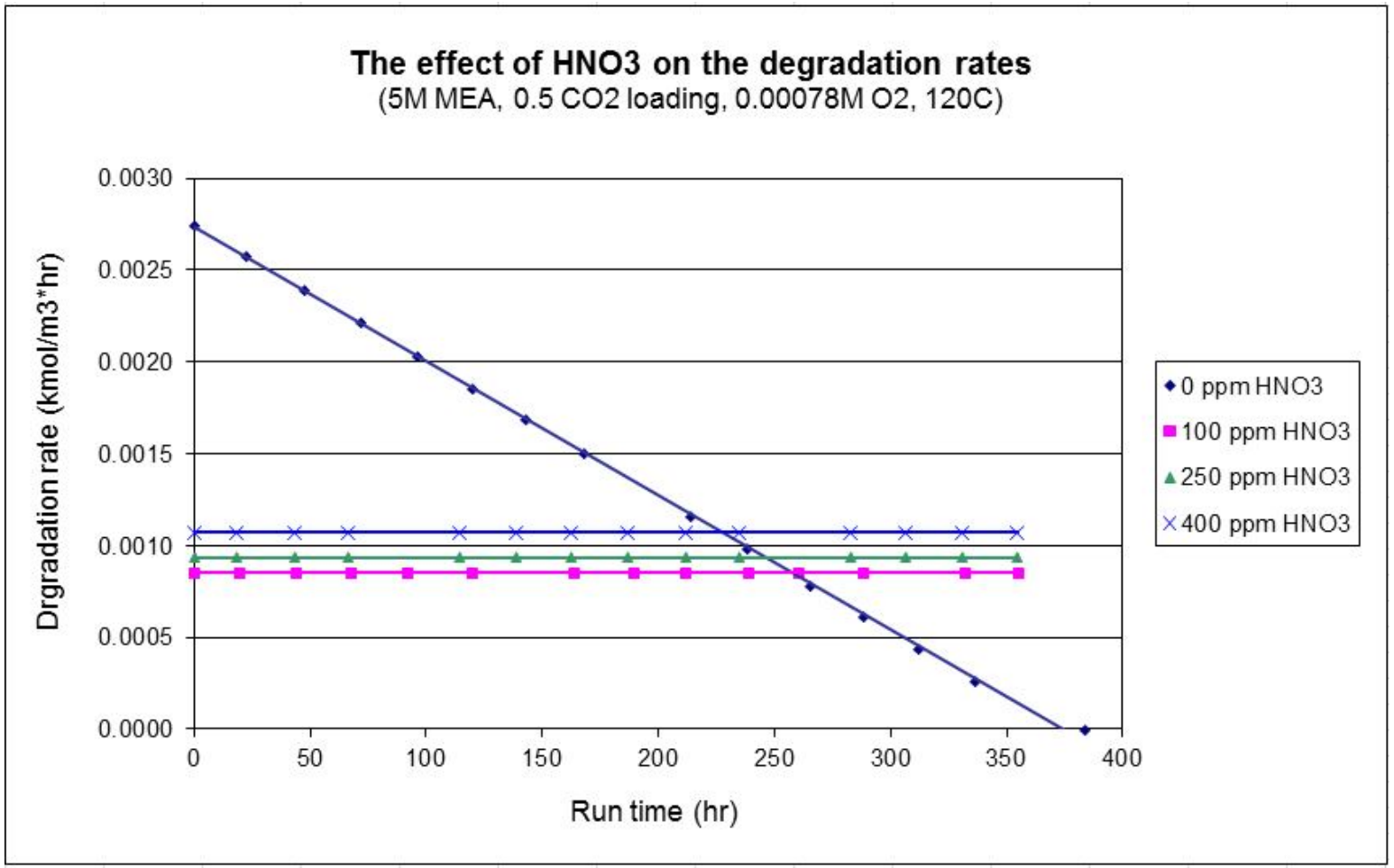

Figure 6.8: The effect of nitric acid (HNO_3) on the oxidative MEA degradation rates (%error: 1.91%, 1.40%, and 1.73% in 100, 250, and 400 ppm HNO_3 systems, respectively). (Original in colour)

Table 6.7: Initial MEA concentrations in the systems containing various concentrations of HNO_3.

HNO_3 concentration (ppm)	**MEA Concentration (M; mol/l)**	**% MEA concentration reduction compared to the base-case system**
0 (base-case)	4.944	
101	4.929	0.31
252	4.912	0.64
403	4.898	0.94

6.6 The oxidative MEA degradation products in systems containing various additives (NaCl, HCl, $FeCl_2$, H_2SO_4, H_2SO_3, and HNO_3) under the base-case conditions

The identification of oxidative MEA degradation products was done by using GC-MS techniques in order to determine the products that were able to be vapourized. A compound was identified by matching its mass spectra with a built-in commercial mass spectra database provided by the National Institute of Standards and Technology version 1998 (NIST98) and also with mass spectra of the standard chemicals in order to ensure accuracy. Since, the degradation products appeared to be similar in every study regardless of the additives, GC analysis of the oxidative MEA degradation products obtained from the base-case system was selected to be used in the product identification, the results of which are summarized in Table 6.8, where molecular weight (MW.) and percent confidence (%) are included for the matching of a mass spectra with the NIST database, while resident time (min) is provided in the validation with standard chemicals. Also, the GC analysis provided peaks of compounds that presented significantly within the base-case system, as illustrated in Figure 6.9. In most mass spectra results that were used to identify degradation products, the database mass spectra did not match the ones obtained from the degradation products. Therefore, the identities of the degradation products are still in question especially the ones with % confident less than 95%. The possible reasons were (i) lack of complete resolution of the peaks, (ii) the compound in the degradation product not being identical to the one in the database, and (iii) a combination of both. Even though some of the products had different residence times when compared to the ones

obtained from the standard chemicals, such compounds were still included as part of the degradation products due to the fact that they showed reasonable similarities in the mass spectra from the NIST98 database. Finally, some of the mass spectra of the products matched using the NIST98 database and the mass spectra obtained using standard chemicals were compared, as presented through Figures 6.10 to 6.21.

Table 6.8: Identification of the oxidative MEA degradation products.

Time (min)	Compound name	Compound code	MS-NIST98 database			Validation with standard chemicals	
			Name	MW.	% confidence	Yes/No	Time (min)
0.844	Carbon dioxide		Carbon dioxide	44		No	
1.470	Water		Water	18		No	
5.740	Monoethanolamine		Monoethanolamine	61	86	Yes	5.740
3.020	3-methylpyridine	A	3-methylpyridine	93	91	Yes	2.880
13.830	1-methyl-azetidine	B	1-methyl-azetidine	71	80	No	
17.859	Glycine anhydride	C	Glycine anhydride	114	70	Yes	25.192
18.114	N-acetylethanolamine	D	N-acetylethanolamine	103	53	Yes	18.585
19.167	2-oxazolidone	E	N/A	N/A	N/A	Yes	19.386
21.053	N/A	F	N/A	N/A	N/A	No	N/A
22.276	Compound A	G	Compound A	115	65	Yes	20.769
22.696	N-methyl caprolactam	H	3-methyl caprolactam	127	58	Yes	10.906
25.011	1-2-hydroxyethyl-2-imidazolidinone	I	1-2-hydroxyethyl-2-imidazolidinone	130	91	Yes	25.549
25.672	Diethyl fumarate	J	Diethyl fumarate	172	59	Yes	24.129
27.372	N/A	K	N/A	N/A	N/A	No	N/A

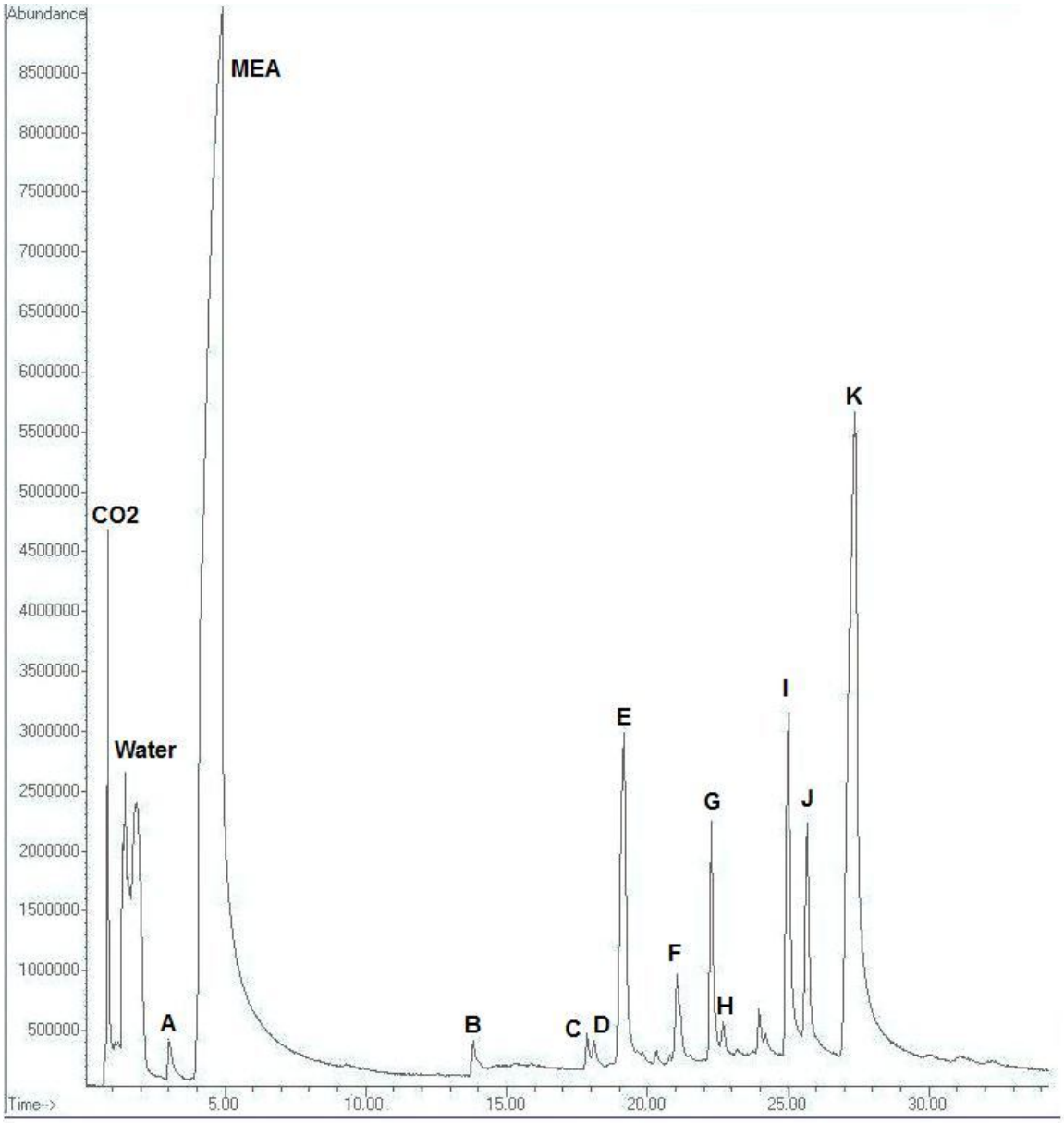

Figure 6.9: GC analysis of the oxidative MEA degradation products obtained from the base-case system. (Original in colour)

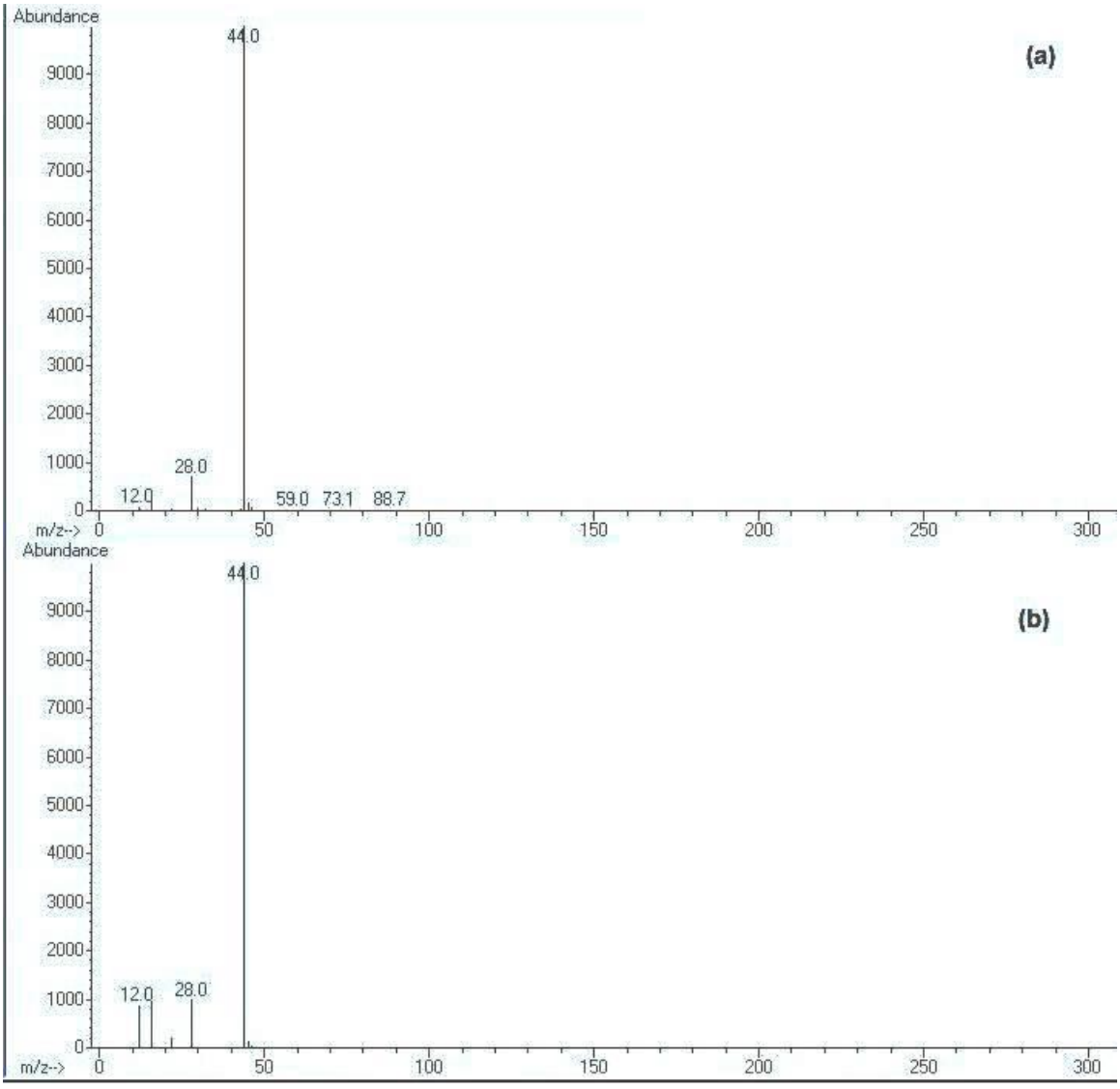

Figure 6.10: Mass spectra of carbon dioxide (CO_2) obtained from (a) the sample solution and (b) MS-NIST98 database. (Original in colour)

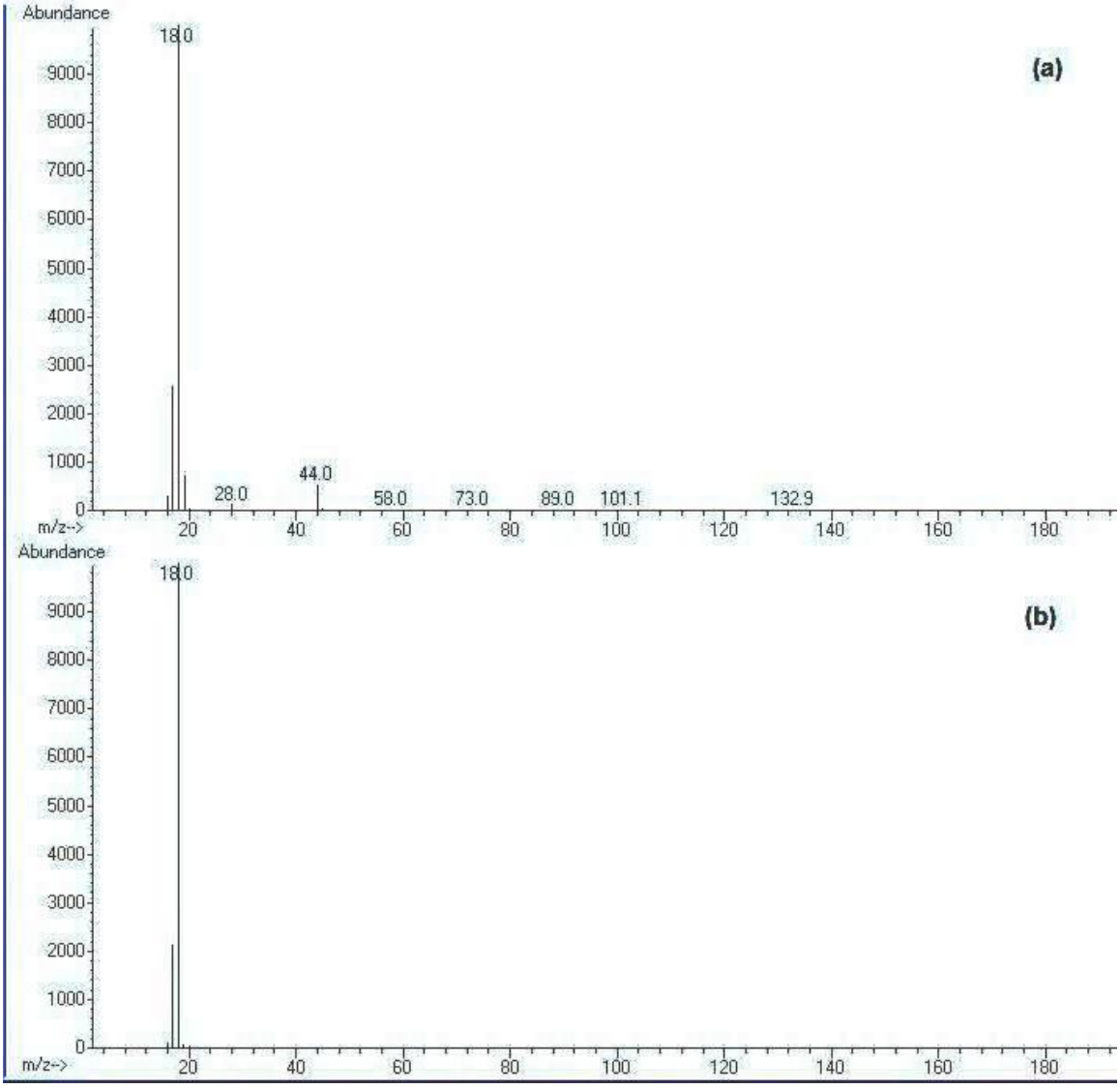

Figure 6.11: Mass spectra of water obtained from (a) the sample solution and (b) MS-NIST98 database. (Original in colour)

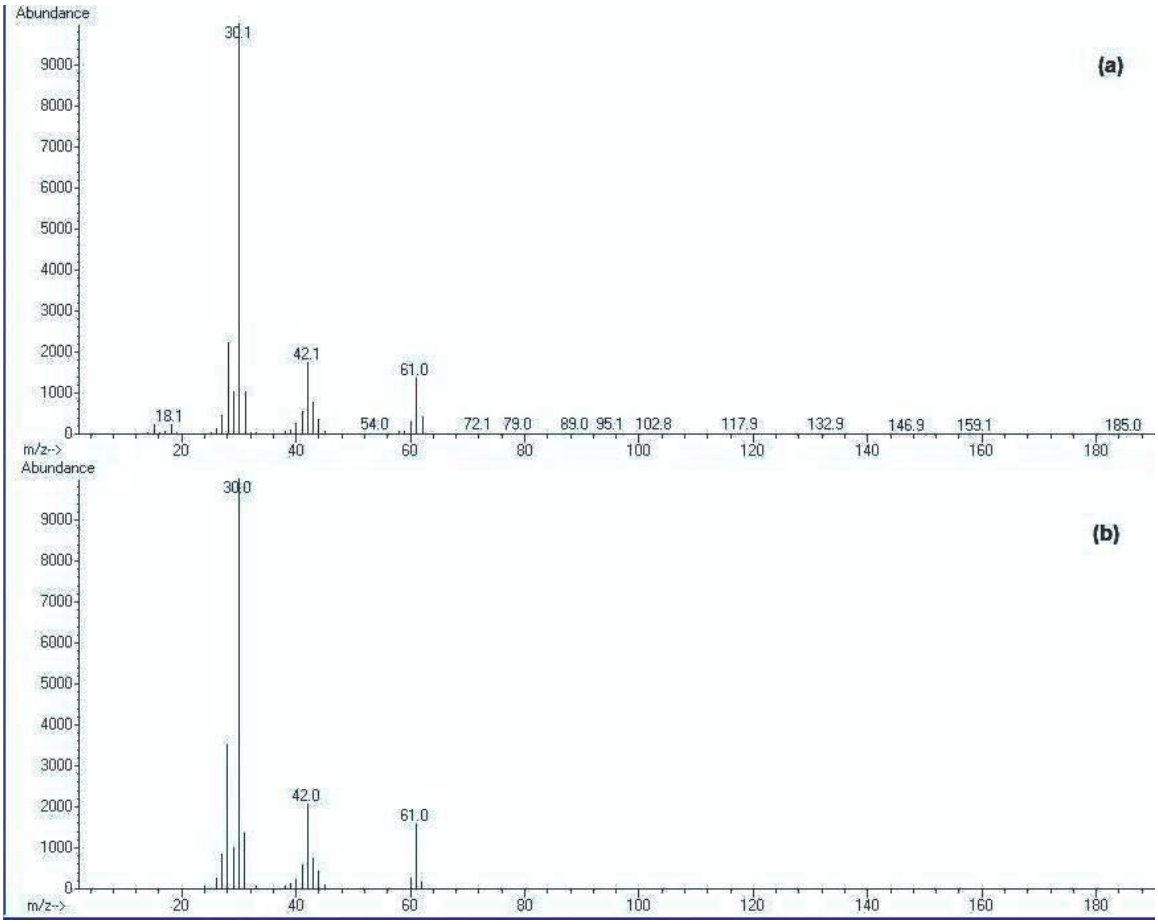

Figure 6.12: Mass spectra of MEA obtained from (a) the sample solution and (b) MS-NIST98 database. (Original in colour)

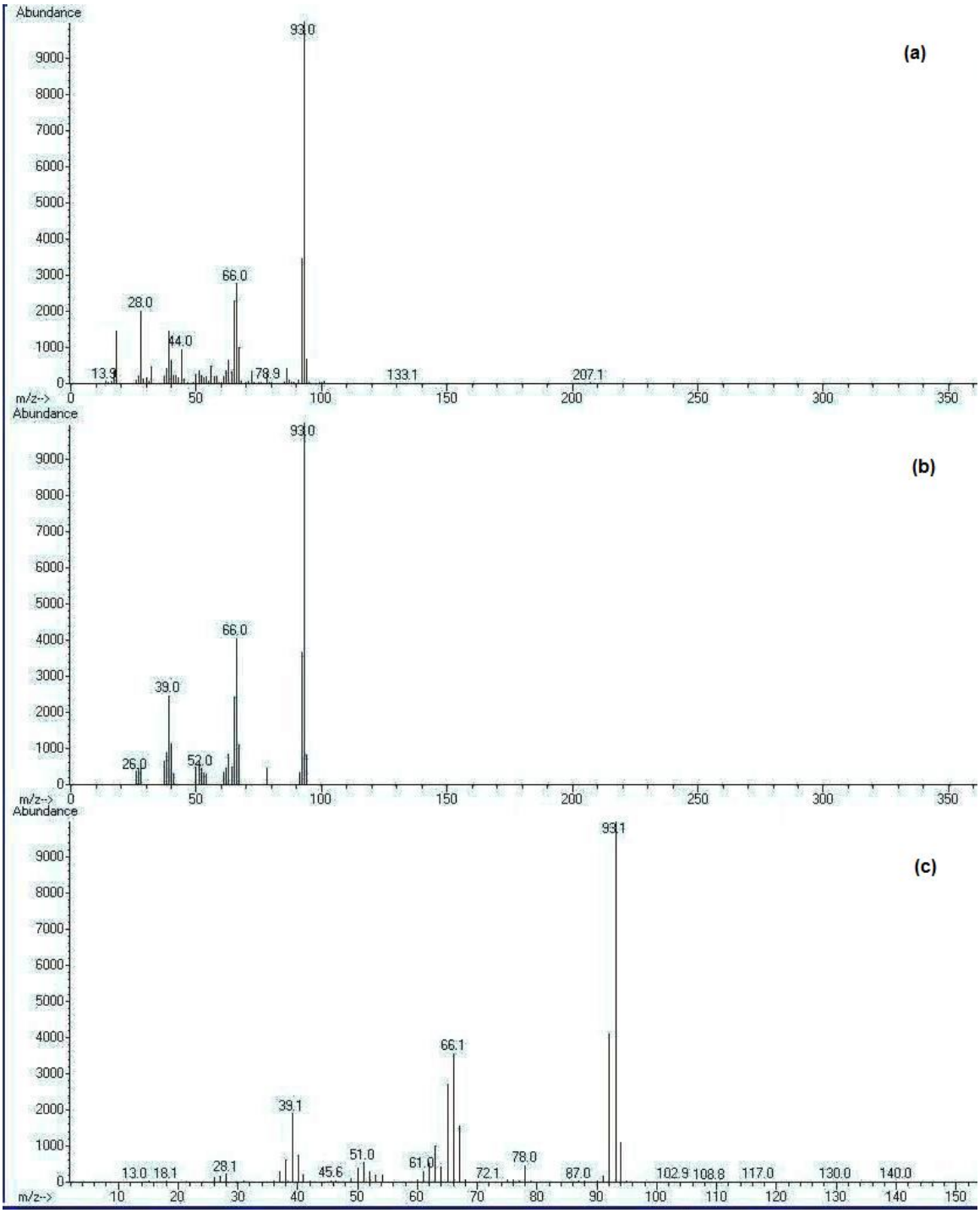

Figure 6.13: Mass spectra of 3-methylpyridine (A) obtained from (a) the sample solution, (b) MS-NIST98 database, and (c) the standard chemical. (Original in colour)

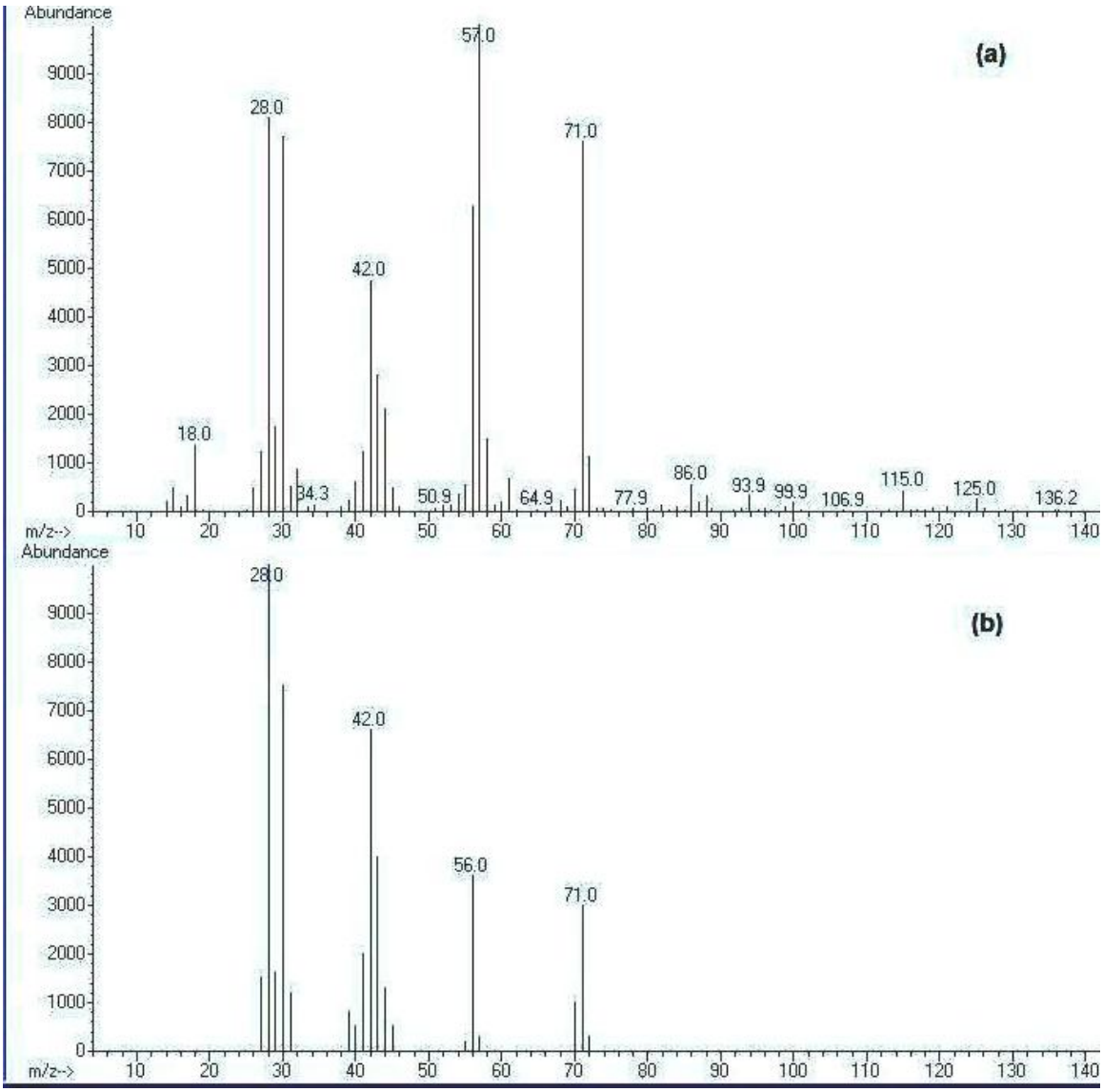

Figure 6.14: Mass spectra of 1-methyl-azetidine (B) obtained from (a) the sample solution and (b) MS-NIST98 database. (Original in colour)

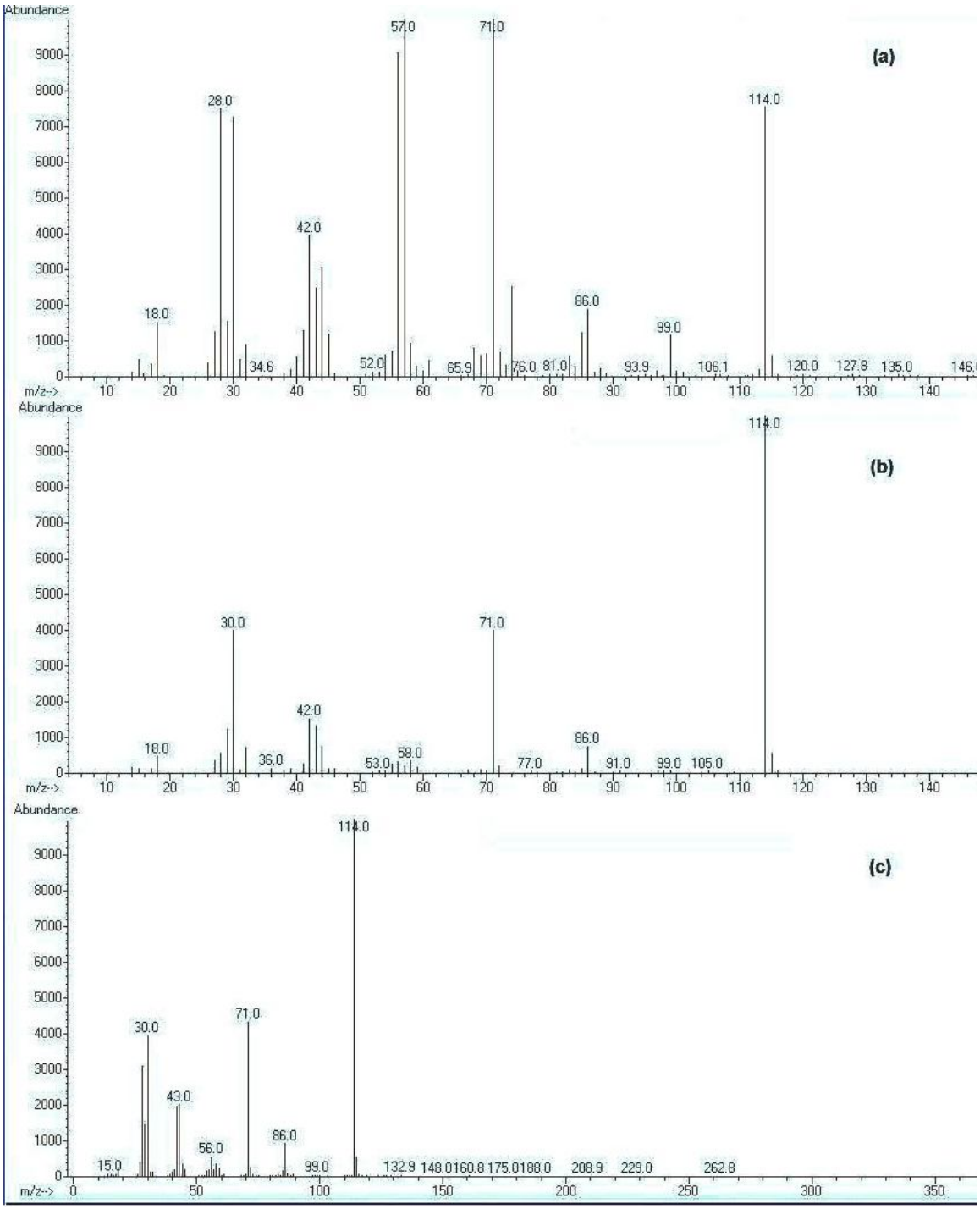

Figure 6.15: Mass spectra of glycine anhydride (C) obtained from (a) the sample solution, (b) MS-NIST98 database, and (c) the standard chemical. (Original in colour)

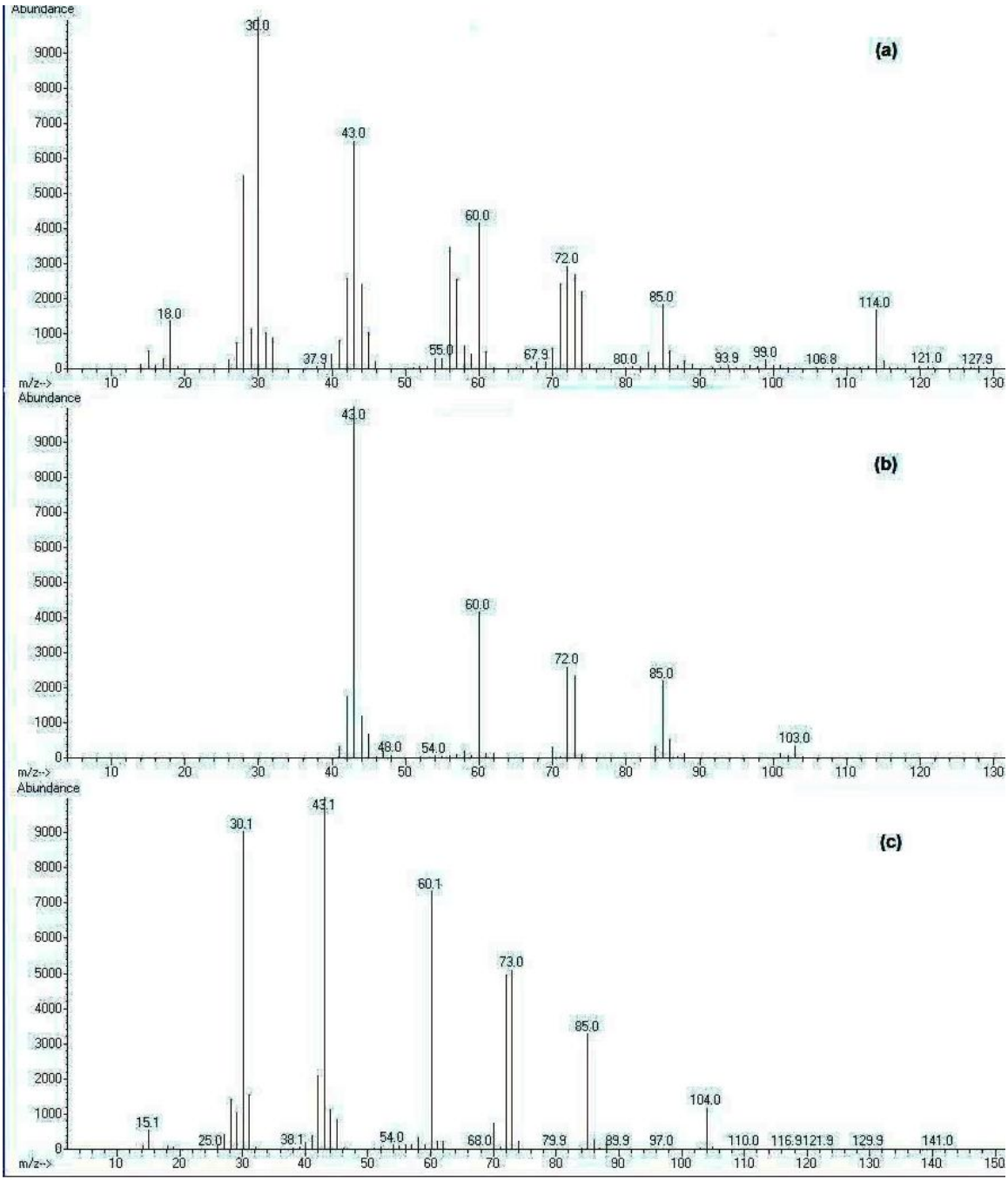

Figure 6.16: Mass spectra of n-acetylethanolamine (D) obtained from (a) the sample solution, (b) MS-NIST98 database, and (c) the standard chemical. (Original in colour)

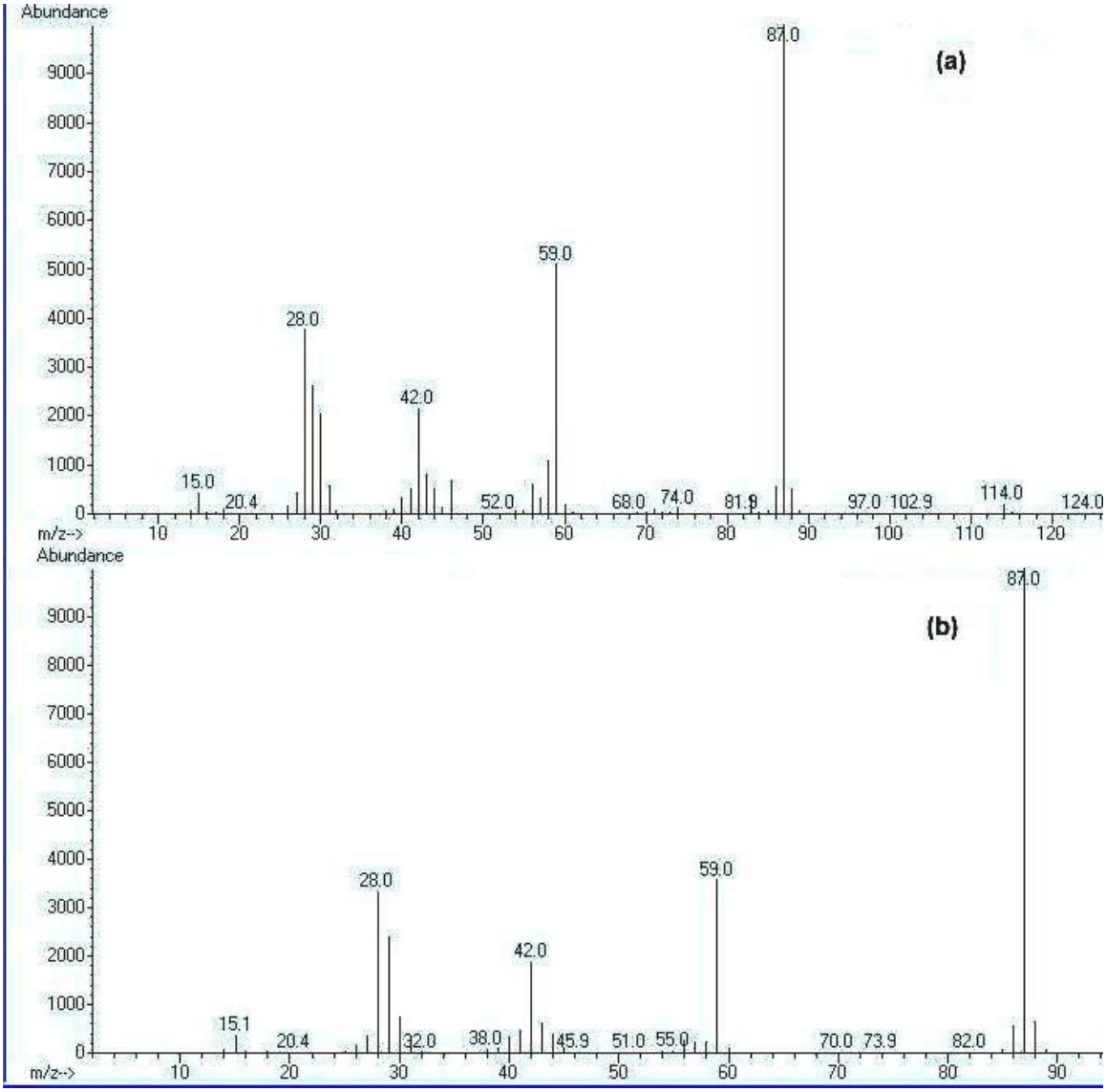

Figure 6.17: Mass spectra of 2-oxazolidone (E) obtained from (a) the sample solution and (b) the standard chemical. (Original in colour)

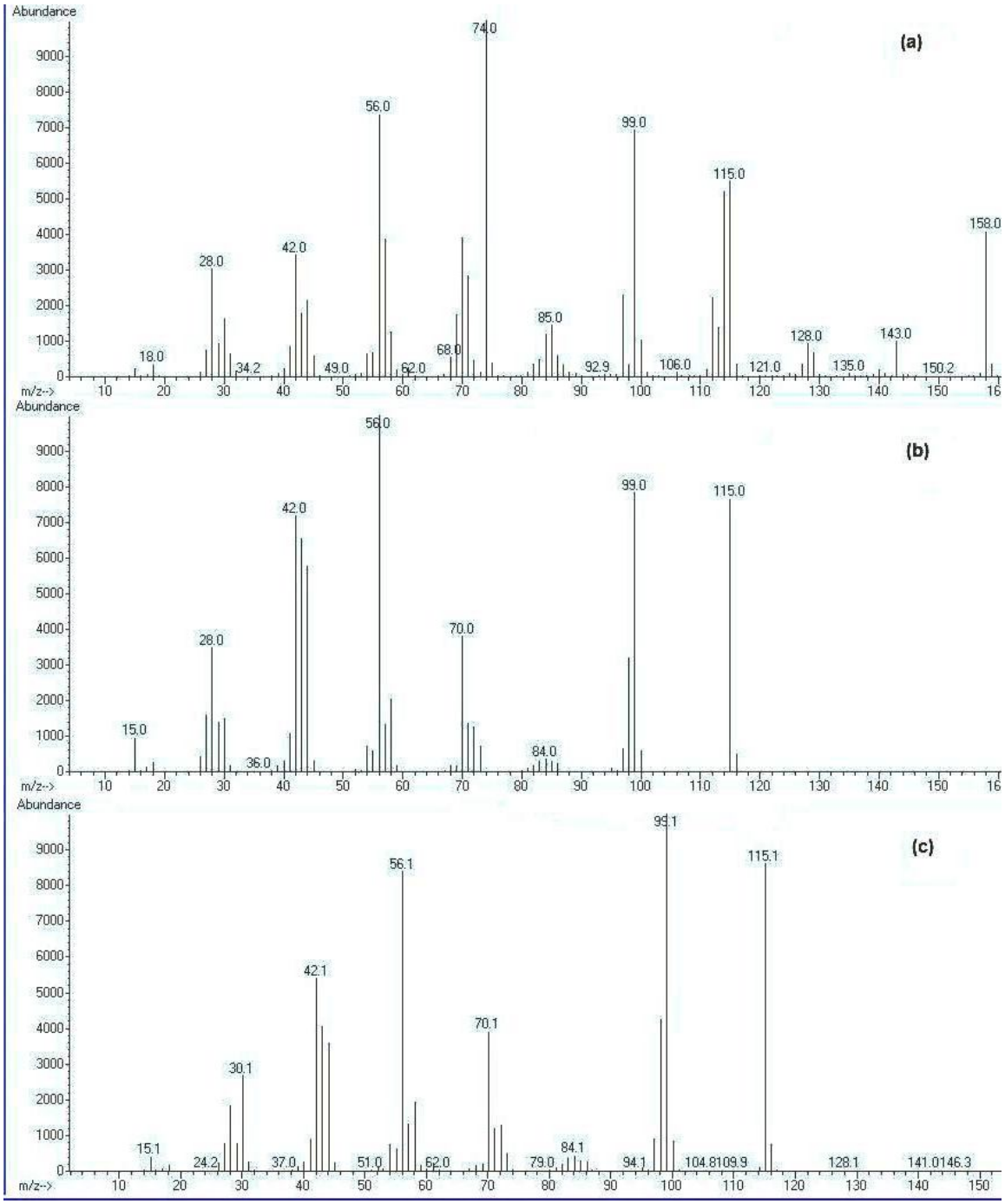

Figure 6.18: Mass spectra of Compound A (G) obtained from (a) the sample solution, (b) MS-NIST98 database, and (c) the standard chemical. (Original in colour)

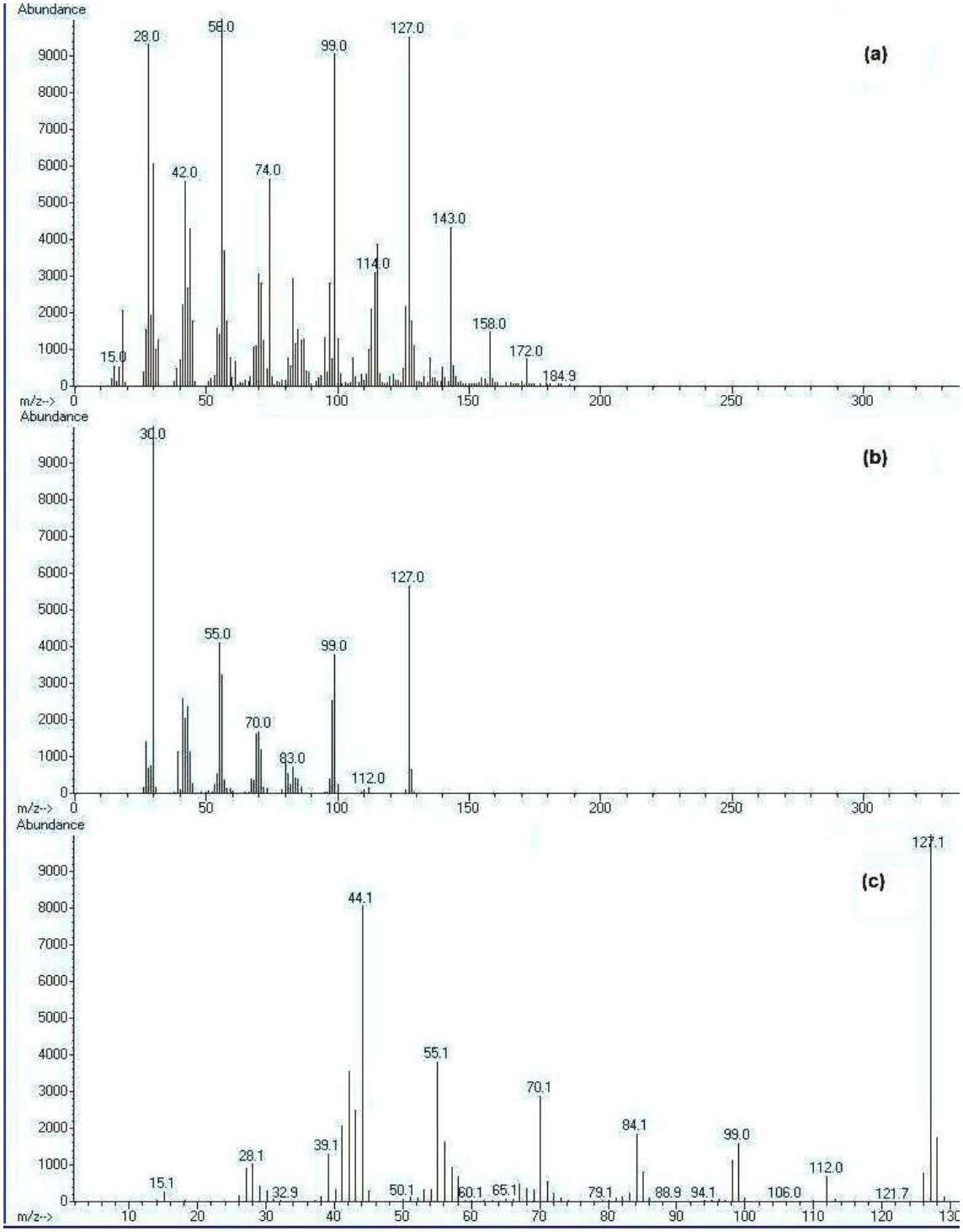

Figure 6.19: Mass spectra of n-methyl caprolactam (H) obtained from (a) the sample solution, (b) MS-NIST98 database, and (c) the standard chemical. (Original in colour)

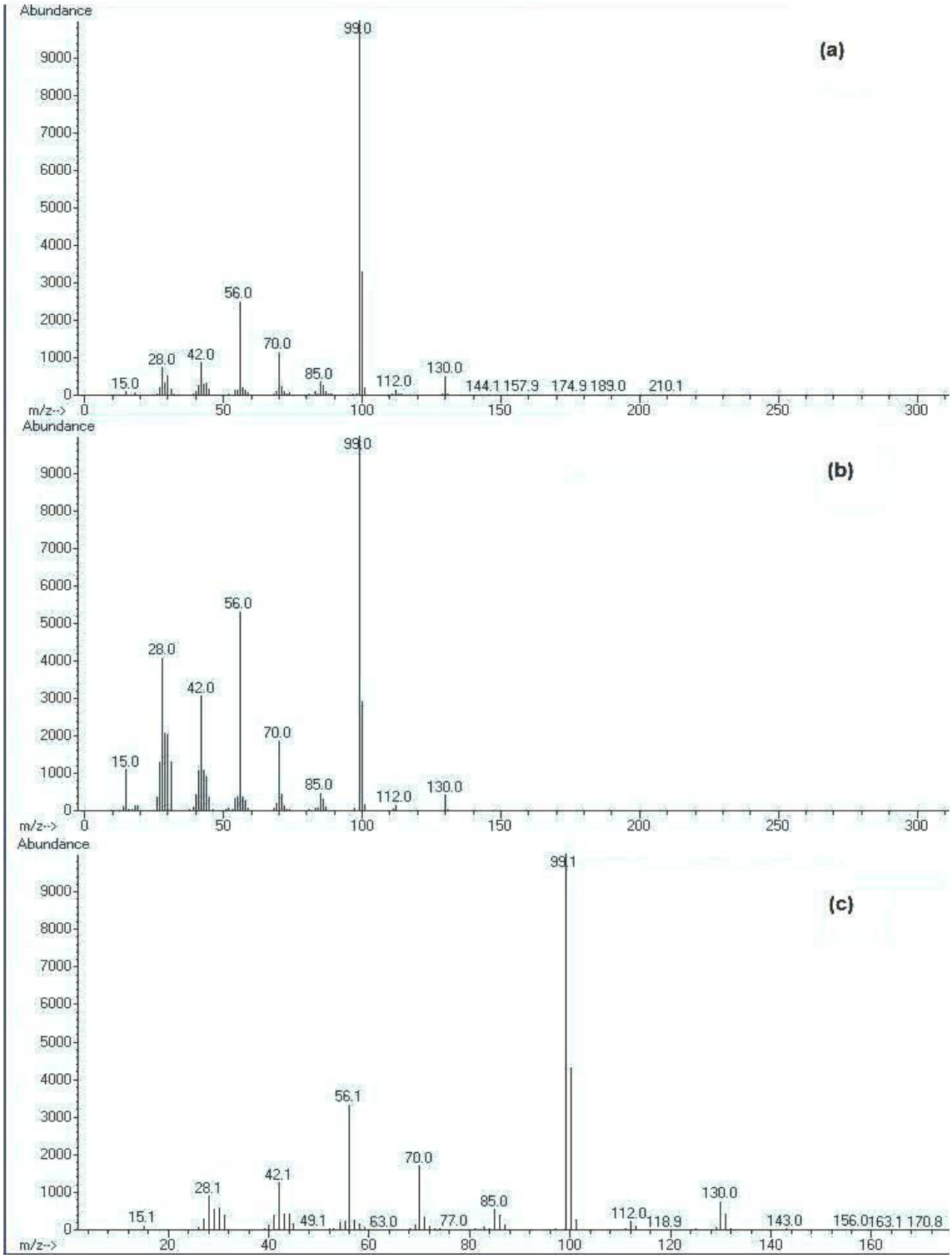

Figure 6.20: Mass spectra of 1-2-hydroxyethyl-2-imidazolidinone (I) obtained from (a) the sample solution, (b) MS-NIST98 database, and (c) the standard chemical. (Original in colour)

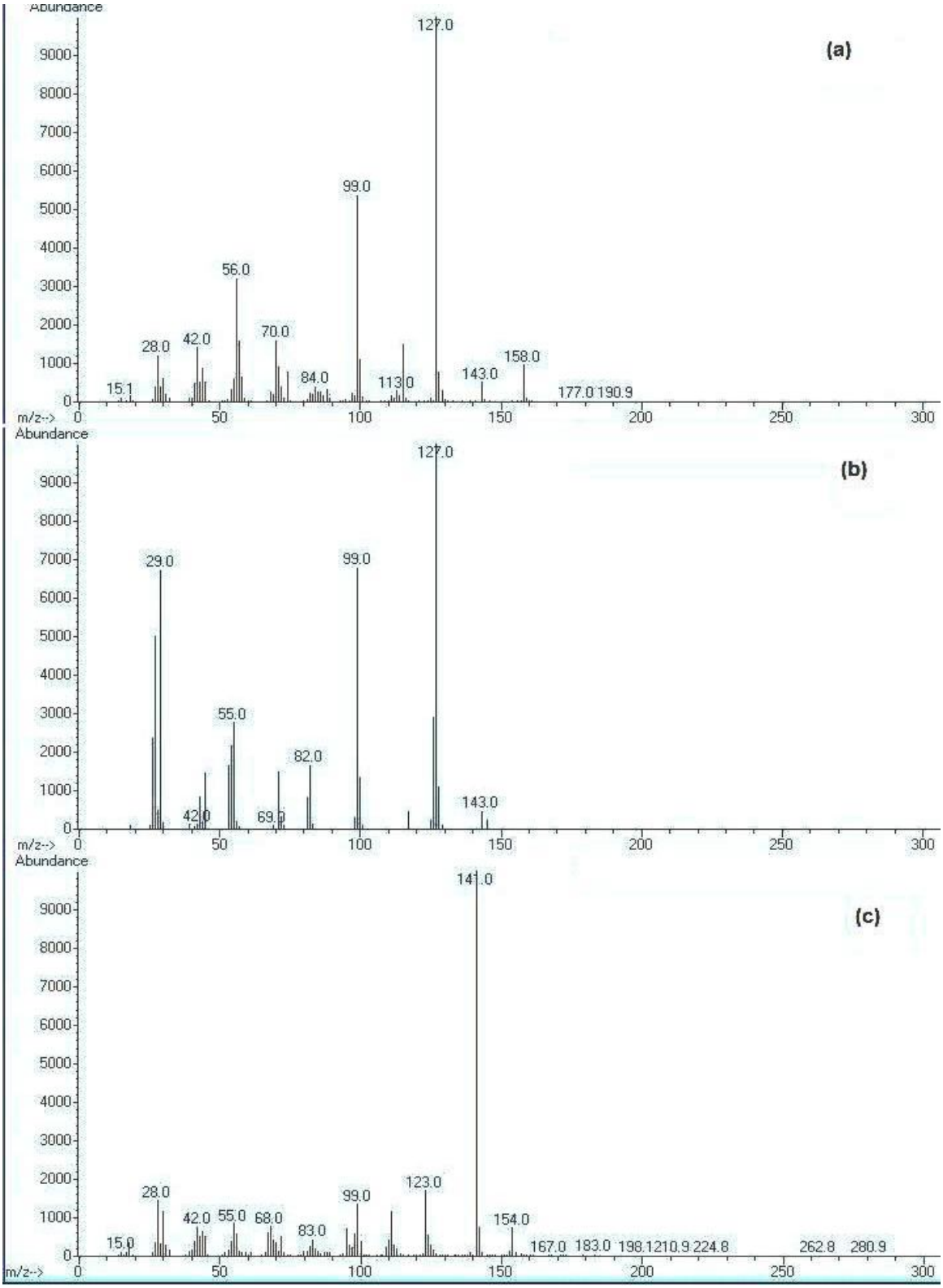

Figure 6.21: Mass spectra of diethyl fumarate (J) obtained from (a) the sample solution, (b) MS-NIST98 database, and (c) the standard chemical. (Original in colour)

6.7 Kinetic study of mixed additives on oxidative MEA degradation

In the kinetic study of the mixed additives on oxidative MEA degradation, hydrochloric acid (HCl), sulphurous acid (H_2SO_3), sulfuric acid (H_2SO_4), and nitric acid (HNO_3) were selected to represent a source of chloride compounds and the aqueous solutions of sulphur dioxide (SO_2), sulphur trioxide (SO_3), and nitrogen dioxide (NO_2) present in a coal fired flue gas, respectively. All the experiments in the kinetic study were performed under the base-case conditions except for one system where two additional temperatures (40°C and 80°C) were introduced in order to study the effect of temperature. The concentrations of the additives were selected based on their positive effects on oxidative MEA degradation, as discussed previously in the single additive systems, and to be equivalent with the kinetic study of carbon steel corrosion. The experimental conditions of the kinetic study of the oxidative MEA degradation are illustrated in Table 6.9. MEA, CO_2 loading, and O_2 concentration were kept constant throughout the degradation study, and the concentrations of the additives were varied between 0 to 2000 ppm of HCl, 0 to 16 of H_2SO_3, 0 to 12 ppm of H_2SO_4, and 0 to 400 ppm of HNO_3.

Table 6.9: The experimental conditions in the kinetic study of the oxidative MEA degradation.

Component	Condition
MEA concentration	5M (1.2% error)
CO_2 loading	0.5 mol CO_2/mol MEA (3.2% error)
O_2 concentration	0.00078M (at 120°C)
Temperature	120°C (±1°C)
Pressure	760 kPa (110 psi)
HCl concentration	0 to 2000 ppm
H_2SO_3 concentration	0 to 16 ppm
H_2SO_4 concentration	0 to 12 ppm
HNO_3 concentration	0 to 400 ppm

Kinetic study is essential to understanding the level of oxidative MEA degradation caused by a given compound. One of the well-known fundamental kinetic correlations is the power law model. In the solutions with mixed additives, the power law model was expressed as:

$$r_{\deg radation} = k_0 \cdot e^{\frac{-E}{RT}} \cdot [MEA]^a \cdot [O_2]^b \cdot [CO_2]^c \cdot [HCl]^d \cdot [H_2SO_3]^e \cdot [H_2SO_4]^f \cdot [HNO_3]^g \quad (6.17)$$

where: r is the degradation rate (kmol MEA/$m^3 \cdot hr$)

k_0 is the pre-exponential factor or collision constant

E is the activation energy (J/mol)

R is the gas constant (8.314 J/(mol·K))

T is the system temperature (K)

[ ] is the concentration (M)

Since the oxidative MEA degradation study focused mainly on the reactions that occurred in the liquid phase, a temperature dependence term in the power law model ($k_0 \cdot e^{\frac{-E}{RT}}$) did not accurately represent the study system due to R being a gas constant. Consequently, it was replaced with a different temperature dependence term ($k_0 \cdot e^{\frac{-H_T}{T}}$), derived based on a system's enthalpy (H; J/mol), which suitably represented the temperature dependence in a liquid phase and which was also a function of temperature. Consequently, equation 6.17 was rearranged to equation 6.18:

$$r_{\deg radation} = k_0 \cdot e^{\frac{-H_T}{T}} \cdot [MEA]^a \cdot [O_2]^b \cdot [CO_2]^c \cdot [HCl]^d \cdot [H_2SO_3]^e \cdot [H_2SO_4]^f \cdot [HNO_3]^g \quad (6.18)$$

where: H_T is the temperature sensitivity constant in liquid phase (K)

Moreover, MEA concentration (5M), O_2 concentration (0.00078M), and CO_2 loading (0.5 mol CO_2 per mol MEA) were kept constant in all the experiments, so equation 6.18 was again rearranged to:

$$r_{\deg radation} = k \cdot e^{\frac{-H_T}{T}} \cdot [HCl]^d \cdot [H_2SO_3]^e \cdot [H_2SO_4]^f \cdot [HNO_3]^g \quad (6.19)$$

where: k is the rate constant

However, in order to distinctively signify the effects of either cation, which was mainly hydrogen ion (H^+), or anions (Cl^-, HSO_3^-, SO_3^{2-}, SO_4^{2-}, and NO_3^-), on the oxidative MEA degradation rates, and to compensate for the absence of any additives in the rate equation, the power law model expressed in equation 6.19 was rearranged to a modified power law equation as presented in equation 6.20:

$$r_{\deg radation} = k \cdot e^{\frac{-H_T}{T}} \cdot [H^+]^d \cdot ([Cl^-]^e + [HSO_3^-]^f + [SO_3^{2-}]^g + [SO_4^{2-}]^h + [NO_3^-]^i) \quad (6.20)$$

where: k is the rate constant

To obtain a reliable rate expression, variables should be varied a minimum of three times, and the number of variables should at least equal to the number of parameters minus one. Thus, there were seven variables (the concentrations of H^+, Cl^-, HSO_3^-, SO_3^{2-}, SO_4^{2-}, NO_3^-, and T) in the mixed-additives systems, which were changed at least three times in order to determine eight parameters expressed as k, d, e, f, g, h, i, and H_T, which demonstrated the orders of reaction and a temperature sensitivity constant. By performing multiple non-linear regressions with the non-linear regression package (NLREG), the modified power law rate equation for the systems containing all four additives (HCl, H_2SO_3, H_2SO_4, and HNO_3) is illustrated in equation 6.21, which provided an acceptable percentage of average absolute deviation (%AAD) of 9.4%.

$$r_{\deg radation} = (8.25E+05)\cdot e^{\frac{-8555}{T}} \cdot [H^+]^{0.37} \cdot ([Cl^-]^{0.24} + [HSO_3^-]^{-0.29} + [SO_3^{2-}]^{-0.02} + [SO_4^{2-}]^{0.05} + [NO_3^-]^{0.17}) \tag{6.21}$$

where the percentage of average absolute deviations (%AAD) was calculated with equation 6.22:

$$\frac{\sum_{i=1}^{n} \left| \frac{r_{Exp} - r_{\Pr edicted}}{r_{Exp}} \right|}{n} \times 100 \tag{6.22}$$

where: r_{Exp} is the experimental degradation rate (kmol MEA/$m^3 \cdot$hr)

$r_{\Pr edicted}$ is the predicted degradation rate (kmol MEA/$m^3 \cdot$hr)

It should be noted that the modified power law rate expression, illustrated in equation 6.21, only represented the system where all the additives (HCl, H_2SO_3, H_2SO_4, and HNO_3) were presented. Even though this work focused mainly on the systems containing all four additives, which represented four different components in a flue gas, it would be beneficial to have some generalized rate equations for the systems containing fewer additives. Therefore, the generalized modified power law rate equation of a single additive system is presented in Table 6.10, where the orders of reaction were kept the same, as illustrated in equation 6.21, but where the rate constant was different. However, the generalized equation for a single system did not represent the systems very well, due to the tremendous %AAD of about 71%.

Table 6.10: The modified power law rate equation of single and four additives system.

Run no.	Temperature (K)	Concentration (M)						Experimental degradation rate (kmol/m^3·hr)	Predicted rate (kmol/m^3·hr)	%ADD
		H^+	Cl^-	HSO_3^-	SO_3^{2-}	SO_4^{2-}	NO_3^-			
1	393	0	0	0	0	0	0	0.00142		
Single additive										
2	393	0.014	0.014	0	0	0	0	0.00051	0.00008	**71.4**
3	393	0.030	0.030	0	0	0	0	0.00074	0.00013	
4	393	0.060	0.060	0	0	0	0	0.00103	0.00019	
5	393	0.00004	0	0.00003	0.000008	0	0	0.00108	0.00058	
6	393	0.00013	0	0.00008	0.000026	0	0	0.00091	0.00065	
7	393	0.00094	0	0.00053	0.000205	0	0	0.00083	0.00081	
8	393	0.00268	0	0.00137	0.000654	0	0	0.00071	0.00094	
9	393	0.00008	0	0	0	0.00004	0	0.00039	0.00002	
10	393	0.00016	0	0	0	0.00008	0	0.00063	0.00003	
11	393	0.00024	0	0	0	0.00012	0	0.00089	0.00003	
12	393	0.00163	0	0	0	0	0.002	0.00085	0.00003	
13	393	0.00388	0	0	0	0	0.004	0.00094	0.00005	
14	393	0.00633	0	0	0	0	0.006	0.00107	0.00007	
$r_{\deg radation} = (3.06E+06)\cdot e^{\frac{-8555}{T}} \cdot [H^+]^{0.37} \cdot ([Cl^-]^{0.24} + [HSO_3^-]^{-0.29} + [SO_3^{2-}]^{-0.02} + [SO_4^{2-}]^{0.05} + [NO_3^-]^{0.17})$ (6.23)										
Four additives										
15	393	0.016	0.014	0.00002	0.000007	0.00003	0.002	0.00147	0.00154	**9.4**
16	393	0.033	0.030	0.00004	0.000013	0.00006	0.003	0.00155	0.00172	
17	393	0.045	0.040	0.00006	0.000020	0.00009	0.005	0.00190	0.00173	
18	393	0.066	0.060	0.00008	0.000027	0.00012	0.006	0.00251	0.00188	
19	313	0.066	0.060	0.00008	0.000027	0.00012	0.006	0.00001	0.00001	
20	353	0.066	0.060	0.00008	0.000027	0.00012	0.006	0.00016	0.00016	
$r_{\deg radation} = (8.25E+05)\cdot e^{\frac{-8555}{T}} \cdot [H^+]^{0.37} \cdot ([Cl^-]^{0.24} + [HSO_3^-]^{-0.29} + [SO_3^{2-}]^{-0.02} + [SO_4^{2-}]^{0.05} + [NO_3^-]^{0.17})$ (6.21)										

CHAPTER SEVEN

THE INHIBITION STUDIES OF CARBON STEEL CORROSION AND OXIDATIVE MEA DEGRADATION

7.1 Inhibitor screening

Several aspects needed to be considered in order to select inhibitors for the inhibition studies of carbon steel (C1020) corrosion and oxidative monoethanolamine (MEA) degradation. They were the process kinetics, the nature of the processes, and the utilization of the process products and/or by-products.

As discussed in previous chapters, (Chapter five section 5.7, and Chapter six section 6.7), the rates of carbon steel corrosion and oxidative MEA degradation were essentially accelerated by the presence of hydrogen ion (H^+), as illustrated in the following equations:

The rate expression of the mixed-additives of carbon steel corrosion:

$$r_{corrosion} = (8.922E+09)\cdot e^{\frac{-6430}{T}} \cdot [H^+]^{0.118} \cdot ([Cl^-]^{0.106} + [HSO_3^-]^{0.007} + [SO_3^{2-}]^{0.006} + [SO_4^{2-}]^{0.006} + [NO_3^-]^{0.102}) \quad (7.1)$$

The rate expression of the mixed-additives of oxidative MEA degradation:

$$r_{\deg radation} = (8.25E+05)\cdot e^{\frac{-8555}{T}} \cdot [H^+]^{0.37} \cdot ([Cl^-]^{0.24} + [HSO_3^-]^{-0.29} + [SO_3^{2-}]^{-0.02} + [SO_4^{2-}]^{0.05} + [NO_3^-]^{0.17}) \quad (7.2)$$

The hydrogen ion (H^+) or so-called proton is the smallest ionic particle with a single positive charge and is well known to be extremely reactive. The hydrogen ion represents the acidity of a solution in terms of a solution pH, which is a value that represents the negative logarithm of hydrogen ion concentration in a solution, as illustrated in equation 7.3:

$$pH = -\log_{10}[H^+] \tag{7.3}$$

where: $[H^+]$ is hydrogen ion concentration in a solution.

Therefore, any inhibitor able to bind with hydrogen ion and lower the ion concentration in a solution would help in reducing corrosion and solvent degradation rates due to less hydrogen ion being available to participate in the process reactions. Generally, such a compound is known as a base. A base is compound that is able to accept hydrogen ion or donate electrons in a form of sharing electrons. Since, the reaction is an acid-base neutralization, it does not involve any electron transfer (e^-) so there is no change in the oxidation number of a corresponding atom. Therefore, a base is compound that probably, to some extent, helps minimize material corrosion as well as oxidative MEA degradation because it provides acid-base neutralization between the base itself and the hydrogen ion.

Another aspect that was taken into consideration in the inhibitor screening was the nature of the processes. Corrosion is electrochemical, which involves reduction-oxidation reactions or Re-Dox reactions. Re-Dox reactions are typically described as chemical reactions which involving electron transfer (e^-), or to be more general, they are reactions in

which atoms have their oxidation number changed. Metal, in the case of this study, carbon steel (1020), loses an electron to the oxidizing agents, or in other words, it is oxidized. On the other hand, oxidative MEA degradation is the process where MEA is degraded in the presence of oxygen and converted into MEA fragments and/or other compounds. Oxygen is potentially catalyzed by metal ions to oxygen-containing free radicals such as superoxide (O_2^-) and hydroxyl radical (·OH), which are known as reactive oxygen species (ROS). Since free radicals are highly unstable due to odd numbers of valent electrons (unpaired electron), they are likely to pick up electrons from other compounds because electrons have a strong tendency to exist in paired rather than unpaired states. Compounds that have been taking up electrons then convert into free radicals, setting up a chain reaction. In the case of the current research, the compound that was attacked by such free radicals was the MEA molecule. The MEA molecule was first converted into an amine radical and then degraded through a series of reactions in the degradation process, which eventually led to solvent loss. Therefore, metal corrosion and oxidative MEA degradation are processes which involving electron transfers either by Re-Dox reactions or free radical-initiating reactions. Therefore, a reducing agent, which is a compound that has a tendency to donate electrons to other compounds or a so-called "electron donor", is able to supply electrons to an oxidizing agent as well as behave as a free radical scavenger by supplying electrons to free radicals, terminating chain reactions. Thus, a "reducing agent" was considered one of the most likely approaches to inhibiting carbon steel corrosion, as well as minimizing the oxidative degradation of MEA.

Another aspect that was taken into account in the inhibitor screening was the utilization of the processes' products and/or by-products. As discussed in Chapter five (section 5.6), the corrosion products were mostly iron oxides and iron hydroxides, and their applications as inhibitors appeared to be limited by their low solubility in aqueous solution. On the other hand, oxidative MEA degradation products, as discussed in Chapter six (section 6.6), appeared to be more applicable because they were highly soluble in aqueous phase. Moreover, the degradation products were mostly amine compounds, which potentially behaved as hydrogen ion scavengers, since they were bases. In addition, by adding the degradation products, not only, to some extent, was it expected that MEA degradation would be inhibited by shifting the reaction to the left but also, there was no additional compound introduced to the system. Consequently, the effects of the oxidative MEA degradation products on carbon steel corrosion were studied as the preliminary inhibitor screening in order to investigate whether if there was any degradation products potentially behaving as a corrosion inhibitor. The preliminary results of the effects of the degradation products on carbon steel corrosion are illustrated in Table 7.1. All the experiments were done under the conditions of 5M MEA (3.1% error), 0.5 CO_2 loading (3.7% error), 0.000351M O_2, 80°C (±1°C), and all the degradation product concentrations were kept the same at 2500 ppm (0.7% error). The results show that, although most of the degradation products appeared to accelerate the carbon steel corrosion, a few products potentially slowed down the corrosion process. Among all those products, compound A, which was shown to essentially slow down the corrosion, was selected as Inhibitor A to be used later on in the inhibition studies of both carbon steel corrosion and oxidative MEA degradation.

In summary, three inhibitors were selected to study the inhibition of carbon steel corrosion and oxidative MEA degradation. They were, Inhibitor A, which was one of the degradation products that appeared to slow down the corrosion process, Inhibitor B, which was a reducing agent in which the derivative was normally used as an oxygen scavenger, and Inhibitor C, which was another reducing agent that reported to behave mostly as a free radical scavenger.

Table 7.1: The effects of the MEA degradation products on carbon steel (1020) corrosion.

Degradation product	**Corrosion rate (mpy)**	**Inhibition efficiency (%)**
Base-case corrosion	**391.6**	**0**
3-methylpyridine	502.4	-28.3
Glycine anhydride	363.9	7.1
N-acetylethanolamine	357.7	8.7
2-oxazolidone	419.6	-7.2
Compound A	***312.2***	***20.3***
N-methyl caprolactam	387.9	0.9
1-2-hydroxyethyl-2-imidazolidinone	467.8	-19.5
Diethyl fumarate	395.5	-1.0

7.2 Experimental conditions

The inhibition studies of carbon steel (C1020) corrosion and oxidative MEA degradation were done by varying three different inhibitors, which were Inhibitor A, Inhibitor B, and Inhibitor C, and the mixed inhibitors, along with their concentrations under the base-case conditions (no inhibitor). The base-case conditions were selected in order to replicate the most severe conditions of each process, where MEA concentration, CO_2 loading, the concentration of hydrochloric acid (HCl) which represented the source of chloride compounds in a flue gas, the concentrations of sulphurous acid (H_2SO_3), sulphuric acid (H_2SO_4), and nitric acid (HNO_3), which represented sulphur dioxide (SO_2), sulphur trioxide (SO_3), and nitrogen dioxide (NO_2) in aqueous solutions, respectively, were fixed and kept the same in both processes. However, O_2 concentrations were different between the corrosion and solvent degradation experiments due to the fact that the corrosion process was operated at atmospheric pressure, while, solvent degradation was operated at elevated pressure (110 psi) in order to accelerate the reaction process. Temperatures were also different, since the corrosion experiment needed to be conducted at the temperature below the boiling point of water in order to prevent rapid vapourization of the heating medium, while the solvent degradation experiment was able to achieve the higher temperature range. The base-case conditions of each process and the reaction rates of the base-case conditions are presented in Table 7.2.

Table 7.2: The base-case conditions (no inhibitor) of the carbon steel (C1020) corrosion and oxidative MEA degradation experiments.

Condition	Carbon steel (C1020) corrosion	Oxidative MEA degradation
MEA concentration	5M (0.9% error)	5M (1.1% error)
CO_2 loading	0.5 mol CO_2/mol MEA (4.3% error)	0.5 mol CO_2/mol MEA (3.2% error)
HCl concentration	2000 ppm (0.4% error)	2000 ppm (8.7% error)
H_2SO_3 concentration	16 ppm (8.3% error)	16 ppm (1.1% error)
H_2SO_4 concentration	12 ppm (1.0% error)	12 ppm (0.5% error)
HNO_3 concentration	400 ppm (1.4% error)	400 ppm (0.2% error)
O_2 concentration	0.000351M	0.00078M
Temperature	80°C (±1°C)	120°C (±1°C)
The rate of reaction	391.6 mpy	0.002512 kmol/$m^3 \cdot$hr

7.3 The calculation of inhibitor's efficiency (%)

The inhibitor's efficiency (%) was calculated using the following equation:

$$\text{Inhibitor's efficiency (\%)} = \left[\frac{R_{uninhibited} - R_{inhibited}}{R_{uninhibited}} \right] \times 100 \qquad (7.4)$$

where:

$R_{uninhibited}$ is the rate of the system without inhibitor (rate of the base-case system).

$R_{inhibited}$ is the rate of the systems with inhibitor.

7.4 The effects of various inhibitors in single inhibitor systems on carbon steel (1020) corrosion and oxidative MEA degradation

7.4.1 Inhibitor A

Inhibitor A is a cyclic amine that has more than one nitrogen atom in the structure.

7.4.1.1 The inhibitor's efficiency of Inhibitor A on carbon steel (1020) corrosion

The corrosion rate and the inhibitor's efficiency of Inhibitor A in systems containing various concentrations of the inhibitor are illustrated in Figure 7.1. The inhibiting efficiency increased with increasing inhibitor concentration. However, a plateau, where there was no further change in the efficiency, was reached at an inhibitor concentration of about 15000 ppm (0.13M) where the maximum efficiency appeared to be 88.9%. The Tafel plots of the systems containing various concentrations of Inhibitor A are also presented in Figure 7.2, and the plots show that the cathodic region was more sensitive to the change of inhibitor concentration than the anodic region, as a larger deviation from the base-case system was observed in the cathodic polarization. This indicated that Inhibitor A helped minimize corrosion by inhibiting the cathodic reaction within the electrochemical reactions.

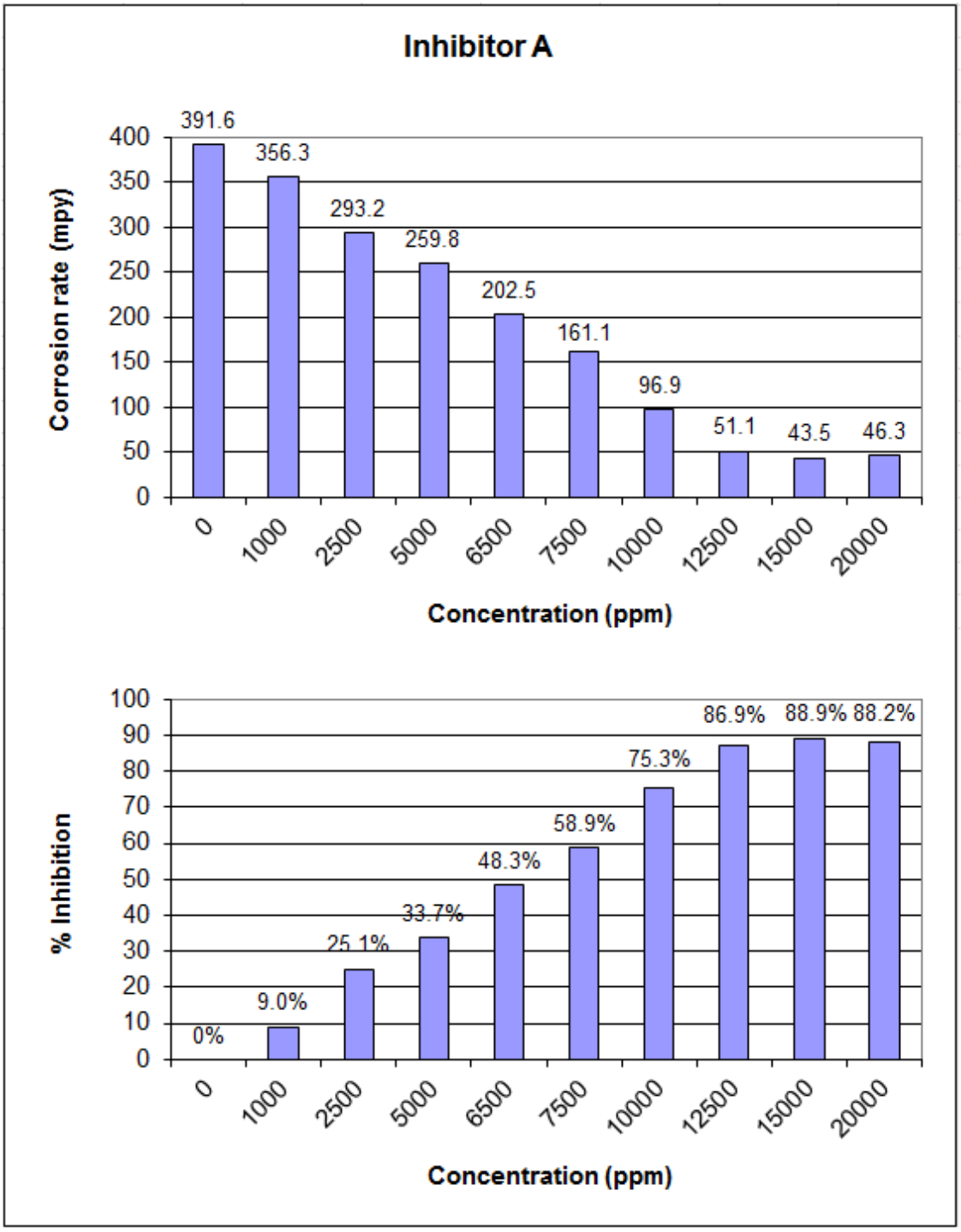

Figure 7.1: The corrosion rate and inhibitor's efficiency of Inhibitor A in the systems containing various concentrations of Inhibitor A (%error: 3.4%). (Original in colour)

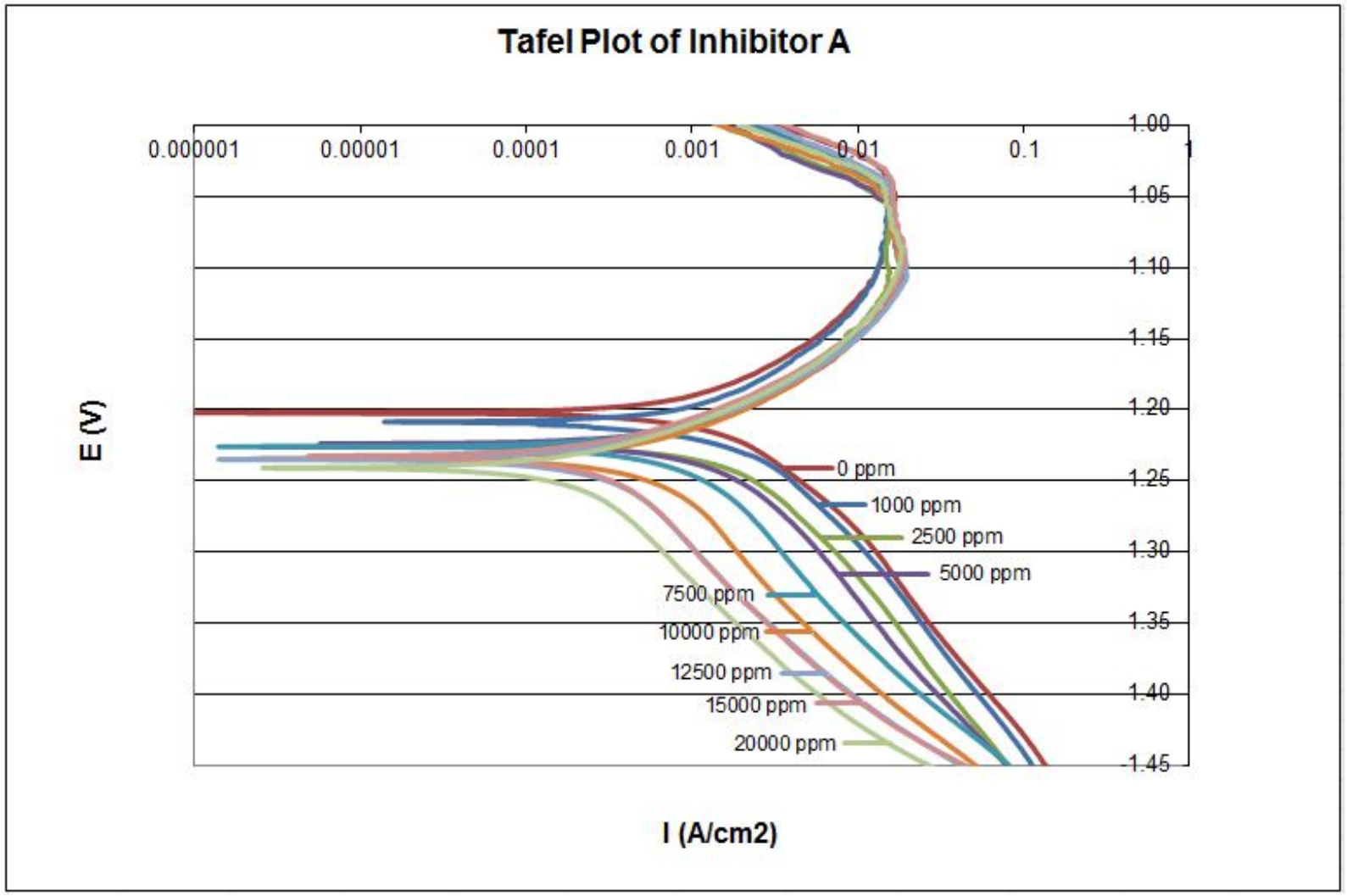

Figure 7.2: Tafel plots of the systems containing various concentrations of Inhibitor A. (Original in colour)

Since Inhibitor A is a base that contains more than one nitrogen atom in its structure, it had a strong tendency to bind with hydrogen ion (H^+) potentially by binding with lone pair electrons of nitrogen atoms, and reduced hydrogen ion concentration in a solution. Thus, when hydrogen ion, which proved to predominantly accelerate the corrosion process (as expressed in equation 7.1) were occupied by Inhibitor A, it led to fewer hydrogen ion being available to participate as oxidizing agents in the electrochemical reactions and eventually led to the reduction of the corrosion rate. Since, the amount of hydrogen ion in a solution is typically represented by the solution pH, the reduction of hydrogen ion concentration due to the acid-base neutralization of Inhibitor A and hydrogen ion was able to be determined by measuring the pH of the system. As a result, the pH of the solutions containing different concentrations of Inhibitor A was measured, and the results are presented in Table 7.3. The results show that pH of the solution increased as Inhibitor A concentration increased, which confirmed that hydrogen ion concentration reduced as Inhibitor A was added to the system. Moreover, Inhibitor A also prevented corrosion by adsorbing onto the metal surface and forming a physical barrier that reduced the metal reactivity in the Re-Dox reactions. The adsorption behaviour described by the interaction between lone pair electrons of the nitrogen atom with electron vacancy in the transition metal, lone pair electrons were able to act as donor electrons and filled in the gap of electron loss due to iron dissolution, leaving the surface with the positive charge (Li et al., 1996). Consequently, Inhibitor A was able to adsorb onto the metal surface by chemisorption and helped protect the surface from participation in any further electrochemical reactions. The adsorption of Inhibitor A onto the metal surface was confirmed from the data provided by GC-MS, which showed that after corrosion occurred, Inhibitor

A concentration in a solution reduced without any formation of additional compound, which indicated that there must be some Inhibitor A left on the metal surface that led to a reduction of the inhibitor concentration. The concentrations of Inhibitor A before and after the corrosion experiments are illustrated in Table 7.4. In summary, Inhibitor A prevented corrosion by behaving as a hydrogen ion scavenger, which helped to reduce hydrogen ion concentration in the solution, and also by adsorbing onto the metal surface, which helped to protect the metal surface from participating in further electrochemical reaction.

Table 7.3: pH of the solutions which containing different concentrations of Inhibitor A (%error: 0.17%).

Inhibitor A concentration (ppm)	pH
0	8.74
2500	8.77
5000	8.81
7500	8.85
10000	8.88

Table 7.4: The concentrations of Inhibitor A before and after the corrosion experiments (%error: 2.8%).

Inhibitor A	Concentration (ppm)	% Concentration reduction
2500 ppm		
Before	2448	
After	2283	7%
5000 ppm		
Before	5103	
After	4449	13%
6500 ppm		
Before	6222	
After	5175	17%
7500 ppm		
Before	7838	
After	6128	22%
10000 ppm		
Before	9889	
After	7104	28%

7.4.1.2 The inhibitor's efficiency of Inhibitor A on oxidative MEA degradation

The inhibiting efficiency of Inhibitor A on the oxidative MEA degradation increased as inhibitor concentration increased, which was indicated from the decrease of the degradation rate. However, the maximum efficiency of Inhibitor A was reached at an inhibitor concentration of 1000 ppm (0.01M), where the degradation rate appeared to be 0.000069 $kmol/m^3 \cdot hr$, which provided an excellent maximum inhibiting efficiency of 97.3%. Unfortunately, the efficiency continually declined when the concentration increased beyond 1000 ppm (0.01M).

The role of Inhibitor A in preventing oxidative MEA degradation was that it bound with hydrogen ion (H^+), which proved to be a primary contributor to solvent degradation (as expressed in equation 7.2) due to the fact that it helped initiate the degradation process by starting a chain reaction. Inhibitor A, which is a base that contains a couple of lone pair electrons of the nitrogen atoms, bound with hydrogen ions through acid-base neutralization, reducing hydrogen ion concentration in the solution, and this resulted in the reduction of the degradation rate. Since the amount of hydrogen ion in a solution can be represented by the pH of the solution, the pH of the solutions containing various concentrations of Inhibitor A are given in Table 7.5. The pH appeared to increase as inhibitor concentration increased, which indicated that the hydrogen ion concentration in the solution was reduced. Moreover, Inhibitor A also reacted with hydrogen ion in that the nitrogen atom in an amino group ($–NH_2$) firstly bound with hydrogen ion in the solution and, then, the newly formed compound split out of the parent molecule (Inhibitor A)

as ammonia (NH_3). The formation of ammonia was confirmed by the results obtained from GC-MS, which showed that Inhibitor A concentration decreased as operating time increased, while the Inhibitor A's derivative, which was a compound that had the exact same structure as Inhibitor A except that it had no amino group in the structure, was produced simultaneously with the decrease of Inhibitor A concentration. In other words, ammonia was produced simultaneously with the decomposition of Inhibitor A to its derivative compound. In addition, it should be noted that the decomposition of Inhibitor A to its derivative compound required days for the reaction to take place, and this was why no Inhibitor A derivative was found in the corrosion experiments, as they took only hours to operate.

However, when Inhibitor A concentration exceeded 1000 ppm, its efficiency in inhibiting solvent degradation was reduced. The reduction of the inhibitor performance could be because Inhibitor A is an amine so it had a strong tendency to behave the same as typical amines by forming an amine radical in the presence of free radicals, which then accelerated a chain reaction of oxidative MEA degradation (Chi and Rochelle, 2002). Therefore, beyond the point where Inhibitor A performed to its maximum efficiency as a hydrogen ion scavenger, amine radical formation began to dominate, which led to the reduction of Inhibitor A performance in inhibiting oxidative solvent degradation.

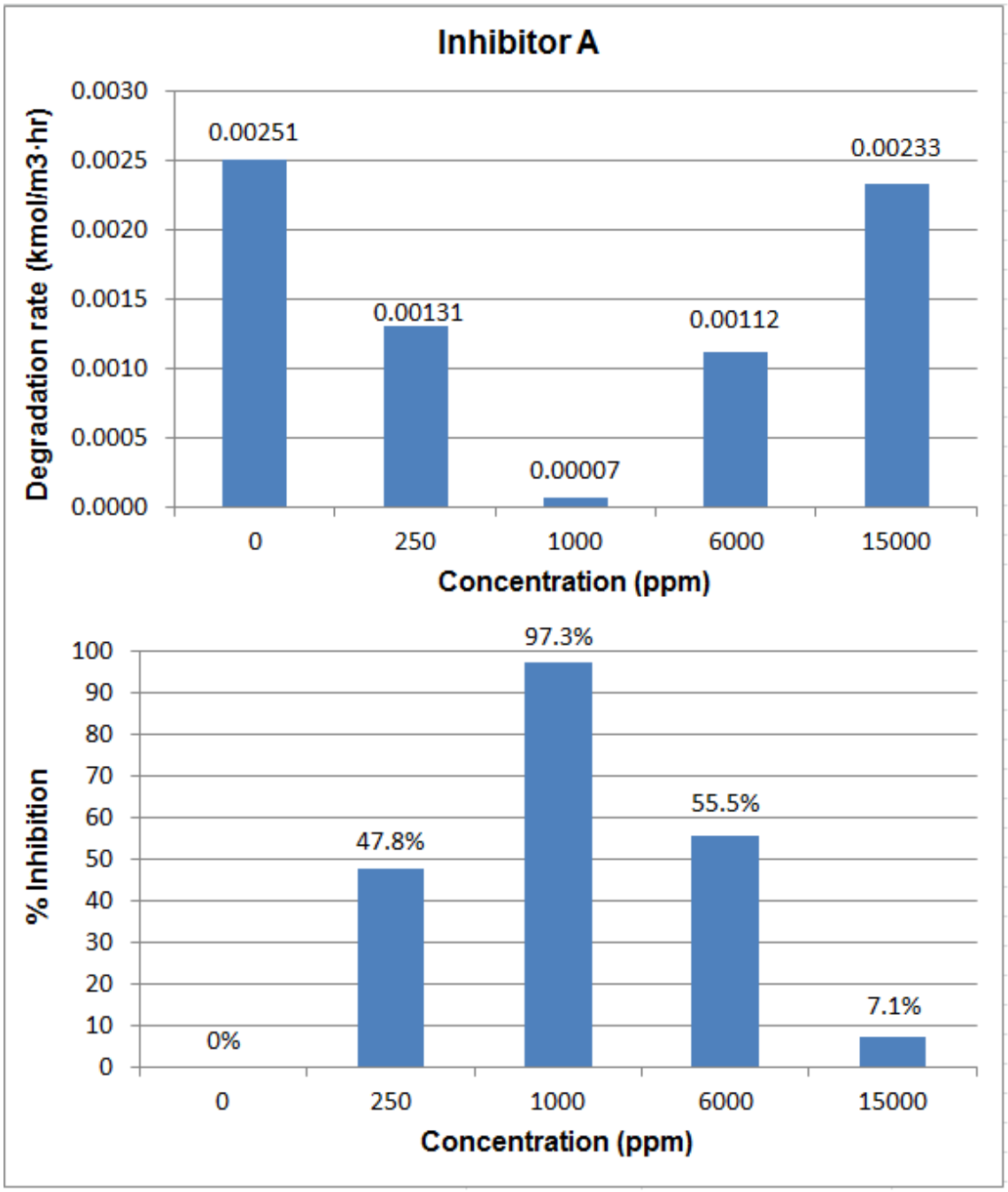

Figure 7.3: The degradation rate and inhibitor's efficiency of Inhibitor A in the systems containing various concentrations of Inhibitor A (%error: 3.8%). (Original in colour)

Table 7.5: pH of the solutions which containing different concentrations of Inhibitor A (%error: 0.21%).

Inhibitor A concentration (ppm)	pH
0	9.01
1000	9.17
6000	9.45
15000	9.52

7.4.2 Inhibitor B

Inhibitor B is a soluble monocation salt of a weak acid compound.

7.4.2.1 The inhibitor's efficiency of Inhibitor B on carbon steel (1020) corrosion

The corrosion rate and the inhibitor's efficiency of Inhibitor B in systems containing various concentrations of the inhibitor are illustrated in Figure 7.4, which shows that the inhibitor's efficiency of Inhibitor B in reducing carbon steel corrosion increased with increasing inhibitor concentration until the maximum inhibiting efficiency was reached at an inhibitor concentration of 100 ppm (0.001M), when its efficiency appeared to be 92.4%. Then, the efficiency continually declined when the concentration exceeded 100 ppm.

The role of Inhibitor B in inhibiting the corrosion process within the concentration range of less than 100 ppm was that it primarily performed as an oxygen scavenger by donating its own electrons to the dissolved oxygen. Since oxygen, which was one of the major oxidizing agents in the electrochemical reactions, was reduced in concentration, the corrosion rate was reduced. The behaviour of Inhibitor B as an oxygen scavenger is supported by the Tafel plots shown in Figure 7.5. The plots show that increasing inhibitor concentration resulted in a shift of the corrosion potential (E_{corr}) to a lower value. The plots illustrated that the change of inhibitor concentration mostly affected the cathodic region, which confirmed that adding Inhibitor B resulted in minimizing the cathodic reac-

tion in the electrochemical process. The reaction between Inhibitor B and dissolved oxygen was also supported by the fact that there was a product of the reaction, which was the oxidized species of Inhibitor B, found in the systems. In addition, it should be noted that, although Inhibitor B was able to donate its electrons not only to the dissolved oxygen but also other species, the reaction between Inhibitor B and dissolved oxygen was likely to be more pronounced, as indicated from the formation of the oxidized species of Inhibitor B, which was an anionic specie that was detected using CE-DAD techniques.

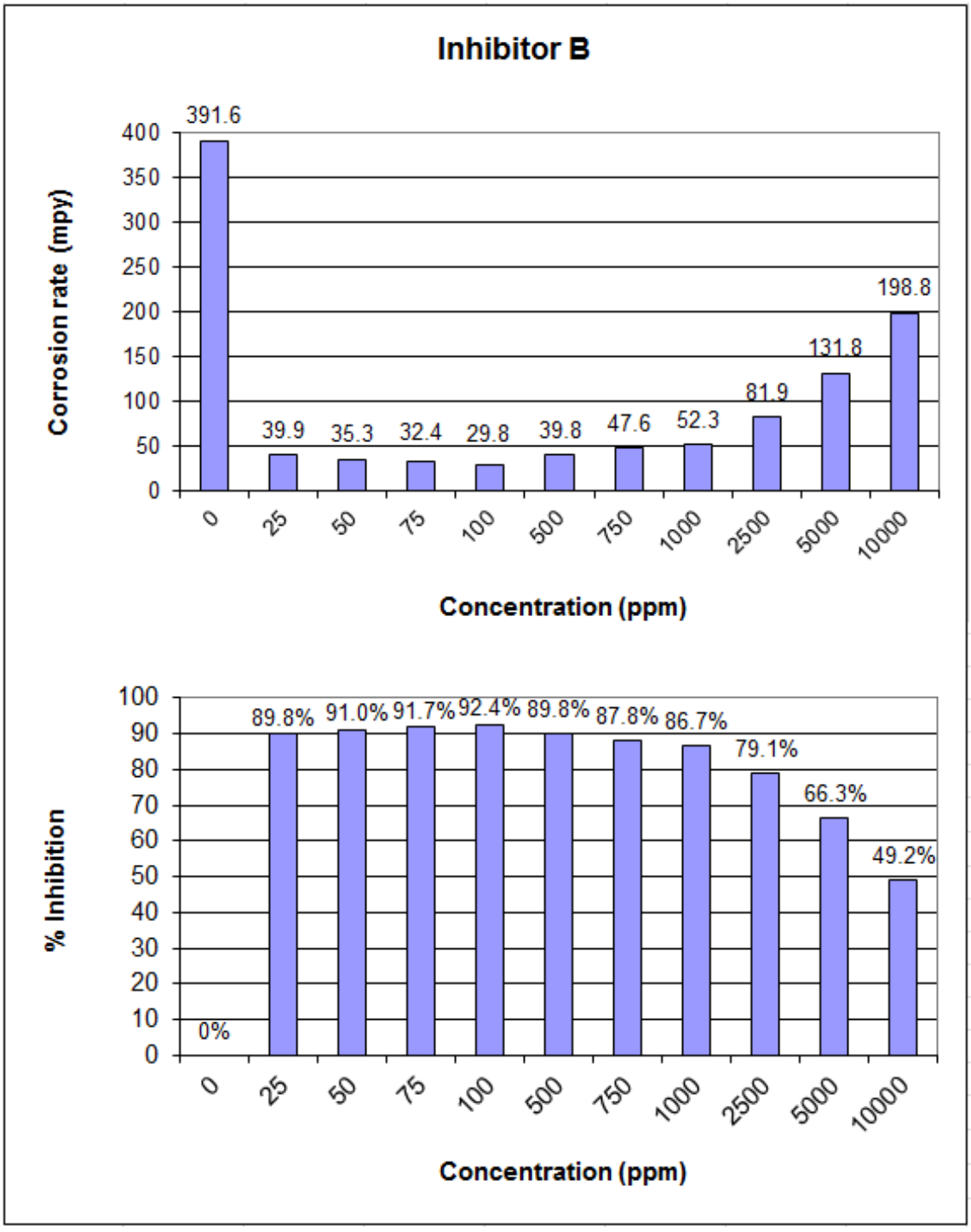

Figure 7.4: The corrosion rate and inhibitor's efficiency of Inhibitor B in the systems containing various concentrations of Inhibitor B (%error: 1.7%). (Original in colour)

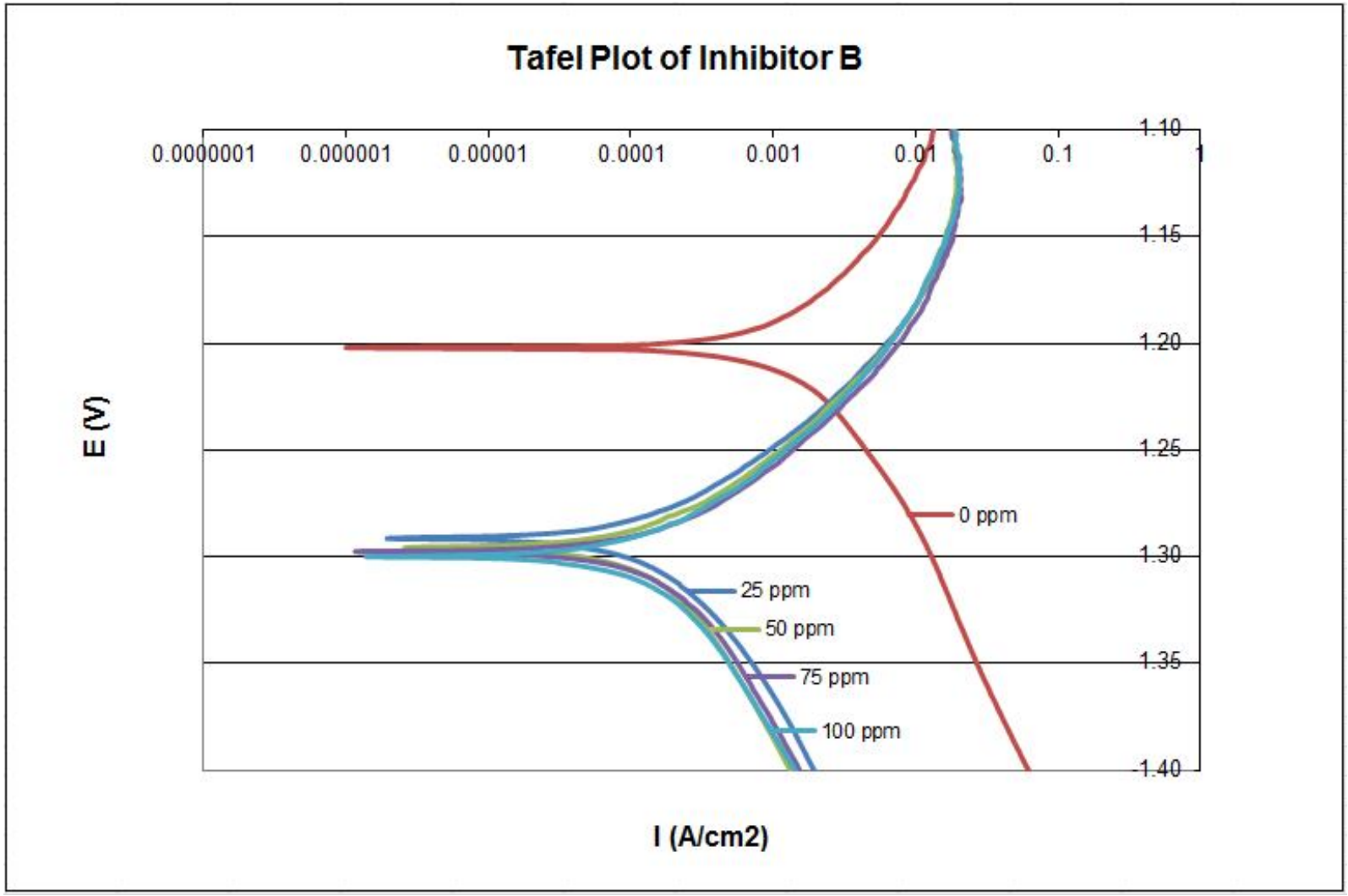

Figure 7.5: Tafel plots of the systems containing Inhibitor B in a concentration range between 0 to 100 ppm. (Original in colour)

However, when the Inhibitor B concentration exceeded 100 ppm, the inhibiting efficiency continually declined. This was because, when the inhibitor concentration increased beyond the optimum point of 100 ppm, the performance of Inhibitor B as an oxygen scavenger reduced. This is confirmed by the Tafel plots presented in Figure 7.6, which show that the deviation of the cathodic region between the systems containing Inhibitor B and the base-case system (no Inhibitor B) became narrower as the inhibitor concentration increased, which indicated that the performance of Inhibitor B as an oxygen scavenger was less effective. Moreover, there was a compound found within the systems containing more than 100 ppm of the inhibitor concentration that was confirmed, by comparison with the standard compound using CE-DAD techniques, to be one of Inhibitor B's derivatives, one that has been reported to have some interference in the oxidation of Inhibitor B (Chen and Rochelle 1998). In other words, Inhibitor B's derivative inhibited the reaction between Inhibitor B and dissolved oxygen. Consequently, the formation of Inhibitor B's derivative is a possible reason for the reduction of Inhibitor B's performance as an oxygen scavenger when the inhibitor concentration exceeded over the optimum point (100 ppm). It should be noted that this derivative can also be formed in systems containing inhibitor concentrations of less than 100 ppm. However, it was too small in quantity to either be detected or to have any effect on the inhibiting performance of Inhibitor B. In summary, Inhibitor B showed excellent performance in minimizing carbon steel corrosion by behaving primarily as an oxygen scavenger.

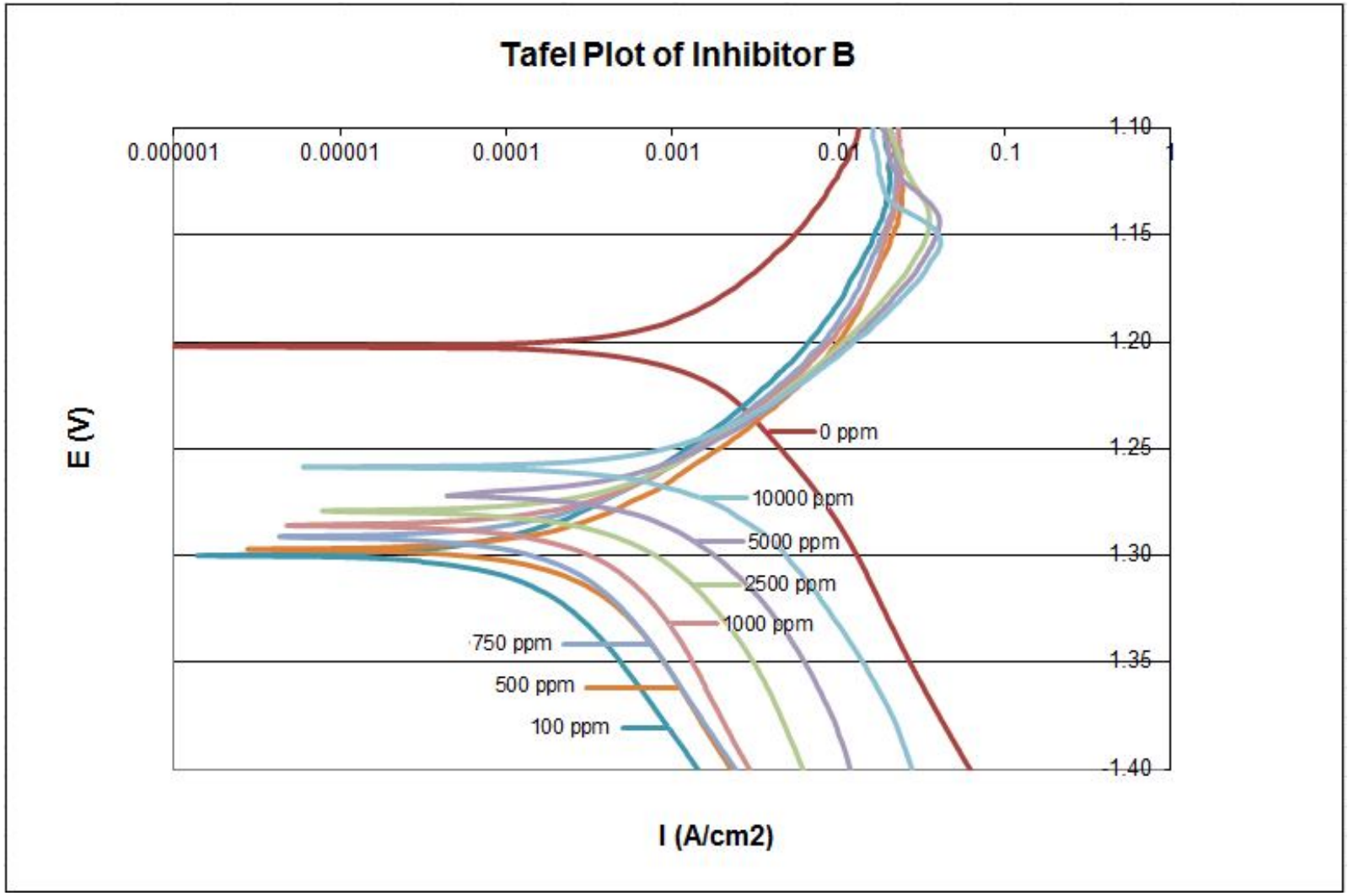

Figure 7.6: Tafel plots of the systems containing Inhibitor B in a concentration range between 100 to 10000 ppm. (Original in colour)

7.4.2.2 The inhibitor's efficiency of Inhibitor B on oxidative MEA degradation

The maximum inhibiting efficiency of Inhibitor B on oxidative MEA degradation appeared to be about 59.9% at inhibitor concentration of 100 ppm (0.001M). The role of Inhibitor B in preventing oxidative MEA degradation was that it behaved as an oxygen scavenger to reduce oxygen concentration in a solution. Oxygen, which is a major contributor to oxidative solvent degradation, partly reacted with Inhibitor B instead of the MEA, resulting in the less MEA oxidation and leading to a reduction in the oxidative MEA degradation rate. Inhibitor B, as previously discussed, reacted with oxygen in a way that it supplied electrons to the oxygen atom, and, then, Inhibitor B itself was oxidized. As presented in Figure 7.7, within the concentration range of 0 to 100 ppm, the efficiency of Inhibitor B increased with increasing inhibitor concentration, and the primary reason for the inhibition effect was the reaction between Inhibitor B and dissolved oxygen. However, when the inhibitor concentration exceeded the optimum point at 100 ppm, the efficiency appeared to reduce. The reduction of Inhibitor B performance when the concentration exceeded the optimum point at 100 ppm was potentially for two reasons. First, the oxidized specie of Inhibitor B itself can be catalyzed to a free radical (Chen and Rochelle 1998), and free radicals are well known to be the primary initiators for a chain reaction in the oxidative degradation process. So, if the oxidized compound of Inhibitor B was able to convert into a free radical, it helped to accelerate the oxidative degradation process by initiating a chain reaction. Another reason that possibly led to the reduction of Inhibitor B performance was the formation of Inhibitor B's derivative, which was the same compound found in the corrosion systems, as discussed in Section 7.4.2.1. This In-

hibitor B derivative appeared to interfere with the reaction between Inhibitor B and oxygen, resulting in lower performance of Inhibitor B as an oxygen scavenger. The formation of the Inhibitor B's derivative was confirmed by comparing it with the standard compound using CE-DAD techniques where the concentration of the Inhibitor B derivative, in terms of peak area, appeared to initially increase and then became constant, as presented in Figure 7.8.

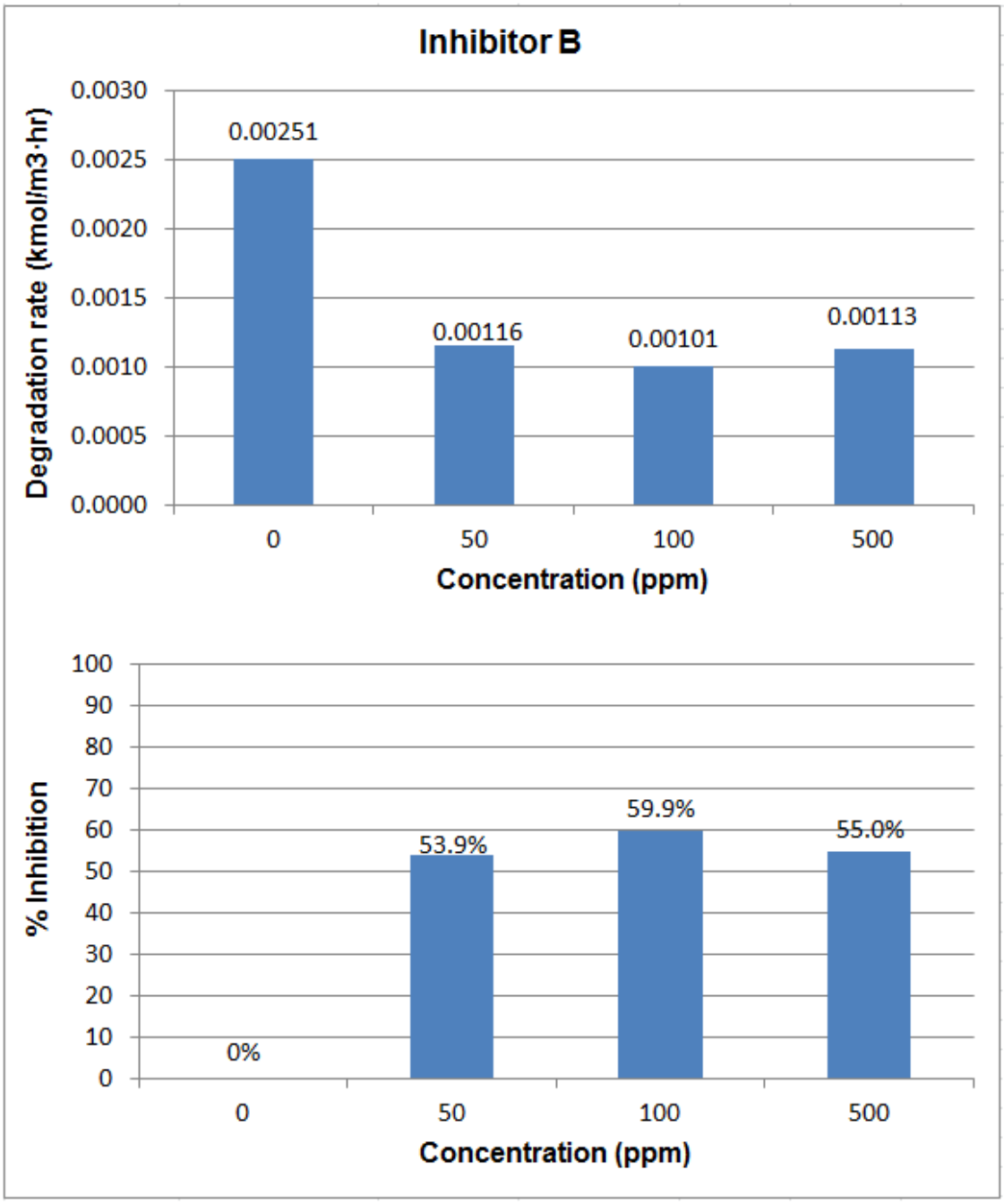

Figure 7.7: The degradation rate and inhibitor's efficiency of Inhibitor B in the systems containing various concentrations of Inhibitor B (%error: 2.1%). (Original in colour)

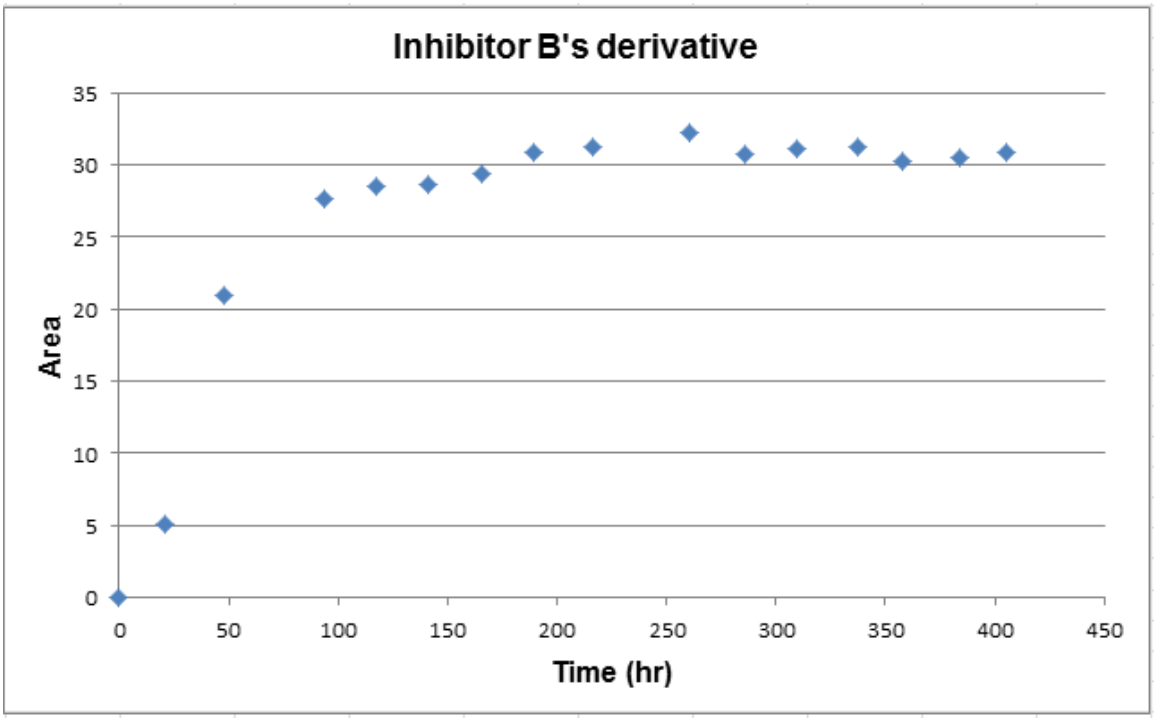

Figure 7.8: Inhibitor B's derivative in the system containing Inhibitor B concentration of 500 ppm (%error: 1.04%). (Original in colour)

7.4.3 Inhibitor C

Inhibitor C is a double cation salt of hydroxycarboxylic acid.

7.4.3.1 The inhibitor's efficiency of Inhibitor C on carbon steel (1020) corrosion

The inhibiting efficiency of Inhibitor C on carbon steel corrosion increased with increasing inhibitor concentration, and the maximum efficiency was reached at an inhibitor concentration of 80,000 ppm (0.28M), where the efficiency appeared to be at 42.7%, as presented in Figure 7.9. The performance of Inhibitor C appeared to stabilize after it reached the maximum point, as there was no significant change in the efficiency with further increases in inhibitor concentration. The role of Inhibitor C in minimizing carbon steel corrosion is that it functioned as a radical scavenger. Free radicals were found to be capable of accept electrons released by the metal surface, which potentially stimulated further iron dissolution, resulting in more material corrosion. In the presence of Inhibitor C, these free radicals tended to react with it so that they gained electrons from the inhibitor itself instead of the metal, which resulted in less metal dissolution and, therefore, less material corrosion. Although the radical scavenging mechanism of Inhibitor C on carbon steel corrosion remains unclear, the behaviour of Inhibitor C as a radical scavenger has been well known. The Tafel plots of the systems containing various concentrations of Inhibitor C are shown in Figure 7.10. The plots illustrate that increasing Inhibitor C concentration affected both anodic and cathodic reactions almost equally.

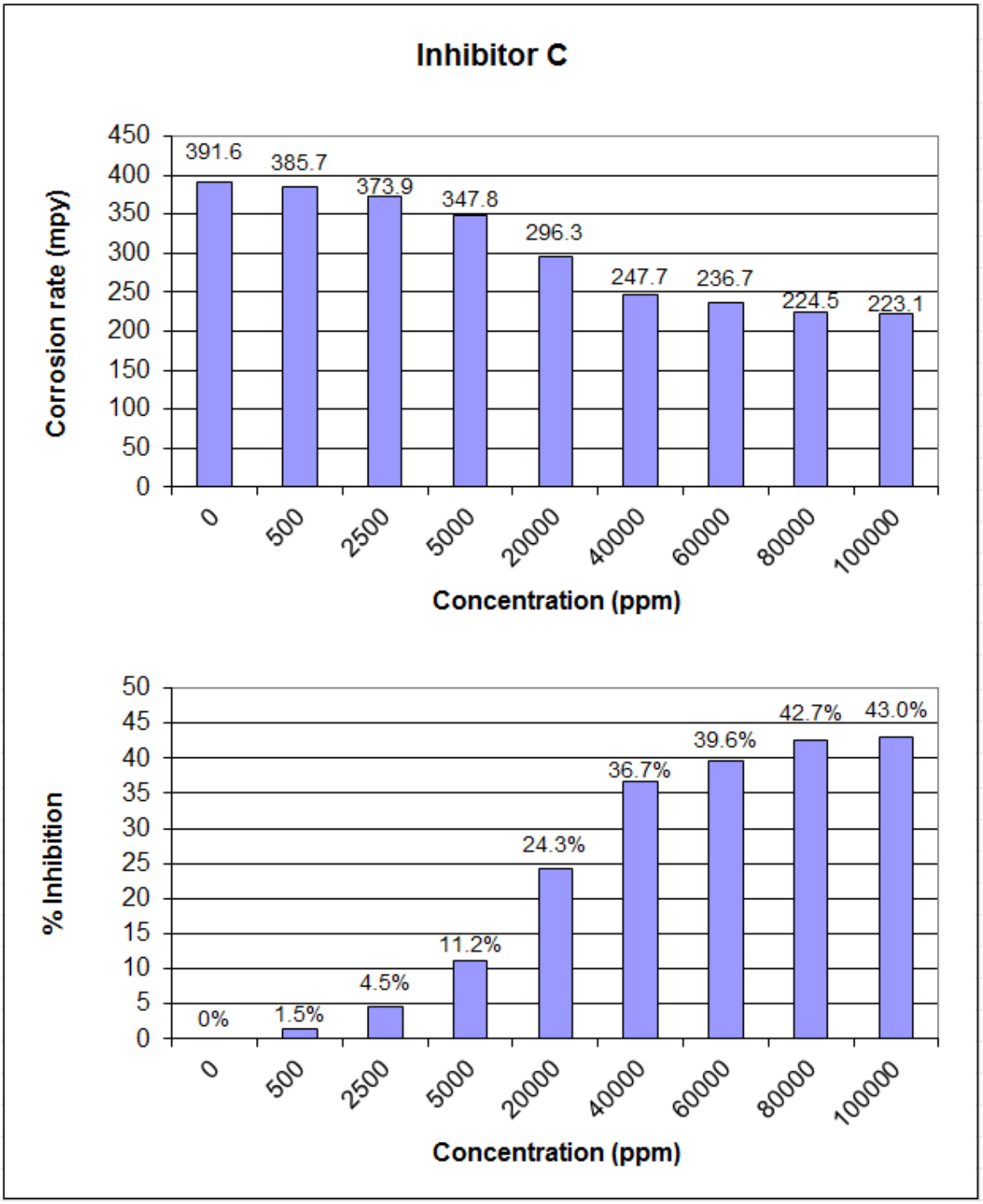

Figure 7.9: The corrosion rate and inhibitor's efficiency of Inhibitor C in the systems containing various concentrations of Inhibitor C (%error: 2.4%). (Original in colour)

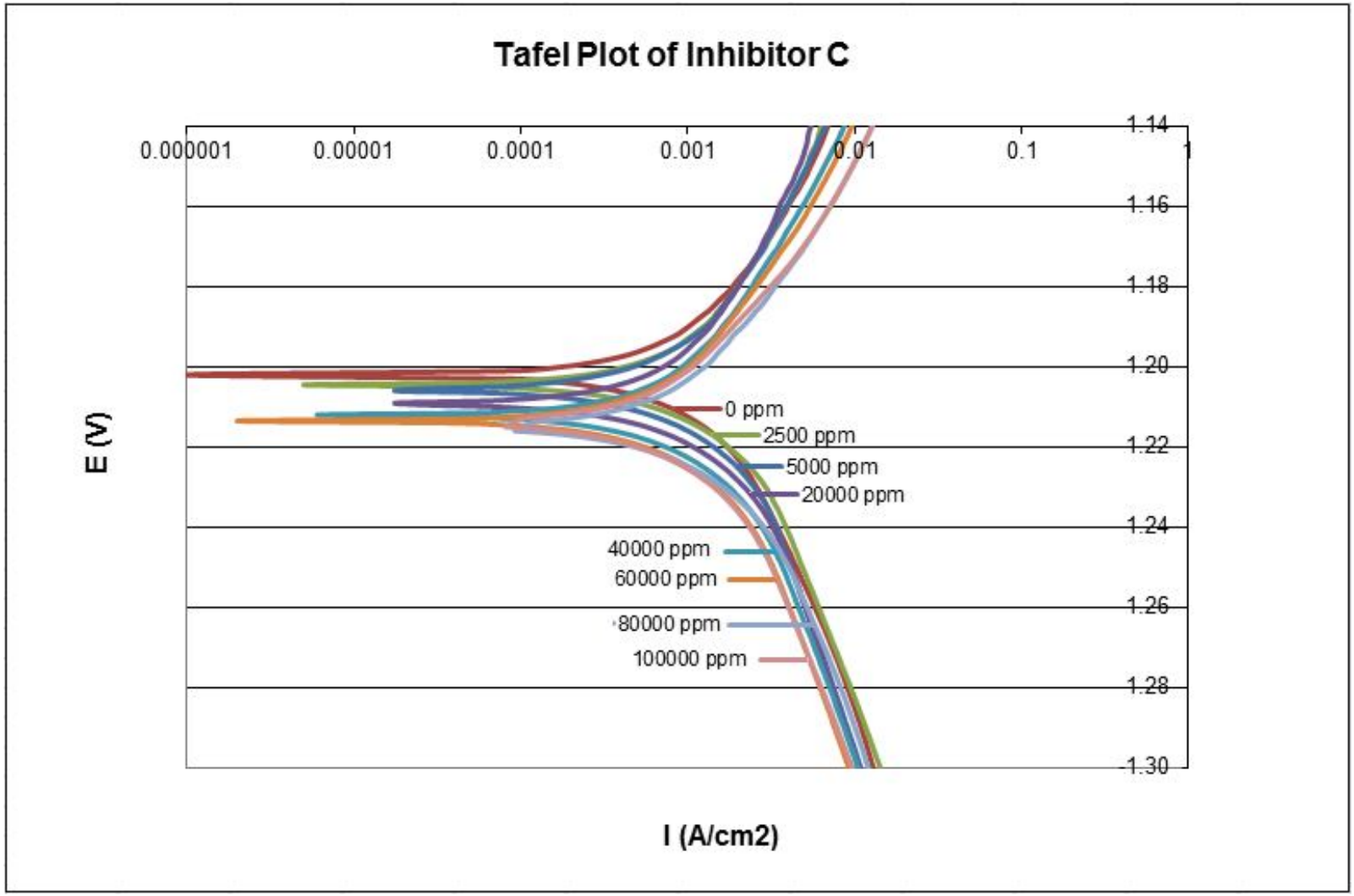

Figure 7.10: Tafel plots of the systems containing various concentrations of Inhibitor C. (Original in colour)

Moreover, Inhibitor C also prevented corrosion by adsorbing onto the metal surface by electrostatic attraction between the anions of the inhibitor and the positively charged metal surface. The adsorption was confirmed by using CE-DAD techniques in order to determine the concentration of Inhibitor C in the solution. The inhibitor concentration decreased after performing the corrosion experiment without producing any additional compounds, which indicated that there must be some Inhibitor C left on the metal surface that led to the reduction of the inhibitor concentration. The concentrations of Inhibitor C both before and after the corrosion experiments are illustrated in Table 7.6. In summary, Inhibitor C helped minimize carbon steel corrosion by behaving as a free radical scavenger and also by adsorbing onto the metal surface. Unfortunately, the inhibitor performance was far from excellent, as its maximum inhibiting efficiency appeared to be only 42.7%.

Table 7.6: The concentrations of Inhibitor C before and after the corrosion experiments (%error: 6.3%).

Inhibitor C	Concentration (ppm)	% Concentration reduction
2500 ppm		
Before	2562	
After	2470	3.6
5000 ppm		
Before	4888	
After	4682	4.2
20000 ppm		
Before	21869	
After	20535	6.1
40000 ppm		
Before	34749	
After	31492	9.4
80000 ppm		
Before	83520	
After	72632	13.0

7.4.3.2 The inhibitor's efficiency of Inhibitor C on oxidative MEA degradation

The inhibiting efficiency of Inhibitor C on oxidative MEA degradation increased with increasing inhibitor concentration, and the maximum efficiency appeared to be at an inhibitor concentration of 40,000 ppm (0.14M), where it provided excellent inhibition efficiency of 92.6%, as presented in Figure 7.11. Oxidative MEA degradation is a process that requires oxygen in the presence of free radicals to initiate a chain reaction of oxidative degradation. Inhibitor C, which is a free radical scavenger, was able to supply its own electrons to the free radicals instead of the MEA molecule, which, then, terminated the chain reaction and resulted in less oxidative degradation of MEA.

However, when the concentration of Inhibitor C exceeded the optimum point at 40,000 ppm, an adverse effect was found in that the inhibiting efficiency declined with further increases in the inhibitor concentration. One possible cause of the reduction of Inhibitor C performance with further increase of inhibitor concentration was the formation of additional compound which found to be a compound that split out from Inhibitor C. This compound was confirmed, by comparison with the standard chemical using CE-DAD techniques, to be acetate. Acetate has been shown to be able to convert to a free radical in an alkaline solution, and it potentially reacted with oxygen to produce peroxy acetate radical, which have been reported to be unreactive with oxygen (Sehested et al., 1986). Consequently, the peroxy acetate radical tended to behave as an additional free radical species that could have induced oxidative MEA degradation, which resulted in the reduction of Inhibitor C performance. It should be noted that the formation of acetate

possibly occurred in all the concentration ranges of Inhibitor C, but the effects of the resulting peroxy acetate radical seemed to be more pronounced in the higher inhibitor concentration ranges due to the greater amount of acetate being generated, which led to the reduction of Inhibitor C performance. In addition, the formation of acetate was supported by the data obtained from CE-DAD techniques, which showed that the Inhibitor C concentration reduced continually throughout the process, as presented in Figure 7.12, which basically indicates that Inhibitor C, to some extent, was degraded into another compound.

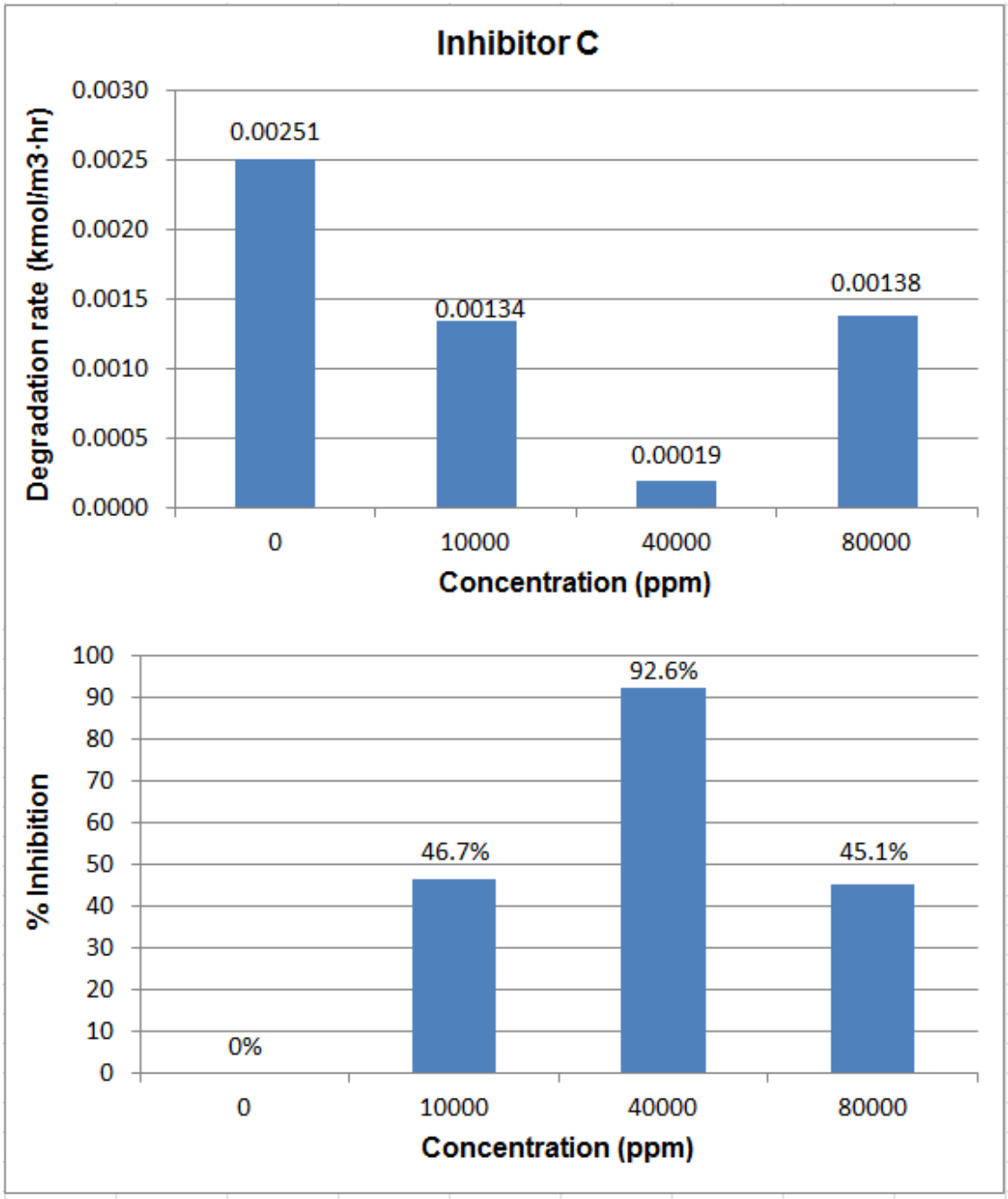

Figure 7.11: The degradation rate and inhibitor's efficiency of Inhibitor C in the systems containing various concentrations of Inhibitor C (%error: 2.9%). (Original in colour)

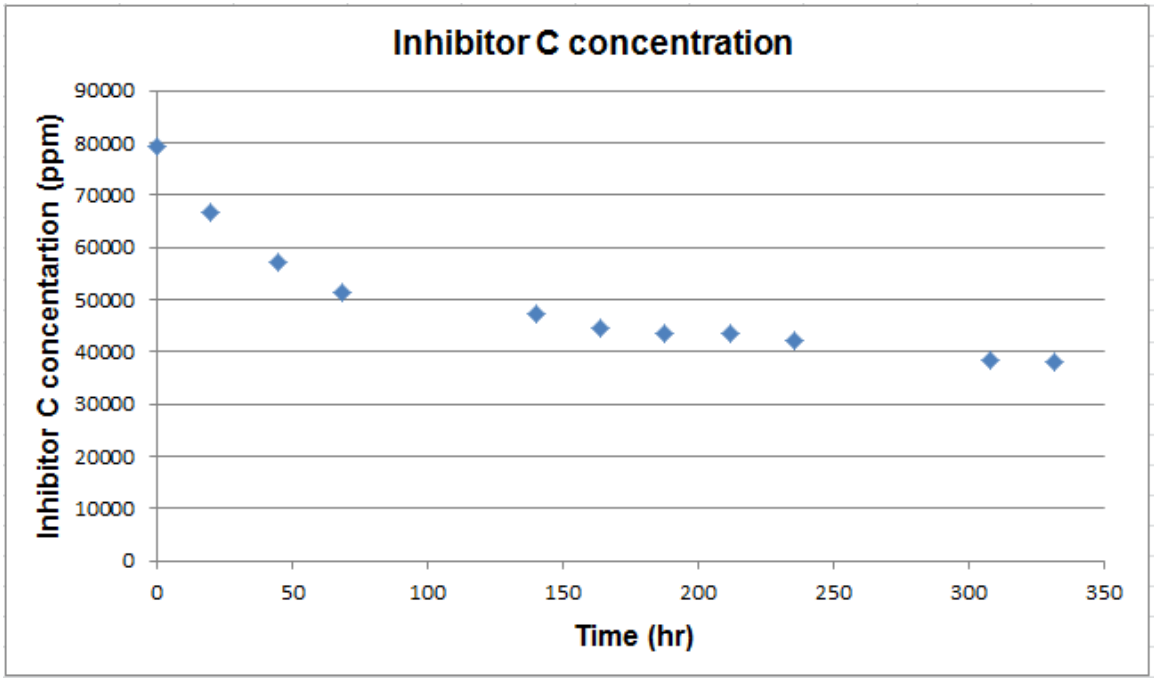

Figure 7.12: Inhibitor C concentration in the degradation system containing 80000 ppm of Inhibitor C (%error: 2.9%). (Original in colour)

7.4.4 The comparisons of inhibitors based on their maximum inhibiting performances

The maximum inhibition performance of various inhibitors is illustrated in Table 7.7. The table shows that Inhibitor A gave excellent inhibiting efficiencies on both carbon steel corrosion and oxidative MEA degradation at 88.9% and 97.3%, respectively. However, the concentration that gave the maximum inhibition performance on carbon steel corrosion (15,000 ppm) was different from the concentration that gave the maximum inhibition performance on oxidative MEA degradation (1000 ppm). Consequently, the difference in these concentrations would probably induce difficulty when it comes to the optimization between these two processes. On the other hand, Inhibitor B provided the maximum inhibitor's efficiencies on both carbon steel corrosion and MEA degradation at a concentration of 100 ppm, where the inhibiting efficiencies appeared to be 94.3% and 59.9% for carbon steel corrosion and oxidative MEA degradation, respectively. Even though, Inhibitor B seemed to provide excellent inhibition performance on corrosion and acceptable performance on solvent degradation, its efficiency was very sensitive to changes of concentration, so the inhibitor must be maintained at a specific concentration (100 ppm) in order to achieve the maximum inhibiting performance. Lastly, Inhibitor C did not provide satisfactory inhibition efficiency for carbon steel corrosion with a maximum efficiency of only 42.7% inhibition at a concentration of 80,000 ppm. However, it provided excellent maximum performance in inhibiting solvent degradation at 92.6% inhibition at the concentration of 40,000 ppm.

Table 7.7: The maximum efficiency of a single inhibitor on both carbon steel (C1020) corrosion and oxidative MEA degradation.

Inhibitor	Carbon steel (C1020) corrosion		Oxidative MEA degradation	
	Concentration (ppm)	**Inhibition Efficiency (%)**	**Concentration (ppm)**	**Inhibition Efficiency (%)**
Inhibitor A	15000	88.9	1000	97.3
Inhibitor B	100	92.4	100	59.9
Inhibitor C	80000	42.7	40000	92.6

According to the previous discussion, only Inhibitor B provided a concentration (100 ppm) that achieved maximum inhibition efficiencies in both carbon steel corrosion and oxidative MEA degradation, but the difficulty in maintaining its optimum concentration will be a challenge. Meanwhile, Inhibitor A and Inhibitor C behaved differently. The concentrations that gave maximum inhibiting performances on the corrosion process were different from the concentrations that gave the maximum performances on inhibiting solvent degradation. However, as far as the efficiency was concerned, Inhibitor A provided excellent efficiencies for the inhibition of both carbon steel corrosion (88.9%) and oxidative MEA degradation (97.3%), while, Inhibitor C provided an exceptional inhibiting performance only on solvent degradation (92.6%). Therefore, in order to obtain the "ultimate" inhibitor to prevent carbon steel corrosion at the same time as inhibiting oxidative MEA degradation, a mix of inhibitors is needed in order to optimize overall inhibition performance. Consequently, the inhibition performances of the mixed inhibitors on carbon steel corrosion and oxidative MEA degradation needed to be studied, where the mixed inhibitors were selected so that the inhibitor that gave the best performance on inhibiting carbon steel corrosion were mixed with the best inhibitor that gave the best performance on inhibiting solvent degradation.

7.5 The effects of mixed inhibitors on carbon steel (1020) corrosion and oxidative MEA degradation

7.5.1 The selection of the mixed inhibitors

The mixed inhibitors were selected to be a combination of the inhibitor that gave the best performance on inhibiting carbon steel corrosion mixed with the inhibitor that gave the best performance on inhibiting oxidative solvent degradation. The following discussion in this section is focused mainly on the selection of the best inhibitor for each system.

For corrosion, Inhibitor A and Inhibitor B both provided excellent maximum inhibition performances at 88.9% and 92.4%, respectively, as presented in Table 7.7. Although, Inhibitor B appeared to give a little bit better performance than Inhibitor A, the major disadvantage of using Inhibitor B was that it was very sensitive to a change in concentration. The concentration must be maintained only at a certain concentration (100 ppm) in order to achieve the maximum inhibitor's performance. In contrast, Inhibitor A appeared to be more stable after it reached the maximum efficiency, as presented in Figure 7.13. Therefore, at the end of the day, Inhibitor A was selected as the best inhibitor to prevent carbon steel corrosion due to the fact that it provided both a very good inhibition efficiency and stability, which would be more beneficial in the practical applications.

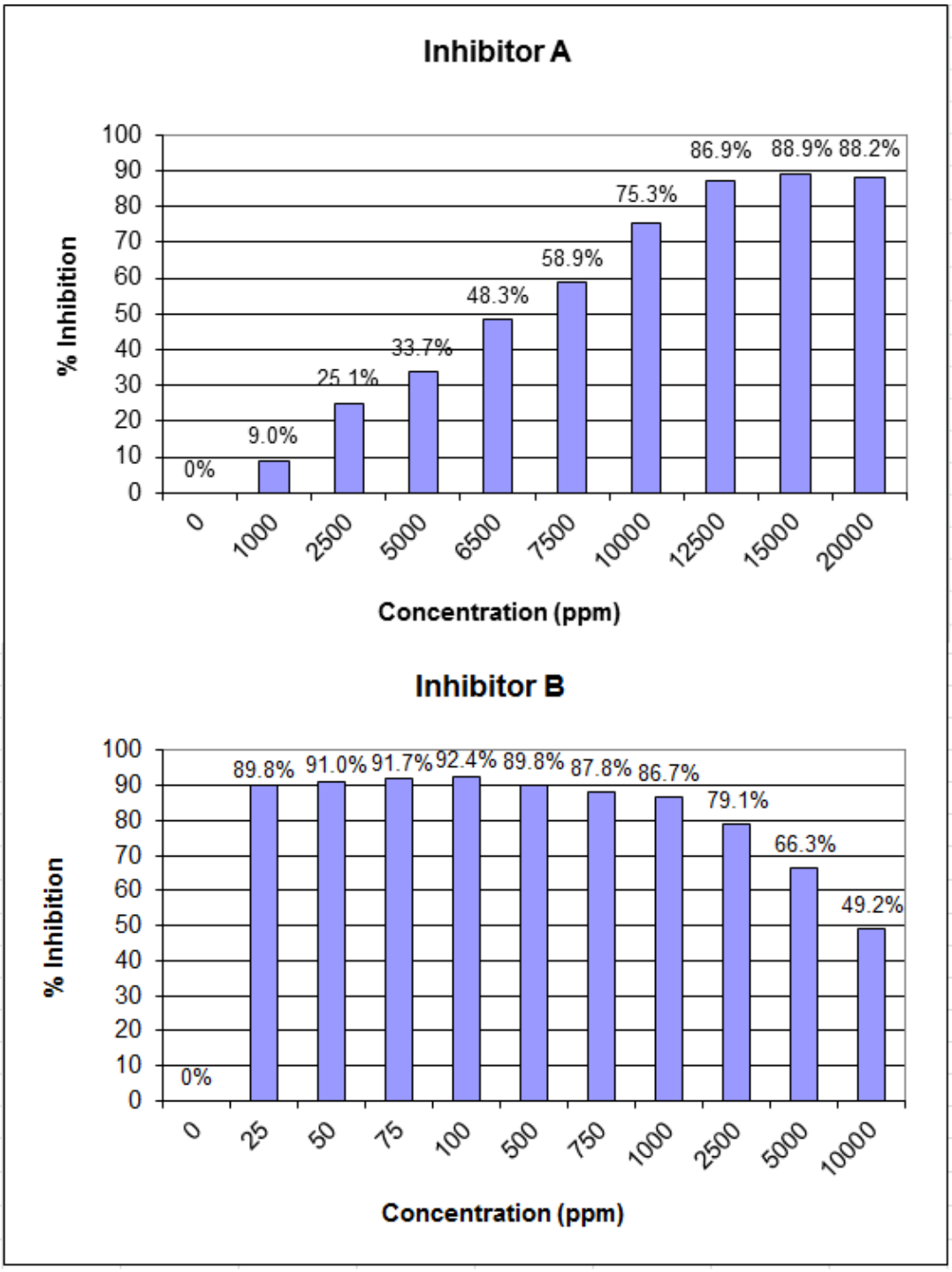

Figure 7.13: The comparison between the performances of Inhibitor A and Inhibitor B.

(Original in colour)

For solvent degradation, Inhibitor A and Inhibitor C both provided excellent maximum inhibition performances at 97.3% and 92.6%, respectively, as presented in Table 7.7. However, the concentration of Inhibitor A that gave the best performance for solvent degradation (1000 ppm) was different from the concentration that gave the best performance for corrosion (15,000 ppm), which it is likely to induce difficulty when trying to achieve optimization between these two processes. Moreover, Inhibitor A had already been chosen as the best inhibitor for minimizing carbon steel corrosion. Therefore, for solvent degradation, Inhibitor C was selected as the best inhibitor to prevent oxidative MEA degradation. It was, therefore mixed with Inhibitor A in the mixed inhibitors study.

In addition, another advantage of using mixed Inhibitors A and C was neither of them is hazardous, as each is rated as having levels of zero in health hazard in the HMIS (Hazardous Materials Identification System), as presented in Table 7.8. So, in terms of both the inhibition efficiency and health safety, Inhibitor A and Inhibitor C appeared to be very reasonable choices to study as a potential mixed inhibitor.

Table 7.8: HMIS (Hazardous Materials Identification System) of Inhibitor A, Inhibitor B, and Inhibitor C.

HMIS classification	Inhibitor		
	Inhibitor A	**Inhibitor B**	**Inhibitor C**
Health hazard	0	2	0
Flammability	2	0	0
Physical hazards	0	0	0

where:

Health hazard

4. Life-threatening

3. Major injury and medical treatment is required.

2. Temporary or minor injury may occur.

1. Irritation or minor reversible injury possible

0. No significant risk to health

Flammability

4. Materials may ignite spontaneously with air.

3. Materials capable of ignition under almost all normal temperature conditions.

2. Materials which must be moderately heated before ignition will occur.

1. Materials that must be preheated before ignition will occur.

0. Materials that will not burn.

Physical hazard

4. Materials which are readily capable of explosive at normal temperature and pressure.

3. Materials that may form explosive mixtures.

2. Materials that are unstable and may undergo violent chemical changes at normal temperature and pressure.

1. Materials that are normally stable but can become unstable (self-react) at high temperatures and pressures.

0. Materials that are normally stable, non-explosives.

7.5.2 The inhibiting efficiency of the mixed inhibitors on carbon steel (C1020) corrosion and oxidative MEA degradation

Inhibitor A and Inhibitor C were chosen to study in the mixed inhibitors systems. The concentrations of the mixed inhibitors were selected based on the concentrations that gave the maximum inhibiting efficiencies of the individual inhibitors on carbon steel corrosion and oxidative MEA degradation. Therefore, the selected concentrations of Inhibitor A were at 1,000 ppm and 15,000 ppm, which provided the maximum inhibiting performances on oxidative MEA degradation and carbon steel corrosion, respectively. For Inhibitor C, the selected concentrations were at 40,000 ppm and 80,000 ppm, which provided the maximum inhibiting performances on oxidative MEA degradation and carbon steel corrosion, respectively. Moreover, three concentration ratios of the mixed inhibitors were selected to represent the combinations of concentrations that gave the best individual performance on the corrosion inhibition (ratio I), the best individual performance on the solvent degradation inhibition (ratio II), and the best performance on both processes together (ratio III).

The results of the mixed inhibitors study on both carbon steel corrosion and oxidative MEA degradation are presented in Table 7.9. In carbon steel corrosion, all the concentration ratios of the mixed inhibitors provided slightly better performance (about two percent better) in the overall inhibition efficiencies on carbon steel corrosion when compared to single inhibitor performance, which indicated that blending inhibitors resulted in synergic effects between the two inhibitors that enhanced the ability to prevent car-

bon steel corrosion. In addition, it showed that the mixed inhibitors in ratio I, which was the combined concentrations of individual inhibitors that gave the maximum inhibiting performance on carbon steel corrosion, provided the highest efficiency on the corrosion inhibition among all the mixed inhibitors ratios.

On the other hand, all the concentration ratios of the mixed inhibitors provided inhibition performances on solvent degradation somewhere in between the efficiencies of individual inhibitors. This indicated that blending inhibitors did not result in synergic effects to enhance the overall efficiency of the mixed inhibitors. It somehow increased the efficiency when compared to one inhibitor but decreased the efficiency if compared to the other inhibitor. The mixed inhibitors ratio II, which was the combined concentrations of the single inhibitors that gave the maximum performance on solvent degradation inhibition, provided the highest inhibiting efficiency on oxidative solvent degradation among all the mixed inhibitor ratios.

Since carbon steel corrosion and oxidative MEA degradation needed to be minimized simultaneously, the mixed inhibitors ratio III appeared to balance the inhibition efficiencies between the two processes. It provided very good inhibition efficiency on carbon steel corrosion at 90.2% inhibition and acceptable performance on oxidative MEA degradation at 65.2% inhibition. Even though the efficiency of the mixed inhibitors ratio III on solvent degradation was not excellent, since it gave an inhibiting performance of only 65.2% inhibition, it should be noted that most of the available corrosion inhibitors tended to accelerate the solvent degradation process and many of the solvent degradation

products potentially induce metal corrosion. Therefore, this study helped to establish "ultimate" inhibitors that were able to inhibit carbon steel corrosion and oxidative MEA degradation simultaneously at an excellent level of 90.2% inhibition and an acceptable inhibition efficiency of 65.2%, respectively, was essentially a successful achievement of this work.

Table 7.9: The mixed inhibitors (Inhibitor A + Inhibitor C) performance with respected to single inhibitor systems (%error: 3.5%).

Inhibitor	Carbon steel (C1020) corrosion		Oxidative MEA degradation	
	Concentration (ppm)	**Inhibition efficiency (%)**	**Concentration (ppm)**	**Inhibition efficiency (%)**
A	1000	9%	1000	97.3%
	15000	88.9%	15000	7.1%
C	40000	36.7%	40000	92.6%
	80000	42.7%	80000	45.1%
A + C: ratio I *(Best for corrosion)*	A + C 15000 + 80000	92.6%	A + C 15000 + 80000	17.3%
A + C: ratio II *(Best for degradation)*	A + C 1000 + 40000	43.9%	A + C 1000 + 40000	93.9%
A + C: ratio III *(Best for each system)*	A + C 15000 + 40000	90.2%	A + C 15000 + 40000	65.2%

CHAPTER EIGHT

CONCLUSIONS AND RECOMMENDATIONS

8.1 Summary of thesis study

This research focused on developing a method for simultaneous inhibition of carbon steel (1020) corrosion and oxidative MEA degradation in the carbon dioxide (CO_2) capture process from simulated post-combustion coal-fired flue gas by absorption with a chemical solvent (monoethanolamine; MEA) with the help of an "ultimate" inhibitor. The work was divided into three main parts: the study of the effect of flue gas composition on carbon steel (1020) corrosion, the study of the effect of a flue gas composition on oxidative MEA degradation, and studies on inhibition of the two processes. The studies of the effect of flue gas composition on both carbon steel (1020) corrosion and oxidative MEA degradation were done by varying additives under the base-case conditions, in which the additives represented different types of components typically present in a flue gas. Thus, two different chloride compounds (sodium chloride; NaCl and ferrous chloride; $FeCl_2$) and hydrochloric acid (HCl) were selected to represent different sources of chlorides in a flue gas. Meanwhile, sulphurous acid (H_2SO_3), sulphuric acid (H_2SO_4), and nitric acid (HNO_3) were selected to represent the aqueous solutions of sulphur dioxide (SO_2), sulphur trioxide (SO_3), and nitrogen dioxide (NO_2), respectively. Moreover, sodium bisulfite ($NaHSO_3$), sodium sulfite (Na_2SO_3), sodium sulphate (Na_2SO_4), and ferrous sulphate heptahydrate ($FeSO_4 \cdot 7H_2O$) were also introduced in the study of carbon steel corrosion. Then, the influences of each component on both carbon steel corrosion and oxidative

MEA degradation were established, along with the rate equations to show the level of aggressiveness of a given compound. Once the behaviours and kinetics of a flue gas composition on both carbon steel corrosion and oxidative MEA degradation had been established, the inhibition study was then performed using information that was obtained from the kinetic studies. Three inhibitors were selected to determine their inhibiting efficiencies on both carbon steel corrosion and oxidative MEA degradation in order to obtain an "ultimate" inhibitor that was able to effectively prevent carbon steel (1020) corrosion while simultaneously inhibiting oxidative MEA degradation.

8.2 Conclusions of thesis study

The effects of various additives: chloride compounds (NaCl, HCl, $FeCl_2$) within the concentrations of 0 to 2000 ppm, sulphate compounds (Na_2SO_4, H_2SO_4, $FeSO_4$) within the concentrations of 0 to 12 ppm, sulfite/bisulfite compounds (H_2SO_3, Na_2SO_3, $NaHSO_3$) within the concentrations of 0 to 400 ppm, and nitric acid (HNO_3) within the concentration of 0 to 400 ppm on carbon steel (1020) corrosion were:

- Sodium chloride (NaCl) slightly increased carbon steel corrosion, mainly due to the influence of chloride ion (Cl^-) because sodium ion (Na^+) had a negligible effect on increasing the corrosion rate because of a much lower standard electrode potential (E_0^0 = -2.71 V) compared to the ferrous ion (Fe^{2+}; E_0^0 = -0.44 V).
- Hydrochloric acid (HCl) strongly accelerated carbon steel corrosion due to hydrogen ion (H^+) being a very strong oxidizing agent (E_0^0 = 0 V).

- Ferrous chloride ($FeCl_2$) slowed down carbon steel corrosion due to the presence of ferrous ion (Fe^{2+}) from the addition of ferrous chloride inhibiting the iron dissolution reaction.
- The effects of cations (Na^+, H^+, and Fe^{2+}) on carbon steel corrosion were that sodium ion did not accelerate carbon steel corrosion because it has a lower standard electrode potential (E_0^0 = -2.71 V) than the metal itself (E_0^0 = -0.44 V). On the other hand, hydrogen ion strongly accelerated the corrosion process since it has a higher standard electrode potential (E_0^0 = 0 V) compared to the metal. Ferrous ion tended to slow down the metal corrosion since it inhibited the iron dissolution reaction.
- The role of chloride ion (Cl^-) in carbon steel corrosion was that it helped accelerate corrosion by combining with ferrous ion (Fe^{2+}) that was released by the metal surface and forming a soluble film of ferrous chloride ($FeCl_2$). Ferrous chloride then helped to stimulate further iron dissolution by dissolving back into the solution, leaving the metal surface open to further attack by the oxidizing agents, which eventually led to more metal corrosion.
- Sodium sulphate (Na_2SO_4), sulphuric acid (H_2SO_4), and ferrous sulphate ($FeSO_4 \cdot 7H_2O$) all increased the corrosion rates. However, no significant difference in the rates between each compound was found. This was because cations (H^+, Na^+, Fe^{2+}) in the compounds had an insignificant effect on the increases of corrosion rates when compared to the effect of sulphate ion (SO_4^2).
- The role of the sulphate ion (SO_4^{2-}) in carbon steel corrosion was that it accelerated corrosion either by behaving as an oxidizing agent by accepting electrons re-

leased by the metal surface, since it had a higher standard electrode potential (E_0^0 = 0.17 V) when compared to the iron dissolution reaction (E_0^0 = -0.44 V), or it potentially led to formation of ferrous sulphate ($FeSO_4$) that was able to be hydrolyzed by water and/or oxygen (O_2) and subsequently liberated the sulphate ion back into the solution to stimulate further iron dissolution (Roberge, 1999).

- Sulphurous acid (H_2SO_3), sodium bisulfite ($NaHSO_3$), and sodium sulfite (Na_2SO_3) either behaved as corrosion accelerators due to hydrolysis reactions or as the corrosion inhibitors, due to their reactions with dissolved oxygen. The difference depended strongly on their concentrations.
- Nitric acid (HNO_3) accelerated corrosion either by nitrate ion behaving as oxidizing agent to accelerate the iron dissolution or the nitrate ion possibly combined with ferrous ion (Fe^{2+}) and formed iron nitrate ($Fe(NO_3)_2$), which has a high solubility in an aqueous solution. The ferrous nitrate then dissolved back into the solution, leaving the metal surface open for further attack by the oxidizing agents.
- The carbon steel (1020) corrosion products appeared to be a combination of goethite (FeOOH; yellow-brown) and magnetite (Fe_3O_4; greyish-black).
- Finally, the modified power law rate equation for the systems containing all four additives (HCl, H_2SO_3, H_2SO_4, and HNO_3) can be illustrated as follows, and it provided an acceptable percentage of average absolute deviation (%AAD) of 8.6%:

$$r_{corrosion} = (8.922E+09)\cdot e^{\frac{-6430}{T}} \cdot [H^+]^{0.118} \cdot ([Cl^-]^{0.106} + [HSO_3^-]^{0.007} + [SO_3^{2-}]^{0.006} + [SO_4^{2-}]^{0.006} + [NO_3^-]^{0.102}) \quad (8.1)$$

The effects of various additives: chloride compounds (NaCl, HCl, $FeCl_2$) within the concentrations of 0 to 2000 ppm, sulphuric acid (H_2SO_4) within the concentration of 0 to 12 ppm, sulphurous acid (H_2SO_3) within the concentration of 0 to 400 ppm, and nitric acid (HNO_3) within the concentration of 0 to 400 ppm on oxidative MEA degradation were:

- Sodium chloride (NaCl) prevented oxidative MEA degradation by reducing oxygen concentration in a solution.
- Hydrochloric acid (HCl), sulphuric acid (H_2SO_4), and nitric acid (HNO_3) essentially accelerated solvent degradation by behaving as catalysts, which helped to accelerate the degradation reactions.
- Ferrous chloride ($FeCl_2$) promoted solvent degradation by helping to elevate oxygen to more active species, such as superoxide ($\cdot O_2^-$) and hydroxyl ($\cdot OH$) radicals. These reactive oxygen species (ROS) then accelerated the oxidative MEA degradation.
- Sulphurous acid (H_2SO_3) behaved as an oxygen scavenger in the concentration range below 250 ppm, which helped to inhibit the oxidative MEA degradation.
- Finally, the modified power law rate equation for the systems containing all four additives (HCl, H_2SO_3, H_2SO_4, and HNO_3) is illustrated as follows, and it provided an acceptable percentage of average absolute deviation (%AAD) of 9.4%.

$$r_{\deg radation} = (8.25E+05)\cdot e^{\frac{-8555}{T}} \cdot [H^+]^{0.37} \cdot ([Cl^-]^{0.24} + [HSO_3^-]^{-0.29} + [SO_3^{2-}]^{-0.02} + [SO_4^{2-}]^{0.05} + [NO_3^-]^{0.17}) \quad (8.2)$$

The inhibition studies of carbon steel (1020) corrosion and oxidative MEA degradation gave the following results:

- Most of the available corrosion inhibitors accelerate the solvent degradation process and many of the solvent degradation products potentially induce metal corrosion. This study helped to establish "ultimate" inhibitors that were able to inhibit both carbon steel corrosion and oxidative MEA degradation processes simultaneously.
- Inhibitor A prevented carbon steel corrosion and oxidative MEA degradation by behaving as a hydrogen ion scavenger, which helped to reduce hydrogen ion concentration in a solution. It provided excellent inhibiting efficiencies of a maximum of 88.9% inhibition on carbon steel corrosion and 97.3% inhibition on oxidative MEA degradation.
- Inhibitor B behaved primarily as an oxygen scavenger. It showed excellent performance on minimizing carbon steel corrosion, where it provided a maximum of 92.4% inhibition, but it showed only a moderate performance on solvent degradation, where it provided a maximum performance of 59.9% inhibition.
- Inhibitor C minimized both carbon steel corrosion and oxidative MEA degradation by behaving as a free radical scavenger. It showed a maximum efficiency of only 42.7% inhibition on carbon steel corrosion but a very good inhibiting efficiency of 92.6% inhibition on oxidative MEA degradation.
- All ratios of the mixed inhibitors (A and C) provided slightly better inhibition performance (about two percentage higher) in overall inhibition efficiency in carbon

steel corrosion when compared to single inhibitor performance. On the other hand, they provided inhibition performances on solvent degradation somewhere in between the efficiencies of the individual inhibitors.

- The mixed inhibitors ratio III (A + C : 15,000 + 40,000 ppm) provided the best overall inhibiting performance, since it balanced the inhibition efficiencies between the carbon steel corrosion and oxidative MEA degradation processes. It provided excellent inhibition efficiency on carbon steel corrosion at 90.2% inhibition and acceptable performance on oxidative MEA degradation at 65.2% inhibition.

8.3 Recommendations for future work

Obtaining an "ultimate" inhibitor (the mixed inhibitors (A + C) ratio III) that was able to effectively prevent carbon steel (1020) corrosion while simultaneously inhibiting oxidative MEA degradation was a successful achievement in this thesis work. However, there are several avenues of future work could help to improve on the results obtained:

- The corrosion products should be identified. Due to equipment unavailability, this study was not able to fully identify the corrosion products generated within the systems. Thus, by using more proper analytical techniques, for example, x-ray diffraction (XRD), the corrosion products can be confidently identified, which would improve understanding of carbon steel corrosion behaviour.

- The oxidative MEA degradation mechanisms should be further studied. Identifying the degradation products produced along the process could potentially provide an idea of the sequential reactions occurring in the solvent degradation mechanisms. Since this work only focused on the kinetics of the oxidative MEA degradation in various additives that represented components typically present within a flue gas, only the final products of oxidative MEA degradation were identified.
- Moreover, the effects of the degradation products on both carbon steel (1020) corrosion and oxidative MEA degradation should be comprehensively studied. Since these products are presented in practical applications of the CO_2 capture process, the level of damage caused by the degradation products should be established.

REFERENCES

1. Aboudheir, A., Tontiwachwuthikul, P., Chakma, A., and Idem, R. (2003). Kinetics of the reactive absorption of carbon dioxide in high CO_2-loaded, concentrated aqueous monoethanolamine solutions. *Chemical Engineering Science, 58* (23-24), 5195-5210.
2. Amornvadee Veawab. (2000). Corrosion and corrosion control in CO_2 absorption process using aqueous amine solutions. Unpublished Doctor of Philosophy, University of Regina.
3. Astarita, G.; Savage, D.; Bisio, A. (1983). Gas treating with chemical solvents; Wiley, New York.
4. Babić-Samardžija, K., Khaled, K. F., and Hackerman, N. (2005). Investigation of the inhibiting action of O-, S- and N-dithiocarbamato(1,4,8,11-tetraazacyclotetradecane)cobalt(III) complexes on the corrosion of iron in $HClO_4$ acid. *Applied Surface Science, 240* (1-4), 327-340.
5. Banaś, J., Lelek-Borkowska, U., Mazurkiewicz, B., and Solarski, W. (2007). Effect of CO_2 and H_2S on the composition and stability of passive film on iron alloys in geothermal water. *Electrochimica Acta, 52* (18), 5704-5714.
6. Bedell, S. A. (2009). Oxidative degradation mechanisms for amines in flue gas capture. *Energy Procedia, 1* (1), 771-778.
7. Bedell, S. A. (2011). Amine autoxidation in flue gas CO_2 capture—Mechanistic lessons learned from other gas treating processes. *International Journal of Greenhouse Gas Control, 5* (1), 1-6.

8. Bello, A., and Idem, R. O. (2006). Comprehensive study of the kinetics of the oxidative degradation of CO_2 loaded and concentrated aqueous monoethanolamine (MEA) with and without sodium metavanadate during CO_2 absorption from flue gases. *Industrial and Engineering Chemistry Research, 45* (8), 2569-2579.
9. Blomen, E., Hendriks, C., and Neele, F. (2009). Capture technologies: Improvements and promising developments. *Energy Procedia, 1* (1), 1505-1512.
10. Bord, N., Crétier, G., Rocca, J., Bailly, C., and Souchez, J. (2005). Simultaneous determination of inorganic anions and organic acids in amine solutions for sour gas treatment by capillary electrophoresis with indirect UV detection. *Journal of Chromatography A, 1100* (2), 223-229.
11. Castaño, J. G., de la Fuente, D., and Morcillo, M. (2007). A laboratory study of the effect of NO_2 on the atmospheric corrosion of zinc. *Atmospheric Environment, 41* (38), 8681-8696.
12. Chakma, A. (1995). An energy efficient mixed solvent for the separation of CO_2. *Energy Conversion and Management, 36* (6-9), 427-430.
13. Chakma, A., Mehrotra, A. K., and Nielsen, B. (1995). Comparison of chemical solvents for mitigating CO_2 emissions from coal-fired power plants. *Heat Recovery Systems and CHP, 15* (2), 231-240.
14. Chakma, A. (1997). CO_2 capture processes - opportunities for improved energy efficiencies. *Energy Conversion and Management, 38* (Supplement 1), S51-S56.
15. Chi, S., and Rochelle, G. T. (2002). Oxidative degradation of monoethanolamine. *Industrial and Engineering Chemistry Research, 41* (17), 4178-4186.

16. Cho, Y., Park, D., Park, D., Woo, H., and Chung, J. (2002). Selective oxidation of hydrogen sulfide to ammonium thiosulfate and sulfur over vanadium-bismuth oxide catalysts, Springer Netherlands.
17. Choi, S. Y., Chung, M. J., and Sung, N. J. (2002). Volatile N-nitrosamine inhibition after intake korean green tea and maesil (prunus mume SIEB. et ZACC.) extracts with an amine-rich diet in subjects ingesting nitrate. *Food and Chemical Toxicology, 40* (7), 949-957.
18. Einar Bardal. (2003). Corrosion and protection. – (engineering materials and processes), Springer.
19. Figueroa, J. D., Fout, T., Plasynski, S., McIlvried, H., and Srivastava, R. D. (2008). Advances in CO_2 capture technology-The U.S. department of energy's carbon sequestration program. *International Journal of Greenhouse Gas Control, 2* (1), 9-20.
20. Goff, G. S., and Rochelle, G. T. (2004). Monoethanolamine degradation: O2 mass transfer effects under CO2 capture conditions. *Industrial and Engineering Chemistry Research, 43*(20), 6400-6408.
21. Goff, G. S., and Rochelle, G. T. (2006). Oxidation inhibitors for copper and iron catalyzed degradation of monoethanolamine in CO_2 capture processes. *Industrial and Engineering Chemistry Research, 45* (8), 2513-2521.
22. Gouda, V. K., and Sayed, S. M. (1973). Corrosion inhibition of steel by sodium sulphite. *Corrosion Science, 13* (9), 653-658.

23. He, X. Y., Deng, H. Y., Li, R., Fei, X. D., Wang, H. Y., and Deng, Z. Y. (2008). Corrosion inhibition of X70 steel in saline solution saturated with CO_2 by thiourea. *Acta Metallurgica Sinica (English Letters), 21* (1), 65-71.
24. Horita, K., Wang, G., and Satake, M. (1997). Spectrophotometric determination of nitrate and nitrite in soil and water samples with a diazotizable aromatic amine and coupling agent using column preconcentration on naphthalene supported with ion-pair of tetradecyldimethylbenzylammonium and iodide. *Analytica Chimica Acta, 350* (3), 295-303.
25. Horowitz, W. (1975). Association of official analytical chemists. (AOAC) methods, 12th ed. (12th edition ed.), George Banta.
26. Howard J. Herzog (1998). Presented at the Fourth International Conference on Greenhouse Gas Control Technologies (August 30 - September 2, 1998), Interlaken, Switzerland.
27. Howard Herzog, Jerry Meldon, and Alan Hatton. (April 2009). Advanced post-combustion CO_2 capture Prepared for the Clean Air Task Force Under.
28. Jones, Denny (1996). *Principles and Prevention of Corrosion* (2nd edition ed.).
29. Kladkaew, N., Idem, R., Tontiwachwuthikul, P., and Saiwan, C. (2009). Corrosion behaviour of carbon steel in the monoethanolamine-H_2O-CO_2-O_2-SO_2 system. *Industrial and Engineering Chemistry Research, 48* (19), 8913-8919.
30. Kladkaew, N., Idem, R., Tontiwachwuthikul, P., and Saiwan, C. (2011). Studies on corrosion and corrosion inhibitors for amine based solvents for CO_2 absorption from power plant flue gases containing CO_2, O_2 and SO_2. *Energy Procedia, 4*, 1761-1768.

31. Knag, M., Bilkova, K., Gulbrandsen, E., Carlsen, P., and Sjöblom, J. (2006). Langmuir–Blodgett films of dococyltriethylammonium bromide and octadecanol on iron. deposition and corrosion inhibitor performance in CO_2 containing brine. *Corrosion Science, 48*(9), 2592-2613.
32. Kohl, A. L., and Nielsen, R. B. (1997). Basic chemistry. Gas purification (fifth edition) (pp. 42). Houston: Gulf Professional Publishing.
33. Lepaumier, H., da Silva, E. F., Einbu, A., Grimstvedt, A., Knudsen, J. N., Zahlsen, K., et al. (2011). Comparison of MEA degradation in pilot-scale with lab-scale experiments. *Energy Procedia, 4*, 1652-1659.
34. Lepaumier, H., da Silva, E. F., Einbu, A., Grimstvedt, A., Knudsen, J. N., Zahlsen, K., et al. (2011). Comparison of MEA degradation in pilot-scale with lab-scale experiments. *Energy Procedia, 4*, 1652-1659.
35. Li, D. G., Feng, Y. R., Bai, Z. Q., and Zheng, M. S. (2007). Characteristics of CO_2 corrosion scale formed on N80 steel in stratum water with saturated CO_2. *Applied Surface Science, 253* (20), 8371-8376.
36. Li, M., He, Z., and Zhou, L. Removal of iron from industrial grade aluminum sulfate by primary amine extraction system. *Hydrometallurgy, In Press, Corrected Proof*
37. Li, P., Lin, J. Y., Tan, K. L., and Lee, J. Y. (1997). Electrochemical impedance and X-ray photoelectron spectroscopic studies of the inhibition of mild steel corrosion in acids by cyclohexylamine. *Electrochimica Acta, 42* (4), 605-615.

38. López, D. A., Schreiner, W. H., de Sánchez, S. R., and Simison, S. N. (2004). The influence of inhibitors molecular structure and steel microstructure on corrosion layers in CO_2 corrosion: An XPS and SEM characterization. *Applied Surface Science, 236* (1-4), 77-97.

39. M. M. Antonijevic and M. B. Petrovic. (2008). Copper corrosion inhibitors. A review.*3*, 1-28.

40. Mandal, B. P., Guha, M., Biswas, A. K., and Bandyopadhyay, S. S. (2001). Removal of carbon dioxide by absorption in mixed amines: Modelling of absorption in aqueous MDEA/MEA and AMP/MEA solutions. *Chemical Engineering Science, 56* (21-22), 6217-6224.

41. Matthias Krumbeck. (March 2007). Post combustion capture from coal, CSLF CCS Workshop Paris.

42. Milton J. Rosen. (2004). Surfactants and interfacial phenomena third edition, New Jersey: John Wiley and Sons, Inc.

43. Mofarahi, M., Khojasteh, Y., Khaledi, H., and Farahnak, A. (2008). Design of CO_2 absorption plant for recovery of CO_2 from flue gases of gas turbine. *Energy, 33* (8), 1311-1319.

44. Paolinelli, L. D., Pérez, T., and Simison, S. N. (2008). The effect of pre-corrosion and steel microstructure on inhibitor performance in CO_2 corrosion. *Corrosion Science, 50* (9), 2456-2464.

45. Peter C Rooney, and Danny D Daniels. (1998). Oxygen solubility in various alkanolamine/water mixtures. *Petroleum Technology Quarterly, Spring 1998,* (Spring 1998), 97-101.

46. Pierre R. Roberge. (1999). Handbook of corrosion engineering, The McGraw-Hill Companies, Inc.

47. R.L. Cook, A.W. Myers, and J. E. Elliott. (2005). Chromate-free on-demand releasable corrosion inhibitors for aluminum.

48. Rooney P. C., Dupart M. S., and Bacon T.R. (1998). Oxygen's role in alkanolamine degradation. *Hydrocarbon Processing (International Edition), 77* (7), 109-113.

49. Samie, F., Tidblad, J., Kucera, V., and Leygraf, C. (2007). Atmospheric corrosion effects of HNO3-Comparison of laboratory-exposed copper, zinc and carbon steel. *Atmospheric Environment, 41* (23), 4888-4896.

50. Sehested, K., Holcman, J., Bjergbakke, E., and Hart, E. J. (1987). Ozone decomposition in aqueous acetate solutions. *The Journal of Physical Chemistry, 91* (9), 2359-2361.

51. Sexton, A. J., and Rochelle, G. T. (2009). Catalysts and inhibitors for MEA oxidation. *Energy Procedia, 1* (1), 1179-1185.

52. Shen, C. H., and Rochelle, G. T. (1998). Nitrogen dioxide absorption and sulfite oxidation in aqueous sulfite. *Environmental Science and Technology, 32* (13), 1994-2003.

53. Soosaiprakasam, I. R., and Veawab, A. (2008). Corrosion and polarization behaviour of carbon steel in MEA-based CO_2 capture process. *International Journal of Greenhouse Gas Control, 2* (4), 553-562.

54. Strazisar, B. R., Anderson, R. R., and White, C. M. (2003). Degradation pathways for monoethanolamine in a CO_2 capture facility. *Energy and Fuels, 17* (4), 1034-1039.

55. Supap, T., Idem, R., Tontiwachwuthikul, P., and Saiwan, C. (2009). Kinetics of sulfur dioxide- and oxygen-induced degradation of aqueous monoethanolamine solution during CO_2 absorption from power plant flue gas streams. *International Journal of Greenhouse Gas Control, 3* (2), 133-142.

56. Teeradet Supap, Raphael Idem, Paitoon Tontiwachwuthikul, and Chintana Saiwan. (2006). Analysis of monoethanolamine and its oxidative degradation products during CO_2 absorption from flue gases: A comparative study of GC-MS, HPLC-RID, and CE-DAD analytical techniques and possible optimum combinations - American Chemical Society.

57. Uyanga, I. J., and Idem, R. O. (2007). Studies of SO_2- and O_2-induced degradation of aqueous MEA during CO_2 capture from power plant flue gas streams. *Industrial and Engineering Chemistry Research, 46* (8), 2558-2566.

58. Veawab, A., and Aroonwilas, A. (2002). Identification of oxidizing agents in aqueous amine-CO_2 systems using a mechanistic corrosion model. *Corrosion Science, 44* (5), 967-987.

59. Wayne, R. P., Barnes, I., Biggs, P., Burrows, J. P., Canosa-Mas, C. E., Hjorth, J., et al. (1991). The nitrate radical: Physics, chemistry, and the atmosphere. *Atmospheric Environment.Part A.General Topics, 25* (1), 1-203.

60. Wilson, D. (1990). Quantifying and comparing fuel-cycle greenhouse-gas emissions : Coal, oil and natural gas consumption. *Energy Policy, 18* (6), 550-562.

61. Xing, X., Gao, B., Zhong, Q., Yue, Q., and Li, Q. (2011). Sorption of nitrate onto amine-crosslinked wheat straw: Characteristics, column sorption and desorption properties. *Journal of Hazardous Materials, 186* (1), 206-211.

62. Zhang, G., Lu, M., Chai, C., and Wu, Y. (2006). Effect of HCO_3^- concentration on CO_2 corrosion in oil and gas fields. *Journal of University of Science and Technology Beijing, Mineral, Metallurgy, Material, 13* (1), 44-49.

63. Zhang, J., Zhang, Q., Ren, H., Zhao, W., and Zhang, H. (2007). Inhibition performance of 2-mercaptobenzothiazole derivatives in CO_2 saturated solution and its adsorption behaviour at fe surface. *Applied Surface Science, 253* (18), 7416-7422.

APPENDIX A

EXPERIMENTAL DATA OF THE CORROSION STUDY

Table A1: The corrosion rates of sodium chloride (NaCl), hydrochloric acid (HCl), and ferrous chloride ($FeCl_2$) systems.

NaCl	
Concentration (ppm)	**Corrosion rate (mpy)**
0	166.35
506	164.6
1005	176.8
1508	175.8
2009	195.1
HCl	
Concentration (ppm)	**Corrosion rate (mpy)**
0	166.35
547	187.4
1094	214.5
1458	244.3
$FeCl_2$	
Concentration (ppm)	**Corrosion rate (mpy)**
0	166.35
510	155.2
1010	126.1
1508	120.0
2033	115.8
2506	109.2

Table A2: The corrosion rates of sodium sulphate (Na_2SO_4), sulphuric acid (H_2SO_4), and ferrous sulphate heptahydrate ($FeSO_4 \cdot 7H_2O$) systems.

Na_2SO_4	
Concentration (ppm)	**Corrosion rate (mpy)**
0.0	166.35
3.3	174.3
6.7	183.7
9.1	205.3
12.5	206.1
H_2SO_4	
Concentration (ppm)	**Corrosion rate (mpy)**
0.0	166.35
2.9	177.0
5.8	195.7
8.7	204.4
11.6	201.3
$FeSO_4 \cdot 7H_2O$	
Concentration (ppm)	**Corrosion rate (mpy)**
0.0	166.35
3.7	191.7
6.1	186.9
9.1	202.6
12.0	211.5

Table A3: The corrosion rates of sulphurous acid (H_2SO_3), sodium sulfite (Na_2SO_3), and sodium bisulfite ($NaHSO_3$) systems.

H_2SO_3	
Concentration (ppm)	**Corrosion rate (mpy)**
0.0	166.35
8	243.6
16	253.6
24	227.6
32	160.3
96	21.6
201	25.4
305	29.7
401	30.6
Na_2SO_3	
Concentration (ppm)	**Corrosion rate (mpy)**
0	166.35
25	255.2
49	77.2
83	19.0
101	20.5
201	25.3
302	26.2
401	29.7
$NaHSO_3$	
Concentration (ppm)	**Corrosion rate (mpy)**
0	166.35
12	259.6
24	22.8
83	24.1
173	21.9
271	26.9
416	37.3

Table A4: The corrosion rates of nitric acid (HNO_3) system.

HNO_3	
Concentration (ppm)	**Corrosion rate (mpy)**
0	166.35
27	235.5
53	272.1
99	312.1
199	311.2
298	327.1
398	344.4

APPENDIX B

EXPERIMENTAL DATA OF THE OXIDATIVE MEA DEGRADATION STUDY

Table B1: The oxidative MEA degradation rates of the base-case system (no additive).

Base-case		
Run time (hr)	**MEA concentration (M)**	**Degradation rate (kmol/m^3·hr)**
0	5.038	0.00274
23	4.954	0.00258
48	4.861	0.00239
72	4.789	0.00221
96	4.788	0.00203
120	4.732	0.00186
143	4.714	0.00169
168	4.687	0.00150
214	4.577	0.00116
239	4.549	0.00098
265	4.546	0.00078
288	4.547	0.00061
312	4.537	0.00044
336	4.491	0.00026
384	4.503	0.00000
Average		**0.00142**

Table B2: The oxidative MEA degradation rates of sodium chloride (NaCl) systems.

NaCl								
500 ppm			1000 ppm			2000 ppm		
Run time (hr)	**MEA concentration (M)**	**Degradation rate (kmol/m^3·hr)**	**Run time (hr)**	**MEA concentration (M)**	**Degradation rate (kmol/m^3·hr)**	**Run time (hr)**	**MEA concentration (M)**	**Degradation rate (kmol/m^3·hr)**
0	4.998	0.00141	0	5.026	0.00108	0	5.007	0.00083
24	4.950	0.00138	23	5.010	0.00108	44	4.986	0.00083
48	4.925	0.00134	44	4.958	0.00108	71	4.998	0.00083
73	4.897	0.00130	71	4.929	0.00108	93	4.973	0.00083
119	4.824	0.00122	118	4.868	0.00108	119	4.933	0.00083
145	4.824	0.00118	143	4.882	0.00108	142	4.889	0.00083
168	4.781	0.00115	167	4.837	0.00108	191	4.842	0.00083
192	4.756	0.00111	191	4.818	0.00108	213	4.864	0.00083
215	4.741	0.00107	214	4.808	0.00108	239	4.796	0.00083
240	4.662	0.00103	239	4.759	0.00108	262	4.809	0.00083
287	4.653	0.00096	289	4.711	0.00108	286	4.816	0.00083
310	4.630	0.00092	312	4.671	0.00108	312	4.764	0.00083
336	4.602	0.00088	336	4.652	0.00108			
360	4.602	0.00084						
383	4.562	0.00080						
Average		**0.00111**	**Average**		**0.00108**	**Average**		**0.00083**

Table B3: The oxidative MEA degradation rates of hydrochloric acid (HCl) systems.

HCl								
500 ppm			1000 ppm			2000 ppm		
Run time (hr)	MEA concentration (M)	Degradation rate (kmol/m^3·hr)	Run time (hr)	MEA concentration (M)	Degradation rate (kmol/m^3·hr)	Run time (hr)	MEA concentration (M)	Degradation rate (kmol/m^3·hr)
0	5.045	0.00051	0	5.030	0.00074	0	5.006	0.00103
24	4.974	0.00051	21	4.966	0.00074	22	4.945	0.00103
48	4.981	0.00051	93	4.927	0.00074	53	4.943	0.00103
72	4.961	0.00051	119	4.914	0.00074	73	4.925	0.00103
97	4.993	0.00051	141	4.899	0.00074	97	4.874	0.00103
121	4.955	0.00051	166	4.873	0.00074	166	4.772	0.00103
146	4.950	0.00051	189	4.826	0.00074	189	4.752	0.00103
168	4.965	0.00051	213	4.838	0.00074	214	4.767	0.00103
192	4.929	0.00051	263	4.791	0.00074	240	4.698	0.00103
216	4.912	0.00051	287	4.821	0.00074	262	4.719	0.00103
242	4.875	0.00051	309	4.806	0.00074	336	4.628	0.00103
312	4.849	0.00051	332	4.733	0.00074	360	4.660	0.00103
337	4.846	0.00051						
Average		**0.00051**	**Average**		**0.00074**	**Average**		**0.00103**

Table B4: The oxidative MEA degradation rates of ferrous chloride ($FeCl_2$) systems.

$FeCl_2$								
500 ppm			**1000 ppm**			**2000 ppm**		
Run time (hr)	**MEA concentration (M)**	**Degradation rate (kmol/m^3·hr)**	**Run time (hr)**	**MEA concentration (M)**	**Degradation rate (kmol/m^3·hr)**	**Run time (hr)**	**MEA concentration (M)**	**Degradation rate (kmol/m^3·hr)**
0	5.063	0.00070	0	5.023	0.00088	0	5.003	0.00098
17	5.044	0.00070	23	4.980	0.00088	18	4.962	0.00098
90	4.934	0.00070	45	4.982	0.00088	45	4.967	0.00098
113	4.907	0.00070	72	4.996	0.00088	67	4.981	0.00098
136	4.900	0.00070	93	4.944	0.00088	138	4.916	0.00098
161	4.882	0.00070	165	4.844	0.00088	162	4.815	0.00098
185	4.882	0.00070	187	4.881	0.00088	186	4.819	0.00098
255	4.857	0.00070	213	4.860	0.00088	211	4.830	0.00098
281	4.821	0.00070	239	4.864	0.00088	235	4.768	0.00098
305	4.818	0.00070	262	4.801	0.00088	284	4.710	0.00098
329	4.797	0.00070	336	4.689	0.00088	306	4.721	0.00098
352	4.799	0.00070						
Average		**0.00070**	**Average**		**0.00088**	**Average**		**0.00098**

Table B5: The oxidative MEA degradation rates of sulphuric acid (H_2SO_4) systems.

H_2SO_4								
4 ppm			8 ppm			12 ppm		
Run time (hr)	**MEA concentration (M)**	**Degradation rate (kmol/m^3·hr)**	**Run time (hr)**	**MEA concentration (M)**	**Degradation rate (kmol/m^3·hr)**	**Run time (hr)**	**MEA concentration (M)**	**Degradation rate (kmol/m^3·hr)**
0	5.021	0.00039	0	5.027	0.00063	0	5.064	0.00089
19	4.987	0.00039	19	4.996	0.00063	20	4.975	0.00089
42	5.009	0.00039	42	4.942	0.00063	44	4.935	0.00089
67	4.999	0.00039	67	4.945	0.00063	68	4.946	0.00089
96	4.936	0.00039	96	4.922	0.00063	92	4.891	0.00089
139	4.941	0.00039	139	4.902	0.00063	120	4.879	0.00089
162	4.906	0.00039	162	4.900	0.00063	164	4.835	0.00089
187	4.940	0.00039	187	4.883	0.00063	190	4.819	0.00089
211	4.893	0.00039	211	4.870	0.00063	212	4.822	0.00089
236	4.903	0.00039	236	4.857	0.00063	239	4.798	0.00089
264	4.928	0.00039	264	4.836	0.00063	261	4.717	0.00089
309	4.892	0.00039	309	4.813	0.00063	288	4.744	0.00089
330	4.868	0.00039	330	4.776	0.00063	332	4.701	0.00089
354	4.880	0.00039				355	4.732	0.00089
Average		**0.00039**	**Average**		**0.00063**	**Average**		**0.00089**

Table B6: The oxidative MEA degradation rates of sulphurous acid (H_2SO_3) systems.

H_2SO_3		
5 ppm		
Run time (hr)	**MEA concentration (M)**	**Degradation rate (kmol/m^3·hr)**
0	4.999	0.00108
18	4.985	0.00108
42	4.979	0.00108
68	4.966	0.00108
92	4.911	0.00108
120	4.883	0.00108
163	4.844	0.00108
188	4.792	0.00108
212	4.777	0.00108
236	4.759	0.00108
259	4.743	0.00108
Average		**0.00108**
15 ppm		
Run time (hr)	**MEA concentration (M)**	**Degradation rate (kmol/m^3·hr)**
0	5.015	0.00091
22	5.012	0.00091
72	4.907	0.00091
95	4.918	0.00091
118	4.895	0.00091
141	4.874	0.00091
165	4.861	0.00091
190	4.839	0.00091
244	4.800	0.00091
263	4.785	0.00091
286	4.762	0.00091
309	4.727	0.00091
337	4.691	0.00091
357	4.701	0.00091
Average		**0.00091**
100 ppm		
Run time (hr)	**MEA concentration (M)**	**Degradation rate (kmol/m^3·hr)**
0	5.010	0.00083
22	5.009	0.00083
45	4.933	0.00083
69	4.997	0.00083
96	4.923	0.00083

166	4.877	0.00083
190	4.849	0.00083
214	4.848	0.00083
240	4.810	0.00083
262	4.807	0.00083
288	4.786	0.00083
333	4.737	0.00083
356	4.707	0.00083
Average		**0.00083**
250 ppm		
Run time (hr)	**MEA concentration (M)**	**Degradation rate ($kmol/m^3 \cdot hr$)**
0	4.894	0.00071
20	4.841	0.00071
42	4.810	0.00071
114	4.771	0.00071
138	4.783	0.00071
162	4.775	0.00071
186	4.787	0.00071
211	4.711	0.00071
282	4.697	0.00071
306	4.652	0.00071
328	4.599	0.00071
Average		**0.00071**
400 ppm		
Run time (hr)	**MEA concentration (M)**	**Degradation rate ($kmol/m^3 \cdot hr$)**
0	4.971	0.00077
18	4.976	0.00077
69	4.950	0.00077
90	4.951	0.00077
115	4.940	0.00077
138	4.904	0.00077
161	4.924	0.00077
187	4.827	0.00077
258	4.803	0.00077
282	4.775	0.00077
306	4.752	0.00077
332	4.738	0.00077
354	4.741	0.00077
Average		**0.00077**

Table B7: The oxidative MEA degradation rates of nitric acid (HNO_3) systems.

HNO_3								
100 ppm			**250 ppm**			**400 ppm**		
Run time (hr)	**MEA concentration (M)**	**Degradation rate (kmol/m^3·hr)**	**Run time (hr)**	**MEA concentration (M)**	**Degradation rate (kmol/m^3·hr)**	**Run time (hr)**	**MEA concentration (M)**	**Degradation rate (kmol/m^3·hr)**
0	5.000	0.00085	0	4.987	0.00094	0	5.020	0.00107
20	4.996	0.00085	19	4.981	0.00094	19	4.982	0.00107
44	4.935	0.00085	44	4.972	0.00094	44	4.936	0.00107
68	4.943	0.00085	67	4.901	0.00094	67	4.892	0.00107
92	4.911	0.00085	115	4.891	0.00094	115	4.827	0.00107
120	4.877	0.00085	139	4.881	0.00094	139	4.873	0.00107
164	4.846	0.00085	163	4.872	0.00094	163	4.803	0.00107
190	4.814	0.00085	187	4.828	0.00094	187	4.785	0.00107
212	4.845	0.00085	212	4.783	0.00094	212	4.748	0.00107
239	4.798	0.00085	235	4.777	0.00094	235	4.708	0.00107
261	4.740	0.00085	283	4.723	0.00094	283	4.676	0.00107
288	4.726	0.00085	307	4.716	0.00094	307	4.666	0.00107
332	4.711	0.00085	331	4.696	0.00094	331	4.661	0.00107
355	4.719	0.00085	355	4.650	0.00094	355	4.612	0.00107
Average		**0.00085**	**Average**		**0.00094**	**Average**		**0.00107**

Table B8: The oxidative MEA degradation rates of the mixed additives Run no. 15 to 18.

Mixed additives		
Run no. 15		
Run time (hr)	**MEA concentration (M)**	**Degradation rate ($kmol/m^3 \cdot hr$)**
0	5.062	0.00147
18	5.029	0.00147
42	4.954	0.00147
66	4.910	0.00147
114	4.821	0.00147
139	4.825	0.00147
162	4.801	0.00147
186	4.729	0.00147
211	4.737	0.00147
238	4.666	0.00147
259	4.654	0.00147
306	4.607	0.00147
331	4.542	0.00147
355	4.506	0.00147
Average		**0.00147**
Run no. 16		
Run time (hr)	**MEA concentration (M)**	**Degradation rate ($kmol/m^3 \cdot hr$)**
0	5.000	0.00155
18	4.947	0.00155
42	4.910	0.00155
66	4.812	0.00155
114	4.727	0.00155
139	4.690	0.00155
162	4.689	0.00155
186	4.609	0.00155
211	4.586	0.00155
238	4.569	0.00155
259	4.536	0.00155
306	4.506	0.00155
331	4.461	0.00155
355	4.427	0.00155
Average		**0.00155**

Run no. 17		
Run time (hr)	**MEA concentration (M)**	**Degradation rate (kmol/m^3·hr)**
0	5.073	0.00190
20	5.057	0.00190
45	5.054	0.00190
69	4.983	0.00190
93	4.952	0.00190
120	4.924	0.00190
165	4.823	0.00190
190	4.733	0.00190
214	4.673	0.00190
240	4.616	0.00190
265	4.574	0.00190
288	4.543	0.00190
335	4.505	0.00190
356	4.458	0.00190
Average		**0.00190**
Run no. 18		
Run time (hr)	**MEA concentration (M)**	**Degradation rate (kmol/m^3·hr)**
0	5.004	0.00251
20	4.979	0.00251
45	4.942	0.00251
69	4.878	0.00251
93	4.836	0.00251
120	4.761	0.00251
165	4.654	0.00251
190	4.639	0.00251
214	4.555	0.00251
240	4.457	0.00251
265	4.402	0.00251
288	4.292	0.00251
335	4.172	0.00251
356	4.138	0.00251
Average		**0.00251**

Table B9: The oxidative MEA degradation rates of the mixed additives Run no. 19 and 20 (Temperature effect).

Mixed additives		
Run no. 19		
Run time (hr)	**MEA concentration (M)**	**Degradation rate ($kmol/m^3 \cdot hr$)**
0	5.046	0.00001
22	5.043	0.00001
47	5.045	0.00001
72	5.037	0.00001
120	5.041	0.00001
142	5.041	0.00001
166	5.041	0.00001
190	5.040	0.00001
216	5.045	0.00001
268	5.041	0.00001
286	5.043	0.00001
311	5.039	0.00001
334	5.033	0.00001
358	5.041	0.00001
384	5.040	0.00001
430	5.035	0.00001
Average		**0.00001**
Run no. 20		
Run time (hr)	**MEA concentration (M)**	**Degradation rate ($kmol/m^3 \cdot hr$)**
0	5.028	0.00016
22	5.013	0.00016
47	4.999	0.00016
72	5.005	0.00016
120	4.992	0.00016
142	4.988	0.00016
166	4.988	0.00016
190	4.991	0.00016
216	4.986	0.00016
268	4.979	0.00016
286	4.970	0.00016
311	4.962	0.00016
334	4.960	0.00016
358	4.951	0.00016
384	4.954	0.00016
430	4.952	0.00016
Average		**0.00016**

APPENDIX C

EXPERIMENTAL DATA OF THE INHIBITION STUDY

Table C1: Inhibitor A performance on carbon steel (1020) corrosion.

Inhibitor A		
Concentration (ppm)	**Corrosion rate (mpy)**	**% Inhibition**
0	391.60	0
1000	356.30	9.0
2500	293.20	25.1
5000	259.80	33.7
6500	202.50	48.3
7500	161.10	58.9
10000	96.89	75.3
12500	51.12	86.9
15000	43.47	88.9
20000	46.31	88.2

Table C2: Inhibitor A performance on oxidative MEA degradation.

Inhibitor A		
250 ppm		
Run time (hr)	**MEA concentration (M)**	**Degradation rate ($kmol/m^3 \cdot hr$)**
0	4.987	0.00131
20	4.949	0.00131
45	4.944	0.00131
69	4.917	0.00131
120	4.851	0.00131
140	4.807	0.00131
164	4.744	0.00131
188	4.697	0.00131
212	4.664	0.00131
236	4.650	0.00131
284	4.618	0.00131
308	4.606	0.00131
332	4.579	0.00131
Average		**0.00131**
% Inhibition		**48.7%**
1000 ppm		
Run time (hr)	**MEA concentration (M)**	**Degradation rate ($kmol/m^3 \cdot hr$)**
0	5.103	0.00007
19	5.097	0.00007
43	5.122	0.00007
67	5.090	0.00007
91	5.085	0.00007
139	5.084	0.00007
164	5.088	0.00007
188	5.102	0.00007
212	5.097	0.00007
236	5.073	0.00007
260	5.073	0.00007
307	5.080	0.00007
330	5.091	0.00007
Average		**0.00007**
% Inhibition		**97.3%**

6000 ppm		
Run time (hr)	**MEA concentration (M)**	**Degradation rate (kmol/m^3·hr)**
0	4.937	0.00112
51	4.788	0.00112
68	4.758	0.00112
92	4.810	0.00112
116	4.747	0.00112
147	4.711	0.00112
164	4.736	0.00112
216	4.623	0.00112
236	4.576	0.00112
260	4.526	0.00112
284	4.503	0.00112
309	4.601	0.00112
332	4.573	0.00112
Average		**0.00112**
% Inhibition		**55.5%**
15000 ppm		
Run time (hr)	**MEA concentration (M)**	**Degradation rate (kmol/m^3·hr)**
0	4.884	0.00233
51	4.778	0.00233
68	4.795	0.00233
92	4.739	0.00233
116	4.708	0.00233
147	4.647	0.00233
164	4.564	0.00233
216	4.426	0.00233
236	4.411	0.00233
260	4.324	0.00233
284	4.262	0.00233
309	4.210	0.00233
332	4.129	0.00233
Average		**0.00233**
% Inhibition		**7.1%**

Table C3: Inhibitor B performance on carbon steel (1020) corrosion.

Inhibitor B		
Concentration (ppm)	**Corrosion rate (mpy)**	**% Inhibition**
0	391.60	0
25	39.93	89.8
50	35.27	91.0
75	32.43	91.7
100	29.79	92.4
500	39.83	89.8
750	47.62	87.8
1000	52.26	86.7
2500	81.88	79.1
5000	131.80	66.3
10000	198.80	49.2

Table C4: Inhibitor B performance on oxidative MEA degradation.

Inhibitor B		
50 ppm		
Run time (hr)	**MEA concentration (M)**	**Degradation rate (kmol/m^3·hr)**
0	4.956	0.00116
23	4.937	0.00116
43	4.967	0.00116
67	4.940	0.00116
119	4.843	0.00116
140	4.823	0.00116
163	4.818	0.00116
187	4.773	0.00116
212	4.770	0.00116
236	4.715	0.00116
260	4.676	0.00116
284	4.651	0.00116
308	4.629	0.00116
331	4.596	0.00116
Average		**0.00116**
% Inhibition		**53.9%**
100 ppm		
Run time (hr)	**MEA concentration (M)**	**Degradation rate (kmol/m^3·hr)**
0	5.028	0.00101
20	5.033	0.00101
44	4.973	0.00101
69	4.943	0.00101
94	4.882	0.00101
117	4.861	0.00101
140	4.846	0.00101
188	4.797	0.00101
212	4.771	0.00101
240	4.773	0.00101
264	4.765	0.00101
288	4.746	0.00101
312	4.711	0.00101
Average		**0.00101**
% Inhibition		**59.9%**

500 ppm		
Run time (hr)	**MEA concentration (M)**	**Degradation rate ($kmol/m^3 \cdot hr$)**
0	5.105	0.00113
21	5.051	0.00113
48	5.027	0.00113
94	5.010	0.00113
118	4.889	0.00113
141	4.877	0.00113
166	4.863	0.00113
190	4.821	0.00113
216	4.774	0.00113
261	4.730	0.00113
286	4.690	0.00113
310	4.711	0.00113
337	4.657	0.00113
358	4.682	0.00113
384	4.684	0.00113
406	4.652	0.00113
Average % Inhibition		**0.00113 55.0%**

Table C5: Inhibitor C performance on carbon steel (1020) corrosion.

Inhibitor C		
Concentration (ppm)	**Corrosion rate (mpy)**	**% Inhibition**
0	391.6	0
500	385.7	1.5
2500	373.9	4.5
5000	347.8	11.2
20000	296.3	24.3
40000	247.7	36.7
60000	236.7	39.6
80000	224.5	42.7
100000	223.1	43.0

Table C6: Inhibitor C performance on oxidative MEA degradation.

Inhibitor C		
10000 ppm		
Run time (hr)	**MEA concentration (M)**	**Degradation rate ($kmol/m^3 \cdot hr$)**
0	4.964	0.00134
26	4.924	0.00134
46	4.890	0.00134
92	4.830	0.00134
115	4.781	0.00134
140	4.766	0.00134
164	4.717	0.00134
189	4.701	0.00134
213	4.692	0.00134
260	4.621	0.00134
284	4.566	0.00134
308	4.536	0.00134
Average		**0.00134**
% Inhibition		**46.7%**
40000 ppm		
Run time (hr)	**MEA concentration (M)**	**Degradation rate ($kmol/m^3 \cdot hr$)**
0	5.292	0.00019
19	5.288	0.00019
43	5.287	0.00019
67	5.240	0.00019
91	5.241	0.00019
139	5.259	0.00019
164	5.262	0.00019
188	5.245	0.00019
212	5.238	0.00019
236	5.225	0.00019
260	5.258	0.00019
307	5.206	0.00019
330	5.231	0.00019
Average		**0.00019**
% Inhibition		**92.6%**

80000 ppm		
Run time (hr)	**MEA concentration (M)**	**Degradation rate ($kmol/m^3 \cdot hr$)**
0	4.715	0.00138
20	4.724	0.00138
45	4.715	0.00138
69	4.644	0.00138
120	4.603	0.00138
140	4.580	0.00138
164	4.550	0.00138
188	4.514	0.00138
212	4.480	0.00138
236	4.430	0.00138
284	4.374	0.00138
308	4.333	0.00138
332	4.252	0.00138
Average		**0.00138**
% Inhibition		**45.1%**

Table C7: Mixed inhibitors (A + C) performance on carbon steel (1020) corrosion.

Mixed Inhibitor A + C		
Mixed inhibitors ratio	**Corrosion rate (mpy)**	**% Inhibition**
Base-case	391.60	0
Ratio I (A + C : 15000 + 80000 ppm)	28.82	92.6
Ratio II (A + C : 1000 + 40000 ppm)	219.60	43.9
Ratio III (A + C : 15000 + 40000 ppm)	38.26	90.2

Table C8: Mixed inhibitors (A + C) performance on oxidative MEA degradation.

Mixed inhibitor A + C		
Ratio I at A + C : 15000 + 80000 ppm		
Run time (hr)	**MEA concentration (M)**	**Degradation rate (kmol/m^3·hr)**
0	4.720	0.00208
26	4.711	0.00208
46	4.637	0.00208
92	4.601	0.00208
115	4.560	0.00208
140	4.506	0.00208
164	4.452	0.00208
189	4.397	0.00208
213	4.327	0.00208
260	4.194	0.00208
284	4.151	0.00208
308	4.112	0.00208
Average		**0.00208**
% Inhibition		**17.3%**
Ratio II at A + C : 1000 + 40000 ppm		
Run time (hr)	**MEA concentration (M)**	**Degradation rate (kmol/m^3·hr)**
0	4.824	0.00015
22	4.855	0.00015
46	4.827	0.00015
70	4.822	0.00015
94	4.824	0.00015
142	4.817	0.00015
165	4.812	0.00015
189	4.824	0.00015
213	4.800	0.00015
237	4.803	0.00015
261	4.790	0.00015
310	4.791	0.00015
Average		**0.00015**
% Inhibition		**93.9%**

Ratio III at A + C : 15000 + 40000 ppm		
Run time (hr)	**MEA concentration (M)**	**Degradation rate (kmol/m^3·hr)**
0	4.834	0.00087
22	4.812	0.00087
46	4.800	0.00087
70	4.778	0.00087
94	4.788	0.00087
142	4.721	0.00087
165	4.659	0.00087
189	4.683	0.00087
213	4.650	0.00087
237	4.639	0.00087
261	4.591	0.00087
310	4.581	0.00087
Average		**0.00087**
% Inhibition		**65.2%**

APPENDIX D

DETERMINATION OF HYDROGEN (H^+), SULFITE (SO_3^{2-}), AND BISULFITE (HSO_3^-) IONS CONCENTRATIONS IN AQUEOUS SOLUTION OF SULPHUROUS ACID (H_2SO_3)

The concentrations of hydrogen (H^+), sulfite (SO_3^{2-}), and bisulfite (HSO_3^-) ions dissociated when dissolving sulphurous acid (H_2SO_3) into aqueous solution were determined by comparing amounts of sulfite and bisulfite ions generated when dissolving sulphurous acid with the calibration curves measured from sodium sulfite (Na_2SO_3) and sodium bisulfite ($NaHSO_3$) in aqueous solutions, respectively, where the ion concentrations were measured by using capillary electrophoresis with diode array detection (CE-DAD). The dissociation of sulphurous acid in water was performed in a concentration range of 0 to 400 ppm (0.001 to 0.005M) acid concentration, and the dissociated data was presented in Table D1 and Figure D1, where hydrogen ion concentration was calculated according to equations D1 and D2.

$$H_2SO_3 \leftrightarrow HSO_3^- + H^+ \qquad \text{D1}$$

$$H_2SO_3 \leftrightarrow SO_3^{2-} + 2H^+ \qquad \text{D2}$$

Table D1: Dissociation of sulphurous acid (H_2SO_3) in water.

Initial H_2SO_3 (M; mol/l)	H_2SO_3 Dissociation		
	H^+ (M)	SO_3^{2-} (M)	HSO_3^-(M)
0	0	0	0
0.00117	0.00099	0.00019	0.00061
0.00244	0.00181	0.00041	0.00099
0.00370	0.00359	0.00095	0.00169
0.00491	0.00476	0.00124	0.00228

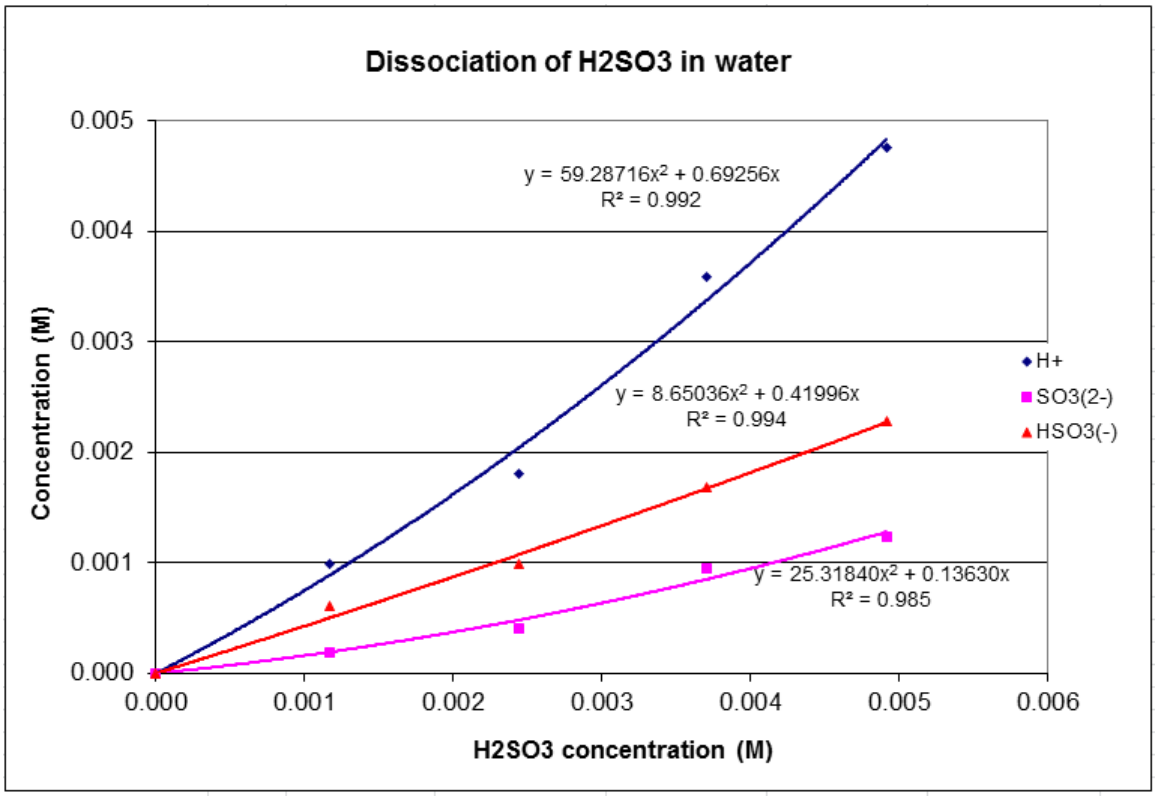

Figure D1: Dissociation of sulphurous acid (H_2SO_3) in water. (Original in colour)